Technical University of Munich

Structure-function relationships of mucin glycoproteins

A thesis presented by

Matthias Marczynski

TUM School of Engineering and Design,

Department of Materials Engineering

Professur für Biomechanik

Technische Universität München

TUM School of Engineering and Design

Structure-function relationships of mucin glycoproteins

Matthias Marczynski

Vollständiger Abdruck der von der TUM School of Engineering and Design der Technischen Universität München zur Erlangung eines

Doktors der Naturwissenschaften (Dr. rer. nat.)

genehmigten Dissertation.

Vorsitzende:	Prof. Dr. Petra Mela
Prüfer der Dissertation:	1. Prof. Dr. rer. nat. Oliver Lieleg
	2. Prof. Dr.-Ing. Ulrich Kulozik

Die Dissertation wurde am 12.10.2021 bei der Technischen Universität München eingereicht und durch die TUM School of Engineering and Design am 07.02.2022 angenommen.

Summary

Over the last decades, mucin glycoproteins have gained increasing attention in the fields of medical research and (bio-)medical engineering. This is, on the one hand, driven by the fact that alterations in the composition and functionality of mucosal systems are associated with a broad range of diseases such as the dry eye syndrome, cystic fibrosis, and certain forms of cancer. On the other hand, mucin glycoproteins possess a number of favorable properties (including excellent hydration, lubricity, and anti-viral and anti-bacterial activity), which make them a promising candidate for biomedical applications. Indeed, an increasing body of scientific literature highlights the diverse potential applications for which purified mucins may be employed. Examples reach from antibacterial, self-lubricating surface coatings on medical products such as contact lenses or catheters to innovative platforms for sustained drug delivery.

Despite the high importance of mucins for many physiological processes and an increasing interest in mucins for medical applications, to date, the mechanistic understanding of how mucins fulfill certain functionalities remains insufficient. In this thesis, different isoforms of lab-purified mucins and enzymatically modified loss-of-function variants generated thereof were employed to address the lack of knowledge concerning the structure-function relationships of mucin glycoproteins. The three states mucins occur in physiologically were recreated: surface-attached mucin layers, mucin-based solutions, and mucin-based hydrogels. With these model systems, the conformation of mucin glycoproteins as well as the binding interactions they can engage in with diverse binding partners were investigated. Moreover, the lubricity of mucin solutions and the barrier properties of mucin hydrogels were probed. The results discussed in this thesis illustrate the complexity of the molecular processes that establish certain physiological functionalities and highlight the importance of structural integrity: even minor defects in the biochemical architecture of mucins can lead to drastically altered physico-chemical properties.

The structure-function analysis presented herein may be of great value for engineering artificial, mucin-inspired macromolecules, which are able to recreate the properties of mucins required for specific (medical) applications. In light of the expected increasing demand for mucins in research, the development of such functional mucin surrogates is highly desired.

Contents

1. Introduction*

Extensive phylogenetic analyses indicated that the ability to produce and secrete mucus was an early milestone in the evolution of the animal kingdom.[1] Genes encoding mucin-like glycoproteins – the main structural and functional component of mucus – were even found in the genomes of members of the most basal metazoan phyla (*i.e.*, animals in the broadest sense) such as *Porifera* (sponges), *Cnidaria* (*e.g.*, corals and jellyfish), and *Ctenophora* (comb jellies).[2, 3] In fact, mucus is considered to be a universal feature that is used by all phyla of the animal kingdom. Accordingly, the composition of mucus, in particular among vertebrates – including humans well as our most distant vertebrate relatives – is highly similar.[2, 4] In addition to mucin glycoproteins, which dictate the biological and physico-chemical properties of mucus, mucosal systems also comprise various secreted proteins, lipids, DNA, salts, and cellular debris as well as intact cells.[5]

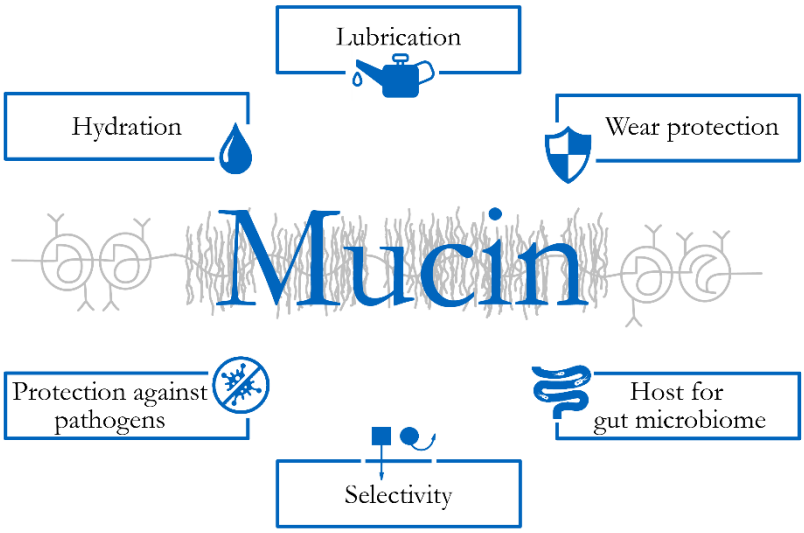

Fig. 1.1: Physiological functions of mucosal systems. Depending on the particular mucosal system mucins are located in, they full different functions including tissue hydration, lubrication, wear protection, accommodation of a healthy microbiome, selectivity, and protection against pathogens.

The functions of mucosal systems are similar throughout the entire animal kingdom (**Fig. 1.1**). Mucus covers all wet epithelial surfaces, and – at least in part – this is necessary to keep mucosal tissues well hydrated. For instance, amphibians secrete mucus on their outer body surface to prevent their skin tissue from drying out.[6] Proper hydration is also important for human mucosal surfaces, even though our tissues are not as much in danger of dehydration. In contrast, the surfaces of our gastrointestinal system as well as the corneal tissue require lubrication, which is essential to prevent tissue damage

* This section follows in part the publications Marczynski *et al.*, Advanced Drug Delivery Reviews (2021) and Marczynski & Lieleg, Biophysics Reviews (2021).

arising from mechanical challenges and reduce damage-induced inflammation.[7, 8] Yet, the functionality of mucus is not limited to dealing with mechanical challenges. For instance, mucus also acts as a protective barrier against potentially harmful objects such as particulate matter, bacteria, or viruses, while – at the same time – regulating the passage of nutrients from the gastrointestinal tract.[9-11]

Owing to these diverse functionalities mucins establish physiologically, the interest in mucins as a functional component in biomedical products has been constantly increasing over the last decades.[12] Moreover, also in the fields of biochemistry and molecular biology, mucin glycoproteins have gained additional attention. In part, this renewed interest in mucins is linked with the intensifying research on the gut microbiome: bacteria can thrive in a mucus gel from which they receive nutrients and complex biological signals. Thereby mucus accommodates and maintains a healthy microbiome.[13-15] Mucins are thus increasingly incorporated into *in vitro* models to better mimic, understand, and engineer such a bacterial microenvironment.[15, 16] Furthermore, mucins are of interest for medical researchers and biologists, *e.g.*, as targetable markers in the context of cancerous tumors or other pathological scenarios.[17-19] As a consequence of this enhanced interest in mucins in recent years, also the demand for functional mucins constantly increased, and this trend is expected to further continue.

Despite the clear importance of mucin glycoproteins in many physiological processes, the mechanistic principles and structural motifs underlying the diverse functionalities of mucins remained mostly enigmatic to this day. This lack of knowledge is likely due to two main reasons: on the one hand, the diverse chemistry and the large molecular weight of mucin glycoproteins as well as the high level of intrinsic structural heterogeneity makes them difficult to characterize. On the other hand, as mentioned above, the availability of functional mucins is limited. Since it has been shown repeatedly that commercially available preparations are structurally and functionally corrupted, high-quality mucins can only be obtained in the laboratory.[20-22] In principle, two different strategies can be employed to obtain a functional protein in the laboratory. First, a protein can be cloned and expressed recombinantly by prokaryotic or eukaryotic cell lines. Owing to the large molecular weight of mucins and their high degree of glycosylation, however, it was not possible yet to obtain entire mucins with this approach. So far, only distinct mucin domains could be produced successfully by generating cDNA libraries from processed mRNA, cloning of the desired cDNA fragments into vectors, and subsequent heterologous expression.[23, 24] Of course, the feasibility of such mucin fragments in both, application-driven and fundamental research is limited. Thus, a second approach is used to obtain whole mucin glycoproteins comprising all structural motifs relevant for their functionalities, *i.e.*, their purification from raw mucus produced by tissues (or eukaryotic cell lines), which naturally express the desired mucin type.

Introduction

The lack of knowledge concerning structure-function relationships of mucins was addressed in this thesis: in the human body, mucosal systems occur in three distinct states – as membrane-tethered polymer layers, solutions, and hydrogels – and each of these systems fulfills specific functions. Here, model systems for native mucosal systems were reconstituted from purified mucins. In addition to a detailed chemical and physical characterization of lab-purified mucins, a side-by-side comparison of model systems generated from both lab-purified mucins and enzymatically modified variants was performed. This top-down approach allowed for identifying the contribution of distinct structural motifs to maintaining an elongated conformation mucins. The conformational state, in turn, dictates the adsorption, lubricating, and binding properties of mucins. Accordingly, also the molecular principles governing mucin lubricity and the barrier properties of mucin hydrogels were investigated. In this context, finally, also the permeability of mucin hydrogels toward the pathologically relevant protein α-synuclein was assessed.

2. Materials & Methods

2.1. Mucin glycoproteins*

Mucins are the functional and primary structural component of all mucinous systems. Physiologically, these mucinous systems occur in three distinct states (**Fig. 2.1 A**). On the one hand, the apical cell layer of all mucosal tissues expresses membrane-tethered mucin glycoproteins, which form a well hydrated, brushy mucin surface layer. On the other hand, mucosal tissues in the human body also produce mucin secretions, which occur either as water-based solutions or hydrogels. Whereas the former exhibit mostly viscous (= liquid-like) properties, in the latter, the elastic (= solid-like) properties dominate. In total, seven different isotypes of such secreted mucins can be distinguished (MUC2, MUC5AC, MUC5B, MUC6, MUC7, MUC8), which are expressed differently throughout the human body.[25, 26] The mucin variants used in this thesis are MUC2, MUC5AC, and MUC5B. The MUC2 isoform is the main component of intestinal mucus hydrogels but is almost entirely absent in all other body regions.[27] In contrast, MUC5AC and MUC5B are mucins with a much broader tissue representation. MUC5AC is the dominating mucin isotype present in gastric mucus and the tear fluid but also occurs in the airways and in the female reproductive tract.[28-30] In these latter two locations as well as in the gallbladder, MUC5B is the most abundant mucin variant.[31, 32] In addition, salivary glands secrete this specific mucin variant into the oral cavity.[32, 33]

The different isoforms of secreted mucins are quite similar to each other in terms of structure and conformation (**Fig. 2.1 B**): the mucin polypeptide backbone contains a long central region comprising a variable number of tandem repeats (VNTRs), which are mostly composed of the amino acids proline, threonine, and serine.[34] This core domain is described best as an intrinsically disordered, elongated chain. On the one hand, this can be attributed to the numerous proline clusters, which have been put forward to prevent the formation of secondary structures – this particular amino acid is too rigid to be incorporated into a locally ordered structure.[35] On the other hand, the high number of threonine and serine residues allows for a dense decoration of the protein backbone with oligosaccharides *via* *O*-glycosidic linkages.[36] Although the detailed composition of these mucin *O*-glycans is quite diverse, there is one specific pattern that occurs more frequently: the oligosaccharide chains are often terminated by anionic sialic acid groups or sulfated glycans.[37, 38] The repulsive electrostatic forces acting between these anionic groups in combination with steric effects

* This section follows in part the publications Marczynski *et al.*, Advanced Drug Delivery Reviews (2021) and Marczynski *et al.*, Biopolymers for Biomedical and Biotechnological Applications (2021).

established by the oligosaccharide chains, are thought to convey a high level of conformational rigidity to the mucin glycoprotein.[39]

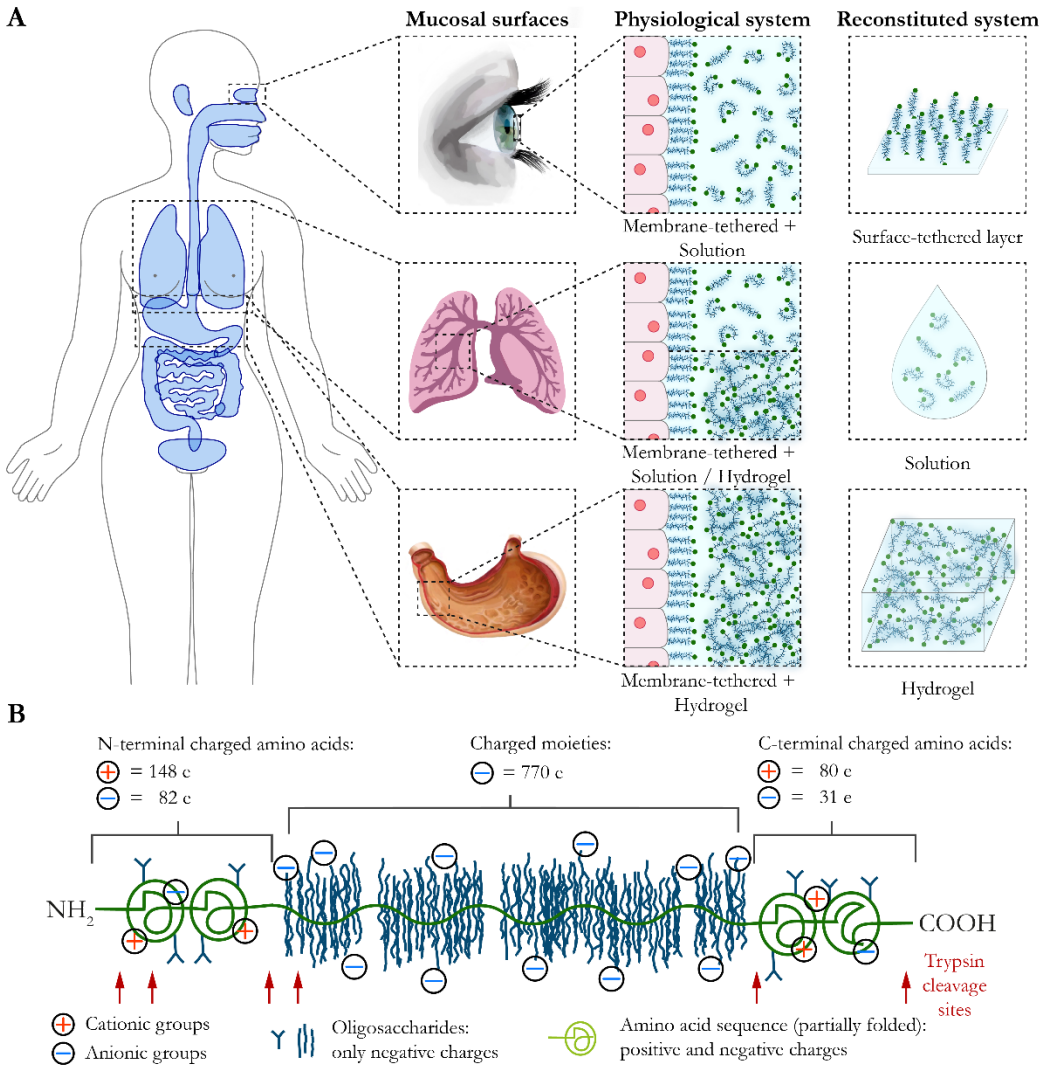

Fig. 2.1: Mucosal systems in the human body and structure of mucin glycoproteins. Mucosal systems cover all wet body surfaces and can occur in three different states: as membrane-tethered mucins on the apical side of mucosal epithelia (*e.g.*, the periciliary layer of the airways), as mucin-based solutions (*e.g.*, the tear fluid), or as mucin-based hydrogels (*e.g.*, gastric mucus). Each of these three states can be reconstituted from purified mucins, which allows studying their properties in a controlled, systematic and highly reproducible manner. The characteristic component of mucus is the mucin glycoprotein (**A**). Schematic of a mucin glycoprotein: a central, highly glycosylated region carrying a large number of anionic sialic acid residues and sulfate groups is flanked by relatively hydrophobic and partially folded termini, which are comprised of hydrophobic and charged amino acids. Red arrows indicate the most likely trypsin cleavage sites as determined by Käsdorf *et al.*[40] (**B**).

From both ends, this polyanionic VNTR region is flanked by (partially) folded terminal domains, which are only sparsely glycosylated (mostly through *N*-glycosidic bonds) and display a mixture of

anionic, cationic and hydrophobic amino acids.[34, 41, 42] In addition, the mucin termini are rich in cysteines, and this allows individual mucin molecules to assemble into oligomers and polymeric networks by forming intermolecular disulfide bridges.[43, 44] One of the key parameters that dictate if mucins form such networks (*i.e.*, a hydrogel) is the mucin concentration in the mucosal system: higher mucin concentrations enable an increased number of inter-mucin interactions. Thus, the formation of an interconnected network is more likely. For instance, in the gastrointestinal tract, the cervix, and in the airways (where mucus exists in the form of hydrogels), the mucin concentration is on the order of ~1-5 %.[45, 46] In contrast, the mucin concentration in the tear fluid and in saliva is rather low (*i.e.*, < 0.02 %), and these mucosal systems behave as viscoelastic liquids.[28, 47]

Different from secreted mucins, membrane-tethered mucins are asymmetric molecules comprising a large, extracellular domain consisting of the VNTR region and a short N-terminal signal peptide that guides the localization of the mucin molecule in the apical cell membrane, and a small, intracellular C-terminus.[48, 49] A single-pass transmembrane domain connects the two subunits and anchors membrane-associated mucins to the cell membrane.[50] As membrane-tethered mucins are integrated into hydrophobic lipid bilayer membranes, it is challenging to purify these mucins variants in their structurally intact form. Because of this difficulties, in the past, secreted mucins have been routinely used as proxies for membrane-tethered mucins.

2.2. Purification of functional mucins

Throughout this thesis, three different variants of lab-purified mucin were used: intestinal mucin MUC2 and gastric mucin MUC5AC*, both of porcine origin, as well as human salivary mucin MUC5B. All mucin isotypes were purified according to a standard protocol published previously in Schömig *et al.* (**Fig. 2.2**).[22] For the purification of the porcine mucin variants, pig small intestines or stomachs were obtained from a local slaughterhouse on the day of processing. After gently rinsing the tissues with tap water, raw mucus was obtained from dissected organs by manually scraping the inner mucosal surfaces with spoons. The collected mucus was pooled and diluted 5-fold in 10 mM sodium phosphate buffered saline (PBS; pH 7.0) supplemented with 170 mM NaCl and 0.04 % (w/v) NaN_3. For homogenization, the diluted raw mucus was stirred at 4 °C overnight. Then, coarse impurities such as food particles and cellular debris were removed *via* two (ultra-)centrifugation steps (first run: 30 min at 17590 × g; second run: 1 h at 158306 × g) using a Beckman Optima L-70

* Porcine gastric mucin MUC5AC is the mucin variant that was predominantly used in this thesis. Detailed information on this variant can be found in **Appendix A1**.

ultracentrifuge (Beckman Coulter, Brea, CA, USA) and a Type 45 Ti fixed-angle rotor (Beckman Coulter). Subsequently, the mucin glycoproteins were isolated by means of size exclusion chromatography (SEC) using an ÄKTA purifier system (GE Healthcare, Munich, Germany) equipped with an XK50/100 column packed with Sepharose 6FF (column volume ~1.64 L) equilibrated in 10 mM PBS. The collected mucin fractions were pooled, and the NaCl concentration of the solution was adjusted to 1 M. Afterwards, the mucin solution was dialyzed against ultrapure water and concentrated by cross-flow filtration using a filter hollow fiber cartridge with a MWCO of 100 kDA (Xampler Ultrafiltration Cartridge, GE Healthcare). The concentrate was lyophilized and stored at -80 °C until further use.

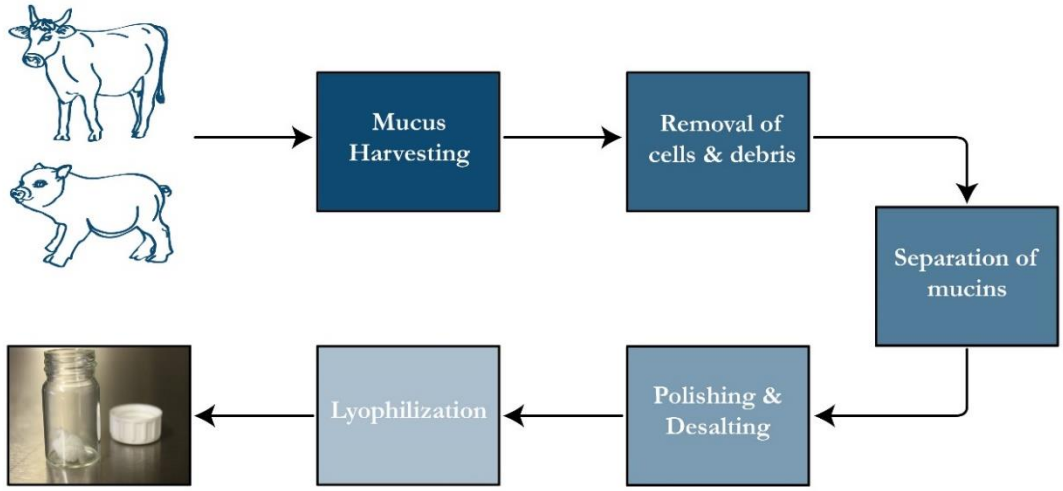

Fig. 2.2: Purification of mucins from mucosal animal tissues. The standard procedure for the purification of functional mucins from mucosal tissues comprises five steps. First, crude mucus is manually harvested from the tissue surface to obtain the mucin containing material that is further processed. The removal of cellular debris and coarse, particulate impurities is followed by a technique that isolates the mucin glycoproteins from most molecular impurities. Afterwards, mucins are desalted and further purified to remove remaining molecular contaminants. Finally, lyophilization yields a protein powder which can be stored for extended time periods.

For the purification of human salivary mucin MUC5B, unstimulated human whole saliva was collected from healthy, non-smoking, 20-30 year old donors, which refrained from consuming food and beverages other than water for at least 1 h prior to saliva donation. Throughout the entire collection procedure, saliva samples were stored on ice. To purify functional mucins, the same protocol as used for porcine MUC2 and MUC5AC was followed.

Different from the standard protocol displayed in **Fig. 2.2**, some modifications can be introduced to simplify and accelerate the mucin purification from animal tissues (see **Appendix A2**). In particular, a partial automatization and simplification of the mucus harvesting procedure can be achieved by

contacting mucosal tissues with an aqueous buffer solution in an aerated bubble column (**Appendix A2**, **Fig. A2.1**), thereby solubilizing the mucins. This step can replace the time-consuming manual harvesting procedure to obtain raw mucus. In addition, the purification procedure can be further simplified by subjecting the harvested raw mucus to several filtration steps (as an initial isolation step after dilution with PBS buffer and overnight homogenization) instead of performing time consuming and costly centrifugation steps. Several combinations of grids made from stainless steel with average mesh sizes on the order of 1 mm to 125 μm yielded mucins with tribological and rheological properties similar to those purified according to the standard protocol (**Fig. A2.2**).

2.3. Re-purification of commercial porcine gastric mucins (PGM)

In addition to manually purified mucins, two variants of commercially available porcine gastric mucin MUC5AC were used in the experiments presented in this thesis. To distinguish lab-purified MUC5AC variants from the commercially available products, the latter ones will be referred to as ‚PGM Type II' and ‚PGM Type III' for the remainder of this work. Crude PGM preparations were obtained from Sigma-Aldrich (St. Louis, MO, USA) as lyophilized powders (PGM Type II: M2378, sialic acid content according to the vendor ≤1.2 %; Sigma Type III: M1778, partially purified, sialic acid content according to the vendor 0.5−1.5 %). The two commercial mucin variants were subjected to the same purification process as the lab-purified mucins. This way, it could be ensured that differences in the behavior of lab-purified and commercial mucins are not solely due to an insufficient purification of the commercial mucin variants.

For re-purification of the commercial PGM variants, 200 mg of each variant were dissolved in 200 mL of 10 mM PBS (pH 7.0) containing 1 M NaCl. After complete dissolution of the lyophilized mucin powders, the solutions were subjected to SEC. Reconstitution of PGM in a buffer containing high NaCl concentrations during the SEC step was chosen to remove impurities that are bound to the PGM *via* electrostatic attraction forces. The collected fractions were then further processed as described above for lab-purified MUC5AC.

The successful removal of proteinous components (other than the mucin glycoproteins) from the commercial mucin preparation could be verified by recording the absorption signal at a wavelength of 280 nm during the SEC step of the purification procedure (**Fig. 2.3 A**). Owing to their large size, mucins are the first proteins to elute from the SEC column, and the corresponding peak in the chromatogram was clearly separated from the main elution peak, which is established by the remaining mucus protein components. After completion of the purification procedure, both the lab-

purified MUC5AC and the commercial PGMs appear as a white product with a cotton candy-like texture (**Fig. 2.3 A**).

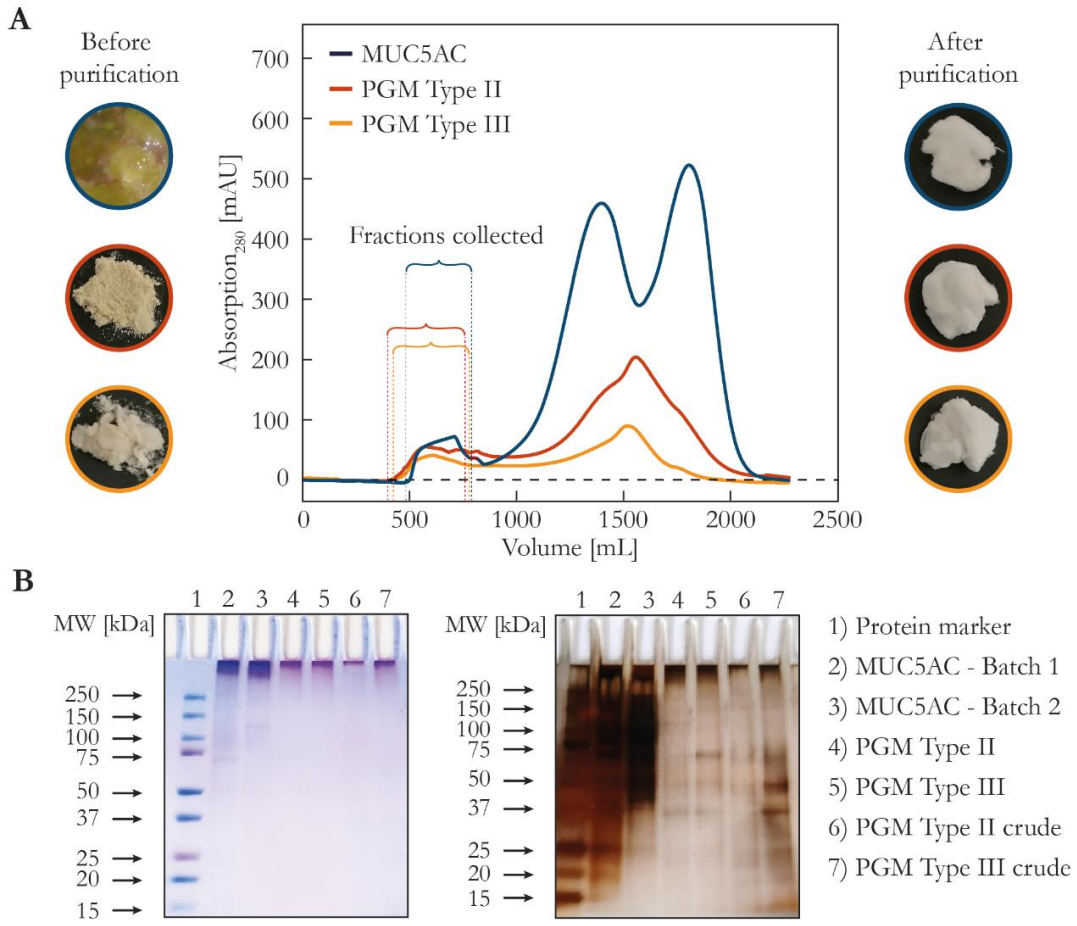

Fig. 2.3: Purity of lab-purified MUC5AC and commercial PGMs before and after (re-)purification. Illustrative examples of size exclusion chromatograms recorded at an absorption wavelength of 280 nm. For each of the three mucin variants, eluate fractions were collected as indicated by the parentheses and further processed. The purification of gastric mucin from mucus yields a white cotton candy-like lyophilisate. Commercially available mucins are obtained as beige powders; after repurification, those PGMs exhibit the same color and morphology as lab-purified (**A**). SDS-PAGE after a combined Coomassie/PAS staining (left) to specifically detect mucins (purple stain) and after silver staining (right) to detect protein contaminants (black stain; **B**).

Moreover, an electrophoretic separation of the isolated mucins on a polyacrylamide gel indicated that all mucin preparations contained significant amounts of mucin as indicated by the distinct purple stains located in the pockets of the gel after applying a combined Coomassie/PAS staining. However, even after (re-)purification, all mucin variants were still contaminated with small amounts of protein components only detectable by performing a highly sensitive silver staining (**Fig. 2.3 B**). A detailed

characterization of both, the lab-purified MUC5AC and the two commercial PGM variants, can be found in **Appendix A1**.

2.4. Chemically modified mucin variants

Distinct chemical motifs of mucin glycoproteins can be removed by treating the mucin preparations with specific enzymes. Firstly, lab-purified MUC5AC is always intimately associated with DNA fragments, which can be efficiently removed by a DNase treatment (**Fig. 3.2 A**). Secondly, anionic sulfate groups or sialic acid residues can be cleaved from the mucin glycan chains using sulfatases or neuraminidases, respectively (**Fig. 3.2 B**). Lastly, the terminal domains of mucins can be removed by a treatment with the protease trypsin. In the latter case, the dense glycosylation pattern protected the central domain of the mucin molecule from being degraded into small fragments. Hence, only the ‚unprotected', non-glycosylated terminal regions were cleaved.

After enzymatic treatment, all mucin variants were purified to remove the enzymes and cleaved fragments; here, the above describe protocol was used starting from the SEC step.

2.4.1. DNase treatment

Some lab-purified mucin variants such as porcine MUC5AC (but not human MUC5B) are typically associated with DNA – even after careful manual purification.[38] Interestingly, in contrast to lab-purified MUC5AC, commercial PGM is essentially devoid of DNA impurities (**Fig. 3.2 A**). For enzymatic removal of mucin-associated DNA, lyophilized mucin powders were first exposed to UV radiation for 1 h for sterilization. Then, the mucins were dissolved at a concentration of 1 mg mL^{-1} in sterile 50 mM Tris−HCl (Carl Roth, Karlsruhe, Germany) buffer (pH 7.5) supplemented with 10 mM $MgCl_2$ (Carl Roth). Per 1 mg of mucin, 50 µL of a 0.1 % (w/v) bovine pancreas deoxyribonuclease I (DNase I) solution (Sigma-Aldrich) was mixed with the mucin solution and incubated at 37 °C overnight while shaking. This DNase-treated mucin was then further purified as outlined above. The successful removal of DNA strands could be verified by an electrophoretic separation on polyacrylamide gels followed by a DNA staining with the DNA sensitive dye SYBR Safe (Thermo Fisher Scientific Inc., Waltham, MA, USA) (**Fig. 3.2 A**). In the following, the DNase-treated MUC5AC is referred to as MUC5AC -DNA.

2.4.2. Sulfatase treatment

To remove terminal sulfate groups from the glycan chains, mucins (MUC5AC as well as MUC5B) were subjected to a sulfatase treatment. Mucin was dissolved under sterile conditions at a concentration of 1 mg mL^{-1} in sterile 200 mM acetate buffer (pH 5.0). Per 1 mg of mucin, 10 U of lyophilized sulfatase powder (S9626-10KU, Sigma-Aldrich) were added to the solution. The reaction was allowed to take place at 37 °C overnight while shaking at 250 rpm (Heidolph Instruments GmbH & Co. KG, Schwabach, Germany). The amount of released sulfate groups was quantified using a commercial quatification kit (QuantiChrom™ Sulfate Assay; BioAssay Systems, Hayward, CA, USA). In the following, the sulfatase-treated mucin variants are referred to as MUC5AC -DNA/-SO_4, MUC5AC -SO_4, and MUC5B -SO_4.

The enzyme used for this treatment was an aryl sulfatase (type H-1 from *Helix pomatia*). Although mucin glycoproteins do not carry aryl sulfate groups but mainly N-acetylglucosamine-6-sulfates (GlcNAc-6-SO3), the H-1 sulfatase showed activity toward GlcNAc-6-SO3. This specific activity was verified by performing the identical enzymatic treatment with heparin as substrate, which also carries GlcNAc-6-SO3 groups.[39]

2.4.3. Neuraminidase treatment

Neuraminidase from *Clostridium perfringens* (N3001, Sigma-Aldrich) was used to remove sialic acid residues from the mucin macromolecules. Mucin was dissolved under sterile conditions at a concentration of 1 mg mL^{-1} in sterile 10 mM PBS (pH 7.0). Per 1 mg of mucin, 1 U of lyophilized neuraminidase powder was added to the solution. The reaction took place at 37 °C overnight while shaking at 100 rpm. For determining the amount of released sialic acid groups, a commercially available quantification kit (Sialic Acid (NANA) Assay Kit (abcam, Cambridge, UK)) was employed as specified by the manufacturer. In the following, the neuraminidase-treated mucin variants are referred to as MUC5AC -DNA/-SA, MUC5AC -SA, and MUC5B -SA. Triple-treated MUC5AC and double-treated MUC5B are referred to as MUC5AC -DNA/-SO_4/-SA and MUC5B -SO_4/-SA, respectively.

2.4.4. Trypsin treatment

An enzymatic treatment of native MUC5AC with the protease trypsin was performed as described in Madsen *et al.*.[51] Trypsin is a serine protease, which cleaves proteins and polypeptides at the carboxyl

side of the basic amino acids arginine and lysine. The dense glycosylation of the mucin core domain prevents the degradation of this specific region, *i.e.*, this treatment cleaves off predominantly terminal mucin domains (**Fig. 2.1 B**).

In brief, purified MUC5AC was rehydrated at a concentration of 1 % (w/v) in a 50 mM ammonium bicarbonate (NH_4HCO_3) solution that was supplemented with 5 % (v/v) of 200 mM dithiothreitol (DTT; dissolved in a 100 mM NH_4HCO_3 solution). The final pH level of the reaction mixture was adjusted to pH 7.8. Iodoacetamide (4 % (v/v), 1 M) dissolved in a 100 mM NH_4HCO_3 solution (adjusted to pH 7.8) was added to alkylate free cysteine residues of the mucin molecules, and the reaction mixture was incubated at RT for 1 h. The reaction was quenched by adding 20 % (v/v) of DTT dissolved in 100 mM NH_4HCO_3 solution. Then, 40 % (v/v) of a 1 mg mL^{-1} solution of trypsin (Sigma-Aldrich; dissolved in a 100 mM NH_4HCO_3 solution) was added to the MUC5AC solution and incubated at 30 °C for 18 h. The enzymatically treated mucin was purified using SEC and crossflow filtration as described above and lyophilized for storage at -80 °C.

2.5. Molecular probes and test particles

Owing to their diverse chemistry, mucins can interact with a broad range of molecules and particles *via* both transient and covalent binding interactions. In this thesis, different probes were used to mechanistically investigate mucoadhesion.

2.5.1. Dextrans

Dextrans are branched polysaccharides whose main chains are comprised of glucose monomers that are linked *via* α-1,6 glycosidic linkages. Branches are connected to the main chain *via* α-1,3 linkages. Dextrans are available in different, defined molecular weights, and with numerous chemical modifications (including anionic, cationic, or hydrophobic derivatives as well as a broad range of fluorophores). Owing to this high level of functional and molecular versality, dextrans are commonly used in research to serve as molecular probes in systematic studies when the impact of a certain parameter (such as size, charge, or hydrophobicity) is of interest. The dextrans used in this thesis as well as the fluorescently labeled variants thereof (labeled with fluorescein isothiocyanate = FITC) were obtained from Sigma-Aldrich or TdB Labs (Uppsala, Sweden) at different average molecular weights (4 and 150 kDa). These dextrans were used to investigate charge-dependent interactions with reconstituted mucinous systems, and the following three variants were used: unmodified (*i.e.*,

electrostatically neutral), carboxymethyl-modified (CM, anionic), and diethylaminoethyl-modified (DEAE, cationic) dextrans.

2.5.2. Peptides and proteins

In addition to dextrans, several synthetic peptides were used to systematically assess binding interactions between tailored molecular probes and mucin glycoproteins. The advantage of these peptides is the great level of tunability they offer as their overall composition can be chosen at will and is only limited by solubility constraints (peptides composed mostly or solely of hydrophobic amino acids may exhibit limited solubility in aqueous environments). With such customized peptides, not only the dependency of mucin binding on the overall net charge, but also the impact of hydrophobic residues or the detailed spatial configuration of charged and hydrophobic patches in molecules on mucoadhesion can be assessed. For instance, in a pilot study, Li *et al.* could demonstrate that the diffusion behavior of synthetic peptides with the same net charge, but different charge arrangements, were fundamentally different from each other in mucin hydrogels.[52]

All peptides used in this thesis were 24-mers synthesized by PEPperPRINT (Heidelberg, Germany). In total, a panel of eight different peptides was used for binding and penetration studies. Six of these peptides were N-terminally functionalized with the fluorophore 5(6)-carboxy-tetramethylrhodamine (5,6-TAMRA; absorption/emission maxima of ~555/580 nm). Since this functionalization would change the net charge of each peptide by -2 e, for compensation, the C-terminal carboxy groups of these peptides were amidated. Thus, the overall change in charge was -1 e for all fluorescent peptides. The two non-fluorescent peptides were synthesized with free N-terminal amines and free C-terminal carboxyl groups. All variants employed in this thesis are listed in **Tables A3.1** & **A3.3**.

Moreover, different proteins were used to study mucin binding interactions. A total of six different variants of the protein α-synuclein (αSN) were obtained from the research group of Prof. Dr. Mireille Claessens (Chair of nanobiophysics, Universiteit Twente, Enschede, NL; for the detailed purification procedure see **Appendix A3**). Although the physiological function of this protein remains, to date, enigmatic, αSN has been linked with the onset of different neurodegenerative disorders such as Parkinson's disease, which are characterized by a progressive deterioration of the neurons in the brain and the nervous system.[53] One of the pathological hallmarks of these diseases is the abnormal deposition of protein aggregates in the afflicted cells, which are mainly composed of amyloid fibrils of the protein αSN.[54] In its native state, human αSN is an intrinsically disordered protein which consists of 140 amino acids and is abundantly present in brain cells and cells of the central nervous

system. The αSN amino acid sequence can be divided into three distinct domains: a central, hydrophobic region (that drives the assembly of αSN into amyloid fibrils) is flanked by an amphipathic N-terminal region (which adopts an α-helical conformation when bound to acidic lipid membranes) and a highly acidic C-terminal region that conveys an overall negative net charge to the αSN protein at neutral pH levels.[55-57] At acidic pH values (as present in the stomach; pH < 4.0), however, the overall net charge adopts positive values (**Tables A3.2** & **A3.3**). Its disordered structure makes αSN prone to misfolding and aggregation, which can be induced by a variety of triggers.[58, 59] These misfolded and aggregated αSN species are not only cytotoxic but can even easily spread in a prion-like fashion from cell to cell. In recipient cells, these αSN aggregates seed the aggregation of native (*i.e.*, disordered) αSN molecules, which, eventually, results in an amplification of fibrils and the spread and progression of specific fibril strain-dependent synucleinopathies.[60, 61]

In addition to αSN, bovine serum albumin (BSA, Sigma-Aldrich), lysozyme (Sigma-Aldrich), and poly-L-lysine (MW ~5 kDa; Thermo Fisher) were used as model proteins to study binding interactions with mucin glycoproteins. BSA is a protein derived from cow blood that is routinely used as model protein in molecular biology. It has its isoelectric point at a pH level of ~4.7,[62] *i.e.*, it is positively charged at pH 4.0 but has a negative net charge at pH 7.0. Lysozyme is a protein with anti-microbial activity obtained from hen egg white. It has its isoelectric point at a pH level of ~11.4,[63] *i.e.*, it is positively charged at all physiologically relevant pH levels. In addition to charged amino acids, both BSA and lysozyme do also contain hydrophobic amino acids. By contrast, poly-L-lysine is entirely composed of the cationic amino acid L-lysine and positively charged at all relevant pH levels (**Tables A3.2** & **A3.3**).

2.5.3. Black carbon (BC) nanoparticles

The term 'black carbon' (BC) describes a broad range of carbon-based nanoparticles, which typically emerge as a result of the incomplete combustion of biomass or fossil fuels.[64] These BC nanoparticles can either originate from natural sources (*e.g.*, volcanic ash), or they emerge as an undesired byproduct of industrial/anthropogenic processes (*e.g.*, cigarette smoke and exhaust fumes).[65, 66] Today, BC is considered one of the most prevalent types of particulate matter polluting air and water, which has a strong adverse impact on the world climate.[67] Moreover, an exposure of humans and to BC can also lead to severe health issues: In their 2012 report, the World Health Organization (WHO) linked an exposure (both long-term and short-term) to BC particles to a multitude of medical conditions including disorders of the respiratory system, cardiovascular conditions, and others.[68] Interestingly, so far, medical research has mostly focussed on describing the pathological effects BC can induce in

the bodies of humans by identifying correlations between particle exposure and the risk of developing a certain disorder. Studies shedding light on the mechanistic origins of such pathological alterations are, however, still scarce. In particular, it appears that the impact particulate matter can have on mucosal barriers has been largely neglected. This is astonishing considering that one of the key functions of mucus is preventing the translocation of harmful objects by trapping and immobilizing them.[9, 10, 69] Since mucosal barriers cover virtually all potential 'entrance gates' into the bodies of humans, this scarcity of studies addressing the influence an exposure to particulate matter may have on both, the integrity and functionality of mucus, appears alarming.

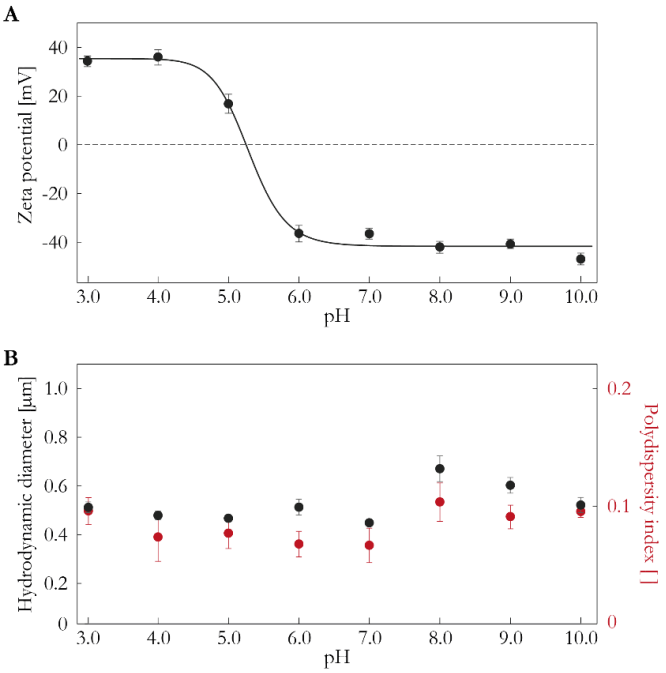

Fig. 2.4: Zeta potential, colloidal stability, and hydrodynamic diameter of BC nanoparticles. At strongly acidic pH levels, BC nanoparticles exhibit a positive zeta potential, whereas the zeta potential is negative at pH levels >5.2 (*i.e.*, the isoelectric point of the BC nanoparticles in water; **A**) When solubilized in ultrapure water, BC nanoparticles form a rather monodisperse (PDI <0.15) dispersion. The hydrodynamic diameter of BC is ~500 nm and is not affected by changes in the apparent pH (**B**).

In this work, interactions between commercially available BC nanoparticles, which have been obtained as a powder (carbon content > 99.9 % (w/w)) from Werth-Metall (Erfurt, Germany), and lab-purified MUC5AC were assessed. Zeta potential measurements indicated that the BC nanoparticles and a strongly positive zeta potential at a pH of 4.0 but a negative zeta potential at a pH of 7.0 (**Fig. 2.4 A**). According to a sigmoidal that was fitted to the measured data, the isoelectric point of the BC nanoparticles is reached at a pH of ~5.2. Moreover, dynamic light scattering (DLS) measurements revealed that the particles have an average hydrodynamic diameter of ~500 nm and the colloidal stability of the nanoparticle dispersion was independent of the apparent pH value (**Fig. 2.4 B**).

2.6. Fluorescence labeling of proteins

Mucins and other proteins (**Table A3.2**) were labeled with different carboxy-modified fluorescing dyes (ATTO-TEC GmbH, Siegen, Germany) by attaching the dye molecules to mucins *via* carbodiimide coupling. Therefore, the respective dye was first diluted to a concentration of c_{ATTO} = 1.0 mg mL^{-1} in MES buffer (10 mM, pH 5.0) at a final volume of 1 mL. Afterwards, 50 mM 1-ethyl-3-(3-dimethyl-aminopropyl)carbodiimide (EDC) and 10 mM sulfo-*N*-hydroxysuccinimide (sulfo-NHS) were added to this solution, and the mixture was allowed to incubate light excluded for 3 h at room temperature. This prolonged incubation time ensured that remaining free EDC was hydrolyzed before the protein of interest was added (to avoid crosslinking of the protein molecules). In parallel, 40 mg of protein were dissolved in 19 mL 10 mM PBS (pH 7.0). Both solutions were mixed thoroughly and allowed to react for 3 h at room temperature. To remove unbound dye molecules the mixture was dialyzed (MWCO = 300 kDa for mucins, MWCO = 6-8 kDa for other proteins) against ultrapure water. The solution was then lyophilized and the freeze-dried powder stored at −80 °C until further use.

2.7. Passively adsorbed and covalent mucin coatings on polymer surfaces

To generate surface-tethered mucin layers, the surfaces of interest can be coated with mucin glycoproteins – either by means of passive, physical adsorption or by covalently linking mucins to them. For passive surface coatings, the objects to be coated were incubated with a mucin solution containing 0.1 % (w/v) mucin at room temperature for 2 h. Afterwards, the surfaces were thoroughly rinsed with ultrapure water, and the coated materials were stored either in ultrapure water or 80 % (v/v) ethanol until further use.

To generate covalent mucin surface coatings, the protocol published by Winkeljann *et al.* was followed.[70] This procedure allows for coating a broad range of (polymeric) materials with mucins. In brief, 96-well plates were treated with oxygen plasma at an oxygen pressure of 0.4 mbar using a power of 30 W for 90 s; this procedure introduced hydroxyl groups into the outermost layer of the polystyrene surface. To each activated well, 100 µL of a 0.1 % (w/v) solution of N-[3-(trimethoxysilyl)propyl]ethylenediamine triacetic acid trisodium salt (TMS-EDTA; abcr, Karlsruhe, Germany) dissolved in 10 mM sodium acetate buffer (pH 4.5) were added, and the wells were incubated at 60 °C for 5 h. Afterwards, the wells were washed thrice with 80 % (v/v) ethanol (100 µL per well) to remove residual TMS-EDTA before the well plates were stored at 40 °C for 18 h. To

activate the terminal carboxyl groups of the silane spacer molecules, each well was incubated with 100 µL of 100 mM 2-(*N*-morpholino) ethanesulfonic acid (MES) buffer (pH 5.0) containing 5 mM 1-ethyl-3-(3-dimethylaminopropyl)carbodiimide hydrochloride (EDC) and 5 mM sulfo-*N*-hydroxysuccinimide (sulfo-NHS; abcr) at room temperature for 30 min. Afterwards, in each well, the EDC/NHS solution was replaced with 100 µL of PBS (pH 7.4; Lonza, Verviers, Belgium) containing 0.1 % (w/v) mucin, and the well plates were stored at 4 °C overnight. Finally, the wells were washed twice with PBS (100 µL per well) and stored in 80 % (v/v) ethanol until further use.

2.8. Techniques to assess the functionality of (re-)purified mucins

Mucus is a complex, multi-component biomaterial that plays an essential role in numerous physiological processes, for instance by acting as a lubricant or a protective barrier against pathogens. Thus, its composition and biophysical properties are meticulously regulated by the human body.[25, 71, 72] However, mucus tends to exhibit a high degree of biological heterogeneity as the concentrations of its constituents vary not only between different individuals but also as a function of age, diet or pathophysiological conditions.[73, 74]

For systematic research, typically, simple model systems are desired, which mimic the properties of the native mucus but, at the same time, offer high levels of reproducibility and enable researchers to control the composition of the material. For this purpose, purified mucins have been commonly used as they are the key macromolecular component that dictate the biological, physico-chemical, and mechanical properties of mucus.[5] To assess the functionality applied and quality of mucin preparations, two mucin-specific properties have been put forward as reliable indicators in particular: on the one hand, functional mucins undergo a sol-gel transition in a pH-dependent manner.[75, 76] On the other hand, solutions reconstituted from high-quality mucin exhibit excellent lubricity.[40, 77]

2.8.1. Oscillatory shear rheology

Most biological materials exhibit a viscoelastic behavior, *i.e.*, neither a purely viscous nor a purely elastic behavior. To describe such viscoelastic materials, the material response σ^* to an induced oscillating deformation γ^* is recorded. The corresponding modulus $G^*(\omega)$ is a complex parameter that can be separated into a real part $G'(\omega)$ describing the elastic material response and an imaginary part $G''(\omega)$ describing the viscous material response (**Fig. 2.5 A**):

$$G'(\omega)=\frac{\sigma_0}{\gamma_0}\cos(\delta) \qquad G''(\omega)=\frac{\sigma_0}{\gamma_0}\sin(\delta)$$

Here, σ_0 and γ_0 denote the amplitude of the shear stress and the shear strain, respectively. The phase shift between the oscillatory stress applied on the material and its strain response (*i.e.*, deformation) is denoted with δ, which is dependent on the angular frequency ω of the stimulation. The viscoelastic properties of the different materials used in this thesis were determined using a research-grade shear rheometer (MCR302, Anton Paar, Graz, Austria).

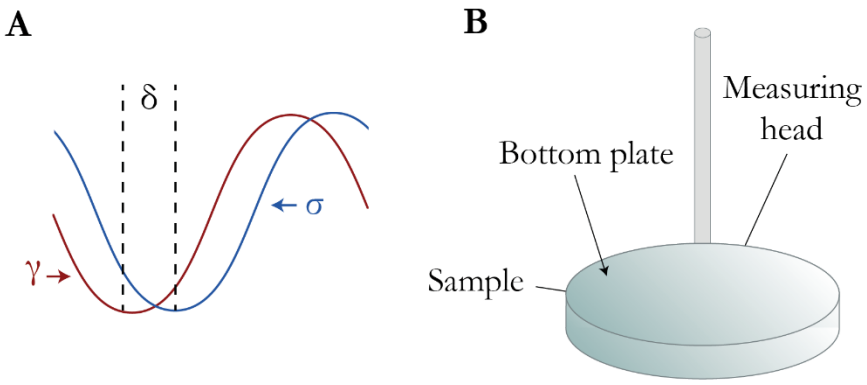

Fig. 2.5: Probing the rheological properties of mucin networks. Phase angle δ between an applied oscillatory shear stress σ (blue) and the material response, *i.e.*, the deformation γ (red; **A**). Schematic drawing of the measuring setup consisting of a temperature-controlled bottom plate and a measuring head used for oscillatory shear measurements (**B**). By performing an oscillating motion the measuring head induces shear stress on the (mucin hydrogel) sample. The deformation of the sample in response to the applied shear stress is recorded by the macrorheometer, which calculates the viscoelastic moduli *G'* and *G"*.

To determine the frequency-dependent viscoelastic parameters of mucin samples, oscillatory shear rheology measurements were conducted using a plate/plate setup (**Fig. 2.5 B**), and the gap between the oscillating measuring head (PP25, Anton Paar) and the stationary bottom plate (P-PTD 200/Air, Anton Paar) was set to a value of d = 150 µm. To ensure linear viscoelastic response of all samples, pre-measurements were conducted in a stress-controlled manner at a torque of M = 0.5 µNm. From those pre-tests, the corresponding strains were determined for each sample. Then, frequency-dependent measurements were conducted in strain-controlled mode using the 1.5-fold value of the strain determined in the pre-measurements. The shear measurements were performed following a logarithmic frequency ramp from f = 0.01-10 Hz. The mucin samples were prepared 1 h prior to measurements at a mucin concentration of 1 % (w/v) in either 10 mM sodium acetate buffer (pH 4.0) or 10 mM PBS (pH 7.0). Per measurement, 150 µL of sample were used, and special care was taken that the sample completely filled the gap between the two opposing plates.

2.8.2. Tribology

To investigate the lubricity of solutions reconstituted from (re-)purified mucins, tribological measurements were performed.

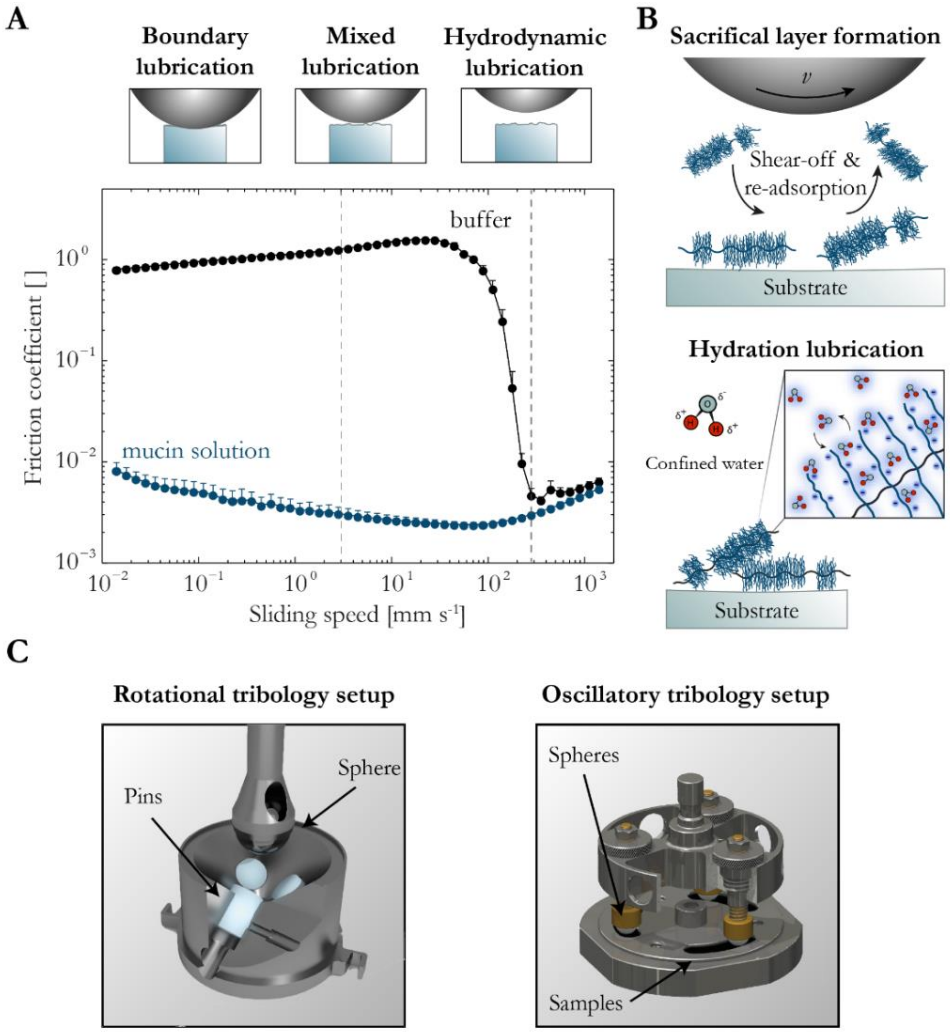

Fig. 2.6: Macromolecular lubrication mechanisms and tribological setups used in this thesis. According to the classical Stribeck theory, typical friction curves can be divided into three distinct regimes: hydrodynamic lubrication, mixed lubrication, and boundary lubrication (**A**). The outstanding lubricating properties of mucins originate from two effects: the continuous shear-off and re-adsorption of mucins (*i.e.*, the formation of a sacrificial layer) and their ability to supply a water film separating the opposing surfaces (*i.e.*, hydration lubrication; **B**). The rotational tribology setup (**left**) consist of a shaft that holds a sphere and a sample holder unit equipped with three cylindrical samples. The measuring head of the oscillatory tribology (**right**) setup offers space for three pins, and the bottom plate allows for mounting three kidney-shaped samples as counterparts (**C**).

During each tribological measurement, the coefficient of friction μ was recorded as

$$\mu(v) = \frac{F_R(v)}{F_N},$$

where $F_R(v)$ denotes the friction force, which is dependent on the sliding velocity v, and F_N denotes the normal force applied onto the probed surface. According to the classical Stribeck theory, three lubrication regimes can be distinguished, which occur in all lubricated contact scenarios: the boundary friction regime, the mixed regime, and the hydrodynamic regime (**Fig. 2.6 A**).

Two molecular processes are responsible for the ability of mucins to provide excellent lubrication: sacrificial layer formation and hydration lubrication (**Fig. 2.6 B**). On the one hand, the sacrificial layer mechanism describes the ability to of mucins to adsorb onto surfaces and readily re-adsorb after shear-off (see **Chapter 2.5.3**).[78] This property allows for the dissipation of friction energy and thus the reduction of the friction coefficient. Hydration lubrication, on the other hand, is based on the ability of mucins to form well hydrated biopolymer layers on a broad range of surfaces (**Figure A4.1**), which can provide a thin water film between two opposing surfaces even at low sliding velocities.[79, 80] Furthermore, under shear forces and pressure, water molecules are exchanged between the polymer and surrounding fluid, which further dissipates friction energy.

Rotational tribology experiments

For rotational friction measurements a commercial shear rheometer (MCR 302, Anton Paar) was equipped with a rotational tribology unit (T-PTD 200, Anton Paar; **Fig. 2.6 C**, **left**) as described previously.[81] The setup comprises a ball-on-3-pins geometry consisting of a rotating sphere made from stainless steel (1.4301, Ø = 12.7 mm, Kugel Pompel, Wien, Austria) and three pins made from polydimethylsiloxane (PDMS, Sylgard 184, Dow Corning, Midland, MI, USA; Ø = 5.5 mm) as counterparts (preparation of PDMS pins: **Appendix A4**). Before each measurement, three pins were inserted into the sample holder and cleaned with 80 % (v/v) ethanol and ultrapure water. The measurements were conducted at room temperature, and the PDMS cylinders were fully covered with lubricant (*i.e.*, either 20 mM 4-(2-hydroxyethyl)-1-piperazineethanesulfonic acid (HEPES) buffer (pH 7.0) or mucin variants dissolved in this buffer at a concentration of 1 mg mL^{-1}). A normal force of F_N = 6 N was applied leading to a contact area of ~8.1 mm^2 and, thus, a contact pressure of $p_0 \approx 0.35$ MPa (according to the Hertzian contact theory using the Young's moduli and Poisson's ratios of steel (E_{steel} = 210 GPa, $\nu_{steel} \approx 0.30$) and PDMS (E_{PDMS} = 2 MPa, ν_{PDMS} using ≈ 0.49)[82]). Friction coefficients were recorded for sliding speeds v ranging from 0.01 to 1000 mm s^{-1} a measuring time of 10 s per data point.

Oscillatory tribology experiments

Oscillatory tribology experiments were performed as described in Winkeljann *et al.*.[83] A custom-made measuring setup was used, which comprised a measuring head equipped with three spheres made from stainless steel (1.4404, Ø = 5.0 mm, *S*q < 0.2 µm; Kugel Pompel; **Fig. 2.6 C**, **right**) as well as three kidney-shaped PDMS samples. The experiments were performed at a constant normal force of F_N = 1.35 N, which resulted in an average contact pressure of $p_0 \approx 0.35$ MPa (which is equivalent to the contact pressure used for rotational tribology experiments). The measuring head was oscillated over a deflection angle range of $0° \leq \varphi \leq 10°$ at a constant sliding velocity of v = 0.1 mm s^{-1}. The setup was lubricated with a mucin solution reconstituted at a concentration of 1 mg mL^{-1}. Since measuring artefacts occur around the turning points of each oscillation, from each stroke only data points between deflection angles of 2° and 8° were used for data evaluation. For each measurement, four cycles (each cycle consisting of a forward and a backward stroke) were recorded, and the first cycle of every measurement was discarded to minimize stick-slip effects affecting the measured friction coefficients. An averaged friction trace $\mu(\varphi)$ was calculated from the forward and the backward stroke of each cycle according to the following equation:

$$\mu(\varphi) = \frac{\mu_f(\varphi) - \mu_b(\varphi)}{2}$$

Here, φ denotes the deflection angle, and $\mu_f(\varphi)$ and $\mu_b(\varphi)$ represent the friction traces obtained during forward and backward strokes, respectively. The obtained function $\mu(\varphi)$ was averaged with respect to φ to obtain an overall friction coefficient representing a multi-cycle friction measurement.

2.8.3. Adsorption measurements

The ability to adsorb onto a variety of surfaces is essential for mucins to provide lubrication. To quantify the adsorption kinetics and the adsorption efficiency of mucin glycoproteins to a variety of surfaces, a quartz crystal microbalance with dissipation monitoring (QCM-D) was employed. This techniques allows for detecting the adsorption of molecules onto the surface of a piezoelectric crystal. The application of an alternating current induces the oscillation of a crystal sensors at its resonance frequency of ~10 MHz. Deposition of mass onto the sensor surface, for instance by the adsorption of molecules, leads to a shift in the sensor‘s resonance frequency. Such a shift in resonance frequency can be correlated with the mass of the adsorbed layer according to the Sauerbrey equation:[84]

$$\Delta f = -\frac{2 f_0^2}{A\sqrt{\varrho\,\mu}}\,\Delta m$$

Here, the parameters A, ϱ, and μ denote the surface area of the piezo crystal, the density, and the shear modulus of the quartz, respectively. Initially, this correlation was developed for thin, rigid layers forming on the sensor surface. If biomolecules adsorb onto the crystal surface, they form viscoelastic layers, which dampen the oscillation of the piezo sensor. In such cases, typically, the Sauerbrey equation does not hold true anymore. Then, in addition to the shift in resonance frequency Δf, a second recorded parameter, the damping signal (ΔD), needs to be taken into account to obtain absolute values for the deposited protein mass.[85]

Adsorption measurements were performed with a qCell T Q2 quartz crystal microbalance with dissipation monitoring (3t-analytik, Tuttlingen, Germany). Sensors with surfaces made from stainless steel (1.4404, 3t-analytik) were used to study mucin adsorption onto hydrophilic substrate. To measure the adsorption of mucins onto hydrophobic surfaces, gold-coated quartz crystals (3t-analytik) were spin-coated with a thin layer of PDMS. For this step, PDMS was mixed in a prepolymer/cross-linker ratio of 10:1 and diluted to 1 % (v/v) in *n*-hexane. 100 µL of this solution were applied to the center of a quartz crystal and distributed by spin-coating (WS-400B-6NPP/LITE spin coater, Laurell Technologies Corporation, North Wales, PA, USA; spin-coater settings: 3000 rpm for 1 min). Afterwards, the PDMS was cured at 80 °C for 4 h. For each adsorption measurement on PDMS, a quartz crystal with a fresh PDMS coating was used; for each adsorption measurement on steel, a quartz crystal was used that was cleaned with piranha solution (a mixture of three parts 95 % sulfuric acid and one part 35 % (v/v) hydrogen peroxide solution) and ultrapure water prior to use. For the adsorption measurements, mucin solutions were prepared at a concentration of 0.1 mg mL^{-1} in sterile-filtered (filter threshold: 0.22 µM) 20 mM (4-(2-hydroxyethyl)-1-piperazineethanesulfonic acid) buffer (HEPES, pH 7.0). Prior to each measurement, the setup was equilibrated in 20 mM HEPES buffer (pH 7.0) at a flow rate of 100 µL min^{-1} until a stable frequency signal was reached. At the beginning of each measurement, 15 min of this HEPES buffer signal was recorded as a baseline. Afterwards, the mucins were injected at a flow rate of 100 µL min^{-1}, and the frequency signal was recorded for at least 45 min. To record secondary binding events (*i.e.*, the binding of other molecules from solution to the pre-adsorbed mucin layers), a buffer signal was recorded for another 15 min after the mucin adsorption has been completed, and this frequency track served as the baseline for the secondary binding study. For the latter, the molecules of interest were injected at a flow rate of 100 µL min^{-1}, and their binding to the surface-bound mucins was recorded for 45 min.

2.9. Techniques to probe the binding of objects to mucins *in vitro*

Owing to their diverse chemistry, mucin glycoproteins can engage in multiple binding interactions with virtually any objects they come in contact with. In this work, the nature of the binding interactions acting between mucins and several molecules and particles were investigated in detail.

2.9.1. Molecule binding to mucin surface layers

Two different assays were employed to quantify the binding of different molecules to surface-attached mucin layers – a depletion assay and QCM-D measurements.

Depletion assay

This assay is an indirect approach to quantify the relative binding affinities of molecules adsorbing from solution to surface-tethered mucin layers. Here, the propensity of mucins to bind molecules was deduced from their ability to deplete (fluorescently labeled) molecules from solution. In detail, the wells of 96-well microtiter plates (Corning Inc., Corning, NY, USA) were coated with mucins either by means of passive adsorption or covalent coupling (see **Chapter 2.7**). Afterwards, the wells were rinsed twice with 200 µL of 20 mM HEPES buffer (pH 7.0) or 10 mM PBS (pH 7.4), and each well was incubated with 200 µL of a test molecule solution at room temperature for 1 h while shaking. After incubation, 100 µL of the test molecule solution were transferred from each well into a fresh well of an uncoated 96-well microtiter plate, and the fluorescence intensity of each sample was determined fluorometrically using a multi-label plate reader (Viktor3, PerkinElmer, Inc., MA, USA).

Unspecific binding to mucins *via* attractive electrostatic forces was systematically investigated using FITC-labeled dextrans (4 kDa and 150 kDa), which are available in different charge states (see **Chapter 2.5.1**). For this assay, the 4 kDa and 150 kDa dextrans were dissolved at a concentration of 0.02 % (w/v) and 0.00125 % (w/v), respectively, in 20 mM HEPES (pH 7.0). Moreover, a panel of seven different FITC-conjugated lectins (Vector Laboratories, Inc. Burlingame, CA, USA) was used at a concentration of 30 µg mL^{-1} in PBS (pH 7.4). The panel consisted of concanavalin A (Con A), Dolichos biflorus agglutinin (DBA), peanut agglutinin (PNA), Ricinus communis agglutinin I (RCA I), soybean agglutinin (SBA), Ulex europaeus agglutinin I (UEA I), and wheat germ agglutinin (WGA).

Assessing mucin binding using QCM-D

A direct approach to qualitatively assess the binding of molecular probes to surface-attached mucin layers is based on QCM-D. This adsorption-based assay was performed as a two-step procedure. First, mucin glycoproteins were allowed to adsorb from solution (0.01 % (w/v) in 20 mM HEPES, pH 7.0) to the surfaces of PDMS-coated QCM-D sensors for 45 min at a flow rate of 100 μL min^{-1}. After rinsing the measuring cell with HEPES buffer for at least 15 min, a solution containing the test molecules (FITC-labeled 150 kDa dextrans at a concentration of 0.05 % (w/v))was injected into the measuring cell, and the resulting shift in resonance frequency (and damping signal) were recorded for another 30 min. For each individual measurement, PDMS coated sensors were freshly prepared as described in **Chapter 2.8.3**.

2.9.2. Molecule binding to mucins in solution

Of course, the binding properties of surface-attached mucins might differ from those of mucins in solution. This is based on the realization that the adsorption of mucins onto surfaces inevitably leads to the occupation of potential binding sites. For instance, the adsorption of mucins onto hydrophobic is facilitated by hydrophobic interactions acting between the surface and the terminal mucin domains.[38, 86] As a consequence these hydrophobic domains will not be available anymore for the binding of other hydrophobic binding partners. Thus, it is often desired to use immobilization-free methods to measure binding affinities.

In this work, the binding of αSN proteins to native and trypsin-treated MUC5AC was quantified in solution using microscale thermophoresis (MST). This technique is based on the detection of changes in the fluorescence signals emitted by a target (αSN) as a function of the concentration of a non-fluorescent ligand (MUC5AC) when a temperature gradient is applied.[87, 88] These changes in fluorescence intensity are based on two effects: on the one hand, the emission intensity of a fluorophore depends on the ambient temperature. On the other hand, molecules exhibit a directed movement a long a temperature gradient – a phenomenon that is referred to as thermophoresis. In particular, a spatial temperature difference ΔT leads to a change in molecule concentration in the region of the elevated temperature, which can be quantified by the Soret coefficient S_T:[88, 89]

$$\frac{c_{hot}}{c_{cold}} = \exp\{-S_T \Delta T\}$$

The Soret coefficient is a function a various parameters, most importantly the type of solvent and molecule specific parameters such as size, charge state, and solvation entropy in the respective

solvent. Since the thermophoresis of a fluorescent target molecule (*i.e.*, αSN) typically differs in the above mentioned parameters from complexes composed of the target molecule and the ligand (*i.e.*, αSN/MUC5AC complexes), relative differences in thermophoresis can be used to retrieve binding affinities from titration series.

Interaction studies between purified gastric mucin MUC5AC and αSN variants were performed on a Monolith NT.115 (NanoTemper Technologies GmbH, Munich, Germany) equipped with a red-green fluorescent reader using a 15 % light-emitting diode and 20 % infrared (IR) power. MST measurements were conducted in acidic acetate buffer (10 mM, pH 4.0) using unlabeled MUC5AC molecules as ligands and fluorescently labeled αSN-AF647 proteins as target molecules. The thermophoretic movement of target molecules was monitored at different molar ratios between ligand and target molecule. Therefore, the sample sets (16 binding mixtures each) were prepared in acetate buffer (10 mM, pH 4.0) containing constant final amounts of αSN (ι_s = 250 nM) and decreasing concentrations of mucin. Each titration series starts with a mucin concentration of 1.33 µM that was stepwise diluted with acetate buffer until a final mucin concentration of ~0.04 nM was reached in the 16th mixture. Each mixture was filled into a glass capillary (premium coated capillaries MO-K005, NanoTemper Technologies GmbH), and for each capillary, the following measurement procedure was applied: first, a baseline for signal normalization was recorded for 5 s. Then, the IR laser was turned on and the thermophoretic movement of the target molecules was recorded for 30 s. Thereafter, the laser was turned off and the reverse diffusion of fluorescently labeled αSN molecules was recorded for another 5 s. For evaluation, the normalized fluorescence intensity signal was plotted against the concentration of the titrated ligand MUC5AC.

2.10. Techniques to assess the barrier properties of mucin hydrogels

Mucus barriers in the human body tract not only regulate the passage of beneficial molecules such as nutrients, hormones, or drugs but also act as a barrier toward noxious substances. The barrier properties of mucin-based hydrogels are – at least to a large extent - regulated by binding interactions acting between the mucins and the objects coming into contact with the mucin hydrogel. In this thesis, two experimental approaches were employed to study the partitioning of molecular probes into mucin hydrogels as well as their translocation process throughout them.

2.10.1. Molecular penetration experiments

The diffusive penetration of mucin hydrogels by different molecules (both model molecules with tailored properties as well as patho-physiologically relevant species) was quantified using a microfluidics chip as an experimental platform. A detailed description of the procedure for the production of wafers and individual microfluidics chips can be found in **Appendix A4** (**Fig. A4.2**). To study the diffusive entrance of molecules into a mucin hydrogel, a well-defined interface between the liquid compartment (containing the test molecules) and the mucin hydrogel is required. Such an interface was obtained by designing the microfluidics chip with finger-like structures (**Fig. 2.7 A**). Here, an aqueous solution containing purified mucins (1 % (w/v) dissolved in ultrapure water) was injected into an inlet channel that connects to several of such finger-like structures (~2 µL per structure), and the mucin solution was gently pushed through the channels. When reaching the end of these channels, the mucin solution stopped due to the special design of the microchannels, which slightly narrow at their tips. This geometry not only induced a slight resistance but also resulted in the formation of flat liquid/air interfaces at the fingertips, which enabled an easy and reliable quantification of the molecular penetration process.

To stabilize these liquid/air interfaces and to avoid their erosion by liquid flux, the formation of mucin gels was initiated on chip by injecting 5 µL of an acidic buffer (10 mM acetate buffer, pH 4.0) into the test reservoir that is connected to the mucin-filled finger structures. (**Fig. 2.7 C, D**). To show successful gelation of the mucin solutions, the Brownian motion of fluorescently labeled polystyrene nanoparticles (Ø = 500 nm) embedded into the mucin phase was tracked. At neutral pH, where mucin solutions form a low viscosity liquid, thermal energy is sufficient to induce particle fluctuations with amplitudes large enough to be easily detected by single particle tracking microscopy. However, once the mucin solution is acidified, a viscoelastic gel is formed and the embedded polystyrene particles become trapped inside the mesh of the acidic mucin gel; consequently, their fluctuation amplitude is strongly reduced (**Fig. 2.7 B**).

With these stabilized mucin gel/liquid interfaces, molecular penetration experiments were performed. For this purpose, the test molecules were dissolved in 10 mM acetate buffer (pH 4.0). FITC-labeled 4 kDa dextrans were reconstituted at a concentration of 0.5 % (w/v), the peptides and proteins (both, fluorescently labeled and non-labeled ones alike) listed in the Tables A2.1 & A2.2 at a concentration of 100 µM. To initiate the penetration experiments, 5 µL of the solutions containing the molecular probes were injected *via* one of the inlets of the 'test reservoir' (**Fig. 2.7 E, F**).

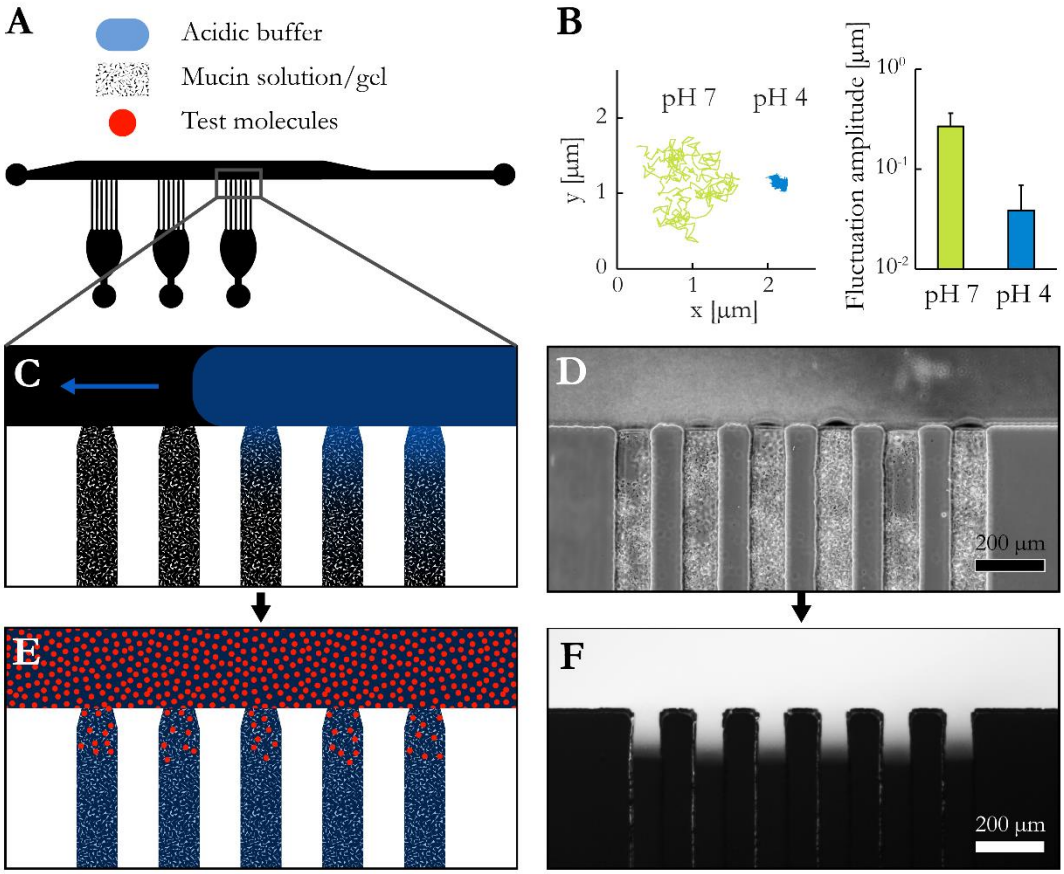

Fig. 2.7: Schematic illustration and microscopic images of the microfluidic setup used for molecular penetration tests into mucin gels. Overview of the microfluidic chip geometry comprising three hand-like structures which are filled with a mucin solution (**A**). Thermal fluctuation behavior of polystyrene nanoparticles embedded in a mucin solution on chip at pH 7.0 (*i.e.*, before acidification) and in a mucin hydrogel at pH 4.0 (*i.e.*, after acidification on chip). The error bars denote the standard deviation as obtained from three independent measurements in which ~20 particles were analyzed each (**B**). Gelation of the mucin solution is initiated by injecting acidic buffer into one of the microfluidic channels (**C**, **D**). After gelation has been induced on chip, the test molecules are injected and allowed to penetrate the mucin gel by diffusion (**E**, **F**).

Fluorescence and phase contrast images of the microchannels were recorded on an inverted light microscope (Leica DMi8, Leica, Wetzlar, Germany) using a 4× and 10× objective (Leica), respectively. Sixteen-bit images were acquired at distinct time points (0, 5, 10, 20, and 30 min after injection of the probe molecules) in both microscopy modes using a digital camera (Orca Flash 4.0 C11440, Hamamatsu, Japan) and the Leica Application Suite X software (version 3.0.4.16529, Leica). For fluorescence microscopy, either a TXR filter cube (Ex.: 560/40, DC: 585, Em.: 630/75, Leica) or a FITC filter cube (Ex.: 480/40, DC: 505, Em.: 527/30, Leica) was used. To ensure that no pixel saturation occurs, the exposure time was adjusted for every image acquired. To process the images

and to determine the penetration profiles, each microchannel was analyzed separately using ImageJ software (public domain, version 1.52a, May 2018) and MATLAB (Math-Works, Natick, MA, USA). For the fluorescence images, a rectangular region of interest (ROI) was defined with a width of 45 px and a height of 560 px. This ROI was selected such that the gel/buffer interface was located 60 px from the top pixel row of the ROI with the largest part of the ROI reaching into the mucin gel phase. The averaged fluorescence intensity recorded for the 30 uppermost pixel lines of the ROI was set as a reference, representing the buffer reservoir with an intensity of 1, which corresponds to a test molecule concentration of 100 %. This allowed for compensating for photobleaching effects and normalizing all other intensity values within the mucin gel channel obtained at different time points during the experiments. For each mucin compartment, that is, the lower 500 pixel lines of the ROI, the measured fluorescence intensity was averaged per pixel line, which yielded an intensity column vector with a length of 500 px for each ROI. Then these intensity values were normalized to the intensity in the buffer reservoir. Subsequently, the averaged and normalized intensity values obtained per line were further averaged over all fingers analyzed at the same time point. For each experimental condition, data from at least two different chips (with up to 18 'fingers' each) was analyzed. The normalized intensity values were then plotted against the channel depth to obtain intensity profiles, and the gel/buffer interface was assigned the coordinate zero.

For phase contrast images, the ROI was defined as a 1000 px long and approximately 35 px wide rectangle in the center of the channel starting at the gel buffer interface. The gray scale values of the images were averaged for each pixel line and normalized to the maximum value measured for that specific channel at any time. In both types of images, that is, fluorescence and phase contrast images, the position of the maximal fluorescence intensity and the position of the internal gel/gel interface, respectively, were determined.

2.10.2. Permeation assay

To study the translocation efficiency of molecules across mucin hydrogels, a second experimental approach was employed. Here, the mucin hydrogel was reconstituted on top of semi-permeable polyethylene terephthalate (PET) membranes (average pore size ~0.4 μm), which comprise the bottom parts of 24-well cell culture inserts (Sabeu GmbH & Co. KG, Northeim, Germany). These membranes allow for the passage of small molecules but retain the mucin hydrogel in the inserts. For these experiments, the formation of a structurally intact mucin hydrogel on top of the membranes is a vital requirement. To achieve that, the lyophilized mucin was dissolved at a concentration of 2 % (w/v) in ultrapure water during shaking at 4 °C overnight. Then, 100 μL of this solution were

pipetted onto the membrane area of each insert. The inserts were then transferred into the wells of a 24-well microtiter plate (Corning Inc.), which had been filled with 750 µL of 10 mM acetate buffer (pH 4.0) each. As described above for the microfluidics setup, also here, contacting the mucin solution with the acidic buffer initiated a sol-gel transition *in situ*. After successful gel formation, a 5 µL drop of acetate buffer containing test molecules in high concentration (5 % (w/v) in the case of FITC-labeled 4 kDa dextrans) was carefully pipetted on top of the mucin hydrogel. After incubation overnight, the amount of test molecules in the acceptor reservoir (*i.e.*, the wells of the microtiter plate), which translocated across the mucin hydrogel, was determined fluorometrically using a Fluoroskan Ascent™ FL microplate fluorometer (Thermo Fisher Scientific).

2.11. Analytical techniques

Two indirect, analytical methods were applied to determine both the purity and structural integrity of purified mucin samples: sodium dodecyl sulfate polyacrylamide gel electrophoresis (SDS-PAGE) and indirect enzyme-linked immunosorbent assay (ELISA).

2.11.1. SDS-PAGE

To qualitatively assess both the purity and the structural integrity of mucins, an electrophoretic separation of mucin samples was performed using an SDS-PAGE. With this technique, the protein components of a sample are separated solely based on their molecular weight, independent of their charge state or structure.

For this purpose, the lyophilized mucin samples of interest were dissolved in ultrapure water at a concentration of 1 % (w/v) during shaking at 4 °C for 1 h. Each mucin solution (~20 µL) was mixed with 2× sample buffer (containing 120 mM tris(hydroxymethyl)aminoethane hydrochloride (TRIS−HCl), 4 % (w/v) SDS (Sigma-Aldrich), 20 % (v/v) glycerol, and 0.02 % (w/v) bromophenol blue sodium salt; adjusted to pH 6.8) in a ratio of 1:1. After thermal protein denaturation (*i.e.*, incubation of the solubilized samples at 95 °C for 5 min), 20 µL of each mixture were loaded onto a precast polyacrylamide gel (TruPAGE Precast Protein Gel 4−20%, Sigma-Aldrich). Additionally, 4 µL of a protein standard solution (Marker Precision Plus Protein Kaleidoscope Standards; Bio-Rad Laboratories Inc., Hercules, CA) were loaded onto a separate lane. The gel was run in SDS running buffer (containing 25 mM TRIS−HCl, 200 mM glycine, 0.1 % (w/v) SDS; adjusted to pH 8.0) at 120 V for 1 h.

To detect mucin glycoproteins, after electrophoretic separation, the gel was subjected to Coomassie staining followed by a Periodic acid−Schiff (PAS) staining. First, the gel was incubated in a Coomassie Blue staining solution (containing 0.1 % (w/v) Coomassie R-250 (Bio-Rad Laboratories, Hercules, CA, USA), 45 % (v/v) methanol, 10 % (v/v) acetic acid) during shaking at room temperature for 1 h. Thereafter, the gel was rinsed twice with tap water and incubated in 10 % (v/v) acetic acid until the background was sufficiently de-stained. Afterwards, the gel was incubated in 0.5 % (v/v) periodic acid (Carl Roth) for 10 min, and then in Schiff's reagent (Carl Roth) for 15 min. Blue stains (resulting from the Coomassie staining) indicate the presence of proteins within the gel matrix, whereas purple stains specifically report the presence of mucin glycoproteins. Another, more sensitive technique for detecting proteins in the gel matrix is to perform a silver staining with the polyacrylamide gel after completed electrophoresis. First, the gel was washed twice in ultrapure water for 5 min each, followed by an incubation in a fixation solution (40 % (v/v) ethanol, 10 % (v/v) acetic acid) for 30 min. After washing the gel twice in 10 % (v/v) for 5 min each, the gel was rinsed twice with ultrapure water. Afterwards, the gel was incubated in a sensitizing solution (15 mM $Na_2S_2O_3$, 25 mM formaldehyde) for 1 min, and then washed twice with ultrapure water. For staining, the gel was incubated in a solution comprising 15 mM $AgNO_3$ and 25 mM formaldehyde for 30 min, rinsed twice with ultrapure water, and incubated in a developer solution (0.3 M Na_2CO_3, 25 µM $Na_2S_2O_3$, 25 mM formaldehyde) until protein bands appeared. To stop the staining reaction, the gel was transferred into a 5 % (v/v) acetic acid solution.

For staining DNA, the gel was incubated for 30 min in an aqueous solution of 0.01 % (v/v) SYBR® Green I (Sigma-Aldrich) during shaking at room temperature. To prevent the fluorescent dye from bleaching, the gel was kept in the dark during incubation. Images were acquired using a UV transilluminator (Bio-Rad Universal Hood II Gel Documentation System).

2.11.2. Indirect ELISA

Performing an indirect ELISA allowed for verifying the presence and the structural integrity of the terminal sequences of mucins attached to a surface. This method is based on the detection of mucins by specific antibodies, which have a very high specificity and sensitivity toward their targets (=antigens). A primary antibody is used to target the antigen of interest. Then, a second antibody is used, which binds the primary antibody with high affinity. This second antibody is coupled with a reporter – the secondary antibodies used in this work were conjugated with the enzyme horseradish peroxidase (HRP), which converts an initially colorless substrate into a colored product. This

conversion reaction will only happen if the secondary antibody has bound to its antigen, the primary antibody.

In brief, the wells of 96-well microtiter plates (Corning Inc.) were coated with mucins either by means of passive adsorption or covalent coupling (see **Chapter 2.7**). Afterwards, each well was rinsed thrice with PBS-Tween (*i.e.*, PBS (pH 7.4) containing 0.1 % (w/v) Tween 20). Then, unspecific binding sites in all wells were blocked by incubating the wells in blocking buffer (comprising 5 % (w/v) milk powder dissolved in PBS-Tween) at 4 °C overnight. On the next day, the blocked wells were again rinsed with PBS-Tween. Afterwards, each well was incubated with 200 µL of a solution containing the primary antibody (diluted 1:400 in blocking buffer) for 1 h while shaking. For this step, a monoclonal antibody was used for the detection of MUC5AC (ABIN966608, antibodies-online GmbH, Aachen, Germany); this antibody targets an epitope within the mucin C-terminus.[90] After incubation at room temperature for 1 h, the wells were rinsed again with PBS-Tween. Then, 200 µL of a solution containing the secondary antibody (goat anti-mouse IgG antibody; ABIN237501, antibodies-online GmbH) conjugated with HRP were added to each well. This secondary antibody was diluted 1:5000 in blocking buffer. Incubation was allowed to take place on a shaker at room temperature for 2 h. Afterwards, the wells were washed with pure PBS (pH 7.4). Thereafter, 100 µL of QuantaRed Working Solution was added to each well. The QuantaRed Working Solution comprised 50 parts QuantaRed Enhancer Solution, 50 parts QuantaRed Stable Peroxide and one part QuantaRed ADHP Concentrate (QuantaRed Enhanced Chemifluorescent HRP Substrate Kit 15159, Thermo Fisher Scientific). After 30 min of incubation at room temperature in the dark, the peroxidase activity was stopped by adding 20 µL of QuantaRed Stop Solution to each well. The well plate was incubated on a shaker for 30 s before the absorbance of the converted substrate was measured with a multilabel plate reader (Viktor3, PerkinElmer). Absorbance was determined at a wavelength of 570 nm using a data acquisition time of 0.1 s.

2.11.3. Quantification of thiol groups

An assay based on the absorption of UV light was used to determine the average number of accessible thiol groups in mucin glycoproteins. This assay is based on the detection of a product with an absorption maximum at a wavelength of 324 nm upon reaction of the reagent 4,4'-dithiodipyridine (DTDP) with the accessible thiol groups present in mucins. The assay was performed as outlined by Riener *et al.*.[91] In brief, a calibration curve was recorded using L-cysteine (Alfa Aesar, Ward Hill, MA, USA). Therefore, DTDP was dissolved in 12 mM HCl at a concentration of 4 mM, and L-cysteine

was dissolved in PBS (10 mM, pH 7.0) at a concentration of 3 mM. Then, 0, 10, 20, 30, or 40 µL of the cysteine solution were mixed with PBS to a total sample volume of 2.875 mL. Then, 125 µL of DTDP solution were added and the reaction was allowed to take place at room temperature for 5 min prior to measuring the absorption behavior of the samples using a UV/Vis photospectrometer (λ = 324 nm; Specord 210, Analytik Jena AG, Jena, Germany). To determine the amount of accessible thiols in mucins, each mucin variant was dissolved in PBS at a concentration of 1 % (w/v). Then, 2.875 mL of each mucin solution were mixed with 125 µL of DTDP solution, and the reaction was allowed to take place at room temperature for 5 min prior to determining absorption at 324 nm. A mixture of 2.875 mL of pure PBS (*i.e.*, devoid of mucins) and 125 µL DTDP solution was used as 'DTDP blank'. To account for the absorption properties of the mucins themselves, the absorption behavior of a mucin solution devoid of DTDP was determined ('mucin blank'). The absorption values measured for these 'blanks' were subtracted from those measured for the samples.

2.12. Statistical analysis

To detect significant differences between two examined groups, two-sample independent *t*-tests were conducted. Prior to testing, the normal distribution of the measured values was verified with either the Shapiro-Wilk-test or the Kolmogorow−Smirnow−Lilliefors-test. Furthermore, homogeneity of variances was tested using the Levene's test. To test for statistically significant differences between two normally distributed populations with homogenous variances, Student's t-tests were performed, whereas Welch's t-test was used in the case of unequal variances. For non-normal distributed populations, the Wilcoxon-Mann-Whitney-test was used. To detect statistical differences between more than two groups, one-way ANOVA (Analysis of Variances) and for pairwise multi-comparison Tukey Post-Hoc tests were performed. The significance level α was set to 0.05, *i.e.*, a *p*-value of $p \leq \alpha$ indicates statistically significant differences.

3. Surface-attached mucin layers

Mucins not only constitute the key component of secreted mucus but they are also expressed as membrane-tethered variants on the luminal side of mucosal tissues (**Fig. 2.1 A**).[25, 48, 92] These membrane-associated mucin layers can be found throughout all mucosal surfaces in the body, where they form well hydrated layers. In fact, keeping mucosal surfaces hydrated is one of the most essential physiological functions of membrane-tethered mucins.[48, 49] Proper hydration is also crucial for a macromolecular surface layer to provide lubrication, and, indeed, these mucins contribute to friction reduction on mucosal surfaces.[93, 94] However, although they form a hydration layer that keeps opposing surfaces separated from each other, the lubricating potential of such surface-anchored mucin layers is less efficient than that of mucin solutions.[70] This can be rationalized as follows: When the lubricity of solubilized mucins is probed, their lubricating performance is based on a combination of two mechanisms – the formation of a sacrificial mucin layer and hydration lubrication (**Chapter 2.8.2**).[79, 95] By anchoring mucins to (epithelial) surfaces, however, the sacrificial layer mechanism is suppressed, and the remaining lubricity is based on the hydration lubrication mechanism alone. Accordingly, especially in the boundary lubrication regime, the lubricating performance of surface-bound mucin layers is not as good as that of solubilized mucins. Lastly, a third important functionality of these mucin layers is the protection of the underlying mucosal tissues from invading pathogens.[96-98] Mucins can prevent pathogens from binding to the cell surface receptors of the underlying tissue by steric hindrance. To keep pathogens distant from mucosal tissues, the individual mucin proteins can extend up to 1.5 μm from the cell surfaces.[48, 99, 100] Delaveris *et al.* (2020) could even show that the conformation of membrane-tethered mucins is linked to the apparent mucin density on the cell surface. At high surface densities, mucins assume an elongated conformation; thus, the distance a pathogen would have to traverse to infect the underlying tissue increases.[100] Another delicate protection mechanism against pathogenic infection is established by the ability of membrane-tethered mucins to act as releasable decoys. Upon pathogen binding to the ligands presented by these mucins, the extracellular domains are split off and released into the luminal space.[101, 102] Continuous mucus turnover eventually leads to the removal of the pathogens from the body.

In humans, a total of eleven different membrane-associated mucin isoforms exists: MUC1, MUC3A, MUC3B, MUC4, MUC12, MUC13, MUC15, MUC16, MUC17, MUC20, and MUC21.[25, 48] The expression patterns of the different variants depend on the particular tissue type.[48] The three most extensively studied variants of those membrane-associated mucins are MUC1, MUC4, and MUC16, which constitute the periciliary layer covering the airway epithelia.[48, 92] At this specific location in the

human body, the membrane-bound mucin layers are covered by secreted mucus, which can be either in a sol state (= liquid) or in a gel state –depending on environmental factors as well as the individual health state.[103, 104] Physiologically, membrane-bound mucin layer do not mix with secreted mucus but rather form two distinct, spatially well-separated phases. For instance, Button *et al.* (2012) could show that, in the airways, the mucus hydrogel does not penetrate the periciliary layer that is constituted by a dense, extracellular mucin brush.[103]

In this chapter of the thesis, surface-attached mucin layers were reconstituted from purified mucins on different surfaces to study their physico-chemical properties, *i.e.*, their adsorption behavior as well as the impact of enzymatic modifications on mucin conformation and adsorption.

3.1. Formation of surface-attached mucin layers *in vitro*[*]

It is a very challenging task to reconstitute artificial mucosal systems comprising membrane-tethered mucin isoforms *in vitro*. This is mainly due to the fact that, in their physiological state, these mucins are well anchored in hydrophobic phospholipid bilayers and thus particularly difficult to purify without structurally damaging them.[105, 106] Hence, for research purposes, model systems mimicking the properties of membrane-tethered are commonly employed instead. Anchoring purified mucins onto surfaces allows for creating a model representation of membrane-tethered mucosal systems. Owing to their high degree of structural similarity and their comparably good availability, secreted mucin isoforms are preferentially used as surrogates for membrane-tethered mucins. Indeed, such surface coatings generated using purified, secreted mucins were shown to successfully recreate some of the functionalities of physiological membrane-tethered mucin layers. For instance, *in vivo*, one of the most striking properties of membrane-associated mucins is their ability to prevent the adhesion of viruses and foreign cells, both eukaryotic and prokaryotic ones, to body surfaces.[100, 107] Several authors could confirm the anti-adhesive properties of adsorbed mucin layers by conducting biofouling tests with bacteria and eukaryotic cells on a range of medically relevant polymeric materials.[108-111]

In vitro, mucins can be attached to different surfaces *via* two routes: either by means of passive adsorption, *i.e.*, the physical deposition of mucins from a solution onto a sample surface, or by covalently grafting the glycoproteins to a surface. When mucin surfaces layers are generated *via* the

* This section follows in part the publications Marczynski *et al.*, Colloids and Surfaces B: Biointerfaces (2020) and Marczynski *et al.*, Biomacromolecules (2021).

first route, the surfaces to be coated are incubated in a solution containing mucins. Both, the amount of adsorbed mucins and the adsorption kinetics of the sorption process, can differ depending on the surface materials and the type of mucin. Both parameters were here assessed using QCM-D measurements. As model surfaces, the polymer PDMS and stainless steel were chosen as these two materials represent typical substrates with non-polar and polar surface properties, respectively. Moreover, these two materials are the ones that were brought in contact during the tribological experiments discussed in **Chapter 4.1**. The adsorption of two different mucin isoforms was investigated: human salivary mucin MUC5B and porcine gastric mucin MUC5AC.

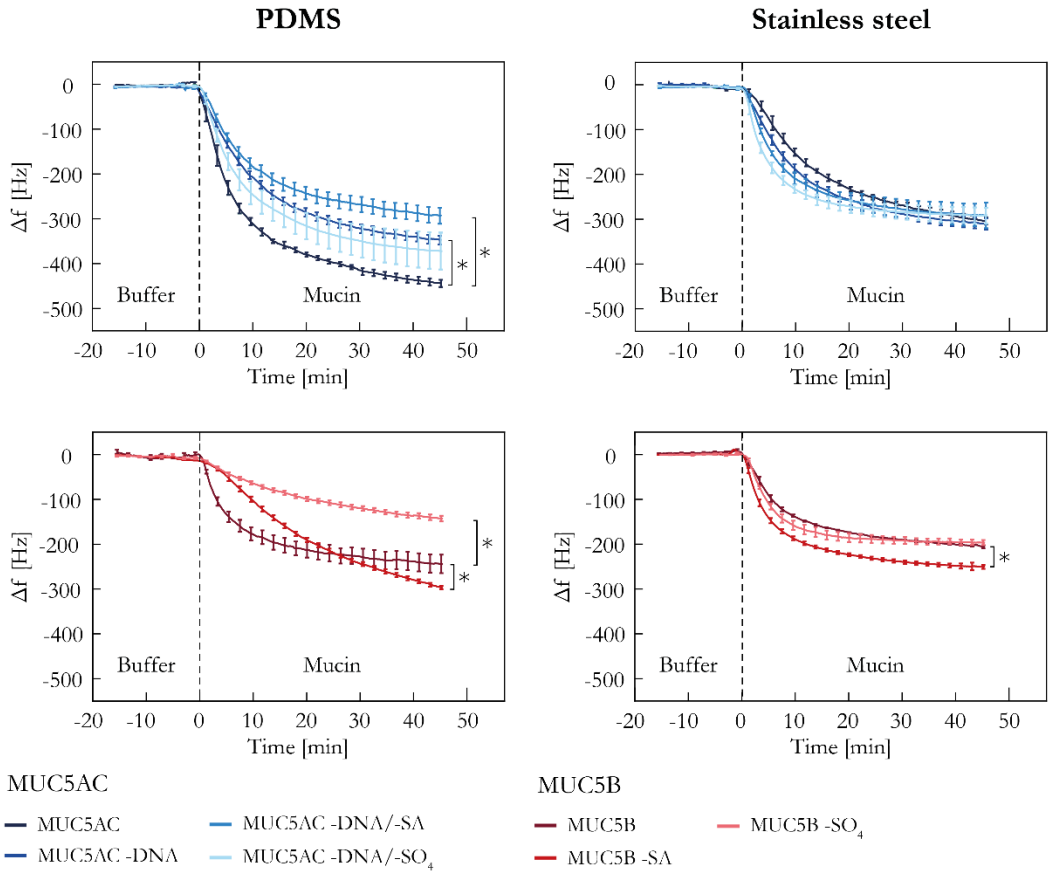

Fig. 3.1: Adsorption behavior of native and enzymatically treated mucins onto PDMS and steel surfaces. Gastric mucin MUC5AC induced a stronger frequency shift than salivary mucin MUC5B on both, hydrophilic steel and hydrophobic PDMS surfaces. The adsorption efficiency of both mucin variants was affected by an enzymatic removal of negatively charged groups; yet, this effect was more strongly pronounced on PDMS. Error bars denote the standard error of the mean as obtained from at least three independent measurements. Asterisks indicate statistical significance ($p < 0.05$) as calculated for the final frequency shift determined after 45 min of adsorption.

With this technique, it has been previously demonstrated that MUC5AC induces a stronger frequency shift on PDMS coated quartz crystals than MUC5B, and this behavior could be reproduced here (**Fig. 3.1**).[40] Moreover, similar results were obtained on steel surfaces (**Fig. 3.1**). Since the measured frequency shift corresponds to the deposited mass, this finding indicated that, despite comparable molecular weights, MUC5AC exhibited increased adsorption onto PDMS compared to MUC5B. Whereas the molecular origin for this difference between MUC5B and MUC5AC remains unclear, these adsorption curves obtained for native mucins could be used as references to which the adsorption behavior of enzymatically treated mucin variants was compared (**Fig. 3.1**).

It is well known that the functionality of mucins is intimately associated with their molecular and structural integrity. For instance, an efficient adsorption onto surfaces is essential for mucins to act as a lubricant. An intentional enzymatic removal of the terminal domains by a trypsin treatment, however, completely abolished the ability of mucins to adsorb onto PDMS surfaces and thus their lubricity.[40] As the adsorption onto such surfaces is mostly governed by hydrophobic interactions acting between the PDMS and the hydrophobic termini of the mucin molecule, the trypsin-treated mucin variants could not engage in binding interactions with the PDMS surface anymore.

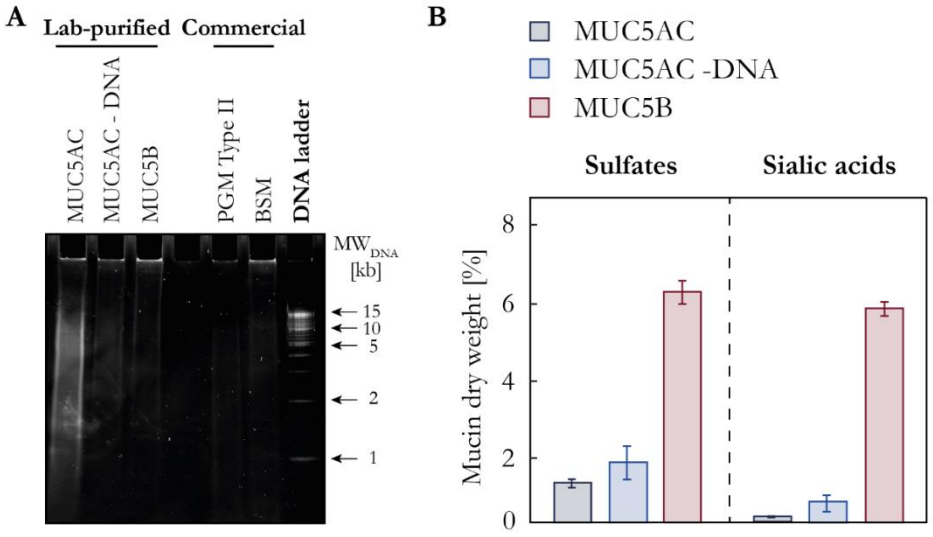

Fig. 3.2: Contamination of mucin samples with DNA & Enzymatic treatment of mucins. Mucin samples were subjected to an electrophoretic separation on a polyacrylamide gel, and the gel was subjected to a staining of the DNA impurities in the gel (white stain) with the dye SYBR Green I. The successful removal of mucin associated DNA impurities from the mucin samples was shown by the reduction of the DNA signal in the MUC5AC -DNA sample compared to the MUC5AC sample. Lab-purified MUC5B as well as the two commercial analogues of MUC5AC and MUC5B (*i.e.*, PGM and BSM) were devoid of DNA contaminations (**A**). The amounts of charged glycans, which were removed from either MUC5AC, MUC5AC –DNA, or MUC5B by an enzymatic treatment with neuraminidase and sulfatase, respectively, were determined using commercially available quantification kits (**B**).

Here, it was assessed whether also more subtle biochemical modifications, *i.e.*, the removal of anionic residues (namely, sialic acids and sulfate groups as well as DNA in the case of MUC5AC) were to affect the adsorption behavior of MUC5AC and MUC5B. Indeed, the extent and pattern of the glycosylation of mucin molecules are subject to a natural plasticity, *i.e.*, variations that occur periodically in time or between different mucus locations.[112, 113] Moreover, such alterations in the composition of mucin glycan chains can also be related to pathogen infection and disease.[114, 115]

Different from MUC5B, MUC5AC typically contains significant amounts of DNA when purified manually (**Fig. 3.2. A**). As DNA strands are strongly polyanionic at physiological pH levels, they confer additional negative charges to the mucin glycoproteins. It appears likely that they are bound to the terminal mucin domains *via* unspecific electrostatic forces acting between cationic amino acid residues located in the mucin termini and anionic phosphate groups of the DNA backbone. These mucin-associated DNA strands can be enzymatically removed by a treatment with DNase. A successful removal of DNA could be verified by an electrophoretic separation of DNase-treated mucin samples on a polyacrylamide gel (**Fig. 3.2 A**). Physiologically, such mucin-associated DNA might lead to additional interactions of mucins with other molecules, which, in turn, might affect other mucin properties such as their ability to form hydrogels at acidic conditions. However, independent of its physiological relevance, the presence of DNA on MUC5AC affected the efficiency of subsequent treatments with sulfatase and neuraminidase. These enzymes were used to cleave sulfate groups and sialic acids, respectively. Larger amounts of sulfate and sialic acid group could be removed from MUC5AC –DNA, *i.e.*, MUC5AC that had been pre-treated with DNase, than from native MUC5AC (**Fig. 3.2 B**): whereas 1.8 % (sulfate) and 0.5 % (sialic acid) of the mucin dry weight, respectively, were removed by the enzymatic treatments in the case of MUC5AC –DNA, cleaved sulfate groups and sialic acids accounted for only 1.4 % and 0.2 % in the case of native MUC5AC. Interestingly, lab-purified MUC5B was essentially free of DNA contaminations (**Fig. 3.2 A**). At the same time, the sulfate and sialic acid contents determined for MUC5B, *i.e.*, 6.2 % and 6.0 % of the mucin dry weight, by far exceeded those in MUC5AC. Overall, the contents of anionic groups quantified for both, MUC5AC and MUC5B, agreed well with those reported in the literature.[116-119]

The intentional removal of negative charges from the mucins resulted in strongly altered adsorption behaviors. On PDMS surfaces, the adsorption efficiency of MUC5B $–SO_4$ was reduced by ~50 % as indicated by the much higher plateau in the frequency shift (**Fig. 3.1**). In contrast, for MUC5B -SA, a stronger final value in the frequency shift was determined after 45 min of adsorption time than for native MUC5B. Interestingly, also the adsorption kinetics obtained for this specific variant (as well as the other modified MUC5B variant) were much slower than for native MUC5B. Whereas for MUC5B a plateau value was reached within in the course of the experiment (*i.e.*, 45 min), this was

not the case for the other variants. By fitting an exponential decay function $\Delta f \sim \exp(-t/\tau)$, where τ denotes the decay time, it was found that τ was increased by an order of magnitude for both enzymatically treated mucin variants ($\tau_{native} \approx 450$ s; $\tau_{-SO4} \approx 1400$ s; $\tau_{-SA} \approx 1700$ s; **Fig. A4.3**). On steel surfaces, a different picture emerged. Here, MUC5B $-SO_4$ displayed a similar adsorption behavior as untreated MUC5B (**Fig. 3.1**). For MUC5B -SA, however, a significantly increased frequency shift indicated improved adsorption properties. The removal of sialic acid moieties might have weakened the electrostatic repulsion mucins experience from the steel surface, thus enhancing mucin adsorption. Although it was surprising that this effect only occurred for MUC5B –SA but not for MUC5B $-SO_4$ (which should have lost probably an even larger amount of charged residues by the enzymatic treatment, **Fig. 3.2 B**), those results indicated that mucin adsorption is always affected when the intrinsic charge state of mucins is modified. For MUC5AC, the adsorption behavior of the three enzymatically treated variants onto steel surfaces was virtually identical to that of native MUC5AC (**Fig. 3.1**). In contrast, when studying PDMS surfaces, all three modified MUC5AC variants showed decreased adsorption efficiencies. Yet, for one of these treated mucins (*i.e.*, MUC5AC -DNA/–SA), this difference was not statistically significant (**Fig. 3.1**).

3.2. Conformation of surface-attached mucin molecules*

It was suggested earlier that the adsorption efficiency of mucins strongly depends on their conformation.[120, 121] This notion is supported by an ELISA performed with MUC5AC and its derived variants: whereas the anti-MUC5AC antibody returned a strong signal for native MUC5AC, hardly any signals could be recorded for the modified variants (**Fig. 3.3**). As the relative absorption values recorded for the enzyme-treated variants were more than an order of magnitude smaller than those determined for native MUC5AC, this suggested that those two mucin properties are indeed related. The monoclonal antibody used for the detection of MUC5AC targets an epitope within the mucin C-terminus.[90] All enzymatic treatments performed with MUC5AC, however, were directed either at the mucin-associated DNA or the glycan chains, but not at the terminal mucin domains.

In general, mucin adsorption onto hydrophobic surfaces is thought to require the hydrophobic protein domains to be present and accessible.[86, 122] A weakening of intramolecular electrostatic repulsion forces (for instance, by removing mucin-associated DNA, sialic acids, and sulfate groups),

* This section follows in part the publications Marczynski *et al.*, Colloids and Surfaces B: Biointerfaces (2020) and Lutz *et al.*, Langmuir (2020).

however, might have led to alterations in the mucin conformation. For instance, after enzymatic modification, the modified mucin molecules might have assumed a rather coiled configuration in aqueous solution, in which the hydrophobic termini of the molecule were well shielded from the surrounding and thus less accessible for binding interactions required for surface adsorption. In contrast, in structurally intact mucins, repulsive electrostatic forces might prevent coiling and, instead, help maintaining an energetically favored elongated conformation, in which the terminal domains are exposed to the aqueous environment and readily available for surface adsorption.[123]

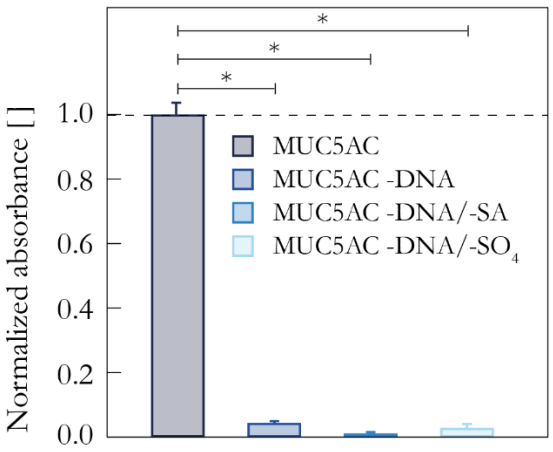

Fig. 3.3: ELISA for the detection of different MUC5AC variants. The measured absorbance values for all samples were normalized to the fluorescence intensity measured for native MUC5AC. Error bars denote the standard error of the mean as obtained from five individual measurements ($n = 5$). Asterisks indicate statistical significance ($p < 0.05$).

In the presence of hydrophobic surfaces, of course, also the adsorption of enzymatically modified mucins from an aqueous solution still can be expected to be entropically favored.[124] However, if the structural configuration of modified mucins were to be such that the hydrophobic binding sites are deeply buried in the protein core, prior to adsorption, these mucins would have to undergo a conformational rearrangement such that the hydrophobic regions become accessible again. Such conformational changes in proteins, however, are comparatively slow processes, which might require more time than the actual surface attachment.[125, 126] Accordingly, proteins, which have to undergo strong conformational changes prior to adsorption might exhibit rather slow adsorption kinetics. Indeed, drastically slower kinetics were recorded for the adsorption of the two enzymatically modified MUC5B variants on PDMS surfaces (**Fig. 3.1**). In agreement with this picture, a dependence of the mucin conformation on the composition and integrity of the mucin glycosylation has been described before by Round *et al.* in an AFM-based study.[127]

The hypothesis that the conformation of mucins might be dictated by their charge state was supported by two additional binding assays conducted with unspecific binding partners, *i.e.*, fluorescently labeled dextrans with different net charges. First, a depletion assay was performed (**Fig. 3.4 A**). Here, the wells of a microtiter plate were coated with mucins and afterwards incubated

with solutions containing one of the three dextran variants. In this setup, the solubilized dextrans were depleted from solution by binding to the adsorbed mucin layer. The fluorescence intensity of the supernatant (containing the remaining unbound dextrans) was determined, and the amount of depleted, *i.e.*, mucin-bound, dextrans was derived. In addition to native MUC5AC, these experiments were performed with MUC5AC –DNA and MUC5AC –DNA/-SO_4 as models for enzymatically modified MUC5AC. The latter one was chosen over the other imaginable double-treated variant as, here, compared to MUC5AC –DNA/–SA, the largest reduction in charge was expected.

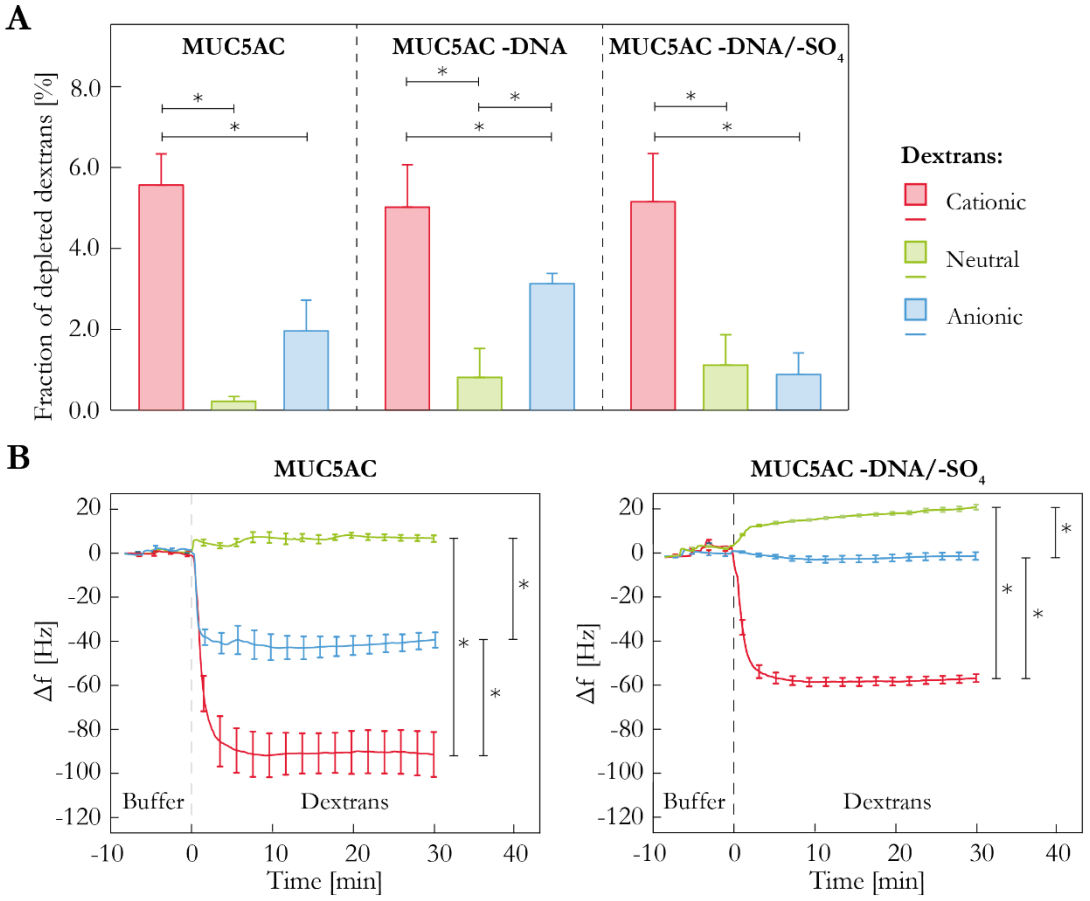

Fig. 3.4: Assessing binding interactions between different dextrans variants and surface-attached layers of three MUC5AC variants. Binding of cationic (blue), neutral (green), and anionic (red) dextrans to adsorbed mucin layers was compared by performing a depletion assay using dextrans with a molecular weight of 150 kDa. The error bars represent the standard error of the mean as obtained from five individual samples ($n = 5$). Asterisks mark significant differences between the dextran groups ($p < 0.05$; **A**). In a second set of experiments, the binding of the same dextran variants as in **A** to pre-adsorbed mucin layers was assessed by recording the mass increase on QCM-D sensors, which occurred as a result of dextran binding to mucins. The error bars denote the standard error of mean as obtained from three individual measurements ($n = 3$). Asterisks mark significant differences ($p < 0.05$; **B**).

Surface-attached mucin layers

The results obtained with this assay indicated that binding interactions between native, untreated MUC5AC and charged dextran molecules were critically affected by attractive electrostatic forces: both cationic and anionic dextrans bound to the surface-attached mucin layers, whereas neutral dextrans did not (or at least in very low numbers). In addition, cationic dextrans showed a slightly higher binding propensity toward MUC5AC than anionic ones (**Fig. 3.4 A**). Although tempting, determining K_D values for the binding of the different dextran variants to mucins is, however, challenging for conceptual and technical reasons. First, the binding of dextrans to binding sites of the mucin molecule can be strongly influenced by previous binding events. For instance, binding of dextrans to the mucin molecule can alter the (local) charge state of the mucin molecule; this, in turn, can result in conformational changes of certain domains of the mucin molecule. Second, binding data obtained in a titration series at high ligand concentrations came with larger experimental errors, which rendered a fitting procedure of those curves unreliable.[39] This increased experimental variability may – at least in part – reflect the complex consequences multiple binding events can have on the mucin molecule.

Although the treatment of MUC5AC with DNase had removed negative charges (as established by the phosphate groups of the mucin-associated DNA strand), the binding affinity of DEAE-dextrans toward MUC5AC –DNA was not affected significantly (**Fig. 3.4 A**). Also the binding properties of unmodified dextrans were not affected by the enzymatic mucin modification. As it was the case for native MUC5AC, these dextrans hardly showed any binding to MUC5AC –DNA (**Fig. 3.4 A**).At the same time, the binding of anionic dextrans to MUC5AC –DNA was slightly enhanced – and this effect can be rationalized by the reduction of repulsive electrostatic forces acting between the DNA-free mucins and the anionic dextrans (**Fig. 3.4 A**). For the binding of the three dextran variants to the double-treated mucin variant MUC5AC -DNA/-SO_4, a different picture emerged. Although a large number of negatively charged motifs (and thus potential binding sites for cationic DEAE-dextrans) was removed from this specific mucin variant, also here, no significant reduction in the amounts of depleted DEAE-dextrans could be detected (**Fig.3.4 A**). In contrast, the amounts of anionic CM-dextrans, which bound to the mucin surface layers, were drastically reduced for MUC5AC -DNA/-SO_4 (**Fig. 3.4 A**). For surface layers obtained with this mucin variant, no significant differences in molecule depletion could be observed between unmodified and CM-dextrans anymore. This outcome is interesting considering that the removal of anionic DNA strands from the mucin glycoprotein should have decreased intermolecular repulsion forces acting between the mucin backbone and the anionic dextrans, which, in turn, should have facilitated binding of anionic dextrans rather than weakening it.

Considering the counterintuitive outcome of the binding tests conducted with CM-dextrans, another quantitative technique was employed to verify the results obtained in the depletion tests: an adsorption-based assay to test dextran binding to the different mucin variants *via* QCM-D. Here, PDSM coated quartz crystals were functionalized with the respective mucin variant before, in a second step, the different dextran variants were flushed into the flow cell, from where they could be depleted by the surface-attached mucins. Also with this technique, it was found that the binding of positively charged DEAE-dextrans to native mucin molecules was very pronounced, whereas the anionic CM-dextrans were depleted to a much lower extent (**Fig. 3.4 B**). The unmodified dextrans did not appear to adsorb to the mucin layers at all. In agreement with the results obtained from the depletion assay, DEAE-dextrans also bound to surface layers reconstituted from the enzymatically treated MUC5AC -DNA/-SO_4, whereas neither unmodified nor CM-dextrans induced a negative frequency shift as it would be triggered by the adsorption of dextrans to the mucin layer (**Fig. 3.4 B**) Since QCM-D measurements are able to detect even subtle changes in the adsorbed mass, this result indicated that almost no anionic dextrans bound to the modified mucin.

At this point, it has to be noted that the outcome of such delicate assays probing binding interactions between mucins and different molecular probes strongly depends on the individual mucin batch.[39, 128] For a complex biological macromolecule as mucin, this is not surprising as the glycosylation pattern of mucin glycoproteins is subject to a certain degree of biological variability: the glycosylation of MUC5AC molecules can vary not only between individual pigs (from whose stomachs the mucins were purified) but also within one and the same animal depending on its health state, diet, and the location from where mucus samples were collected.[129, 130] As a consequence, slight variations in the dextran binding patterns were found when a different purification batch of lab-purified mucin was compared (**Fig. A4.4**). For this specific purification batch, enzymatic removal of anionic charges from the mucin molecules resulted in a strong reduction of the capability to deplete DEAE-dextrans. This result can be rationalized by the fact that anionic motifs (*i.e.*, sulfate residues and sialic acids) constitute very likely target sites for the unspecific binding of cationic molecules *via* attractive electrostatic forces.[131] In consequence, the removal of anionic moieties reduced the binding propensity of cationic dextrans toward charge-reduced mucins. Again, also anionic CM-dextrans bound to the surface layers reconstituted from enzyme-treated mucins in significantly smaller amounts than to MUC5AC layers. (**Fig. A4.4**).

Taken together, the results obtained from both binding experiments indicated that – in addition to removing potential binding sites for cationic molecules – an enzymatic cleavage of anionic residues from mucin glycoproteins can also affect the binding capability of mucins toward anionic molecules. At this point, it is important to recall that the most likely target motifs on mucins, which could allow

for the binding of those anionic molecules, are located in the termini of the mucin glycoprotein (*i.e.*, in the non-glycosylated regions of the peptide backbone, which were not targeted by the treatments). If the conformation of the (largely unfolded) mucin is well elongated, *i.e.*, if those termini are accessible, molecule binding to those terminal groups should be easily possible. In turn, conformational changes as, for example, brought about by weakened intramolecular repulsion forces (as expected for, *e.g.*, DNA/sulfate-reduced mucins), could reduce the accessibility of these terminal domains, eventually lowering the efficiency of the binding of anionic CM-dextrans.

3.3. Imaging of surface-adsorbed mucins*

Having established that a removal of negatively charged mucin domains – even if the cleaved motifs account only for an almost negligibly small fraction of the total mucin molecule weight – might result in local and/or global conformational changes, atomic force microscopy (AFM) was employed to image the conformations of the respective mucin molecules (for details on sample preparation and the imaging procedure, see **Appendix A4**).

For these AFM experiments, the focus was on MUC5B, since for this specific mucin isoform, differences in adsorption behavior between native MUC5B and the enzymatically treated variants could be observed on both types of surfaces, hydrophobic PDMS and hydrophilic steel samples (**Fig. 3.1**). However, since these materials exhibited comparatively large surface roughness values on the nanoscopic length scale, HOPG (highly oriented pyrolytic graphite) and mica surfaces were used as hydrophobic and hydrophilic model substrates for AFM-based imaging. It has been demonstrated previously that the deposition technique considerably influences the conformation of the adsorbing mucin molecules.[127, 132] Thus, to recreate the scenario used for adsorption (and lubrication) experiments, a solution containing freely diffusing mucins was deposited on top of the substrates to allow mucins to adsorb from solution onto the respective substrate surface. Furthermore, such a setup might best resemble the physiological situations as, for instance, present in the eye.

On hydrophilic mica surfaces, all three MUC5B variants adopted compact, globular conformations with similar heights and diameters (as indicated by the line scans) in the range of ~0-10 nm and ~0-20 nm, respectively (**Fig. 3.5 A**). The widths of the frequency distributions of height and diameter values, however, were different and significantly shifted toward larger values for enzymatically treated

* This section follows in part the publications Marczynski *et al.*, Colloids and Surfaces B: Biointerfaces (2020) and Lutz *et al.*, Langmuir (2020).

mucin variants (**Fig. A4.5** & **Table A4.1**). In addition, at least for MUC5B –SA, an increasing occurrence of aggregates could be observed with increasing mucin concentration. This effect, however, was not detectable for native MUC5B and MUC5B –SO_4 (**Fig. A4.5** & **Table A4.1**). Furthermore, all MUC5B variants adsorbed onto mica to a similar extent (in terms of detected number of particles and coverage, **Fig. A4.5** & **Table A4.1**).

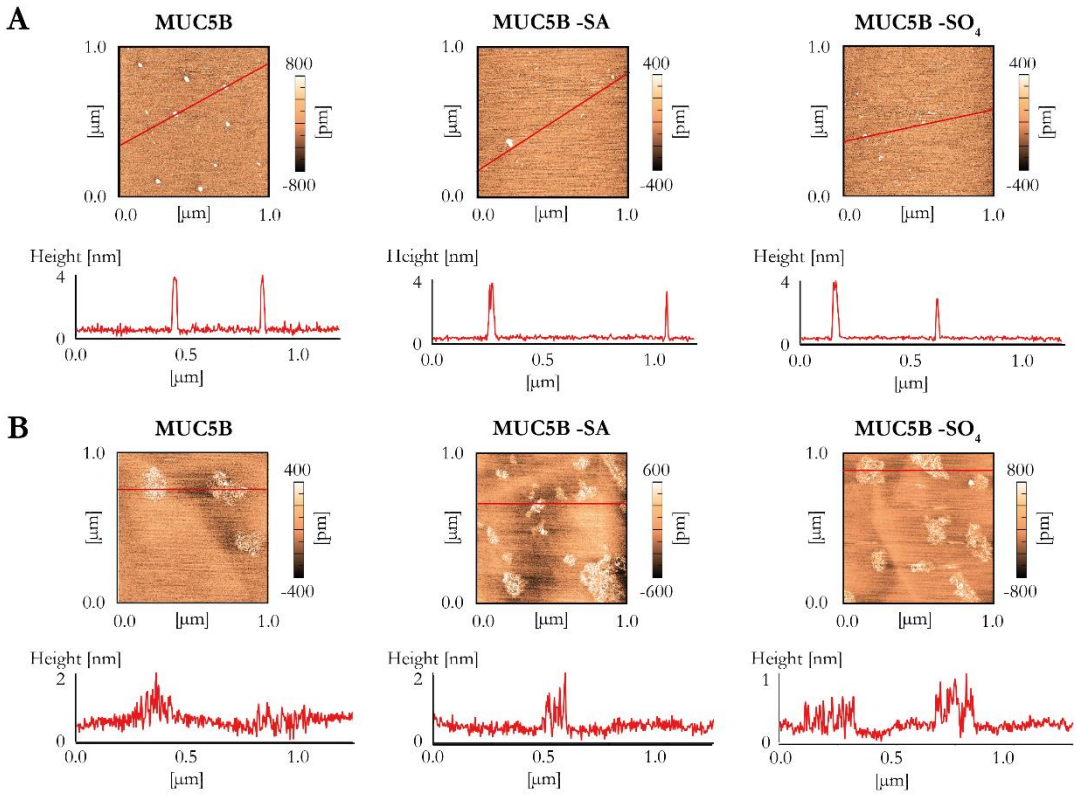

Fig. 3.5: Adsorption behavior of native and enzymatically treated MUC5B variants on mica and HOPG surfaces as visualized by AFM imaging. Images were taken with an AC40TS cantilever in a HEPES solution containing a mucin concentration of 0.010 mg mL^{-1} and 0.001 mg ml^{-1}, respectively, on hydrophilic mica (**A**) and hydrophobic HOPG surfaces (**B**). Each image covers an area of 1 µm x 1 µm. Line scans are given for sections indicated by red lines.

Whereas all three mucin variants exhibited a globular conformation when deposited onto mica surfaces, the same molecules adopted an extended appearance on HOPG surfaces with heights of 1-2 nm (**Fig. 3.5 B**). For the mucin concentration used for imaging on this kind of surface (*i.e.*, 0.001 mg mL^{-1}), all three mucin variants showed patches of isolated or overlapping molecules covering the HOPG substrate. Sections with different heights and widths were observable, which most likely corresponded to the differently glycosylated domains of the mucin molecule; this observation agreed with what was suggested previously by McMaster *et al.*.[133] Thus, at first glance, these images seemed to support the postulation of Zappone *et al.* that the global conformation of

mucin molecules is dominated mostly by steric hindrance between the glycan chains rather than electrostatic repulsion.[134] However, in the past, it has been demonstrated repeatedly that the conformation mucins adopt when deposited onto surfaces critically depends on several other parameters such as the surface energy and the surface topography. In fact, the surfaces used for the binding assays and AFM imaging, respectively, differed in these parameters, which might – at least in part – explain the differences between the expected and the imaged conformations of enzymatically modified mucins.[135, 136]

To clarify the role of electrostatic forces in establishing and maintaining the conformation of mucin glycoproteins, a numerical model was developed (for details see **Appendix A5**). The goal of this model was to compare structural parameters of thermally fluctuating mucins that describe the configuration of the macromolecule – both in the presence and absence of negative charges (as established by sulfate groups and sialic acids) in the mucin backbone. To set up a numerical model, the complex structure of the mucin glycoprotein was segmented into small beam elements, which were assigned longitudinal charge profiles as specified in **AppenidxA5**. The mucin-associated DNA strands could not be included into this numerical model as the total amount of mucin-associated DNA is difficult to determine and might vary strongly between purification batches . Of course, the simulated mucin glycoprotein represented only a simplified model, which is why the absolute numbers of the quantities determined from the simulation should be considered to be estimates.

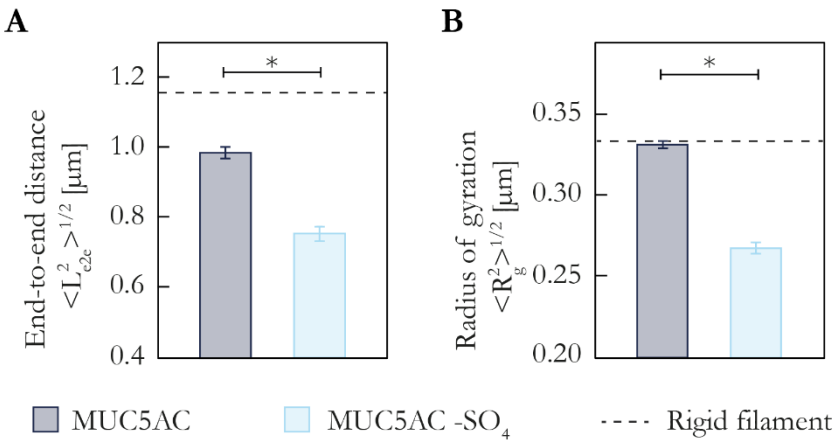

Fig. 3.6: Results obtained from a numerical simulation of native MUC5AC and charged-reduced MUC5AC –SO_4. The structural parameters end-to-end distance $<L_{e2e}^2>^{1/2}$ (**A**) and radius of gyration $<R_g^2>^{1/2}$ (**B**), which are considered representative for the conformation of macromolecules, were calculated for two variants of simulated mucin molecules: native MUC5AC and charge-reduced MUC5AC –SO_4. The error bars depict the standard error of the mean as obtained from five independent simulation runs ($n = 5$). Asterisks mark significant differences ($p < 0.05$).

At a neutral pH of 7.0, for MUC5AC, values for the average end-to-end distances and the radii of gyration were obtained that are close to values that would have been obtained for a rigid, well-elongated molecule (**Fig. 3.6**). Thus, the high density of negatively charged groups in the central area of the mucin macromolecule, indeed, seemed to contribute to maintaining the elongated conformation of the mucin molecules established by rather strong intramolecular repulsive forces (**Fig. 3.6**). However, the molecule simulation also included steric effects – and these might have contributed significantly to the outcome of these simulation experiments.

The validity of the numerical mucin model was checked by comparing the conformation of an enzymatically untreated mucin (neglecting any mucin-associated DNA) at neutral (7.0) and acidic (4.0) pH levels (**Fig. A5.1**). This step was motivated by experimental results from the literature, which have reported a clear compaction of the mucin glycoprotein when the pH of the solvent was decreased from a neutral to an acidic level.[137, 138] Indeed, this behavior could be reproduced by the numerical mucin model (**Fig. A5.1**). When mucin charge profiles corresponding to neutral and acidic buffer conditions were applied (**Table A5.1**), a reduction of both, the end-to-end distance and the radius of gyration of the simulated mucin by factors of ~4.5 and ~2, respectively, were observed. Having confirmed that the developed model could successfully reproduce charge-driven conformational changes (induced by alterations in the pH) that had been reported in the literature, the same model was used for the prediction of conformational changes of the mucin macromolecule upon removal of anionic residues (**Fig. 3.6**). Indeed, when anionic sulfate groups were removed from the charge profile used for modeling, a rather compacted mucin conformation could be obtained as demonstrated by a significant reduction of both, the end-to-end distance and the radius of gyration. In conclusion, the numerical model supported the experimental outcome obtained from different binding experiments (**Fig. 3.3** & **3.4**), *i.e.*, a compaction of the mucin molecule upon removal of repulsive electrostatic forces. Thus, the contradictive results obtained by AFM imaging, indeed, might have resulted from differences in intrinsic material parameters (since mica and HOPG have been used as model substrates in AFM experiments instead of steel and PDMS).

For simulated mucins, where the other anionic motif, *i.e.*, sialic acid groups, were removed, the same outcome was obtained – albeit more weakly pronounced (**Fig. A5.2**). This reflected the lower density of sialic acid groups on the mucin glycoproteins compared to sulfate residues. At this point, it also has to be emphasized that the numerical model reflected a simplified scenario. It allowed for making statements on the conformational changes of monomeric mucins only; yet, physiologically, gastric mucins typically occur in an oligomeric state. Moreover, the conformational change depicted in the simulated mucins might have even underestimated the structural alterations native mucins undergo upon removal of anionic charges, since DNA could not be included.

Overall, the results of both, binding experiments performed in the lab and a numerical simulation of the mucin molecule, indicated that mucins undergo conformational changes in a pH-dependent manner. Moreover, also the enzymatic reduction of charged groups from mucins induced conformational changes in the mucin glycoprotein. These findings challenge the hypothesis proposed by Zappone *et al.* that the impact of electrostatic forces on the conformation of mucins were to be negligible.[134] In fact, electrostatic repulsion seems to critically modulate the conformational state of mucins – at least in *in vitro* experiments.

3.4. A possible physiological role of mucin-associated DNA*

Based on the results discussed above, it can be speculated that the DNA associated with MUC5AC might compensate for the relatively low amount of sialic acid and sulfate residues present in this mucin isoform compared to MUC5B. Thus, by its association with gastric mucin, DNA might help keeping the mucin glycoprotein in an extended state. Whereas at neutral pH levels the mucin is able to maintain an extended configuration on its own, at acidic pH levels, this might be more difficult. Yet, such acidic conditions might better represent the physiological environment gastric mucins occur in better than the neutral pH levels probed in the binding experiments. Interestingly, the numerical simulations of the different mucin variants (which did not consider the association of MUC5AC with DNA) predicted that, at an acidic pH of 4.0, the protonation of anionic residues on the polypeptide chain would induce a compaction of the mucin molecule (**Fig. A5.1**). Given that the pK_a value of phosphate groups in phosphodiester bonds is ~1,[139] the majority of the phosphate groups in the mucin-associated DNA would likely still be in their deprotonated (*i.e.*, anionic) state at pH 4.0. Thus, at all physiologically relevant pH levels, the DNA strands will contribute additional negative charges and, consequently, intramolecular repulsion forces to the mucin glycoprotein. However, as neither the detailed amount of DNA bound per mucin molecule nor the exact position on the mucin glycoprotein where DNA strands bind to are known, it was not possible to include this aspect into the numerical mucin model. Yet, it seems reasonable to assume that DNA strands likely bind *via* attractive electrostatic forces to positively charged amino acid side chains (which are only accessible in the terminal domains). Moreover, the high density of anionic glycan chains might render binding of polyanionic DNA molecules to the central region difficult. Of course, other DNA binding

* This section follows in part the publication Lutz *et al.*, Langmuir (2020).

mechanisms, for example, *via* physical entanglement with glycan side chains or *via* hydrogen bonds are also possible.[140]

In addition to their contribution to maintaining the conformation of MUC5AC, DNA strands might also fulfill a protective function. Indeed, several pathogens have developed strategies to enzymatically target mucin motifs.[141, 142] For instance, sialic acid residues are known as binding sites for different viruses and are thus targeted by viral neuraminidases to set immobilized viruses free again.[143-145] Moreover, several bacterial species reside in respiratory or gastrointestinal mucus where they can forage on mucin glycoproteins.[146, 147] Mucin desulfation is thought to be one of the first steps of mucin degradation, and, for this purpose, specialized bacteria secrete specialized sulfatases.[148, 149] Subsequently, the desulfated mucin glycan chains can be decomposed by the action of glycosidases to release monosaccharides, which are subsequently metabolized by the bacterial community.[146] An unusual activity that had been reported for a glycosidase from *Prevotella* strain RS2 highlighted the evolutionary adaptation of bacteria to the mucosal environments they inhabit: the reported enzyme specifically cleaved terminal 6-SO3-GlcNAc from sulfated mucin oligosaccharide chains, which represented a novel activity within the so-called *glycoside hydrolase family 20 (GH20)*.[150] Yet, as demonstrated in **Fig. 3.2 B**, the efficiency of an enzymatic attack by sulfatases (and neuraminidases) was reduced when MUC5AC was in its physiological, *i.e.*, DNA-associated, state. Thus, it can be speculated that these DNA strands might function as a protective physical obstacle that limits the accessibility of the respective target sites on mucins, thereby retarding enzymatic degradation.

4. Mucin solutions

In addition to membrane-tethered mucins, which are expressed on the apical surfaces of mucosal epithelia, mucosal tissues in the human body also secrete mucins. Secreted mucus either occur as mucin-based solutions or mucin-based hydrogels (the latter will be discussed in detail in **Chapter 5** of this thesis). The former exhibit mostly viscous (= liquid-like) properties, whereas in the latter the elastic properties (= solid-like) dominate. In total, seven different isotypes of such secreted mucins can be distinguished, *i.e.*, MUC2, MUC5AC, MUC5B, MUC6, MUC7, MUC8, and MUC19. Although those secreted mucins are, in terms of structure, quite similar to each other, they are expressed differently throughout the mucosal systems of the human body.[25, 151] Details can be found in **Chapter 2.1** of this thesis.

The necessity of mucus model systems has already been discussed in the previous chapter. Like membrane-tethered mucosal systems, also secreted mucus is subject to a high degree of intrinsic variability in its composition. This aspect complicates research on secreted mucus and makes it often difficult to interpret experimental results obtained with native mucus samples.[152, 153] Thus, also in the context of mucus solutions, for research purposes, it can be favorable to use model systems based on purified mucins, which mimic selected properties of mucus but offer a much higher level of control and reproducibility. In the past, buffered solutions reconstituted from purified mucin glycoproteins have already been intensively studied, and the potential of these model systems to be used in biomedical applications has been highlighted.[12, 154] Examples of such putative applications of mucin solutions include mucin-based eye drops and tribo-supplements, which can be administered to patients suffering from *xerostomia* (colloquially referred to as 'dry mouth syndrome') or osteoarthritis *via* oral sprays or injection into the synovial cleft, respectively. In fact, mucins are already being used for a commercially available saliva substitute, 'Saliva Orthana', which is distributed by A/S Orthana Kemisk Fabrik, subsidiary of Biofac A/S, Kastrup, Denmark. According to the manufacturer, this product is supplemented with mucins extracted from porcine gastric linings (http://www.biofac.dk/products/artificial-saliva/; 08/24/2021). However, so far, the topical application of this product in clinical trials failed to remedy the symptoms dry mouth patients suffer from.[155, 156] In fact, when 'Saliva Orthana' was employed as a lubricant in *in vitro* tribology setups, its lubricating properties were not significantly different from those of simple buffer solutions – neither at low physiological mucin concentrations nor at high, unphysiological mucin concentrations.[95, 157]

Physiologically, mucin concentrations can vary strongly between different mucosal systems. In part, this concentration depends on the function the respective mucosal system has to fulfill: for instance,

in the tear fluid and in saliva, where the main task mucins are responsible for is providing lubrication and protecting the tissue from mechanical damage, the mucin concentration is relatively low (~0.01 % in the tear fluid[28] and 0.02-0.03 % in saliva[158, 159]). To mimic 'artificial', liquid mucus, mucins are typically employed at concentrations which are on a similar order of magnitude. For example, Song *et al.* could show that porcine gastric mucins MUC5AC, indeed, can serve as excellent lubricants at concentrations as low as ~0.01 % – at least when they are purified carefully in the lab.[77] At this point, it needs to be stated that the term 'purified mucin' as used here refers to products that researchers obtained when they purified mucins in the lab. Of course, these preparations still contain a certain amount of impurities as well as – yet, to a smaller extent – other mucin variants. One critical advantage of using purified mucins is that the intrinsic physicochemical properties of the functional key component of mucus, the mucin glycoproteins, can be studied independently of other mucus components. Moreover, in such simpler model systems, it is possible to investigate the influence of selected chemical conditions (*e.g.*, different pH levels or ionic strength, added molecules) in a controlled manner. In fact, in the previously mentioned publication by Song *et al.*, it was demonstrated that the lubricity of mucin preparations is resilient against variations in mucin concentration, pH, and ion concentrations, which can occur in physiological scenarios.[77]

4.1. Molecular motifs relevant for mucin lubricity*

In the previous chapter, the adsorption behavior of mucins onto different surfaces was investigated, and it was demonstrated that lab-purified mucins efficiently adsorb onto both, hydrophobic and hydrophilic surfaces. Indeed, efficient (re-)adsorption is a parameter that critically affects the ability of mucins to provide lubrication (**Fig. 2.6 B**).[78, 160] Still, also mucin coatings can provide a certain level of lubricity when they are coupled covalently onto surfaces.[70, 111, 161] This ability is based on the high hydration level of mucins which gives rise to a mechanism referred to as hydration lubrication.[79, 162] Physiologically, however, lubricity is predominantly brought about by solubilized mucins as they occur in the tear fluid and saliva. In this physical state, the mucin macromolecules can readily adsorb (and re-adsorb after shear off) onto surfaces, *i.e.*, they create a sacrificial layer and thus prevent opposing surfaces from coming into direct contact.[121, 163] Indeed, in the past, several studies indicated that solutions of purified mucins exhibit exceptional lubricity over a wide range of probed velocities. Especially in the physiologically relevant regime of boundary lubrication, mucin solutions excel at

* This section follows in part the publication Marczynski *et al.*, Colloids and Surfaces B: Biointerfaces (2020).

reducing friction.[164] Moreover, Biegler *et al.* (2016) could show that the lubricities recorded for a solution of purified human salivary mucin MUC5B at a physiological concentration of 0.02 % (w/v) and for native, unstimulated saliva were similar.[165] In the same publication, it was shown that both, native saliva and MUC5B solutions alike, lose lubricity in a dose dependent manner when exposed to cationic astringents such as aluminum ions – a mechanism which was suggested to be closely linked to the sensation of astringency.[166, 167]

In fact, lubricity was recently put forward as an indicator for the quality of a mucin sample.[22, 168] This is based on the realization that structural alterations of mucins as they can, *e.g.*, occur when harsh purification procedures were to be applied, lead to a compromised lubricity of mucin glycoproteins. For instance, Crouzier *et al.* showed that the (partial) deglycosylation of mucins, *i.e.*, the chemical removal of the mucin glycan chains, resulted in a complete loss of their lubricating properties:[164] over the entire range of probed velocities, solutions reconstituted from the deglycosylated mucins performed similarly bad as a buffered, aqueous solution devoid of mucins. Importantly, in comparison, the native mucin variant showed excellent lubricity at all probed velocities. In the same publication, the authors showed that the lubricating performance of the deglycosylated mucins could – at least partially – be restored by grafting polyethylene glycol chains to the 'naked' mucin protein backbone. This latter set of experiments indicated that the lubricating properties of the deglycosylated mucins was abolished due to a loss of its water-binding capacity. Indeed, by measuring the hydration state of the different mucin variants, it was demonstrated that the glycan-reduced mucins had bound a significantly smaller amount of water molecules. Overall, this study highlighted the importance of hydration lubrication for mucins to reduce friction between two opposing surfaces.

A different study performed by Käsdorf *et al.* showed that also the impairment of the second mechanism important for mucin lubricity, *i.e.*, the formation of sacrificial layers, results in a loss of mucin lubricity.[40] Here, the hydrophobic terminal domains were removed from lab-purified mucins (both, MUC5AC and MUC5B) by means of a trypsin treatment, upon which these mucins lost their ability to adsorb onto hydrophobic PDMS surfaces. In contrast to the deglycosylated variants, here, the hydration states of the different trypsinated mucin variants were not different from the native variants. By grafting hydrophobic phenyl-functionalized dextrans to the digested mucins, their lubricating properties could be, in part, restored.

In the previous chapter of this thesis, it was already demonstrated that the removal of anionic motifs, which comprise only a minor fraction of the entire mucin glycoprotein, resulted in drastic changes in their adsorption behavior onto both, hydrophilic and hydrophobic surfaces (**Fig. 3.1**). Since efficient adsorption onto the surfaces to be lubricated is one of the key mechanisms facilitating good

lubrication, such alterations in adsorption efficiency and kinetics were expected to affect the lubricity of the modified mucin variants.

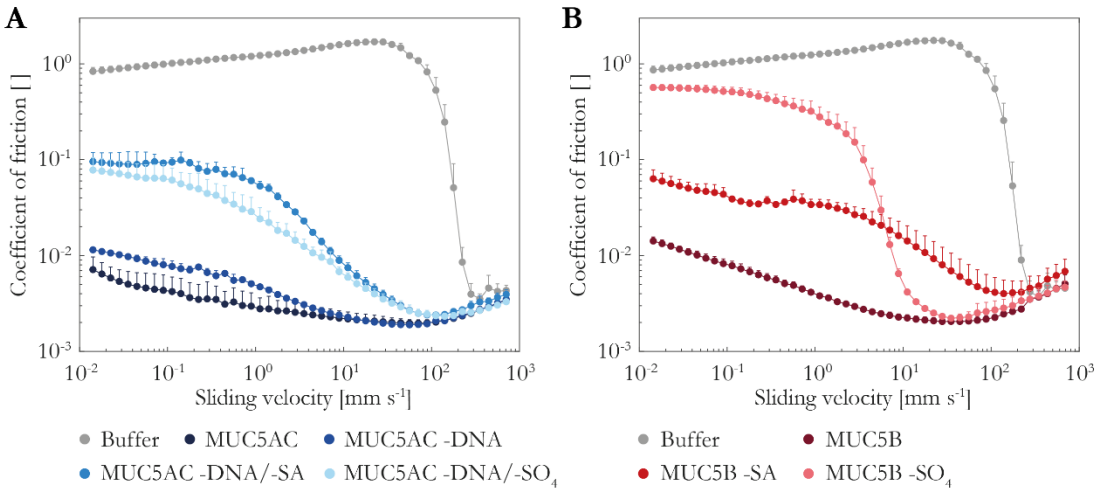

Fig. 4.1: Lubricity of aqueous solutions containing either native or enzymatically modified mucins probed with a rotational tribology setup. Rotational tribology measurements were performed with a steel/PDMS pairing using different mucin solutions as lubricants (1mg mL^{-1} mucin dissolved in 20 mM HEPES, pH 7.0). This figure shows friction curves obtained from rotational tribology measurements for solutions of either MUC5AC (**A**) or MUC5B (**B**), respectively. HEPES buffer devoid of any mucins was included as a reference. Error bars denote the standard error of the mean as obtained from at least three independent measurements (n = 3).

To verify this hypothesis, first, friction measurements were conducted using a stationary contact tribology setup. Here, a steel sphere was contacted with three pins fabricated from PDMS. This particular material pairing was selected as such a hard-on-soft pairing comprising both a hydrophilic and a hydrophobic surface is commonly employed in bio-tribological studies to mimic, *e.g.*, the tongue-palate interface.[163, 169] The steel sphere was rotated at a constant normal load but with varying velocities ranging from 0.01 to 1000 mm s^{-1}. This ensured that friction could be probed in the three relevant lubrication regimes: hydrodynamic lubrication (at high velocities), mixed lubrication, and boundary lubrication (at slow velocities).[40]

Solutions reconstituted from the different native and enzymatically modified variants of MUC5AC (*i.e.*, native MUC5AC, MUC5AC –DNA, MUC5AC –DNA/–SA, and MUC5AC –DNA/–SO_4) and MUC5B (*i.e.*, native MUC5B, MUC5B –SA, and MUC5B –SO_4) were used as lubricants at concentrations of 0.1 % (w/v). At this particular concentration, solutions of high-quality mucins reliably excelled in providing lubrication in the past – and the same result was obtained here (**Fig. 4.1 A** & **B**).[40, 165, 170]

However, upon removal of sialic acids from the mucin glycan chains, the lubricity of MUC5B solutions was considerably reduced, and the friction coefficient at low sliding speeds, *i.e.*, in the boundary lubrication regime, was increased by almost one order of magnitude compared to unmodified MUC5B solutions (**Fig. 4.1 B**). The loss of boundary lubrication was even stronger when sulfate groups had been removed from the salivary mucins; the lubricity of this particular variant was only slightly better than that of a simple HEPES buffer. This more drastic effect on mucin lubricity triggered by the removal of sulfate groups compared to the removal of sialic acid residues can be explained as follows: Both motifs account for approximately 6 % of the total mucin dry weight (**Fig. 3.2 B**). However, since they differ strongly in their molecular weights, also the absolute numbers of these groups present in mucins are very different. On the one hand, *N*-acetylneuraminic acid (NANA), the only type of sialic acids humans are able to produce, has a molecular weight of ~300 g mol^{-1}.* Sulfate groups, on the other hand, have a molecular weight of only ~100 g mol^{-1}. Hence, sulfate groups contribute roughly three times as many negative charges to mucins than sialic acids. Intramolecular, repulsive electrostatic forces acting between these anionic groups were previously shown to help maintaining the native, elongated conformation of mucins – in addition to steric effects (**Chapter 3.3**). Consequently, the removal of these charged groups leads to a reduction of intramolecular repulsive forces and thus to conformational alterations. It can be expected that removing a large fraction of the negative charges (*e.g.*, sulfate groups) from the mucin backbone results in strong conformational changes, whereas the removal of only a small fraction of all negative charges (*e.g.*, sialic acids) may induce less pronounced alterations. Indeed, this notion was also supported by the numerical model presented in **Chapter 3.3**. Here, a (theoretical) removal of sulfates resulted in a strong reduction of both, the end-to-end distance and the radius of gyration of the simulated mucin (**Fig. 3.6**). The same parameters, however, were only slightly reduced for simulated sialic-acid reduced mucins (**Fig. A5.2**). As outlined above, these results were in accordance with adsorption measurements conducted with the different MUC5B variant on PDMS: the sulfate-reduced mucins only induced a small shift in resonance frequency upon adsorption onto the sensor surface and showed the slowest adsorption kinetics out of the three MUC5B variants (**Fig. 3.1**). Rapid adsorption (and re-adsorption after shear-off), *i.e.*, fast adsorption kinetics, however, is pivotal for establishing sacrificial layers and providing lubrication between opposing surfaces. Consequently, as this property was impaired most strongly for MUC5B –SO_4, this specific variant also performed worst during the tribology measurements (**Fig. 4.1 B**).

* Interestingly, most other mammals including pigs can produce also another type of sialic acids, *N*-glycolylneuraminic acid, which has a slightly larger molecular weight and is incorporated in small amounts into the mucins produced by these animals.[152, 153]

A different picture emerged for MUC5AC variants that had been treated with only neuraminidase or sulfatase (MUC5AC –SA and MUC5AC –SO_4). Here, too, only either sialic acid residues or sulfate groups were enzymatically cleaved. Different from analogous experiments conducted with the different MUC5B variants, no differences in terms of lubricity could be recorded for the modified MUC5AC variants compared to solutions of unmodified MUC5AC (**Fig. A4.6**). At this point, it is important to recall that gastric mucin MUC5AC – at least when purified from manually harvested raw mucus – typically contains a certain amount of DNA as a contaminant. Furthermore, in **Chapter 3.1** it has already been demonstrated that the efficiency of an enzymatic treatment targeting the anionic mucin motifs was affected by the presence or absence of DNA strands. DNA strands associated with MUC5AC hampered the efficiency of further enzymatic treatments (**Fig. 3.2 B**). Accordingly, the treatment of unmodified (*i.e.*, DNA-associated) MUC5AC with sulfatase or neuraminidase alone did not remove an amount of negative charges that was large enough to compromise the lubricity of these mucin variants.

Thus, next, the impact of mucin-associated DNA on mucin lubricity was investigated by performing rotational tribology experiments with MUC5AC –DNA. Interestingly, the enzymatic removal of the mucin-associated DNA alone did not impair the lubricating properties of MUC5AC solutions (**Fig. 4.1 A**). A second enzymatic treatment of this MUC5AC –DNA variant with either neuraminidase or sulfatase, however, yielded solutions of mucins (*i.e.*, MUC5AC –DNA/–SA and MUC5AC -DNA/–SO_4) that exhibited drastically reduced lubricity (**Fig. 4.1 A**). In either case, the friction coefficient in the boundary regime was increased by one order of magnitude compared to the value obtained when using untreated MUC5AC solutions as lubricants (**Fig. 4.1 A**). As for MUC5B, also here, the reduction in lubricity can be rationalized by the loss of (a sufficiently large fraction of) negatively charged motifs. This loss, in turn, enabled the mucins to adapt a conformation that was unfavorable for adsorption onto hydrophobic PDMS surfaces and, thus, prevented efficient lubrication (**Fig. 3.1**).

For the (enzymatically treated) mucin variants that failed to provide proper lubrication, it can be hypothesized that the time span required for re-adsorption of these mucins onto PDMS after shear-off was the main factor limiting mucin lubricity: after an initial shear-off from the surface, the modified mucins might have adapted an energetically favored conformation, in which the hydrophobic termini were shielded from the aqueous environment. To re-adsorb to the hydrophobic PDMS surface, mucins would have to undergo a 'backwards' conformational rearrangement such that the hydrophobic domains become exposed again. Such conformational changes, however, are comparatively slow and time consuming processes. Thus, the modified mucin variants might have

been unable to re-adsorb quickly enough to the surfaces and no sacrificial mucin layer was formed. In turn, sufficient lubrication could not be provided.

This hypothesis was supported by tribology measurements that were performed in an oscillatory fashion. Here, a migrating contact setup was used instead of constant contact setup (**Chapter 2.8.2**). Solutions of native MUC5B (which performed well in the rotational tribology measurements) and the worst performing MUC5B variant, MUC5B –SO_4, were used as lubricants. Owing to the migrating contact geometry, a hampered re-adsorption of the modified mucin variant should not affect the lubricity of the mucin solutions as drastically as in the rotational setup.

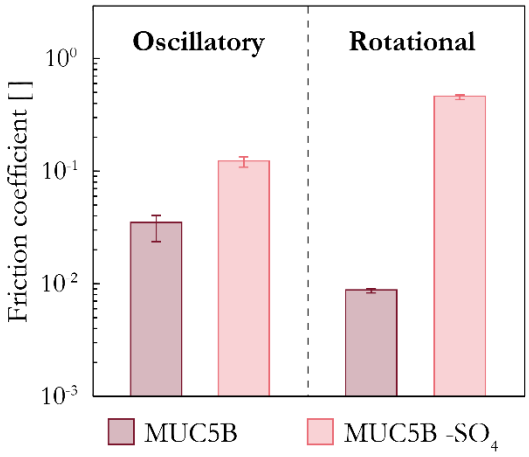

Fig. 4.2: Lubricity of aqueous solutions containing either native MUC5B or MUC5B –SO_4 probed in an oscillatory tribology setup. Oscillatory tribology experiments were performed with 1 mg mL^{-1} solutions of either native MUC5B or MUC5B -SO_4. The error bars denote the standard error of the mean as obtained from at least three independent measurements (n = 3).

Indeed, it was found that MUC5B –SO_4 was able to provide decent lubrication even in the boundary lubrication regime, *i.e.*, at slow sliding velocities of v_s = 0.1 mm s^{-1}, **Fig. 4.2**): now, the friction coefficient measured for MUC5B –SO_4, $\mu_{-\text{sulfate}}(\varphi)$, exceeded that obtained for native MUC5B, $\mu_{\text{native}}(\varphi)$, by a factor of only ~3. In comparison, when probed in rotational mode, the corresponding friction coefficients differed by a factor of ~30 (**Fig. 4.2**). Importantly, for both scenarios, the same material pairing (steel/PDMS) was used. This outcome confirmed that the speed of the mucin adsorption/re-adsorption process is indeed a main factor determining the lubricity of a mucin solution in constant contact mode, and that this parameter is affected by the removal of charged glycans – most likely by triggering conformational changes.

4.2. Why do commercial mucins exhibit compromised lubricity?*

In addition to lab-purified mucins (which had been used in the two above mentioned studies), in the past, commercially available mucin variants, in particular commercial porcine gastric mucin (PGM; 'Type II' and 'Type III' from Sigma-Aldrich), were regularly used for research focusing on mucin lubricity. With those industrial mucins, however, results were obtained that were often very different from analogous experiments conducted with lab-purified mucins or native mucus.[10, 21, 171, 172]

Indeed, when the lubricity of mucin solutions reconstituted from either lab-purified MUC5AC or commercial PGM was probed in a constant contact setup, it was found that the MUC5AC variant exhibited excellent lubricity with friction coefficients below 10^{-2} over the entire range of sliding velocities encompassing five decades (**Fig. 4.3**). Importantly, in the boundary lubrication regime, *i.e.*, under conditions where the structural integrity of mucins affects the lubricity of mucin solutions the most, the friction coefficients determined with lab-purified MUC5AC samples were ~100-fold lower than those recorded with solutions constituted of repurified commercial PGM, which showed hardly any lubricity: compared to results obtained with a simple buffer solution alone (which returned a typical Stribeck curve; **Fig. 4.3**, gray curve), the mixed lubrication regime was only slightly shifted toward slower sliding velocities when commercial PGMs were added to the buffer solution. At slow sliding velocities (*i.e.*, in the boundary lubrication regime) the friction coefficient reached values of ~1 for both, simple buffer and PGM solutions (**Fig. 4.3**).

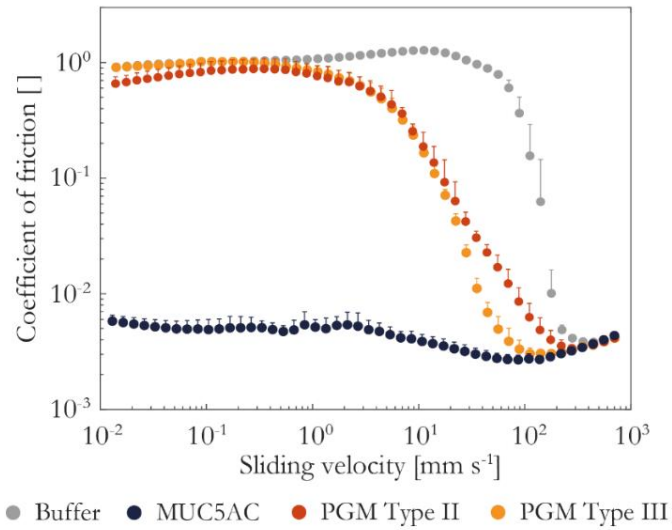

Fig. 4.3: Lubricity of lab-purified MUC5AC and commercial PGM variants Tribology measurements were performed with a steel/PDMS pairing in a ball-on-pins setup using different mucin solutions (0.1 % (w/v)) as lubricants. HEPES buffer devoid of any mucins is included as a reference (gray curve). Each point represents the mean value as obtained from three technical repetitions ($n = 3$) at a given sliding velocity and the error bars denote the corresponding standard error of the mean.

* This section follows in part the publications Marczynski *et al.*, Biomacromolecules (2021), and Marczynski *et al.*, Advanced Drug Delivery Reviews (2021).

Mucin solutions

Although having demonstrated that both PGM variants have lost the ability to lubricate surfaces, the origin of this loss in functionality was not evident. A parameter that is intimately related to the functionality of a lab-purified protein sample is its purity, and this may also apply to porcine gastric mucins. For instance, it was reported that, *in vitro*, the lubricating performance of lab-purified mucins could be impaired by the intentional addition of 'contaminating' proteins.[77] Indeed, gastric mucus, from which both, the commercial PGMs as well as the lab-purified MUC5AC, were obtained, is a mixture of various ingredients including a variety of proteins, lipids, carbohydrates, nucleic acids, and inorganic salts in addition to mucin glycoproteins.[5] When mucins are isolated in the laboratory by size exclusion chromatography (SEC), most of these additional mucus components can be removed (**Fig. 2.3 A**). Recording the absorption signal at a wavelength of 280 nm during mucin isolation from gastric mucus showed that mucins constitute only a minor fraction of the entire mucus proteome (**Fig. 2.3 A**). Owing to their high molecular weight, mucins were the first proteins to elute from the SEC column, and the corresponding peak in the chromatogram was clearly separated from the main elution peak, which was established by the remaining mucus protein components.[22] Interestingly, when re-purified by means of SEC, the commercial mucins also exhibited a second elution peak in the chromatogram (**Fig. 2.3 A**), which demonstrated that a considerable amount of protein impurities could still be removed from the commercial mucin preparations.

However, for the tribology experiments presented in **Fig. 4.3**, already the (re-)purified mucin variants were used. Thus, the purity of these purified preparations was also assessed – this time by means of an electrophoretic separation of the components on a polyacrylamide gel. All samples, lab-purified MUC5AC variants as well as the re-purified commercial PGMs, contained significant amounts of mucins as indicated by the distinct purple stains located in the pockets of the gel after a combined Coomassie/PAS (**Fig. 2.3. B**). However, when a highly sensitive silver staining procedure was applied to the polyacrylamide gels (instead of the less sensitive Coomassie staining), it was found that – even after (re-)purification – all mucin variants were still contaminated with small amounts of non-mucin components. A comparison of the band patterns obtained for the commercial PGM variants before (*i.e.*, 'PGM Type II/III crude') and after purification (*i.e.*, 'PGM Type II/III') verified the successful reduction of contaminants from those industrial PGMs. Considering the rich biochemical diversity of mucins (comprising anionic, cationic, and hydrophobic residues) it is not surprising, that the purified mucins still contained other molecules. Mucin glycoproteins cannot only interact with each other, but also with other proteins and small molecules through both transient and covalent bonds.[173, 174] Since the SEC step conducted as part of the purification procedure was performed at mild conditions (*i.e.*, without the addition of reducing or denaturing agents to the running buffer and at room temperature), the mucins might still have been associated with small amounts of other mucus

components. Only the harsh reducing and denaturing conditions during the sample preparation for polyacrylamide gel analysis allowed for efficient unbinding and subsequent electrophoretic separation of the mucin-associated molecules, which had eluted together with mucins during SEC.

Since this purity analysis did not yield a satisfying explanation for the loss in lubricity that had been measured for the two commercial PGM variants, next, the adsorption behavior of all mucin variants onto the two types of surfaces used in tribology experiments was assessed. It was found that adsorption of MUC5AC onto PDMS induced very pronounced frequency shifts of ~400 Hz. In contrast, the shifts in resonance frequency induced by the two PGM variants upon adsorption were ~2−2.5 times smaller (**Fig. 4.4**).

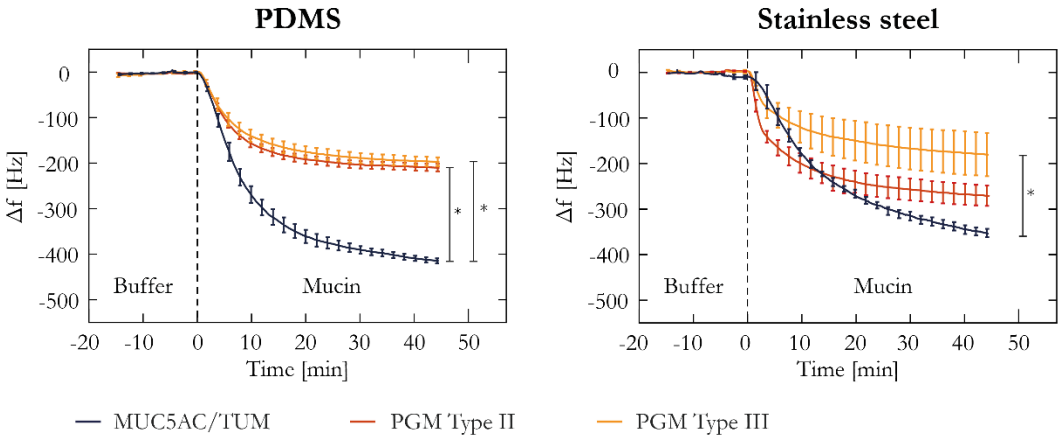

Fig. 4.4: Comparison of the adsorption behavior of lab-purified MUC5AC and the two re-purified PGM variants onto hydrophobic and hydrophilic surfaces. QCM measurements report the frequency shift resulting from the adsorption of mucins onto PDMS and steel surfaces, respectively. For both surface types, the adsorption signal was strongly reduced for the two PGM variants compared to MUC5AC. Each curve represents an average curve as obtained from three technical repetitions per condition ($n = 3$); the error bars denote the corresponding standard error of the mean. Asterisks indicate statistically significant differences ($p < 0.05$) between the different mucin variants as calculated for the final frequency shift determined after 45 min of mucin adsorption.

The strength of such a shift in resonance frequency detected in QCM measurements directly correlates with the mass of the molecular layer adsorbed onto the sensor surface.[175] In principle, differences in molecular weight between commercial and lab-purified mucins (either due to the binding of contaminants such as DNA or from the partial degradation of the mucins) could explain the differences in the amounts adsorbed onto PDMS. However, such differences in molecular weight would have led to similar differences in the QCM signal when mucin adsorbed onto stainless steel surfaces. Yet, this was not the case: the relative difference was smaller on steel than on PDMS (**Fig. 4.4**). Thus, the poor adsorption behavior of commercial mucins onto PDMS surfaces probably

rather reflected reduced levels of hydrophobic interactions with the hydrophobic PDMS surface. Since hydrophobic motifs are predominantly located in the mucin termini, such a picture would be consistent with the hypothesis that the termini of commercial mucins are either inaccessible due to conformational changes or (at least partially) absent.[176] If the first scenario were to be true, the results on simulated mucins suggest that strong structural alterations within the backbone of the commercial mucins should be present (**Fig. 3.6**). In any case, the results obtained during QCM measurements would underscore the notion that commercial mucins might have lost some critical moieties, which are crucial for their adsorption and lubrication abilities.

To challenge the hypothesis that the commercial mucins were structurally altered, the reactivity of a monoclonal antibody against coatings generated from the three mucin variants was probed in an indirect ELISA. To compensate for the reduced adsorption abilities of the commercial PGMs and to ensure sufficient coating densities for all three variants, the mucins had been covalently coupled to the bottoms of the wells of a microtiter plate. Indeed, this coupling method yielded surface layers with comparable coating densities for all mucin variants (**Fig. A4.7**). The ELISA returned a strong signal for lab-purified MUC5AC but hardly any signal for the two commercial PGMs – the relative absorption values obtained for the PGMs were by two orders of magnitude smaller than the one measured for MUC5AC (**Fig. 4.5 A**). Since the coating densities obtained for the three mucin variants were all on the same order of magnitude, the low signals detected for the two PGM variants were not due to a smaller amount of PGM molecules on the well plate (compared to lab-purified MUC5AC). Instead, this assay indicated that the antibody, which was directed against a distinct motif located in the mucin C-terminus[90], was unable to bind to the PGM molecules.

The picture that has emerged so far would be consistent with the idea that the two PGM variants had lost their non-glycosylated termini. Direct information on the structural integrity of the different mucin variants as well as on the protein composition of the samples could be obtained by detecting peptide fragments in mass spectrometric analyses originating from a trypsin treatment (**Appendix A1**). For mucin glycoproteins, the most peptide fragments were expected to originate from the terminal regions of mucins as the dense glycosylation of the mucin core was shown to shield this domain from proteolytic digestion.[40]

By matching all peptide hits detected during the mass spectrometric analysis against a porcine proteome database, it could be verified that all three mucin samples contained gastric mucins – among several other proteins (**Fig. A4.5 B** & **Tables A1.1**-**A1.3**). Next, the total numbers of matches assigned to each protein in each of the three samples, for which at least three hits had been detected, were compared. In the case of the MUC5AC sample, gastric mucin 5AC by far outnumbered all other

detected proteins and thus scored first: ~29 % (with 217 out of a total of 743 matches) were assigned to gastric mucin 5AC (**Fig. 4.5 B** & **Table A1.1**). In contrast, in the two PGM samples, gastric mucin only occurred on the eighth place (with 5 out of a total of 70 matches) and ninth place (with 9 out of a total of 172 matches), respectively, on the list of detected proteins (**Fig. 4.5 B** & **Tables A1.2** & **A1.3**).

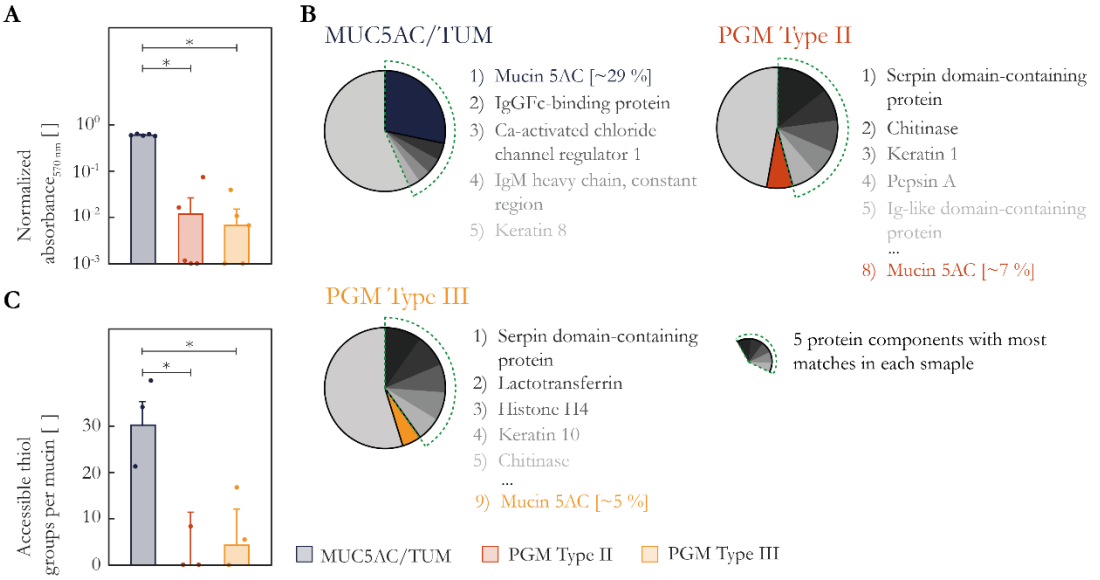

Fig. 4.5: Assays to assess the structural integrity of the three different mucin variants. An ELISA was performed to test for the presence of the terminal domains *via* binding of an anti-MUC5AC antibody. The error bars represent the standard error of the mean as obtained from five independent samples ($n = 5$). The asterisks indicate significant ($p < 0.05$) differences (**A**). Mass spectrometric analysis of the three mucin variants: during mass spectrometric analysis ~29 % of all detected peptide fragments were assigned to gastric mucin 5AC in the sample containing lab-purified MUC5AC. However, only ~7 and ~5% of all detected matches were assigned to gastric mucin 5AC in the PGM Type II and Type III samples, respectively (**B**). Accessible thiol groups located in the mucin termini were quantified spectroscopically. The error bars represent the standard error of the mean as obtained from three individual samples ($n = 3$), and asterisks indicate significant ($p < 0.05$) differences (**C**).

At this point, it is important to note that the numbers of peptide fragments detected for the different proteins in each sample did not reflect the exact quantitative composition of the three mucin preparations due to two reasons: first, since the proteins in the mucin samples came in various sizes (and thus with different numbers of target sites for tryptic digestion), the number of peptide fragments that could be theoretically obtained during sample preparation varied between different proteins. Second, the dense glycosylation of the mucin core region affected the result of the trypsin treatment; the glycosylated domain was efficiently protected from proteolytic degradation. Both their large size and the presence of posttranslational modifications (*i.e.*, the mucin glycan chains) rendered

the identification of such non-fragmented mucin cores challenging. Hence, only mucin peptides which originated from cleavable mucin domains, *i.e.*, the mucin termini, could be detected. In fact, it can be speculated that the total amount of mucins (whether fully intact or not) might have been drastically underestimated in all samples.

Next, the amino acid sequences of all peptide fragments that had been assigned to gastric mucin in each sample were compared with the amino acid sequence that is deposited in the porcine proteome database for gastric mucin 5AC (accession number A0A287ANG4; 07/24/2021). A sequence coverage value of ~24 % was obtained for lab-purified MUC5AC (**Figs. A1.1** & **A1.4**). For the two PGM samples, however, sequence coverage values of only ~0 % and ~2 % were obtained (**Figs. A1.2** & **A1.4**). At this point, it has to be emphasized that the amino acid sequence deposited in the porcine proteome database for gastric mucin 5AC did most likely not cover the full length of the actual amino acid sequence. Indeed, when the amino acid sequence of this entry is compared to the one that is predicted for porcine gastric mucin based on a computational analysis of the respective genomic sequence (NCBI Reference Sequence XP_020938242; 24/07/2021), large sections of the reported sequence are not covered by the amino acid sequence deposited in the UniprotKB database (**Fig. A1.3**). In fact, the database entry covers only 3330 amino acids, whereas the computed sequence has a predicted length of 5809 amino acids. The database sequence comprises mainly the mucin termini, whereas large sections of the glycosylated core protein are not covered (**Fig. A1.3**). With this fact in mind, the sequence coverages values were determined again – however, this time, only the mucin termini were taken into account (as these sections of the computed amino acid sequence are reliably covered by the database entry). As terminal domains, those regions were defined, for which von-Willebrand domains are reported and which are devoid of serine/threonine tandem repeats (**Figs. A1.1** & **A1.2**). By doing so, an even larger sequence coverage value of ~32 % was obtained for lab-purified MUC5AC. In contrast, the sequence coverage values determined for the two PGM variants remained negligibly small (~1 % and ~2%, respectively; **Fig. A1.4**). This detailed analysis of the mass spectrometric data confirmed the hypothesis that the two PGM variants, indeed, are likely to have almost entirely lost their terminal domains.

To support the results obtained by ELISA and the mass spectrometric analysis, the numbers of accessible thiol groups in the three mucin variants were quantified. This experiment was based on the following rationale: If the mucin termini were to be absent, the number of accessible thiol groups can be expected to be lower in such damaged mucins than in structurally intact mucins, since the vast majority of cysteines (*i.e.*, the amino acid residues carrying thiol groups) is located in the mucin

termini. Indeed, significantly larger numbers of such accessible thiol groups per mucin molecules were measured for lab-purified MUC5AC than for the two commercial PGM variants (**Fig. 4.5 C**).

Together, ELISA, mass spectrometric analysis, and the thiol quantification assay indicated that the commercial PGM variants have (almost entirely) lost their terminal domains. Indeed, the vendor, from which the commercial PGMs were purchased, states on the corresponding product pages that the PGM variants were obtained from hog stomachs by treatment with the protease pepsin (followed by other purification steps; https://www.sigmaaldrich.com, product numbers M2378 & M1778, accessed on 08/24/2021). It is reasonable to assume that – similar to trypsin – pepsin might have cleaved most of the stomach proteins and peptides into small fragments including the non-glycosylated (= unprotected) termini of the mucin molecules. Of course, it cannot be ruled out that some PGM molecules may still carry remnants of their terminal peptide sequences.

4.3. Probing binding interactions established by commercial mucins*

In addition to providing lubricity, mucus also establishes an important barrier toward pathogens. The defense strategy of mucus is – at least in part – based on the ability of mucins to establish binding interactions with intruding bacteria or viruses, thus preventing them from reaching the tissue surface.[10, 16, 177, 178] Having shown that commercial mucins have lost their non-glycosylated termini, they can be expected to interact with unspecific binding partners in a different manner than intact, lab-purified mucins. This expectation is based on the realization that cationic residues in the mucin glycoprotein are mostly located in those non-glycosylated domains of the mucin molecules. Interestingly, when a depletion assay was performed with the three dextran variants used before (*i.e.*, cationic, neutral, and anionic ones), only subtle differences in the dextran binding behavior could be detected between lab-purified and commercial mucin variants (**Fig. 4.6**).

All three mucin variants depleted cationic and anionic dextrans significantly better than neutral dextrans (which, as expected, did not interact strongly with mucins; **Fig. 4.6**). This finding was somewhat surprising for the two PGM variants considering that these mucins have lost their terminal domains. Only in these termini, however, cationic binding sites should have been accessible for the binding of anionic dextrans – in the central region of the mucins, cationic amino acid residues are typically shielded by the dense glycosylation pattern. Thus, this outcome suggested that not only the

* This section follows in part the publication Marczynski *et al.*, Biomacromolecules (2021).

terminal domains of commercial mucins might have been damaged during the purification of commercial PGMs. In addition, also the mucin glycan chains might have been affected such that parts of the protein backbone became exposed and were thus accessible for anionic dextrans.

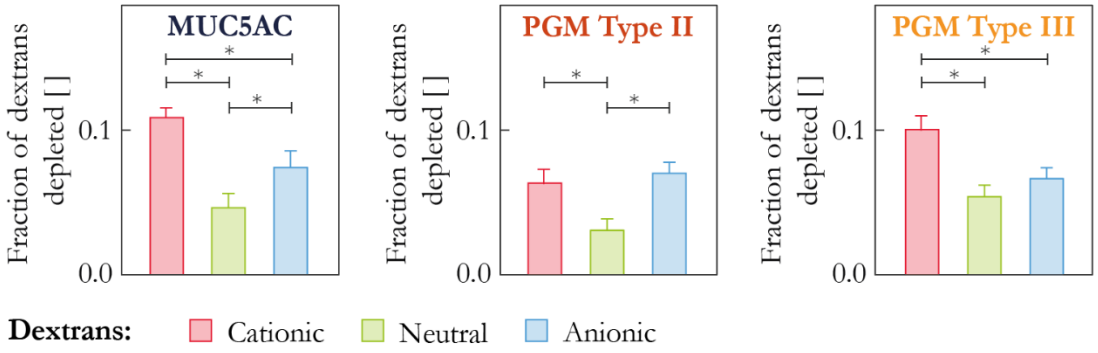

Fig. 4.6: Depletion of dextrans from solution by surface-attached mucin layers. Binding of cationic, neutral, and anionic dextrans to covalently linked mucin surface layers was compared for the three mucin variants MUC5AC, PGM Type II, and PGM Type III. The error bars represent the standard error of the mean as obtained from four individual samples ($n = 4$). Asterisk mark significant differences ($p < 0.05$).

Considering that glycan chains account for ~80-90 % of the molecular mass of mucins, it was expected that such damages of the mucin glycosylation would lead to differences in the molecular weight between commercial PGM and lab-purified MUC5AC. In the past, a broad spectrum of values ranging from ~1 MDa to up to ~15 MDa was reported for the molecular weight of gastric mucin.[179-181] Of course, the outcome of such measurements depends on the purity (and structural integrity) of the mucins and the technique used to estimate the molecular weight. In this thesis, the molecular weights of the different mucin variants were estimated by means of SEC-MALLS (size exclusion chromatography coupled with multi-angle laser light scattering). A significantly larger molecular weight of ~9.1 MDa was determined for lab-purified MUC5AC than for the two PGM variants (~2.4 and ~2.5 MDa, respectively; **Fig. A1.5 A, B**). Since the protein backbone alone accounts for only ~0.6 MDa, these differences in molecular weights indicated that, indeed, the glycan chains of the commercial PGMs might have been altered, too. To verify this notion, in a next step, the glycan chains of all mucin variants were chemically removed from the protein backbone, broken down into monosaccharide units, and subsequently quantified using HPAEC-PAD (high-performance anion-exchange chromatography with pulsed amperometry detection). Indeed, although the determined ratios of the individual monosaccharides were relatively similar for the different mucins, lab-purified MUC5AC, by far, comprised larger total amounts of glycans than the two commercial PGM variants (**Fig. A1.5 C**).

The alterations in the quantities (and types) of saccharides were also reflected by a lectin binding assay, in which the capability of covalently bound mucin layers to deplete fluorescently labeled lectins (**Fig. 4.7**) with various sugar binding affinities from aqueous solutions was assessed.

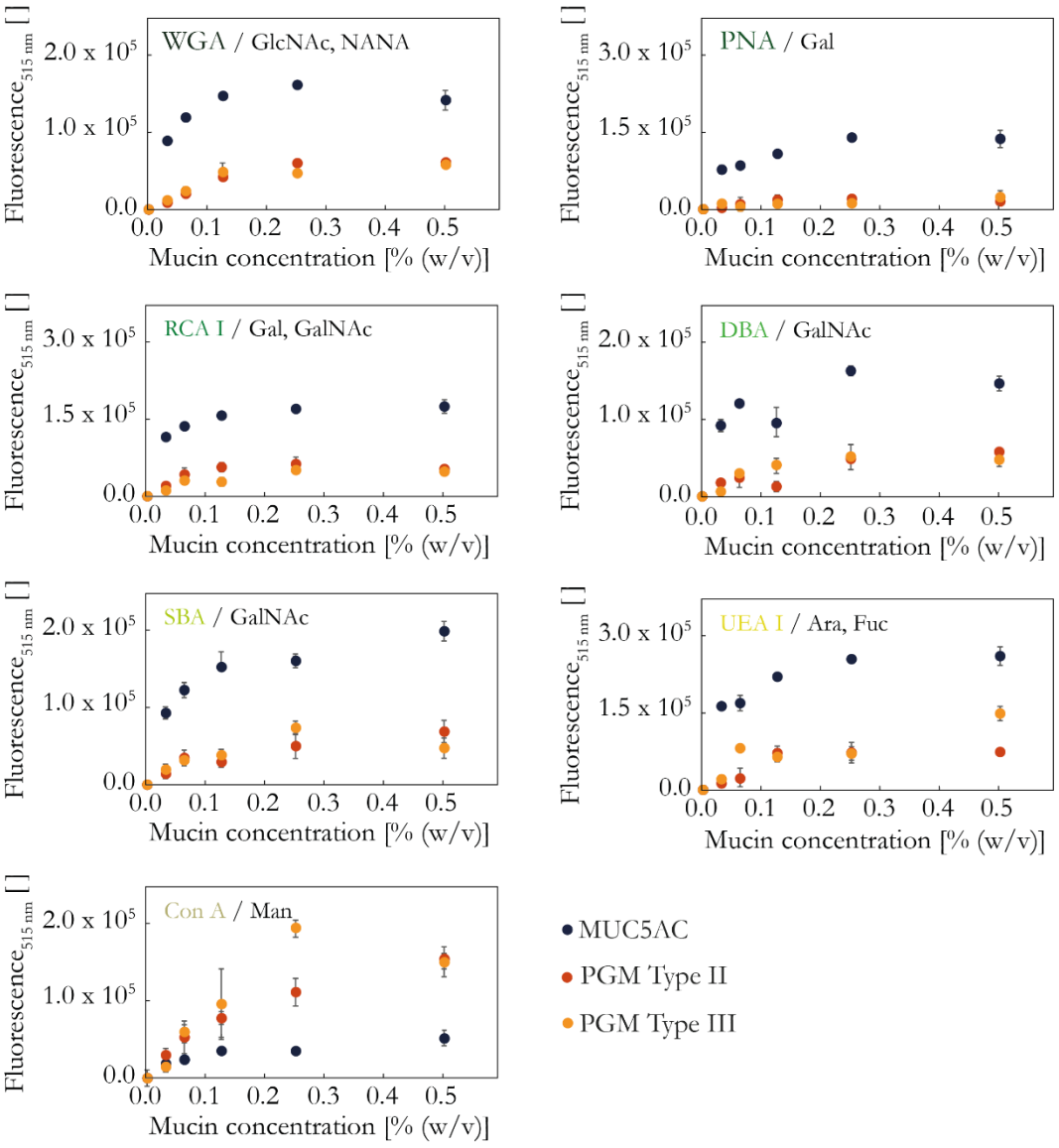

Fig. 4.7: Lectin binding assay. The saccharide-specific binding of a panel of seven lectins to seven different saccharide motifs, which typically constitute the glycan chains of glycoproteins, was probed for surface-bound mucin layers. The fluorescence intensity of the depleted, mucin-attached lectins was correlated with the amount of depleted lectins. At each probed mucin concentration a similar experimental outcome was observed. The error bars represent the standard deviation as obtained from four ($n = 4$) individual experiments. To account for differences in surface coating density, the data points have been corrected accordingly.

Mucin solutions

A panel of seven different lectins was used, which targeted, in total, seven different saccharide motifs: arabinose (Ara), fucose (Fuc), galactose (Gal), mannose (Man), *N*-acetylgalactosamine (GalNAc), *N*-acetylglucosamine (GlcNAc), and *N*-acetylneuraminic acid (NANA). The majority of the employed lectin variants bound in significantly higher numbers to lab-purified MUC5AC coatings than to commercial PGM coatings – independent of the mucin concentration used to generate the (covalent) surface coatings. An exception was the lectin concanavalin A (Con A), which has a high affinity for terminal mannose residues;[182] this lectin bound in large amounts to both commercial PGM variants but only in small numbers to lab-purified MUC5AC. This result suggested that mannose moieties might have become exposed and accessible to lectin binding due to alterations in the glycan composition during the extraction and purification of commercial PGM.

Interestingly, for this assay, the strongest signals were not necessarily obtained for those saccharides, which were identified to be the most abundant in the mucin glycosylation pattern (**Fig. A1.5 C**). For instance, in the case of lab-purified MUC5AC, the assay returned higher values for fucose residues (which were targeted by the lectin UEA I) than for *N*-acetylglucosamine (to which the lectin WGA bound). This can be rationalized as follows: Lectins did not report on the total glycan composition but rather on the occurrence of glycan moieties terminating the mucin glycan chains. Owing to the dense decoration of the mucin protein backbone with glycan chains, the accessibility of basal target sites located closer to the mucin backbone might have been strongly limited.

As demonstrated by the results presented in this and the previous subchapter (**Chapter 4.2**), commercially available porcine gastric mucins are structurally damaged. As a consequence, model systems reconstituted from these commercial mucins were unable to reproduce the physico-chemical properties of native mucus. For instance, these commercial PGMs have lost their ability to lubricate surfaces (**Fig. 4.1**).[172, 183] Moreover, it has been reported that these commercial mucins fail to form hydrogels at acidic conditions.[20, 21] As these terminal domains were shown to be particularly important for mucins to undergo a sol-gel transition, this further supports the notion that the terminal sequences of commercial mucins were removed during the purification procedure.[34, 76, 152] Accordingly, results obtained with such damaged mucins are questionable, at best. Unfortunately, these commercial mucin variants are still routinely used for research purposes – regardless of their poor quality.[184-186]

5. Mucin hydrogels

In an aqueous environment, secreted mucins can assemble into polymeric networks. This assembly process is driven by the formation of both, transient and covalent intermolecular bonds established by hydrophobic interactions, attractive electrostatic interactions, hydrogen bonds, and disulfide bridges. A key parameter that dictates if mucins form such a network (*i.e.*, a hydrogel) is the concentration of mucins in the mucosal system: higher mucin concentrations allow for an increased number of inter-mucin interactions, and thus the formation of an interconnected network is more likely.[187] Indeed, in gastrointestinal, cervical, and airways mucus (where mucus occurs as hydrogels), the mucin concentration is on the order of ~1-5 %.[31, 45, 46] Sellers *et al.* found that hydrogels reconstituted from lab-purified gastrointestinal mucins at physiological concentrations exhibited viscoelastic properties comparable to those of native mucus.[188] The viscoelastic properties of a mucin-based system, however, depend also on a number of other factors including the concentration of certain ions such as calcium,[189-191] variations in pH,[75, 189] or the presence of other molecules, which are able to act as cross-linkers between mucin fibers.[192-194] In this context, an additional level of complexity is introduced by the fact that all of the parameters discussed above can vary depending on the location of the respective mucosal system in the human body and the health state of the individual.[195, 196] For instance, in patients suffering from cystic fibrosis, the mucin concentrations in airway mucus can be up to 3 times as high as those found in healthy individuals.[196, 197] Accordingly, the elasticity of these mucus hydrogels is abnormally high, since a higher number of mucins allows for an increased occurrence of inter-mucin interactions.[198] Such diseased mucus barriers, however, might not be able to fulfill their physiological functions.

5.1. pH-dependent sol-gel transition of mucin preparations*

Physiologically, mucus hydrogels cover all epithelial tissues and establish the first line of defense intruding pathogens encounter when they enter the human body. Here, mucin glycoproteins are the key structural components that constitute the scaffolds of such mucus gels. Of course, when working with a mucus gel model system, this model should also be able to recreate the ability to form a hydrogel. Accordingly, in addition to good lubricity, also the ability to transition from a solution into a gel was proposed as a criterion for good quality of a mucin preparation. Experimentally, the

* This section follows in part the publications Marczynski *et al.*, Biomaterials Science (2018) & Marczynski *et al.*, Biomacromolecules (2021).

conversion from a mucin solution into a hydrogel can be initiated by a decrease in pH; this sol-gel transition typically takes place at pH values of ~4 and below.[75, 76, 199] Indeed, at a neutral pH level (pH 7.0), aqueous preparations containing either lab-purified intestinal mucin MUC2 or gastric mucin MUC5AC were both dominated by their viscous properties, *i.e.*, they were present as viscoelastic solutions (**Fig. 5.1 B**). When the pH was reduced to an acidic level (pH 4.0), it was found that the mucin preparations were dominated by their elastic properties over the entire range of probed frequencies, *i.e.*, they successfully transitioned into hydrogels (**Fig. 5.1 A**).

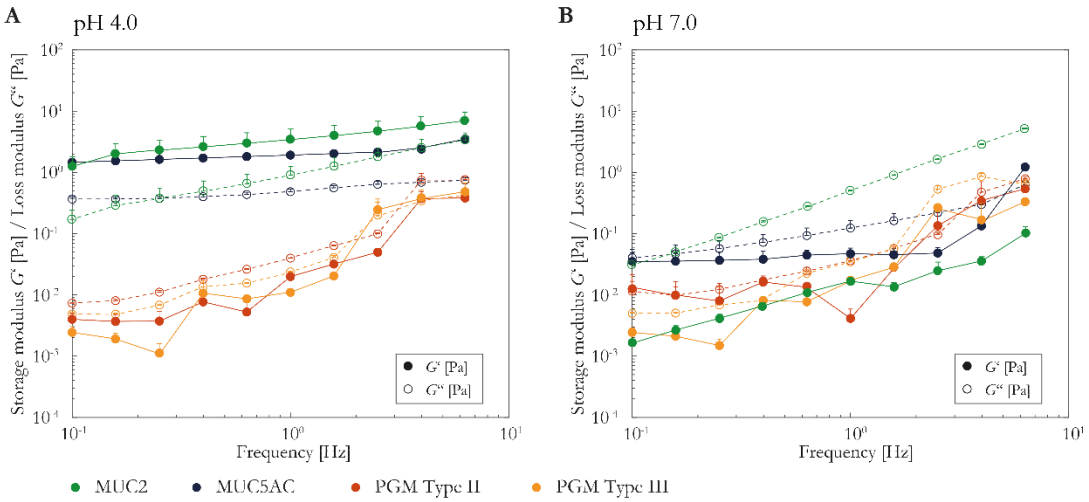

Fig. 5.1: pH-dependent gelation of solutions reconstituted from lab-purified mucins (MUC2, MCU5AC) or commercial gastric mucin. The viscoelastic frequency response of mucin samples is shown for both acidic (pH 4.0) and neutral (pH 7.0) buffer conditions. Closed symbols and solid lines denote the storage modulus *G'* and open symbols and dashed lines the loss modulus *G"*. Error bars represent the standard error of the mean as obtained from three independent measurements ($n = 3$).

Decreasing the pH from neutral to acidic values of ~4.0 led to an increase in the viscoelastic moduli of these mucin preparations by ~2 orders of magnitude (**Fig. 5.1**) – and similar shifts were reported in the literature.[75, 200] Here, the gel formation is thought to be induced by local conformational changes of the mucin glycoprotein, which occur in response to the reduction of the pH level to 4.0.[76] Such changes in conformation can be explained by the protonation of the carboxyl groups in the side chains of glutamic acid and aspartic acid residues in the mucin termini. In their protonated, *i.e.*, charge-neutral state, carboxyl groups are unable to engage in intramolecular salt bridges with cationic amine groups, which may cause the mucin termini to unfold. Such an unfolding of the mucin molecule results in the exposure of hydrophobic regions and free thiols, which are hidden in the conformation of the protein at neutral pH levels.[34, 76] These now exposed binding sites, in turn, allow for inter-mucin crosslinking *via* hydrophobic interactions and the formation of disulfide bridges.[34]

Indeed, the importance of both, hydrophobic interactions and disulfide bonds between mucins for the formation of a mucin network has been demonstrated before: for instance, eliminating hydrophobic interactions by adding surfactants to a mucin gel reduced its viscoelastic moduli.[189] Moreover, decreasing the number of disulfide bonds by adding reducing agents resulted in a reduction of the viscoelastic moduli of native mucus.[201, 202] On the other hand, mucus barriers could be reinforced by an exposure to oxidizing agents, which facilitated the formation of additional disulfide bonds.[203]

Of course, to a certain degree, also the viscoelastic properties of mucins are subject to batch-to-batch variations. For instance, a different batch of lab-purified MUC5AC* formed hydrogels even at a neutral pH of 7.0. The elastic modulus of this particular mucin hydrogel further increased upon acidification reaching shear moduli on the order of ~30 Pa (determined at an oscillating frequency of 1 Hz; **Fig. A4.8**). Such an atypical gelation behavior, *i.e.,* the domination of elastic properties at neutral pH levels, typically hints towards the presence of cross-linking agents in the mucin sample, which facilitate the formation of a polymeric network even at neutral pH; such an explanation might also apply to the mucin batch in question. In fact, several authors have reported before that different isotypes of immunoglobulins (IgA, IgG, and IgM) can form cross-links between individual mucins on the one hand and between mucins and other objects such as viruses on the other hand.[204-206] In agreement with this notion, a higher content of those immunoglobulins was detected in MUC5AC/KTH (~5.0 %) than in MUC5AC (~3.4 %; **Tables A1.1** & **A1.4**). A second factor contributing to the variability of the viscoelastic properties of mucins might be the mucin glycan pattern, which is also subject to a certain degree of intrinsic biological variation.[207, 208] Such variations in mucin glycosylation may result in slight differences in mucin conformation, which, in turn, can affect the binding capability toward other molecules – including inter-mucin interactions.[127]

A different picture emerged for the two commercial PGM variants: independent of the sample pH, preparations of the two commercial PGM variants were dominated by their viscous properties at all tested frequencies, *i.e.*, they remained in the 'sol' (= solution) state and did not transition into hydrogels in a pH-dependent manner (**Fig. 5.1**). This finding is in accordance with several previous studies, which reported that commercial PGM does not form hydrogels but remains a viscoelastic solution.[20-22] The loss of the ability to form hydrogels in a pH-dependent fashion can be rationalized by the absence of the terminal mucin domains: as outlined above these domains are critical to establish inter-mucin interactions, which drive gel formation. Since both, hydrophobic domains and

* MUC5AC/KTH: This particular batch of MUC5AC was purified in the lab of Prof. Dr. Thomas Crouzier (Division of Glycoscience) at the Royal Institute of Technology (KTH) in Stockholm, Sweden.

thiol groups, are mostly present in the mucin termini, the PGM mucins were unable to form cross-linked mucin networks.

5.2. Charge-dependent barrier properties of mucin hydrogels*

Physiologically, mucus systems serve as physical barriers towards the entrance and distribution of pathogens. In addition, mucus barriers in the gastrointestinal tract regulate the passage of drugs, nutrients, and further beneficial molecules.[5, 9] To achieve those functions, the apical surface of mucosal epithelia is lined with a mucus hydrogel (**Fig. 5.2**). The thickness of such layers as well as the expression profiles of the corresponding mucin genes vary between different mucosal tissues.[25]

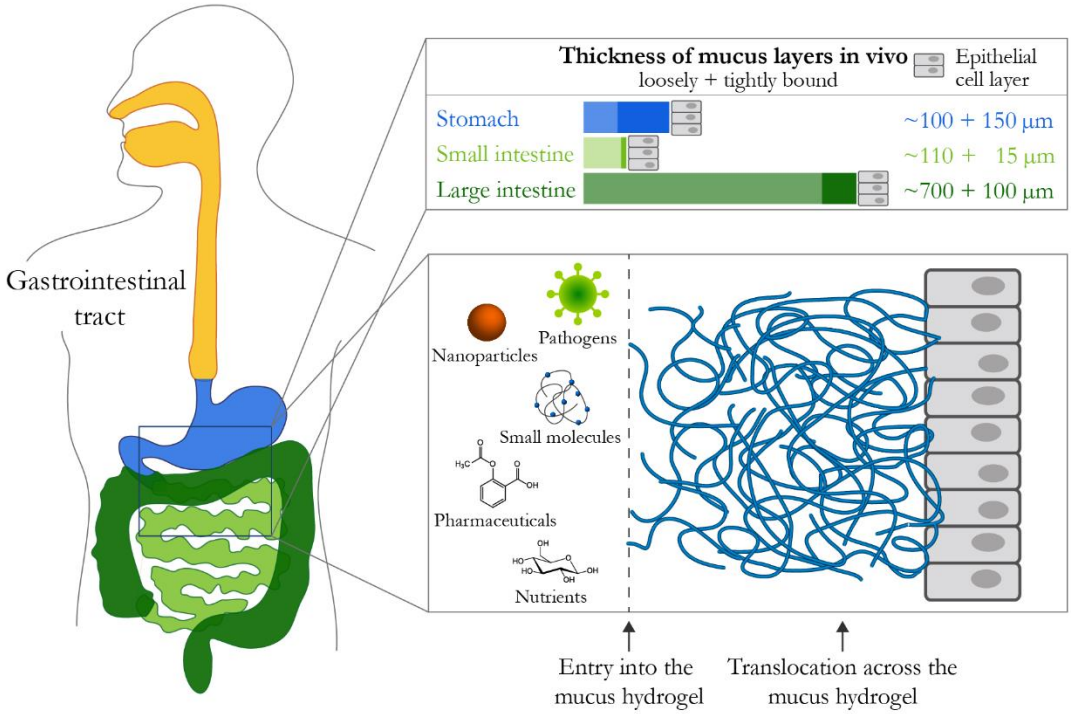

Fig. 5.2: Mucosal barriers in the gastrointestinal tract. Mucosal tissues at different locations in the human body exhibit mucus layers with distinct thicknesses. Those mucosal barriers consist of a thin, tightly bound layer adjacent to the epithelial cell surface (indicated in dark color) and a thick, loosely bound mucus layer located at the luminal end of the mucosal tissue (indicated in lighter color). The mucus barriers regulate the passage of molecules (including nutrients and drugs) and particles (such as viruses of nanoparticles).

* This section follows in part the publications Marczynski *et al.*, Biomaterials Science (2018) and Jiang *et al.,* Advanced Functional Materials (2021).

Mucin hydrogels

In the stomach, MUC5AC is the most abundant mucin; here, it forms mucus layers with a total thickness of ~250 μm (**Fig. 5.2**).[209] Across these gastric mucus layers, a pH gradient is maintained (*i.e.*, strongly acidic luminal pH and neutral pH at the apical side of the epithelial cell layer) by continuous secretion of bicarbonate ions.[210] Such pH gradients serve as buffering barriers for the protection of the gastric mucosa against the harsh conditions in the stomach. In contrast, intestinal mucus mainly comprises MUC2 and exhibits a typical thickness of ~100 μm in the small intestine and up to ~800 μm in the large intestine, respectively (**Fig. 5.2**).[211-213]

The human body continuously secrets and sheds mucus to ensure the removal of trapped pathogens and noxious particles. Mucus turnover times vary considerably between different sites of the gastrointestinal tract. For instance, in the case of intestinal mucus, this turnover time is estimated to be in the range of one to a few hours.[7, 214] This mucus renewal mechanism is crucial for maintaining the protective function of this hydrogel barrier.[215] At the same time, however, it renders the transport of pharmaceuticals across this layer challenging, since drug molecules need to migrate 'upstream' through the self-renewing mucus layer to reach the epithelial layer where they can be resorbed by the cells. Indeed, efficient and targeted administration of pharmaceuticals is, to date, one of the most challenging tasks modern medicine has to deal with as the mucus turnover times set the time scale at which pharmaceuticals need to achieve diffusive transport across the mucus layer. It has been postulated that inert, non-mucoadhesive objects were always more efficient in penetrating mucin hydrogels than charged objects.[216-218] So far, most research in the field of mucus permeability, however, made use of nanoparticle systems. Systematic experimental studies analyzing the mucus penetration behavior of small molecules, *e.g.*, drug molecules, as a function of their physico-chemical properties are, to date, rare. In fact, it is *a priori* not clear if the mucosal transport of small molecules follows the same physico-chemical principles that govern the transport of nanoparticles. Thus, in the next section of this thesis, the penetration of hydrogels reconstituted from either intestinal mucin MUC2 or gastric mucin MUC5AC (which served as model systems for intestinal mucus and gastric mucus, respectively) by fluorescently labeled dextran molecules was investigated. In these experiments, the focus was on charge-dependent effects, which is why cationic, electrostatically neutral, and anionic dextrans were used as simple molecular probes.

From a technical perspective, this called for a different experimental approach then those typically used to study the permeability properties of hydrogels: whereas particle tracking is a suitable approach for characterizing the diffusion of nanoparticles in hydrogels, this is not feasible with small molecules. Moreover, single particle tracking is typically performed with particles that are artificially embedded into a hydrogel.[219-222] Thus, this technique does not take into account partitioning effects, *i.e.*, the entry process of objects into the hydrogel barrier. However, this molecular entry is the first step of

the mucus penetration process and is suspected to critically influence the translocation efficiency of a molecule ensemble.[223] To overcome this limitation, in this thesis, a microfluidics setup was employed as an experimental platform. In such an *in vitro* environment, a stable gel/liquid interface could be generated on-chip, which allowed for the spatio-temporal analysis of both, the molecular entry into and the molecule translocation processes across mucin hydrogel barriers.[52, 224]

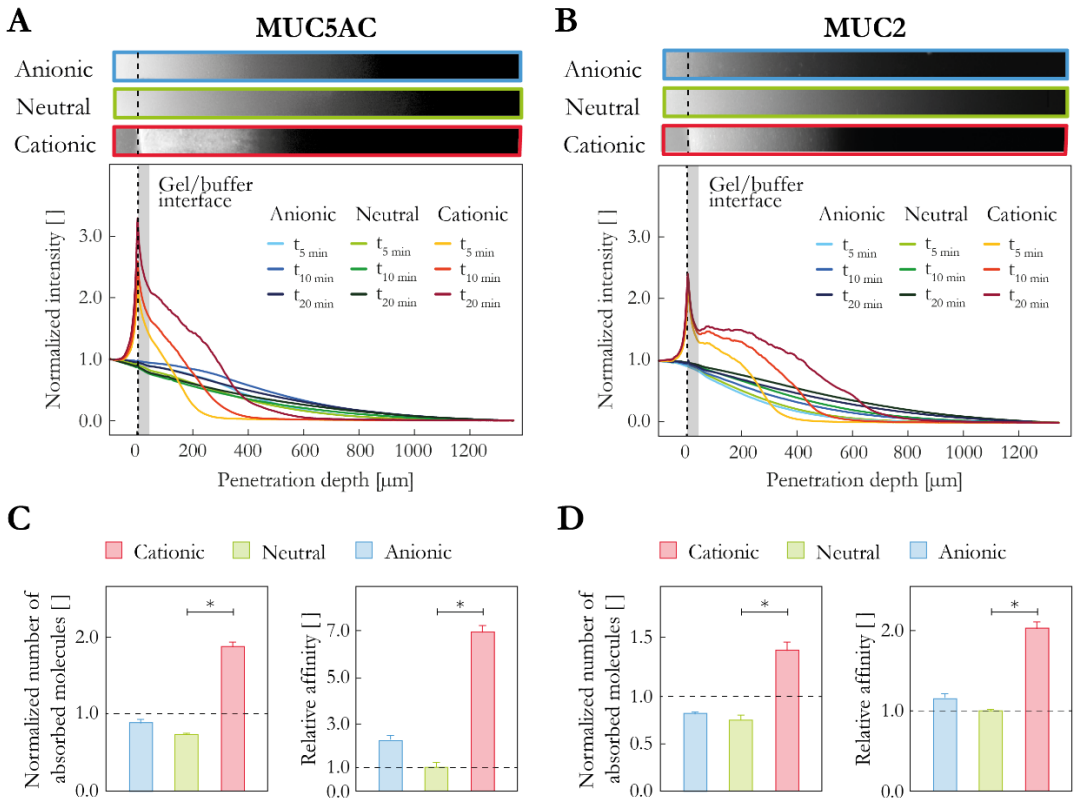

Fig. 5.3: Penetration behavior of different dextran variants into mucin hydrogels. The barrier properties of mucin hydrogels reconstituted from MUC5AC were compared to those of hydrogels comprising MUC2 (**A**, **B**). Different variants of fluorescently labeled dextran molecules were used as molecular probes, and typical fluorescence images corresponding to the profiles shown in the graph are depicted in the top part of subfigures **A**) and **B**), respectively. The number of dextran molecules that penetrated the hydrogel within the first 10 min of the experiment was normalized to the number of molecules that would be present in the first 50 µm of the mucin gel (shaded in gray) if the local dextran concentration in the gel would be identical to that in the buffer reservoir (indicated by the dashed horizontal line in **C**) and **D**), left). The error bars denote the standard error of the mean as obtained from analyzing at least seven 'fingers' each ($n \geq 7$), and asterisks indicate statistically significant differences ($p < 0.05$). The binding affinities of the three dextran variants to mucins were determined by a dextran depletion assay, and the values were normalized to that of neutral dextrans (indicated by the dotted horizontal line in **C**) and **D**), right). The error bars denote the standard error of the mean as obtained from five wells each ($n = 5$), and asterisks indicate statistically significant differences ($p < 0.05$).

Mucin hydrogels

To study the diffusive entrance of dextran molecules into a mucin hydrogel, a well-defined and stable interface between the liquid donor compartment and the hydrogel was required. Such an interface was achieved by using a microfluidics chip comprising finger-like structures (**Fig. 2.7**), in which the mucin hydrogels were generated *in situ* by injecting an acidic buffer solution into the 'reservoir' of the chip. Protons from this buffer were allowed to diffuse into the mucin solution, and this reduction in pH induced mucin gelation on chip (compare **Chapter 5.1**).

With this stabilized mucin gel/liquid interface, molecular penetration experiments were performed using fluorescently labeled test molecules that were injected *via* one of the inlets of the 'test reservoir'. As a molecular platform for these experiments dextrans with molecular weights of ~4 kDa were used. The rationale for this choice was as follows: dextrans are relatively inert macromolecules which, by themselves, do not carry any charged or hydrophobic moieties. However, they can be chemically modified such that they become either positively or negatively charged. The former was achieved by grafting diethylaminoethyl (DEAE) groups to the polysaccharide, whereas the latter was realized by grafting carboxymethyl (CM) groups to the dextran macromolecule. Moreover, the hydrodynamic radii of those dextrans are all in the range of a few nanometers and thus about two orders of magnitude smaller than the mesh size of mucin gels formulated at the mucin concentrations used here.[225] This ensured that geometric hindrance effects as responsible for the trapping of comparatively large polystyrene particles described before can be neglected for the penetration process of dextrans into mucin gels.

When determining the penetration profiles of unmodified (= uncharged) dextran molecules penetrating hydrogels reconstituted from MUC5AC, a roughly exponential decay of fluorescence intensity with increasing penetration distance was observed (**Fig. 5.3 A**, green curves). Such a profile is consistent with an unrestricted diffusion of the dextran molecules from a reservoir with a high, constant molecule concentration into a compartment with absorbing boundary conditions at its far end, *i.e.*, a 'sink' as represented by the relatively large volume of the 'hand' structure filled with mucins. A similar behavior was obtained for CM dextrans (**Fig. 5.3 A**, blue curves), although a slight 'shoulder' in the penetration profiles was present here. In marked contrast to those rather feature-less penetration profiles, for cationic DEAE-dextrans, a pronounced accumulation peak at the liquid/gel interface was obtained (**Fig. 5.3 A**, red curves). Within the time frame of the experiments conducted here, *i.e.*, within 20 min after the test molecules had been injected, the height of this accumulation peak seemed to increase with time. This, however, was an artifact arising from the normalization of the penetration profiles to the fluorescence intensity in the buffer compartment, which had been applied to compensate for photobleaching effects (**Fig. A4.9**: non-normalized profiles). In parallel to this accumulation of molecules at the gel surface, darker areas in the buffer

zone located right in front of the buffer/gel interfaces could be observed. This feature occurred at the beginning of the penetration experiment for positively charged dextrans but was absent for neutral and negatively charged dextrans (which carried the identical fluorophore as the positively charged dextran variants). Thus, this feature seemed to be linked to the charge state of the dextran molecules used for the penetration tests, and it indicated a local depletion of molecules from those areas.

Given those two features, *i.e.*, an accumulation of positively charged molecules at the liquid/gel interface and a local depletion of those molecules in the 'atrium' of the gel, it was *a priori* not clear for which dextran species the entry process into the bulk volume of the mucin gel was most efficient. One could assume that neutral dextrans, which did not show any detectable interaction with the gel matrix, entered the gel at higher numbers than anionic or cationic dextrans since the former do not experience any entrance barrier. However, when the number of molecules which were absorbed into the first 50 μm of the gel after different time intervals were calculated, the opposite was observed (**Fig. 5.3 C**; left): after a penetration time of 10 min, the local concentration of both neutral and anionic dextrans was lower in the gel than it was initially in the buffer reservoir. However, a slightly higher number of anionic dextrans than neutral dextrans was found in the first 50 μm of the mucin gel. This finding agreed with the observation that the corresponding penetration profiles showed a slight shoulder-like feature, *i.e.*, a rather flat regime right after the buffer/gel interface. This feature indicated that also those anionic dextran variants interacted with the mucin gel matrix – and this finding was consistent with the results obtained for binding experiments conducted with surface-attached mucins (**Fig. 3.4**). In contrast to the other two dextrans, after the same time span of 10 min, the concentration of cationic dextrans in the mucin gel even exceeded the initial concentration of these molecules in the buffer compartment. This result suggested that relatively strong binding interactions between solubilized DEAE-dextrans and mucin macromolecules promoted the partitioning of those charged dextrans into the mucin gel.

To verify the hypothesis that both charged dextran variants bind to mucins, albeit with different affinities, a depletion assay was conducted. This approach allowed for determining relative differences between the binding affinities of test molecules toward mucin molecules. The amount of dextrans depleted from solution after incubation was measured and relative affinities of the different dextran variants toward (passively adsorbed) mucin surface coatings were derived. Indeed, the results obtained from this dextran depletion assay revealed different binding affinities of the three dextran variants (**Fig. 5.3 C**; right). Since the penetration profiles of neutral dextrans indicated that this polysaccharide variant does not bind significantly to mucin glycoproteins, this dextran variant was used as a reference and its binding affinity to mucin coatings was set to one. Compared to these

neutral, unmodified dextrans, the cationic DEAE-dextran molecules showed high-affinity binding to MUC5AC, and a relative affinity that was about 7 times as high as for neutral dextrans could be calculated. This strong binding affinity of cationic dextrans toward mucin can be rationalized by the large number of anionic binding sites present in the glycosylated core domain of mucin glycoproteins (established by sialic acids and sulfate groups). Interestingly, also anionic dextrans exhibited a higher affinity toward mucins than neutral dextrans; here, the calculated value was about twice as high as the reference determined for neutral dextrans (**Fig. 5.3 C**, right). This result reflected low-affinity binding of the anionic dextrans to the cationic amino acid residues (*i.e.*, arginine, histidine, and lysine at the experimental pH of 4.0) located in the terminal regions of the mucin molecule. Indeed, owing to the lower number of positive charges in these terminal mucin domains compared to the high density of negative charges in the core region of the glycoprotein, the binding affinities of the mucin macromolecule toward cationic and anionic molecules could be expected to be different.

So far, the molecular penetration experiments had been performed with mucin gels comprising purified gastric mucin MUC5AC, and such a reconstituted MUC5AC gel is a reasonable model for gastric mucus. In intestinal mucus, however, the dominant mucin type is MUC2. Thus, next, hydrogels comprising MUC2 were used for molecular penetration experiments. For these hydrogels, a similar molecular penetration behavior could be observed as described for MUC5AC gels above: positively charged dextrans showed a strong accumulation peak at the buffer/gel interface, whereas neutral and negatively charged molecules did not (**Fig. 5.3 B**). In contrast to the experiments conducted with MUC5AC, the penetration profiles of anionic dextrans did not exhibit a 'shoulder'-like feature but, instead, were virtually indistinguishable from those of neutral dextrans. Consistently, also the amount of molecules, which had successfully entered the first 50 μm of the MUC2 gel was only increased for the cationic DEAE-dextrans compared to neutral dextrans but not for anionic CM-dextrans (**Fig. 5.3 D**, left). Different from the results obtained with gastric mucins MUC5AC, comparably low binding affinities of anionic dextrans toward intestinal mucin glycoproteins MUC2 as for neutral dextrans were obtained (**Fig. 5.3 D**, right). Yet, as outlined above, the binding properties of different mucin batches can vary (**Fig. A4.10**)– and these differences might be even more pronounced if batches of different mucin isoforms are compared to each other.

In conclusion, the experiments conducted with these two mucin variants demonstrated a selective accumulation of molecules at the liquid/gel interface of mucin hydrogels that occurred as a function of the molecule charge: whereas this phenomenon was strongly pronounced for cationic molecules, it was only weakly pronounced for anionic molecules and completely absent for neutral molecules.

5.3. A mathematical model to predict the charge dependent transport of molecules in mucin hydrogels*

Although the penetration experiments described so far shed light on the charge dependent penetration efficiency of molecules into mucin hydrogels, results obtained with the microfluidics setup alone are unable to provide a physiologically accurate model of molecular transport into and across mucus barriers. For mucus-penetrating molecules to reach the epithelial surface of a mucosal tissue, they not only have to enter the mucus gel but they need to cross the whole mucosal barrier. Since all mucus layers are continuously being replenished by the human body, only those molecules have a chance of arriving at the epithelial surface, which travel through the mucus barrier fast enough.

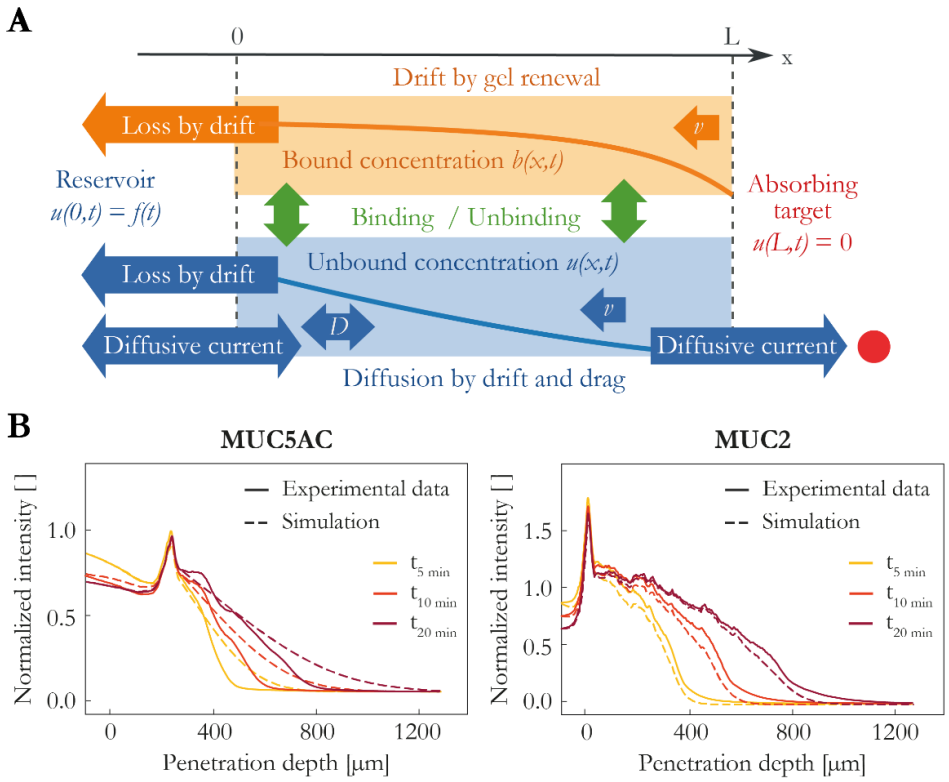

Fig. 5.4: Mathematical model of the penetration behavior of microscopic objects into self-renewing mucus gels. Schematic representation of the model, which incorporated the diffusive transport of molecules through mucus and accounted for transient binding of molecules to the mucin network and the convective transport of molecules away from the apical surface (**A**). Experimental intensity profiles for the penetration of cationic, mucin-binding dextrans into MUC5AC and MUC2 hydrogels could be well described by the simulated profiles, illustrating consistency of the proposed mathematical model. (**B**)

* This section follows in part the publication Marczynski *et al.*, Biomaterials Science (2018).

Thus, a theoretical model was developed, which captured the experimental facts presented so far but could also extrapolate to physiologically relevant scenarios from the field of drug delivery. In a first step, a basic mathematical model was established to reproduce the charge-dependent penetration behavior of molecules into static, reconstituted mucin gels. This model combined the diffusive transport of molecules through a hydrogel layer with transient binding of these molecules to the mucin glycoproteins. In a second step, a counteracting, retrograde transport of molecules at a velocity v was introduced to account for the continuous renewal of the mucus gel layer *in vivo* (**Fig. 5.4 A**). In both transport scenarios, the molecules were either in a free state (described by the concentration of unbound molecules $u(x,t)$) or bound to mucin glycoproteins (described by the concentration of bound molecules $b(x,t)$). A diffusion constant of $D_u = D$ (*i.e.*, free diffusion in a viscous environment) was assigned to unbound, *i.e.*, diffusing molecules, whereas $D_b = 0$ for bound molecules. Charged dextrans could switch between those two states, whereas uncharged dextrans were assumed to always remain in the free, unbound state as they did not show interactions with mucins during binding or penetration experiments. At the far end of the mucin gel, an absorbing boundary condition was defined, *i.e.*, molecules that have successfully diffused through a mucus layer of certain thickness (and thus have reached the target region) were removed from the system. Initial calculations (for $v = 0$ to match the experimental situation on-chip) indicated that the penetration profiles of cationic dextrans could only be reproduced if a heterogeneous mucin concentration $m(x)$ was assumed such that there was an increased density of mucin glycoproteins at the buffer/gel interface. Indeed, this assumption appeared reasonable as locally increased mucin levels were observed at the buffer/gel interface (**Fig. A4.11**). With such a heterogeneous mucin profile $m(x)$, the time-dependent penetration profiles of cationic, mucoadhesive dextrans into MUC5AC and MUC2 hydrogels could be reproduced very well (**Fig. 5.4 B**).

Having verified that the model could successfully reproduce the molecular penetration process observed for reconstituted mucin gels on-chip, next, the model was extended such that it could describe a physiologically more relevant scenario of mucosal transport. In particular, the effect of mucus renewal was included. It was assumed that 'fresh' mucus is secreted at the same velocity $v = 0.1\ \mu m\ s^{-1}$ (estimated from published renewal times[7, 214]) as 'old' mucus is removed on the luminal side, such that the thickness of the mucus layer remains constant. Thus, both bound and unbound molecules experienced retrograde flow (convective transport) away from the cell/mucus interface. In the following, the transport of two different types of objects was modelled: first, the transport of molecules with a hydrodynamic radius of $R = 1.4$ nm (representing 4 kDa dextrans)[226] and thus a large diffusion constant of $D = 175\ \mu m^2\ s^{-1}$, and second, the transport of nanoparticles (which are, for instance, commonly used as drug carriers) with a hydrodynamic radius of $R = 50$ nm and,

correspondingly, a small diffusion coefficient (D = 5 µm² s⁻¹). These diffusion constants were estimated using the Stokes-Einstein relation (**Appendix A6**).

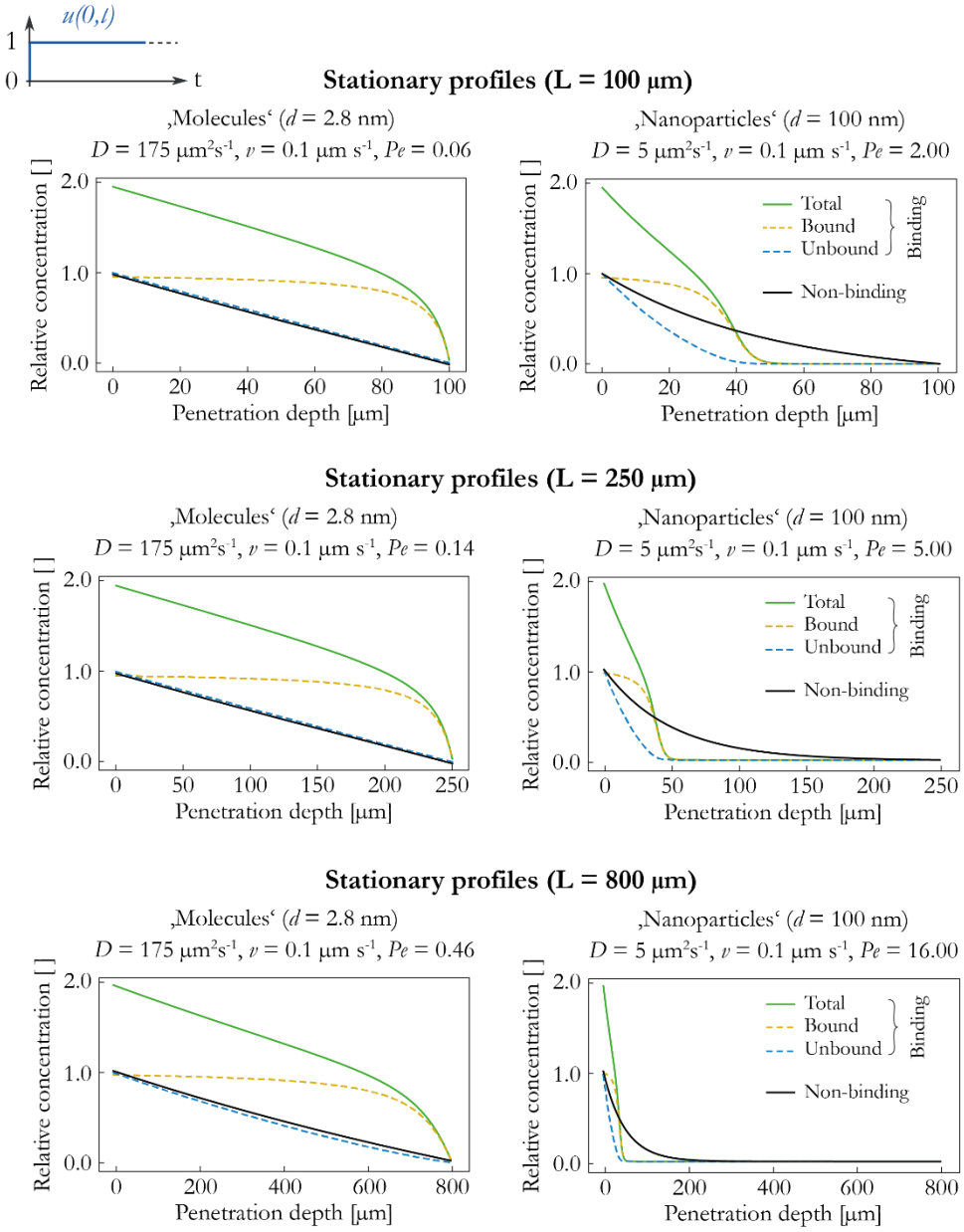

Fig. 5.5: Stationary penetration profiles as obtained for simulated molecules and nanoparticles when a constant molecule/nanoparticle concentration at the mucus surface was assumed. A constant mucin concentration profile $m(x) = m_0 = 1$ was applied, and mucus self-renewal was modelled by assuming a constant retrograde flow with a velocity of v = 0.1 µm s⁻¹. Two scenarios were calculated: a non-binding scenario (black profiles) and a binding scenarios (green profiles, which can be divided into profiles for bound (orange profiles) and unbound molecules/nanoparticles (blue profiles).

For both, molecules and nanoparticles, stationary concentration profiles were calculated for a non-binding scenario (**Fig. 5.5**, black profiles) and a binding scenario (**Fig. 5.5**; green profiles; unbound

dextrans/nanoparticles are represented by blue profiles and bound dextrans/nanoparticles by yellow profiles). Furthermore, three physiologically relevant mucin layer thicknesses (100, 250, and 800 μm) were compared, which represented the thicknesses of the mucus barriers in the small intestine, the stomach, and the large intestine, respectively. In all cases, a constant density of mucin glycoproteins $m(x) = const.$ across the mucin gel was assumed, and the kinetic rate constants describing binding and unbinding events were estimated as described in **Appendix A6**.

For any relevant amount of substance to reach the target at $x = L$, diffusion must be able to overcome the convection created by mucus renewal (*i.e.*, 'drift'). The shape of the stationary profiles in **Fig. 5.5** reflected this 'tug of war': a significant fraction of the molecules reached the right boundary of the mucus gel only if the drift did not dominate over diffusion. A dimensionless number characterizing the relative strength of drift compared to diffusion is the Peclet number $Pe = \frac{v L}{D}$. For $Pe < 1$ diffusion dominated over drift, whereas drift dominated over diffusion for $Pe > 1$, *i.e.*, in a non-binding scenario, the condition $Pe < 1$ guaranteed that diffusion could outperform drift. Indeed, in such a non-binding model, the shape of the molecule concentration profile was completely determined by the dimensionless Peclet number (**Fig. 5.5**, black profiles). When binding of diffusing molecules to and from the hydrogel constituents was included, this criterion was generalized by defining an effective Peclet number $Pe_{\mathrm{eff}} = (1+a) \times Pe$, where a denotes the ratio of bound to unbound molecules (**Appendix A6**). Accordingly, in the model that accounted for transient molecule binding, the criterion $Pe_{\mathrm{eff}} < 1$ described a scenario where diffusion dominated over drift. The penetration profiles calculated for model 'molecules' across self-renewing mucus-gels illustrated that a moderate binding affinity does not greatly reduce the transport efficiency of mucus-binding molecules – provided that the diffusing molecule is small enough such that its diffusive spreading (when the molecule is in its unbound state) is fast enough to overcome the convective drift of the gel (**Fig. 5.5**). An increased partitioning of molecules into the hydrogel compensated for those molecules, which were located in a bound state at a given time point, and thus were not transported.

In contrast to the scenario obtained for molecules, diffusion is much slower for nanoparticles. Thus, increased partitioning was not sufficient to compensate for nanoparticle binding, and the most efficient transport scenario was achieved for non-mucoadhesive nanoparticles (**Fig. 5.5**, black profiles). Moreover, the simulations suggested that, for molecules, the outcome of the penetration process should be more or less insensitive toward the thickness of the mucin gel. In contrast, the calculated penetration profiles for nanoparticles indicated that these larger objects are unable to overcome thick, self-renewing mucin barriers in high numbers – even if the nanoparticles were non-mucoadhesive (**Fig. 5.5**).

So far, a constant concentration of penetrating molecules was assumed at the mucus/buffer interface. In a physiologically relevant drug delivery scenario, however, this is not always a good approximation, since a drug dose (as, *e.g.*, released from a pill) will only be present at the mucosal interface for a finite amount of time τ_0. Thus, a time-dependent concentration profile of such drug molecules in the buffer compartment was introduced such that their concentration was constant: $u(0,t) = 1$ for a time span of $\tau_0 = 1800$ s but returned to zero afterwards (**Fig. 5.6**).

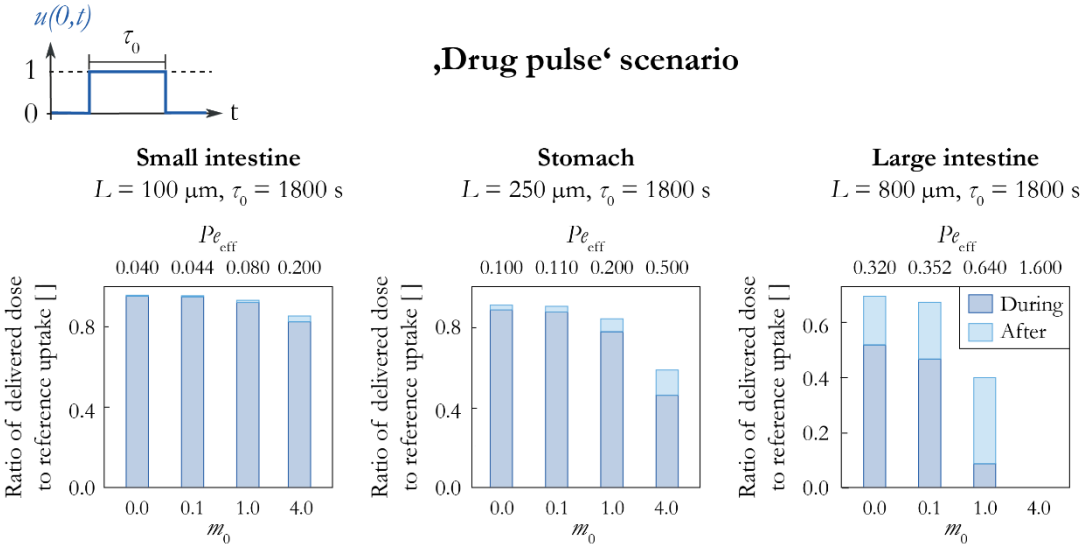

Fig. 5.6: Simulated absorption of molecules at the right boundary of a self-renewing mucin gel. Mucus self-renewal was modelled by assuming a constant retrograde flow with a velocity of $v = 0.1$ µm s^{-1}. Scenarios with different mucus gel thicknesses L were compared for different, spatially constant (bulk) mucin concentrations m_0 in a 'drug pulse' scenario. The drug pulse duration was set as $\tau_0 = 1800$ s. The columns indicate the ratio of the delivered dose of molecules normalized to the reference molecule uptake into the mucin gel layer during/after the duration of the drug pulse.

The three panels of **Fig. 5.6** depict results obtained for three different mucin gel lengths, again corresponding to the different physiological values of mucus gel thickness. In each panel, the ratio of the molecule dose absorbed into the target at $x = L$ to a reference substance uptake into the mucin gel is shown as a bar graph for different binding strengths (as represented by the apparent bulk mucin concentration m_0: no binding was represented by a mucin concentration of $m_0 = 0$, and transient binding with increasing strength was modelled by mucin concentrations of $m_0 = 0.1, 1, 4$). The reference substance uptake was given by the total substance uptake from the lumen into the mucus gel layer. The columns are divided into the amount of molecules absorbed during the pulse (dark blue, 'during') and after the pulse has passed (light blue, 'after'). A substantial amount of substance only reached the target, if $Pe_{\text{eff}} < 1$ (**Fig. 5.6**).

For the largest modelled mucin gel thickness, *i.e.*, 800 μm, and the highest modelled mucin concentration m_0 = 4 (where $Pe_{eff} > 1$), the model predicted that neither mucoadhesive nor non-mucoadhesive molecules would translocate across the self-regenerating mucin gel layer anymore (**Fig. 5.6**, right panel). This calculation was consistent with experimental results (which even did not capture the dynamic mucus renewal): also here, the concentration of penetrated molecules was close to zero at gel depths of 800 μm and beyond (**Fig. 5.3 A**, **B**). For lower mucin concentrations and thinner mucus gels, however, a significant fraction of the translocated molecules should arrive at the target region after the 'drug pulse' has subsided. This phenomenon represented a delayed drug delivery effect, which becomes increasingly important for thicker mucus barriers.

5.4. Impact of mucoadhesion on drug delivery across mucus barriers*

Both experimental and theoretical results indicated that mucoadhesion does not necessarily prevent the efficient penetration of molecules into and across mucin hydrogels. Instead, a non-zero binding affinity of molecules toward mucin gels as observed for cationic DEAE-dextrans resulted in an enhanced partitioning of these molecules into the gel phase. This increased partitioning, in turn, can compensate for a reduced diffusive spreading of those mucin-binding molecules across the gel: although mucoadhesive molecules spend a certain fraction of time in a mucin-bound state during which they cannot diffuse, a larger number of those molecules is absorbed into the gel phase. If the binding affinity is not too high, all those absorbed molecules are capable of performing a 'sticky' random walk (= diffusion interrupted by transient binding events) across the hydrogel. In contrast, for non-binding molecules there is no energetic advantage to enter the gel phase, and they penetrate the gel simply by free diffusion. Therefore, these findings suggest that charged molecules can translocate mucus barriers with comparable efficiencies as neutral, non-mucoadhesive molecules (**Fig. 5.7**). An enrichment of charged molecules within mucus due to enhanced partitioning can compensate for transient molecule binding, thus providing an equally efficient transport across mucosal barriers as in scenarios where mucoadhesion is absent.

For certain classes of pharmaceuticals, *e.g.*, antibiotics, it seems possible that an enrichment of those molecules in the mucus phase can be advantageous: if those pharmaceuticals are directed against certain bacteria which colonize mucus, they will reach a therapeutically efficient dose in the mucus gel more easily if they are mucoadhesive. In such a scenario, the target cells (*i.e.*, the bacterial invaders)

* This section follows in part the publications Marczynski *et al.*, Biomaterials Science (2018) and Marczynski & Lieleg, Biophysics Reviews (2021).

are located within the mucus phase, thus full mucus translocation is not even required for an efficient treatment – but might still be achievable provided that the binding affinity of those antibiotics toward the mucus constituents is not too high. In contrast, if the binding affinity of pharmaceutical objects toward mucin molecules is too high, these mucoadhesive objects will accumulate at the gel/buffer interface without actually penetrating the mucin gel (**Fig. 5.7**). This is, for instance, the case for mucoadhesive drug carrier vehicles such as nanospheres, which can bind simultaneously to several mucin macromolecules *via* multiple binding sites present on the particle surface. Such trapped objects will be rapidly removed from the gastrointestinal tract by mucus renewal without reaching the gastrointestinal epithelium (**Fig. 5.7**, right).

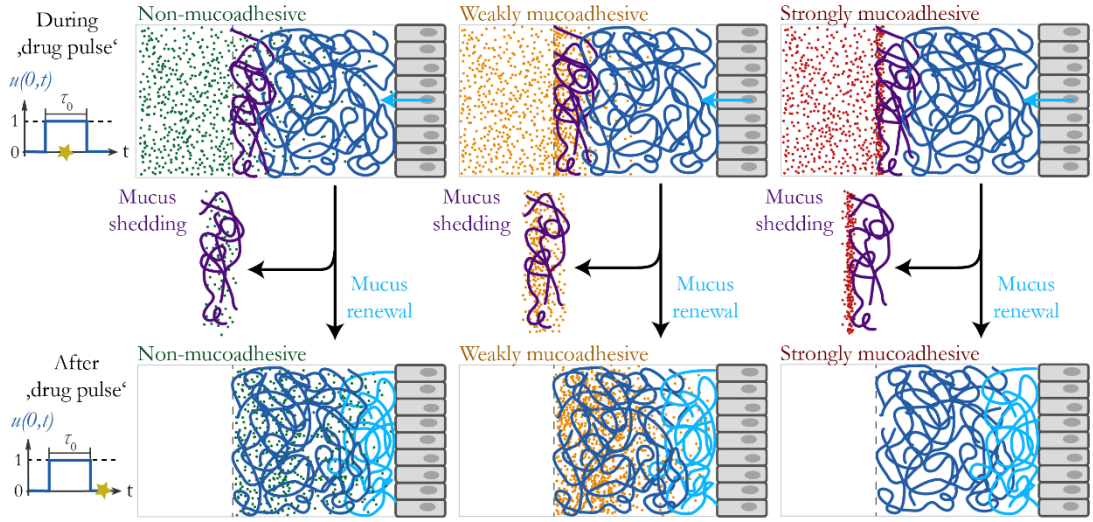

Fig. 5.7: Schematic illustration of the charge-dependent penetration of mucin gels during and after a 'drug pulse'. In a physiological situation, molecular transport across mucus layers is countered by continuous mucus secretion from the apical cell layer of mucosal membranes (indicated in light blue) and shedding of mucus on the luminal side of the mucus layer (indicated in purple). During a 'drug pulse', molecules can partition from the lumen of the gastrointestinal tract into mucus and travel across this hydrogel. The penetration efficiency of molecules or nanoparticles into and across mucin gels depends on the binding strength of those objects to mucus constituents, *e.g.*, the mucin network, and the mucus renewal rate.

Mucoadhesive nanospheres, however, are a convenient administration form of medication.[227, 228] In fact, they can still be used for efficient drug administration if one of the two following scenarios is met: first, they can be rendered non-mucoadhesive if they are coated with inert molecules such as polyethylene glycol. Such 'stealth' particles might be capable of translocating across physiological mucus barriers (**Fig. 5.5**). Second, these drug carrier particles can serve as a lasting depot for pharmaceuticals at the liquid/mucus interface where they release their cargo into the gastrointestinal lumen. Now, mucoadhesion of those drug carrier objects will ensure that the duration of the locally

applied drug pulse will be extended, thus broadening the time window for successful mucus translocation.

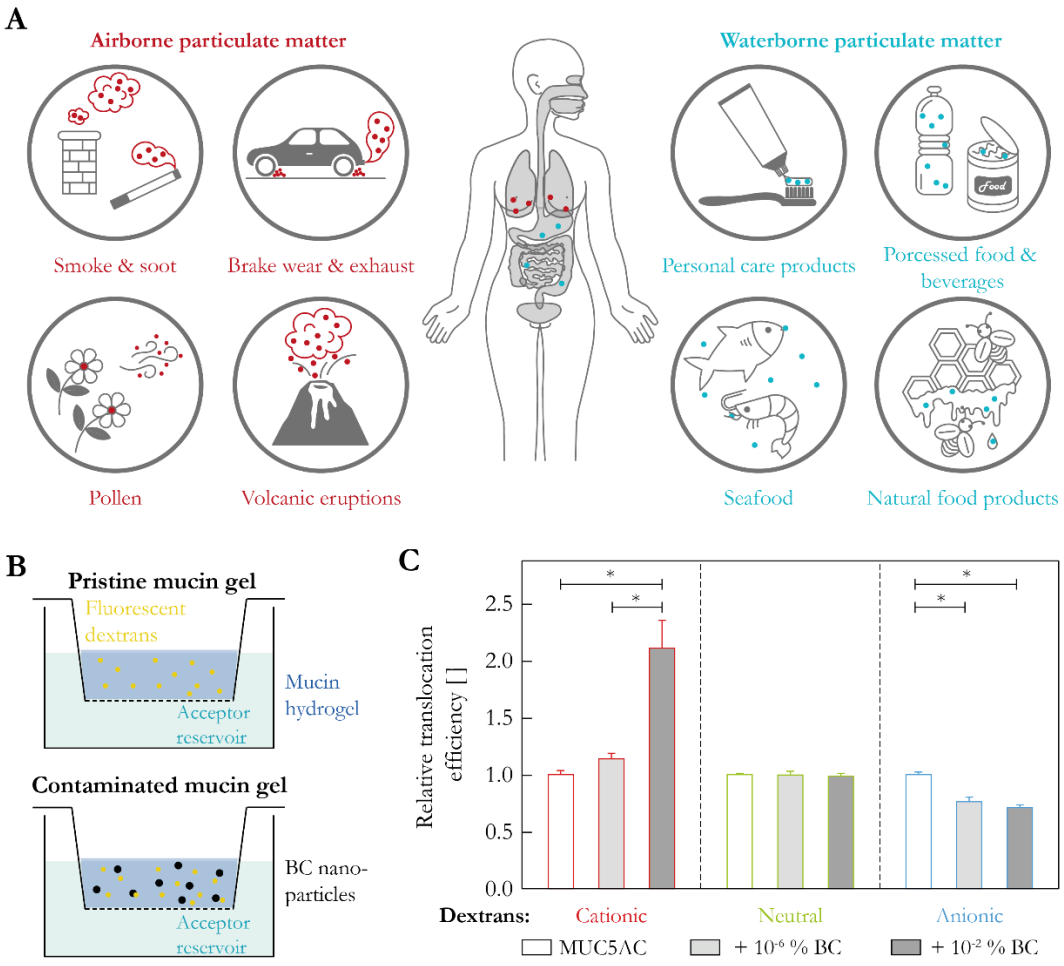

Fig. 5.8: The impact of black carbon nanoparticles on the barrier properties of mucin hydrogels. Sources of particulate matter and entrance gates into the human body. Relevant particulate pollutants can either be of natural origin or the byproducts of anthropogenic activities. (**A**). A permeation assay was used to determine the translocation efficiency of differently charged dextran variants across mucin hydrogels. Mucin hydrogels (either with or without BC nanoparticles) were reconstituted on top of microtiter plate inserts, and solutions containing fluorescently labelled dextrans were pipetted on top of the hydrogels (**B**). After incubation overnight, the amount of dextrans, which translocated across the mucin hydrogel, was quantified fluorometrically. Data was normalized to the amounts of dextrans which translocated across pristine mucin gels. The error bars denote the standard deviation as obtained from eight individual samples ($n = 8$). Asterisk mark significant differences ($p < 0.05$; **C**).

Taken together, the experimental results and the mathematical model presented here illustrated the complexity of molecular transport phenomena across mucus barriers. They challenge the prevailing assumption that mucoadhesion always needs to be avoided to achieve good penetration of molecules through mucus. In fact, the theoretical model indicated that an increased partitioning of

mucoadhesive objects into mucin-based hydrogels can compensate for a more unrestricted spreading of non-mucoadhesive objects.

From a physiological point of view, however, an additional level of complexity is introduced by the fact that the mucus barriers in the human body, are constantly challenged by environmental pollutants (**Fig. 5.8 A**) – and these contaminants may alter the permeability of mucus barriers toward succeeding diffusing objects. Such (particulate) pollutants can either originate from natural sources (*e.g.*, pollen, desert dust or volcanic ash), or they emerge as an unwanted byproduct of industrial/anthropogenic processes (*e.g.*, brake wear or soot originating from the combustion of biomass; **Fig. 5.8 A**). In most cases such as those exemplarily mentioned above, mucus barriers of the human body are unintentionally challenged with such microscopic objects, *i.e.*, as a consequence of environmental pollution. Sometimes, however, mucus is confronted with micro- or nanoparticles as a consequence of an intentional uptake of air/water contaminated with particulate matter, *e.g.*, through the inhalation of cigarette smoke. Independent of the route *via* which any of such particles may enter the human body, they almost always encounter certain mucosal barriers, where they can interfere with the barrier properties of mucus. To assess the impact of such nanosized mucus contaminants on the molecular transport processes in mucin hydrogels, the translocation of (fluorescently labeled) dextrans across mucin barriers was quantified both in the presence and absence of black carbon (BC) nanoparticles (**Chapter 2.5.3**). These particles were chosen as an illustrative model system for airborne particulate matter (such as cigarette smoke).[229] The BC concentrations were chosen such that they represented two physiologically relevant scenarios: a concentration of 10^{-2} % represents the amount of BC that accumulates in the airway mucus of active smokers, whereas a concentration of 10^{-6} % corresponds to the apparent BC doses found in the airway mucus of secondhand smokers, *i.e.*, people that do not actively smoke but are regularly exposed to tobacco smoke.[230] The mucin hydrogels (both gels containing BC nanoparticles and pristine gels) were reconstituted on top of semi-permeable membranes, which comprised the bottom parts of inserts for microtiter plates (**Fig. 5.8 B**). These membranes allowed for the passage of small molecules (such as the 4 kDa dextrans used here) but retained the mucin hydrogel in the insert. A small drop of a solution containing fluorescently labeled dextrans was then pipetted on top of the mucin hydrogel, and – after overnight incubation – the amount of dextrans, which successfully translocated the mucin hydrogel, was quantified.

With this permeation assay, it was observed that cationic dextrans exhibited an increased translocation efficiency across mucin gels that were contaminated with BC nanoparticles, whereas, at the same time, the translocation of anionic mucin gels was hampered – and both effects were dependent on the concentration of BC nanoparticles added (**Fig. 5.8 C**). In contrast, no significant

differences were observed for the translocation behavior of electrostatically neutral control dextrans (**Fig. 5.8 C**). This outcome can be rationalized as follows: at an acidic pH of 4.0, *i.e.*, the pH level at which the permeation experiments were performed, BC nanoparticles are strongly cationic (**Fig. 2.4 A**). QCM-D measurements indicated that these cationic BC particles bind to mucins – and, most likely, this was due to attractive electrostatic forces acting between the positively charged particles and anionic mucin glycan chains (**Fig. A4.12**). When present in mucin hydrogels, BC nanoparticles, on the one hand, occupy potential binding sites for cationic dextrans in the mucin network. On the other hand, penetrating cationic dextrans experience electrostatic repulsion originating from the positive net charge of the trapped BC nanoparticles. Together, these two effects lead to an increased translocation of cationic dextrans across contaminated mucin hydrogels. For anionic dextrans, the opposite effects occur: BC particles provide additional binding sites for CM-dextrans and reduce electrostatic repulsion acting on the dextrans. As a consequence, the translocation process for anionic dextrans is slowed down.

In conclusion, in the context of drug delivery across mucus, mucoadhesion is a key parameter that certainly needs to be considered with care when designing pharmaceuticals or drug carrier particles for mucosal penetration. Yet, the results obtained with nanoparticle-loaded mucin gels indicated that molecular transport processes across such mucin-based hydrogels (*e.g.*, native mucus) are not dictated by the mucin network alone, but are critically influenced by the presence of other constituents. Although the effect of altered permeability of mucin hydrogels was demonstrated for BC nanoparticles only, it seems reasonable to assume that other mucus 'contaminants' (environmental pollutants such as microplastics as well as intrinsic mucus components such as other proteins or lipids) might affect the barrier properties of mucin hydrogels as well.

5.5. Permeability of MUC5AC hydrogels toward α-synuclein*

So far, in this thesis, the effect of the charge of penetrating molecules on the barrier properties of mucin hydrogels was assessed. However, molecules, which come in contact with human mucus barriers in the gastrointestinal tract through ingestion of food and beverages are typically not uniformly charged and display a combination of both, polar/charged and non-polar properties.

* This section follows in part the publication Marczynski *et al.*, Biomacromolecules (2019).

Accordingly, the penetration behavior of such complex molecules might differ strongly from that of simple polysaccharides.

In the last few years, the protein α-synuclein (αSN) has gained particular interest in the context of muco-penetration as this protein is known to be associated with neurodegenerative disorders such as Parkinson's disease (accordingly, these diseases are referred to as synucleinopathies).[231, 232] Indeed, recent research indicated that the pathogenesis of synucleinopathies might begin in the enteric nervous system of the gastrointestinal tract.[233, 234] This hypothesis is based on clinical studies, which demonstrated that patients suffering from Parkinson's disease typically had experienced gastrointestinal problems years (or even decades) before disease-specific symptoms such as motor deficits emerged.[235] Indeed, αSN-expressing enteroendocrine cells (*i.e.*, hormone producing cells in the gastrointestinal tract) facing the gastrointestinal lumen were suspected to provide a direct pathway for pathological, misfolded αSN species to the central nervous system.[236] It seems likely that the uptake of misfolded αSN from the gastric lumen can induce or promote misfolding of αSN in enteroendocrine cells. Since misfolded αSN species can spread in a prion-like fashion,[60, 237] this could lead to the sequential emergence of synucleinopathies: first, in the gastrointestinal mucosa and, later (by propagation), in the brain.[238, 239] However, for αSN molecules to reach the gastrointestinal epithelium, they have to overcome a mucus layer protecting the mucosal tissues.[9] Since αSN contains a combination of motifs relevant for mucoadhesion, *i.e.*, a hydrophobic central region as well as both, negatively and positively charged domains (**Appendix A3**), it might be prone to mucin binding. Although, the penetration behavior of αSN into and its translocation across mucin hydrogels had not been investigated yet, this process might be crucial for understanding how αSN-related disorders can originate from the gastrointestinal tract.[240]

To assess if αSN is a mucoadhesive molecule, microscale thermophoresis (MST) experiments were performed (**Fig. 5.9**). In these experiments, purified porcine gastric mucin MUC5AC was titrated against fluorescently labeled αSN (αSN-AF647). The MST experiments resulted in a binding curve that changed sharply at a MUC5AC concentration of ~20 nM. For low and high ligand concentrations, plateau values for the normalized thermophoresis signal were obtained, which reflected the unbound state of αSN (*i.e.*, fraction of mucin-bound αSN molecules ~0%) and the saturated state (*i.e.*, fraction of mucin-bound αSN molecules ~100%), respectively (**Fig. 5.9**). This data clearly demonstrated that monomeric αSN binds well to lab-purified MUC5AC. For excreted or ingested αSN species to be taken up by enteric nerves, however, they would first have to pass the mucosal barrier – and the mucoadhesive properties of αSN might prevent this.

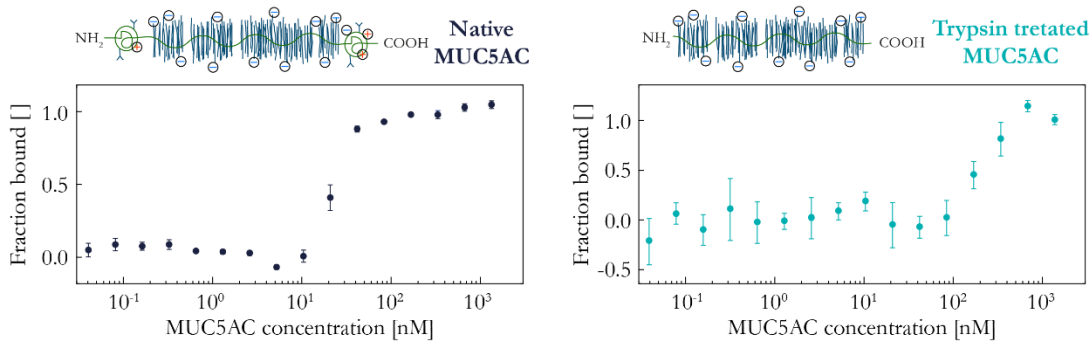

Fig. 5.9: Microscale thermophoresis (MST) experiments conducted with native and trypsin treated MUC5AC. Shown are the fraction of αSN molecules bound to mucin molecules as derived from the normalized fluorescence intensity signal obtained in MST measurements for native as well as trypsin treated MUC5AC. The error bars represent the standard error of the mean as calculated from three independent samples (n = 3).

To test if the binding interactions between αSN and MUC5AC are that strong that the diffusion of αSN across the mucin hydrogel might be prevented, the same microfluidics setup as introduced in **Chapter 5.2** was used. The penetration profiles of fluorescently labeled monomeric αSN molecules partitioning into acidic MUC5AC hydrogels displayed a sharp accumulation peak. However, different from what had been obtained from penetration experiments performed with cationic DEAE-dextrans, the accumulation peak (represented by a band of maximum fluorescence intensity) was now located within the mucin hydrogel (**Fig. 5.10 A**). Here, the fluorescence intensity corresponded to the number of αSN molecules travelling through the mucin hydrogel over time, and the intensity peak represented a local accumulation of αSN within the mucin hydrogel. The peak had an intensity value that, at all times except for t_0 (*i.e.*, directly after injection of αSN into the test reservoir), strongly exceeded the value measured in the buffer reservoir.

In the mucin gel region just behind this peak, *i.e.*, in areas through which the fluorescence band had already traveled, the fluorescence signal was lower than that in the reservoir, which suggested a depletion of the fluorescently labeled αSN-AF647 molecules from this region. Both of those features, *i.e.*, an accumulation peak and a local depletion of molecules just behind this accumulation peak, had already been observed for cationic DEAE-dextran molecules penetrating mucin gels before (**Fig. 5.3 A, B** & **A4.10**) – and this effect was attributed to molecular partitioning into the hydrogel. However, different from those previous penetration experiments conducted with simple polysaccharides, the αSN accumulation peak did not remain located at the buffer gel interface. Instead, within the 30 min time period considered here, the position of this peak continuously travelled with time and seemed to follow a time dependence of $\sim\sqrt{t}$ (**Fig. 5.10 B**), which suggested

that mainly diffusive processes were responsible for moving this peak through the mucin gel. Thus, in spite of its strong mucoadhesive properties, a certain fraction of αSN molecules successfully penetrated mucin hydrogels. On a time scale of 30 min (which is comparable to physiological mucus turnover times[7]), the αSN molecules reached penetration depths on the order of the thickness of mucus layers that naturally occur in the stomach and the small intestine (~100−250 µm).[212, 213]

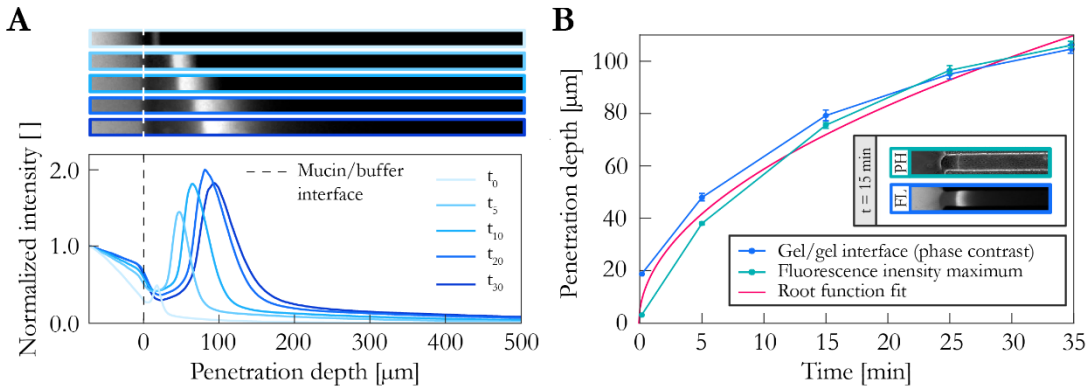

Fig. 5.10: Penetration behavior of αSN into MUC5AC hydrogels. Intensity profiles obtained for AF647-labeled αSN molecules penetrating a 1% (w/v) MUC5AC hydrogel at distinct time points. Each curve represents data obtained from averaging seven distinct channels (n = 7). Typical fluorescence images corresponding to the intensity profiles at the five distinct time points are shown in the panels above (**A**). Comparison of the time-dependent positions of the "internal" gel/gel interface observed in phase contrast images and the peak in the fluorescence profiles. Error bars denote the standard error of the mean as obtained from seven experiments (n = 7). Exemplary microscopy pictures of both features are shown as an inset for t = 15 min. The red curve represents a root function fitted to the experimental data (**B**).

Having established that αSN has mucoadhesive properties that affect its transport across mucin gels, next, the physico-chemical interactions responsible for this mucoadhesion were investigated. Based on previous experiments with model molecules and nanoparticles, it was expect that both electrostatic forces and hydrophobic interactions could play a role. To test the impact of the latter, the MST experiments were repeated with trypsin treated MUC5AC (*i.e.*, mucins that had lost their terminal domains). With such trypsin treated mucins, the binding curve was shifted to higher mucin concentrations by approximately an order of magnitude (**Fig. 5.9**). This demonstrated that, in the absence of the hydrophobic terminal domains of MUC5AC, the efficiency of αSN binding was reduced. This, in turn, indicated that hydrophobic interactions might, indeed, contribute to αSN/mucin binding. However, since αSN binding was still possible, electrostatic interactions seem to play a role as well. Indeed, MST measurements conducted with untreated mucins at elevated temperatures indicated that electrostatic interactions were dominant: for intact mucin, no temperature dependence of αSN-binding was detected (**Fig. A4.13**), and such a T-dependence might be expected only if hydrophobic interactions were to critically contribute to αSN binding. However, when a

truncated αSN variant missing large sections of the polycationic domain of αSN (αSN 60-140; **Tables A3.2** & **A3.3**) was tested, the binding curve was shifted to lower mucin concentrations at an elevated temperature (**Fig. A4.13**). This indicated that hydrophobic interactions dominated mucin binding for this particular variant.

5.6. Structural rearrangement of MUC5AC hydrogels*

The penetration behavior of αSN into mucin gels showed features that were not observed for simple dextrans before: for cationic dextrans, which bound to mucins with high affinity, an accumulation at the gel/buffer interface was observed. In contrast, for αSN, a fluorescence peak (corresponding to a peak in αSN concentration) travelled across the mucin gel in a 'wave-like' fashion. Moreover, mucoadhesion of charged dextrans could be fully explained by electrostatic interactions. The mucoadhesive properties of αSN, however, seemed to be brought about by an interplay of electrostatic and hydrophobic interactions. Thus, it seems possible that the interaction between αSN and mucins might have given rise to additional effects other than plain binding. For example, αSN might have affected the conformation of individual mucins and induced the formation of mesoscopic mucin structures.

To assess the effects of αSN binding to MUC5AC in mucin hydrogels, fluorescence confocal laser scanning microscopy (CLSM) was employed. Here, plain mucin hydrogels exhibited a relatively homogeneous morphology, whereas very different images were recorded for mucin networks that had been incubated with αSN (**Fig. 5.11 A**): when αSN was present, the mucin filaments were arranged into bundles, and the hydrogel matrix appeared to exhibit large pores with diameters on the order of micrometers (**Fig. 5.11 A** & **A4.14**). When quantifying these CLSM images by determining the area covered with fluorescent structures, a statistically significant reduction of this value was observed for samples containing αSN (**Fig. 5.11 A**). The data discussed so far implied that αSN molecules induced a severe structural rearrangement of mucin hydrogels, and αSN might function as a crosslinking molecule connecting single mucin filaments thus establishing the formation of mucin fibrils. Such a reorganization of the mucin network can also be expected to result in changes in the optical density of the mucin gel phase – and these alterations should be detectable by phase contrast microscopy. Indeed, when the mucin gel texture before and after the penetration of fluorescently labeled αSN-AF647 was compared, alterations in the optical appearance of the mucin hydrogel were

* This section follows in part the publication Marczynski *et al.*, Biomacromolecules (2019).

observed after αSN penetration (**Fig. 5.11 B**). The same result was obtained when unlabeled αSN was used, whereas the fluorophore AF647 alone did not induce changes in the optical appearance of the mucin gels (**Fig. 5.11 B**).

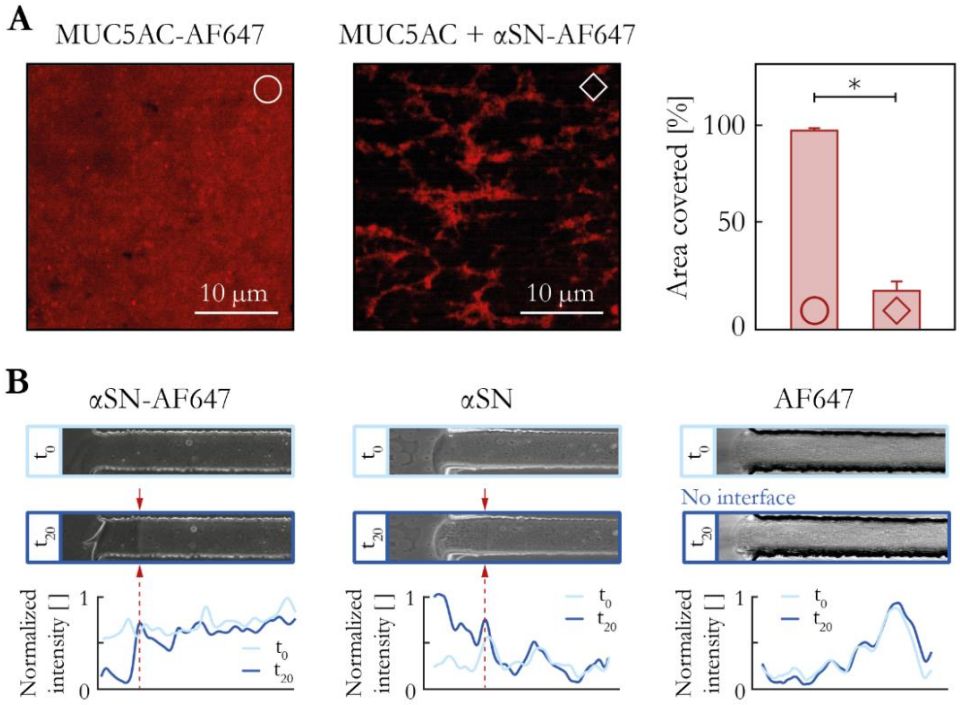

Fig. 5.11: Structural rearrangement of the mucin hydrogel by αSN as detected by fluorescence CLSM and phase contrast microscopy. Fluorescence CLSM images of mucin networks either in the absence or presence of αSN-AF647. For each condition, the area fraction covered with fluorescent structures was determined and averaged for four frames ($n = 4$). Error bars denote the standard deviation, and asterisks indicate statistically significant differences ($p < 0.05$) in the fraction of covered area (**A**). Phase contrast images of MUC5AC gels before and 20 min after injection of the indicated test molecules. For each condition, at least three chips ($n \geq 3$) were evaluated. The profiles represent the normalized intensity vs. the gel depth. The arrows and dotted lines in indicate the position of an internal gel/gel interface. Hydrogel areas, which have been penetrated by αSN, showed an altered texture. Free fluorophore AF647 alone did not lead to structural alterations in the MUC5AC gel (**B**).

This showed that the rearrangement of the mucin network was achieved by the αSN protein itself and not by (hydrophobic) interactions established by the AF647 dye. After αSN penetration, the texture of the penetrated mucin gel regions differed from that of unpenetrated gel areas located at deeper channel positions, and the treated and untreated gel regions were separated by a sharp interface that migrated toward larger channel depths with increasing time (**Fig. 5.10 B**, inset). When the position of this internal gel/gel interface was compared to the position of the fluorescence peak described before, a good correlation was obtained (**Fig. 5.10 B**). This further underscored the

hypothesis that the penetration of αSN molecules into mucin gels was responsible for the structural rearrangements in the mucin gel.

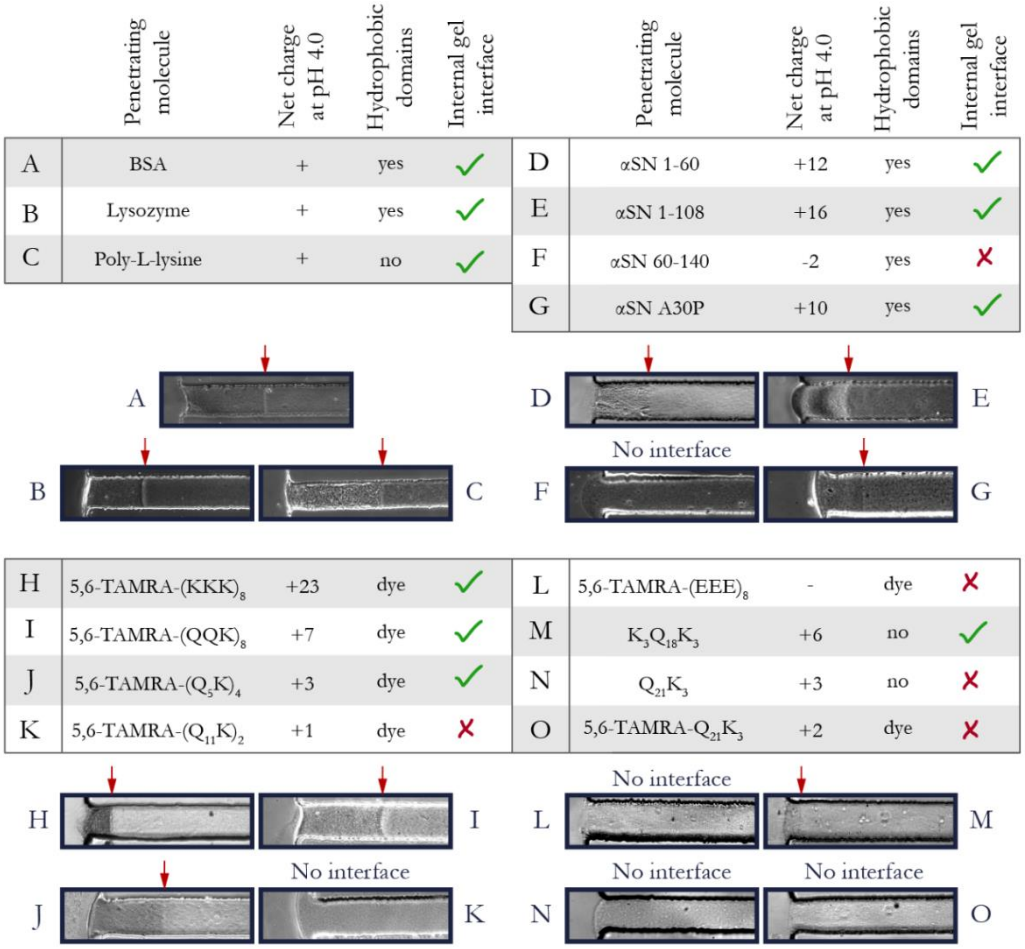

Fig. 5.12: Penetration behavior of different proteins and peptides. The tables display the charge state of the respective molecules at pH 4.0, and the presence/absence of hydrophobic domains. The range of tested molecules included proteins such as BSA (**A**), lysozyme (**B**), and poly-L-lysine (MW ~5 kDa; **C**) as well as different αSN mutant variants (**D**-**G**). Additionally, synthetic peptides as listed in **H**-**O** were tested to identify molecular motifs required for altering the mucin hydrogel texture. Green ticks and red crosses indicate if an internal gel/gel interface was formed (green tick) or not (red cross) after the respective molecule had penetrated a mucin gel. Phase contrast images display the hydrogel appearance 20 min after injection of the test molecules. The arrows indicate the positions of the internal gel/gel interfaces (if present). For each condition, at least three chips ($n \geq 3$) were evaluated.

Having established that αSN proteins induced the restructuring of mucin hydrogels, next, the structural motifs responsible for this process were identified. First, the penetration experiments were repeated with two common model proteins: BSA and lysozyme, which – similar to αSN – both carry a positive net charge at pH 4 (**Table A3.2**). Indeed, phase contrast images showed the occurrence of

a similar internal gel/gel interface within the mucin hydrogel as discussed for αSN above. The hydrogel areas that had been penetrated by αSN exhibited textural changes compared to non-penetrated gel regions (**Fig. 5.12 A**, **B**). Thus, the hydrogel rearrangement was probably not triggered by a specific sequence within the αSN amino acid chain but seemed to be a rather generic effect (putative) crosslinkers may have on mucin hydrogels.

In addition to wildtype αSN, the permeability of mucin hydrogels toward four different αSN mutant variants was probed (**Tables A3.2** & **A3.3**): The first three variants were deletion mutants lacking different motifs of the αSN amino acid sequence (αSN 1−60, αSN 1−108, and αSN 60−140), and the fourth variant comprised a single amino acid substitution at position 30 (αSN A30P: here, alanine at position 30 was substituted by proline)* Only three of those αSN variants induced the virtually identical effect as wildtype αSN (**Fig. 5.12 D**, **E**, **G**). The αSN 60−140 mutant, however, failed to alter the hydrogel texture (**Fig. 5.12 F**). This specific truncated variant lacks the positively charged domain that is present in the other three αSN mutant variants (and wildtype αSN). As indicated by MST measurements, it can be speculated that mucin binding of this particular variant was established by hydrophobic interactions rather than electrostatic forces (**Fig. A4.13**). Together, these experiments suggested that the physical properties of the αSN polypeptide seemed to be sufficient for inducing structural rearrangements of the mucin matrix; at least two mucin binding domains were required for this.

To systematically test the influence of charged motifs on mucin reorganization, a set of custom-made, synthetic peptides with finely tunable charge states was used (**Tables A3.1** & **A3.3**). Indeed, when the penetration behavior of the fully cationic polypeptide poly-L-lysine (MW ≈ 1-5 kDa) and the fluorescent 24-meric analogue 5,6-TAMRA-$(KKK)_8$ was probed, the formation of an internal gel/gel interface was observed in both cases (**Fig. 5.12 C**, **H**); these findings agreed with the expectation that positively charged motifs can induce mucin gel reorganization. Fully replacing the positively charged amino acids by negatively charged ones, however, eliminated the formation of the internal interface (**Fig. 5.12 L**). Having shown that positively charged motifs in molecules can trigger the reorganization of the mucin gel architecture by establishing electrostatic interactions, next, the number of those cationic patches required in a single peptide to obtain this effect was determined. Thus, the penetration behavior of a set of cationic peptides with similar molecular weights but different charge densities was probed (**Fig. 5.12 I-K**). Only one of those constructs failed to create structural alterations of the mucin gel: for the 5,6-TAMRA-$(Q_{11}K)_2$ peptide, neither an internal

* The A30P variant is a patho-physiologically relevant mutant of wildtype αSN that is found in patients suffering from a specific familial form of Parkinson's disease.[227]

gel/gel interface nor structural changes in the penetrated gel regions occurred (**Fig. 5.12 K**), and this particular peptide has a very low net charge of +1.

Consistent with the results presented so far, the following hypothesis can be formulated: single mucin filaments can be cross-linked by such molecules that carry at least two spatially separated binding sites. Thus, cationic groups might connect two different mucin molecules *via* electrostatic forces acting on the anionic, glycosylated mucin region (**Fig. 5.13 A**). To verify this hypothesis, two non-fluorescent and otherwise featureless oligo-glutamine based peptides carrying a lysine triplet either at both termini ($K_3Q_{18}K_3$) or at the C-terminus only ($Q_{21}K_3$) were employed. In full agreement with the expectation formulated above, the $K_3Q_{18}K_3$ peptide led to the formation of an internal gel/gel interface and altered the texture of MUC5AC gels after penetration (**Fig. 5.12 M**). In contrast, the $Q_{21}K_3$ peptide (which carried only one cationic binding site) did not induce any detectable structural alterations in the mucin gel (**Fig. 5.12 N**).

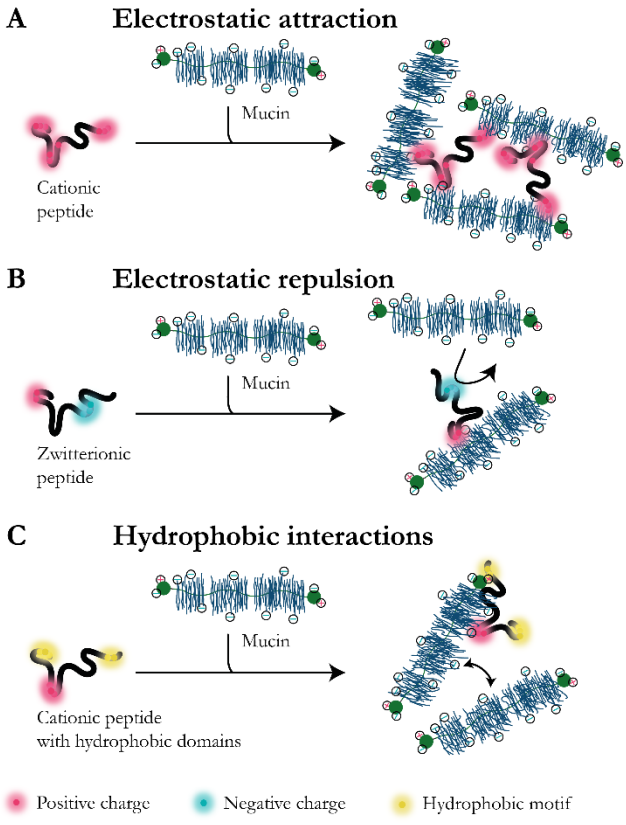

Fig. 5.13: Schematic representation of mechanisms that may contribute to mucoadhesion and the ensuing re-organization of mucin networks. Peptides with two or more positively charged motifs within their peptide sequence are thought to cross-link mucin molecules *via* electrostatic forces and thereby rearrange the microstructure of an existing mucin gel (**A**). Electrostatic repulsion between negatively charged motifs within the peptide backbone and/or the carbohydrate residues of mucin molecules, however, inhibit the cross-linking of mucin molecules (**B**). Moreover, peptides may bind to mucins *via* short-ranged hydrophobic interactions. Intermolecular electro-static repulsion between mucin molecules, however, prevents cross-linking (**C**).

Why did αSN 60−140 and the 5,6-TAMRA-$(Q_{11}K)_2$ peptide fail to alter the mucin hydrogel texture, although both molecules carry a number of cationic groups, which – in theory – should be able to establish binding interactions with mucins? In those particular molecules, the individual cationic groups are spatially isolated within the peptide sequence, and this seems not to be sufficient to

constitute mucin binding sites. The attractive electrostatic forces originating from them might not be sufficient to compensate for the electrostatic repulsion forces acting between the anionic glycan residues of two mucins and between mucins and anionic groups of αSN and the 5,6-TAMRA-$(Q_{11}K)_2$ peptide, respectively (**Fig. 5.13 B**). However, it needs to be emphasized that even molecules with a negative net charge might still be able to cross-link mucin molecules *via* electrostatic interactions if they carry cationic binding sites that are sufficiently strong to overcome these repulsive electrostatic forces. This might, for instance, apply to αSN molecules in only slightly acidic or alkaline environments, for example, in the intestinal lumen where αSN exhibits a negative net charge (**Tables A3.2** & **A3.3**).

How do hydrophobic interactions fit into this picture? As outlined above, hydrophobic interactions seem to contribute to the mucoadhesive behavior of αSN. Hence, it seems possible that cross-linking of mucin molecules can be achieved not only by cationic but also by hydrophobic binding sites on a protein/peptide. To test this hypothesis, the penetration experiments were performed with another oligo-glutamine based peptide carrying the hydrophobic fluorophore 5,6-TAMRA at the N-terminus and a cationic lysine triplet at the C-terminus (5,6-TAMRA-$Q_{21}K_3$). A rearrangement of the mucin network, however, did not occur for this bi-functionalized peptide (**Fig. 5.12 O**). At the buffer conditions used here (10 mM sodium acetate resulting in a Debye length of λ_D ~3.1 nm), electrostatic forces (both attractive and repulsive ones) might have a longer range than hydrophobic interactions. Thus, it can be speculated that the electrostatic repulsion forces acting between mucin filaments prevented them from getting close enough for hydrophobic interactions to be established. – and this might have prevented mucin cross-linking (**Fig. 5.13 C**). However, stronger hydrophobic interactions as, for example, brought about by larger hydrophobic areas, which can be generated by introducing hydrophobic amino acids into the peptide backbone, might be sufficient to overcome mucin−mucin repulsion. Experimentally, however, this is not trivial to test as synthetic oligopeptides containing hydrophobic amino acids tend to be insoluble in aqueous solutions. Alternatively, a moderately large hydrophobic sequence incorporated into a peptide sequence might be strong enough to act as a mucin-binding domain if it were to be located sufficiently far away ($\gg\lambda_D$) from the second mucin binding domain. Then, the electrostatic repulsion between two neighboring polyanionic mucin filaments could be weak enough to be overcome by hydrophobic forces.

Having established that αSN proteins can induce the remodeling of mucin hydrogels, it is *a priori* not clear how such a restructuring of the mucin network into a more porous matrix would affect its permeability towards luminal contents – both benign ones (such as nutrients) as well as malign ones (such as succeeding αSN molecules or pathogenic species such as certain bacteria or viruses). The *in vitro* results discussed so far indicated that the penetration of αSN molecules into mucin gels and

their translocation across them seemed to be facilitated by the restructuring process αSN molecules induce. Thus, in a last step, the penetration behavior of both, non-mucoadhesive (*i.e.*, neutral) and strongly mucoadhesive (*i.e.*, cationic) dextrans into mucin hydrogels that had been pre-penetrated and restructured by αSN was investigated. When the diffusive entry of these two molecule species into both, restructured and native mucin hydrogels, was investigated, it was found that the penetration profiles at both conditions were virtually identical (**Fig. A4.15**). This finding suggested that a rearrangement of the mucin network did not greatly affect the penetration behavior of small molecules, *i.e.*, those molecules which are smaller than the initial pore size of the untreated mucin hydrogel. However, it seems possible that the αSN-induced restructuring of the mucin network may facilitate the penetration of (potentially pathogenic) larger objects such as bacteria that, otherwise, would be retained by the mucin matrix due to size filtering. Yet, even in a restructured hydrogel, mucin molecules might be able to fulfil their protective functionality by immobilizing these large objects through binding interactions as these large objects typically bind to several mucins simultaneously.

At this point, it has to be emphasized that, in the gastrointestinal tract, the expression of MUC5AC, the mucin variant used for the penetration experiments, is limited to the stomach of healthy human beings. The characteristic mucin variant present in the intestine is MUC2.[241] However, as indicated in **Fig. 5.3**, the penetration experiments conducted with purified porcine MUC5AC and MUC2 as gel matrices and dextrans as molecular probes returned highly similar results for both mucin variants. This, in turn, motivates that also mucin gels reconstituted from other gel-forming mucin variants (such as MUC2) might react similarly to αSN as described here for MUC5AC gels.

In previous research, it was speculated that the ingestion of food products made from animal tissue containing (misfolded or mutated) αSN species might seed the aggregation of native αSN in the cells of the gastrointestinal epithelium from where it can spread in a prion-like fashion.[240] Indeed, the results presented here seem to support this hypothesis: in the course of the experiment, αSN molecules penetrated to depths of the mucin hydrogels that correspond to the thicknesses of thin physiological mucus barriers (**Fig. 5.10 A**). In fact, the thickness and the continuity of mucus layers can be corrupted as a consequence of chronic disorders of the gastrointestinal tract.[242, 243] Owing to their weakened mucus barriers, such patients might be particularly susceptible towards the development of αSN-associated diseases after ingestion of contaminated food products. Moreover, here, it was demonstrated that a mucin gel rearrangement can be accomplished not only by αSN but also by other proteins and peptides (**Fig. 5.12**). Accordingly, it seems likely that a remodeling of the mucin network might be a phenomenon that occurs regularly in freshly secreted mucus and does not necessarily imply pathological conditions.

6. Summary & Outlook*

One of the biggest complications inherent in research focusing on biomaterials is the complexity and heterogeneity of the biomaterials of interest. Typically, they comprise complex mixtures of large biomacromolecules as well as a broad range of small molecules and ions. Moreover, the concentrations of all those ingredients can vary not only between different individuals but also as a function of age, diet or pathophysiological conditions. As a consequence, it can be very challenging to decipher the molecular principles and components responsible for a certain behavior of a biomaterial. Thus, progress in both, academic research and the development of bio-enhanced products for applications in biomedical engineering or drug delivery, is not only affected by the limited availability of biological materials but also requires samples of good quality and known composition.

There are numerous established examples, where only one or very few key components dictate the biological, physico-chemical, and mechanical properties of a biomaterial.[244-247] This overarching principle was detected by a bottom-up-approach originating from the field of biophysics: first, researchers isolated selected bio-macromolecular components from a raw biological material, then they reconstituted them into a simplified model system, and they compared their properties to those of the respective native biological system. In fact, such model systems not only offer high levels of reproducibility, but they also enable researchers to control the composition of the material and to assess subsequent alterations in its properties. With such an approach, it was, *e.g.*, possible to identify how specific structural features of a macromolecule establish certain functionalities in the material of interest. In addition, model systems comprising a relatively low number of well-characterized components can help to investigate – step-by-step – how selected physiological/environmental factors (*e.g.*, alterations in ionic strength, pH, or temperature, enzymatic activity, impurities) shape the various functionalities of the biomaterial. Two prominent examples where such a bottom-up-approach using reconstituted model system has proven to be highly valuable are artificial actin cortices modelling the cytoskeleton[248-250] and extracellular matrix mimics, which are typically based on collagen scaffolds[251, 252].

Another complex, multi-component biomaterial that has gained increased attention during the last decades is mucus.[5] The key component of this biomaterial, *i.e.*, the mucin glycoprotein, was the objective of this thesis. Mucosal systems are involved in several physiological tasks such as

* This section follows in part the publications Marczynski *et al.*, Biomacromolecules (2021), Marczynski *et al.*, Advanced Drug Delivery Reviews (2021) and Marczynski & Lieleg, Biophysics Reviews (2021).

biolubrication, protection against hostile germs, and regulation of drug/nutrient uptake in the gastrointestinal tract.[25, 71] To better understand how those different functions of mucus are brought about, many groups have used model systems based on purified mucin glycoproteins.[253] With those purified mucins, it was possible to create simpler substitutes for native mucus, and these surrogate systems, indeed, could replicate some of the unique properties of native mucus. One critical advantage of using (lab-)purified mucins is that the intrinsic physicochemical properties of the functional key component of mucus, the mucin glycoproteins, can be studied independently, *i.e.*, in the absence of other mucus components.

Of course, when using model systems based on purified mucins, one has to make sure that the mucins incorporated into the model are structurally intact and functional. Therefore, it is crucial that mucins are carefully isolated in the lab using gentle procedures. Of course, these preparations may still contain a certain amount of impurities as well as – yet, to a smaller extent – other mucin variants.[128, 176] In the past, however, lots of research was also conducted using commercially purified mucins (such as the PGM variants 'Type II' and 'Type III' sold by Sigma-Aldrich or 'Orthana mucin' distributed by A/S Orthana Kemisk Fabrik). With those industrial mucins, often results were obtained that were very different from analogous experiments conducted with lab-purified mucins or native mucus.[10, 21, 109, 171, 172, 176, 219, 254] A side-by-side comparison of lab-purified gastric mucin ('MUC5AC') and the commercially available analogues ('PGMs') performed in this thesis demonstrated that the PGM variants have been structurally damaged in different ways (**Chapters 4.2** & **4.3**): on the one hand, the hydrophobic termini had been removed during their purification. On the other hand, damage had also been afflicted on the mucin glycan chains. These structural alterations were responsible that the PGMs have almost entirely lost their ability to act as a lubricant, to form hydrogels (with anti-viral properties), and to create cell-repellent surface layers.[109]

However, even subtle structural alterations of the mucin molecule led to pronounced losses in functionality. In the **Chapters 3** and **4.1**, it was shown that the enzymatic removal of negatively charged glycan residues (or DNA as in the case of lab-purified MUC5AC) resulted in drastic changes in the adsorption behavior and lubricating properties of mucins. A numerical simulation of the mucin molecule (**Chapter 3.3**) clarified that these losses in functionality can be attributed to changes of the conformational state of mucins upon removal of negative charges from the mucin core region: weakening of the intramolecular repulsion, which is responsible for maintaining the elongated conformation of mucins, resulted in a 'collapse' of the mucin molecule.

In light of these experimental insights, the following picture emerged: Structural integrity of the mucin molecule is crucial for it to fulfill its diverse functionalities (**Fig. 6.1**), and a careful purification process is required to isolate such functional mucins from crude mucus.

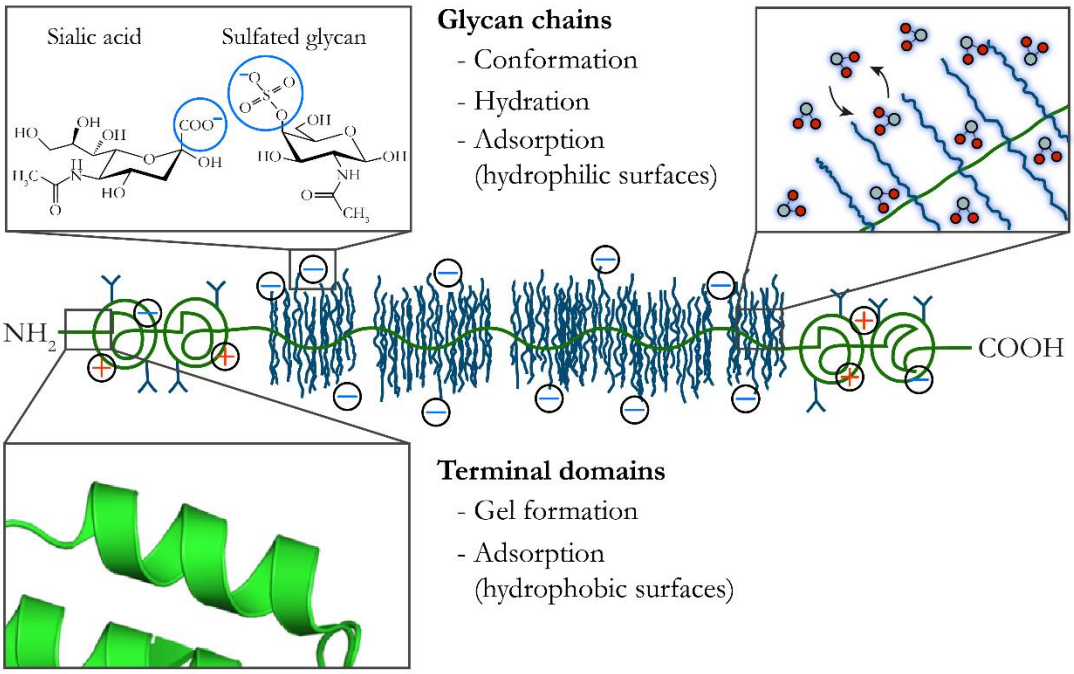

Fig. 6.1: Structure-function analysis of mucin glycoproteins. The mucin molecule is a biomacromolecule with diverse functionalities, which are brought about by different structural motifs. The glycan chains are important to maintain an elongated conformation, and both, electrostatic repulsion and steric effects, contribute, here. Moreover, the glycan chains guarantee proper hydration of the mucin molecule and are likely to facilitate adsorption to hydrophilic surfaces. The hydrophobic mucin termini enable adsorption to hydrophobic surfaces and are critical for mucins to form a network *via* intermolecular linkages.

At least two structural key features of mucin glycoproteins are pivotal for their broad functionality (**Fig. 6.1**): the hydrophobic termini of the macromolecule and the mucin glycan pattern. For instance, the ability to serve as a lubricant is realized by mucin molecules through their ability to efficiently adsorb onto virtually any kind of (hydrophobic or hydrophilic) surface. Structural damages to either the hydrophobic terminal domains or the glycan-decorated core region of mucin, however, compromise the adsorption of mucins to the respective surfaces. This, in turn, will result in an insufficient coverage of the surfaces with lubricating mucin molecules, which corrupts both sacrificial layer formation and hydration lubrication. The detailed mechanisms hindering the surface adsorption process of mucins can be manifold: a loss of the hydrophobic mucin termini, for example, prevents mucin adsorption onto hydrophobic surfaces (such as PDMS).[40] Likewise, damages inflicted on the mucin glycans may result in reduced mucin adsorption onto hydrophilic or charged surfaces; This

type of damage can also affect mucin adsorption to hydrophobic surfaces if they are severe enough to induce conformational changes in the glycoprotein such that the termini are not accessible anymore. Such a loss or inaccessibility of the mucin termini can also compromise the ability of mucins to form a polymeric network (and thus a hydrogel; **Chapter 5.1**). These networks are thought to be established by a combination of intermolecular disulfide bridges and attractive electrostatic as well as hydrophobic forces acting between individual mucin glycoproteins.[34, 189] Of course, other structural components of the mucin glycoprotein, *e.g.*, uncharged glycans, might play an important role for the physiological functions discussed in thesis as well. For instance, steric effects arising from the glycan chains might help maintaining the elongated mucin conformation.[255] However, at this point, it remains unclear to what extent these particular motifs contribute to mucin functionality – this is an open question that future research will have to address.

There are also other (physiological) functions mucins may contribute to, and those could not be explored within in the scope of this work. Indeed, in the past years, academic research has increasingly focused on the question of how mucins can regulate microbial gene expression. For instance, recent research indicated that mucin glycans seem to be able to attenuate the virulence of certain pathogens.[256] Moreover, mucin glycans play an important role in shaping and maintaining a healthy microbiota, *e.g.*, by providing a nutrient source for certain commensal species only.[15] In addition, mucins help regulating the spatial organization of microbial populations and thereby maintain a stable microbiome, for instance, in the gastrointestinal tract.[257, 258] Thus, it is crucial that the mucins selected to study such effects possess an intact glycosylation pattern (which should discourage researchers to use commercial PGM variants).

In addition, mucins have gained increasing attention in the field of medical research in the past years – either as building blocks for drug carriers/depots or even as active compounds. The presence of different functional groups such as cysteines, amines, and sialic acids renders mucins available for different chemical conjugation methods; of course, for successful conjugation, intact mucins are required as well. With such chemical modifications, it is not only possible to attach mucins to a broad range of surfaces but they can also be incorporated into organic and inorganic frameworks such mucin-based hydrogels and nanoparticles. Those mucin-based objects constitute valuable tools in the field of drug delivery: here, mucins can serve as biocompatible and easy-to-modify structural elements that allow to load the carrier objects with a broad range of molecules and enable the controlled release of pharmaceuticals. In typical examples of drug carriers made from hybrid materials making use of purified mucins, the main component of the composite matrix is established by other (bio-)polymers such as PEG[259], gelatin[260], cellulose[261], and chitosan[262]. In those examples, the negative net charge of mucins conveys additional properties to the matrix the mucins are integrated into; for instance,

mucin-enriched hydrogels can be better loaded with cationic drugs and retard the release of positively charged cargos.[263, 264] In more advanced approaches, mucin-based drug carriers were engineered such that they released their cargo, *i.e.*, the drug molecules, only when a suitable trigger event occurred (such as the exposure to a physiological salt concentration or disease-specific nucleic acids).[264, 265]

In addition to drug delivery applications, mucins are also promising candidates for other medical products, which make use of their physico-chemical properties. For instance, the hydrating and lubricating properties of mucins may be exploitable. Patients suffering from *keratoconjunctivits sicca* (colloquially referred to as 'dry eye syndrome') or the *Sjögren syndrome* experience an irritation of the ocular tissue, eye redness, and pain resulting from inflammations.*[266] Owing to their excellent water binding capacity, administering purified mucins as eye drops might help to rehydrate the corneal surfaces. Similarly, *xerostomia* ('dry mouth syndrome') patients might greatly benefit from mucin-based sprays to remedy oral dryness. In addition, when used as component of a mouth wash, the anti-biofouling properties of mucins could help preventing the colonization of our teeth.[16] Although some potential applications have been pinpointed in this section, it is unlikely that the full potential mucins hold as components of medical product has been explored already.

All these examples presented above highlight the great potential mucins hold for the treatment of various medical conditions. As a consequence, the demand for functional mucins can be expected to further increase in the near future – potentially to a point where it can no longer be covered by lab-purified mucins alone. Thus, inspired by the modular composition of mucins, researchers aimed at creating synthetic mucins (or polymers featuring defined motifs replicating natural mucin domains) to meet this enhanced demand.[267] In these approaches, typically, a small set of simple monomers (carbohydrates or small, organic molecules) was assembled into synthetic mucin surrogates, which emulated the structure, physical properties, and functionalities of native mucins or certain mucin domains. Variations in monomer composition, monomer sequence, and chain length allowed for creating mucin mimics with tailored properties.[268-271] So far, however, no fully synthetic analogues that could reproduce all the versatile functionalities of natural mucins could be synthetized. In this context, a thorough understanding of the structure-function relationships of mucin glycoproteins and the mechanistic principles governing mucin functionalities is of critical importance. Thus, the structure-function analysis performed in this thesis may be of great value for engineering artificial, mucin-inspired polymers in the future.

* The origin of these disorders lies in an increased tear evaporation due to an dysfunction of the Meibomian glands.[266]

Appendix

Appendix A1: Detailed characterization of the MUC5AC glycoprotein*

To determine the detailed protein composition of lab-purified MUC5AC and the two re-purified, commercial PGM variants, samples of these mucins were subjected to a mass spectroscopic analysis. For this purpose, from each lyophilized mucin sample, 1 mg was dissolved in 50 mM ammonium bicarbonate buffer (pH 7.8) containing 6 M guanidine hydrochloride. The proteins were reduced by adding dithiothreitol (DTT) to a final concentration of 10 mM, and the samples were incubated at 55 °C for 1 h. Subsequently, the samples were alkylated by adding 2-iodoethanol to a final concentration of 1 % (v/v) to prevent covalent mucin crosslinking *via* disulfide bonds; here, the incubation was conducted at room temperature for 30 min in the dark. Afterwards, the samples were transferred into prewetted Microcon filter tubes (Ultracel YM-10, Merck Millipore, Burlington, MA), centrifuged at 12000 xg for 10 min, and washed thrice with 50 mM ammonium bicarbonate buffer. Then, 0.5 µg trypsin (Promega/SDS Bioscience, Madison, WI) dissolved in 200 µL of 0.2 M ammonium bicarbonate buffer (pH 7.8) were added to each sample, and the reaction mixtures were incubated at 37 °C overnight. The resulting peptides were collected in new collection tubes by two consecutive centrifugation steps (each run at 12000 xg for 10 min) in 50 µL of 50 mM ammonium bicarbonate buffer. The obtained solutions were freeze-dried, and the obtained powder was dissolved in 0.1 % (v/v) formic acid for the subsequent mass spectrometric analysis. Peptide analysis was performed with a nanoACQUITY Ultra Performance Liquid Chromatography system coupled to a Q-TOF mass spectrometer (Xevo Q-TOF, Waters, Milford, MA) as described previously.[272] In brief, the peptides were loaded onto a C_{18} trap column (Symmetry 180 µm × 20 mm, 5 µm; Waters) followed by washing with 1 % (v/v) acetonitrile, 0.1 % (v/v) formic acid at 15 µL min^{-1} for 10 min. The samples eluted from the trap column were separated on a C_{18} analytical column (75 µm × 100 mm, 1.7 µm; Waters) at a flow rate of 225 nL min^{-1} using 0.1 % (v/v) formic acid as solvent A and 0.1 % (v/v) formic acid in acetonitrile as solvent B in a stepwise gradient: 0.1−10 % B (0−5 min), 10−30 % B (5−32 min), 30−40 % B (32−35 min), 40−85 % B (36−38 min), 85 % B (38−40 min), 85−0.1 % B (40−42 min), and 0.1 % B (42−60 min). The eluting peptides were sprayed into the mass spectrometer (capillary and cone voltages set to 2 kV and 35 V, respectively), and tandem mass spectrometry (MS/MS) spectra were acquired using automated data-directed switching between the MS and MS/MS modes using the instrument software (MassLynx V4.0 SP4). Each sample was

* This section follows in part the publication Marczynski *et al.*, Biomacromolecules (2021).

analyzed two to three times at different predefined mass ranges (400−800 and 800−1600 m/z). In each analysis, the five most abundant signals of a survey scan (different mass ranges, 1 s scan time) were selected by charge state, and the collision energy was applied accordingly for sequential MS/MS fragmentation scanning (50−1800 m/z range, 1 s scan time). The MS raw data files were processed using Mascot Distiller (version 2.4.3.2, Matrix Science, London, U.K.) and the resulting files were submitted to a local Mascot (Matrix Science, version 2.3.2) server using the *Sus scrofa* (Pig) proteome (49,792 sequences) downloaded from the UniprotKB database. The following settings were used for the database search: trypsin-specific digestion with two missed cleavage allowed; ethanolylated cysteine as fixed and oxidized methionine as variable modifications; peptide tolerance of 100 ppm; fragment tolerance of 0.2 Da. Peptides with Mascot ion scores exceeding the threshold for statistical significance ($p < 0.05$) were selected. Proteins identified with at least two (or more) unique peptides were considered.

In the MUC5AC sample, a total of 67 different proteins was identified (**Table A1.1**). Only those protein matches were considered, for which at least three independent hits were recorded during the mass spectroscopic analysis. In this sample, gastric mucin MUC5AC by far outnumbered all other detected proteins: ~29 % (*i.e.*, 217 out of a total of 743 detected matches). In contrast, in the two PGM samples, gastric mucin MUC5AC only comprised a minor fraction of the detected hits with ~7 % (*i.e.*, 5 out of a total of 70 matches) and ~5 % (*i.e.*, 9 out of a total of 172 matches), respectively.

Table A1.1: Mass spectrometric analysis of MUC5AC. 67 different proteins were identified in this sample when the matches were tested against a porcine (*Sus scrofa*) protein database. Gastric mucin MUC5AC is highlighted in bold font.

#	Description: gene (protein)	No. of significant matches	No. of significant sequences
1	**MUC5AC (Mucin 5AC = gastric mucin)**	**217**	**60**
2	FCGBP (IgGFc-binding protein)	35	23
3	CLCA1 (Calcium-activated chloride channel regulator 1)	32	16
4	N/A (uncharacterized protein) = IgM heavy chain constant region	26	12
5	KRT8 (Keratin, type II cytoskeletal 8 isoform 2)	23	11
6	BPIFB1 (Long palate lung and nasal epithelium protein 1)	20	12
7	H4F3 (Histone H4)	17	7
8	H1-3 (Histone H2B)	16	6
9	ACTG1 (gamma-Actin)	15	9
10	AGR2 (Anterior gradient protein 2 homolog)	14	6
11	A2M (alpha-2-Macroglobulin)	13	8
12	ACTN4 (alpha-Actinin-4)	12	6
13	FLNB (Filamin B, beta)	12	8
14	HBB (Hemoglobin subunit beta)	11	6

15	GAPDH (Glyceraldehyde-3-phosphate dehydrogenase)	10	6
16	OLFM4 (Olfactomedin 4)	10	8
17	MUC2 (Mucin 2)	9	6
18	ALDH1A1 (Retinal dehydrogenase 1)	9	4
19	ATP5F1B (ATP synthase subunit beta)	9	6
20	CKMT1A (Creatine kinase, mitochondrial 1A)	9	6
21	KRT1 (Keratin-1)	8	4
22	DMBT1 (Deleted in malignant brain tumors 1 protein)	8	4
23	LDHB (L-Lactate dehydrogenase B chain)	8	5
24	LGALS3 (Galectin-3)	8	5
25	PDIA6 (Protein disulfide-isomerase A6)	7	4
26	N/A (uncharacterized protein) = Immunoglobulin lambda like polypeptide 5	7	3
27	ALB (Serum albumin)	7	5
28	HSPA1B (heat shock 70 kDa protein 1B)	7	4
29	FCN2 (Ficolin-2)	7	4
30	HSPA8 (Heat shock protein family A member 8)	6	4
31	MUC1 (Mucin 1)	6	2
32	RPL10A (60S ribosomal protein L10a)	6	4
33	VCP (15S Mg(2+)-ATPase p97 subunit)	6	4
34	HSP90B1 (Endoplasmin = heat shock protein 90kDa beta member 1)	6	5
35	HADHA (Trifunctional enzyme subunit alpha, mitochondrial)	6	3
36	HSPE1 (10 kDa heat shock protein, mitochondrial)	6	3
37	GOT2 (Aspartate aminotransferase, mitochondrial)	5	4
38	RPLP0 (60S acidic ribosomal protein P0)	5	3
39	HSP90AA1 (heat shock protein HSP 90-alpha)	5	4
40	PDIA3 (Protein disulfide-isomerase A3)	5	2
41	LOC100624785 (Tubulin beta chain)	5	3
42	PRDX1 (Peroxiredoxin-1)	5	3
43	N/A (uncharacterized protein; immunoglobulin light chain constant region)	4	2
44	N/A (uncharacterized protein; immunoglobulin heavy variable 3-23)	4	2
45	KRT18 (Keratin 18)	4	3
46	PGD (6-Phosphogluconate dehydrogenase, decarboxylating)	4	4
47	GKN1 (Gastrokine-1)	4	4
48	RPS2 (40S ribosomal protein S2)	4	2
49	GSTP1 (Glutathione S-transferase P)	4	3
50	PSME1 (Proteasome activator complex subunit 1)	4	2
51	H2AJ (Histone H2A type 1-J)	4	2
52	H3C15 (Histone H3	4	2
53	ANXA4 (Annexin A4)	3	2
54	PIGR (polymeric immunoglobulin receptor)	3	2
55	CLIC1 (Chloride intracellular channel protein 1)	3	2
56	RPSA (40S ribosomal protein SA)	3	2
57	GPI (Glucose-6-phosphate isomerase)	3	2

58	CKB (Creatine kinase)	3	2
59	UGDH (UDP-glucose-6-dehydrogenase)	3	3
60	TAGLN2 (Transgelin-2)	3	2
61	ATP5F1A (ATP synthase F1 subunit alpha, mitochondrial)	3	3
62	HBA (Hemoglobin subunit alpha)	3	2
63	LGALS3BP (Galectin-3-binding protein)	3	3
64	LOC100513601 (Ig-like domain-containing protein)	3	2
65	LGALS4 (Galectin-4)	3	2
66	ENO1 (Enolase 1)	3	2
67	SPTAN1 (Spectrin alpha chain, brain)	3	2

In the two re-purified PGM samples, a total of only 14 and 23 different proteins were identified, respectively (**Tables A1.2** & **A1.3**). If ranked in a descending order based on the number of detected matches for the different, gastric mucin MUC5AC only takes rank 8 and 9, respectively.

Table A1.2: Mass spectrometric analysis of re-purified PGM Type II. 14 different proteins were identified in this sample when the matches were tested against a porcine (*Sus scrofa*) protein database. Gastric mucin MUC5AC (*i.e.*, PGM) is highlighted in bold font.

#	**Description: gene (protein)**	**No. of significant matches**	**No. of significant sequences**
1	LOC106504545 (Serpin domain-containing protein)	10	5
2	CHIA (Chitinase)	6	3
3	KRT1 (Keratin 1)	6	3
4	PGA (Pepsin A)	5	1
5	N/A (uncharacterized protein; immunoglobulin heavy variable 3-23)	5	2
6	TFF1 (Trefoil factor 1)	5	2
7	N/A (uncharacterized protein) = IgM heavy chain constant region	5	2
8	**MUC5AC (Mucin 5AC)**	**5**	**3**
9	CD63 (CD63 antigen)	4	1
10	PGB (Pepsin B)	4	2
11	TFF2 (Trefoil factor 2)	4	2
12	MUC2 (mucin 2)	4	2
13	KRT10 (Keratin 10)	4	3
14	PSCA (Prostate stem cell antigen preproprotein)	3	2

Table A1.3: Mass spectrometric analysis of re-purified PGM Type III. 23 different proteins were identified in this sample when the matches were tested against a porcine (*Sus scrofa*) protein database. Gastric mucin MUC5AC is highlighted in bold font.

#	Description: gene (protein)	No. of significant matches	No. of significant sequences
1	LOC106504545 (Serpin domain-containing protein)	17	8
2	LTF (Lactotransferrin)	15	9
3	H4F3 (Histone H4)	13	5
4	KRT10 (Keratin 10)	13	8
5	CHIA (Chitinase)	11	5
6	KRT1 (Keratin 1)	11	7
7	LOC100302368 (Trypsinogen isoform X1)	9	4
8	N/A (uncharacterized protein) = IgM heavy chain constant region	9	6
9	**MUC5AC (Mucin 5AC)**	**9**	**6**
10	FCN2 (Ficolin-2)	8	4
11	Lysozyme C-1	7	3
12	N/A (uncharacterized protein) = Immunoglobulin lambda like polypeptide 5	7	3
13	PGA (Pepsin A)	6	2
14	N/A (uncharacterized protein; immunoglobulin light chain constant region)	5	3
15	KRT2 (Keratin 2)	4	3
16	PGB (Pepsin B)	4	2
17	MVP (Major vault protein)	4	2
18	MUC2 (Mucin 2)	4	2
19	H2BC11 (Histone 2B)	4	3
20	TPM1 (Tropomyosin alpha-1 chain)	3	2
21	CTSC (Cathepsin C)	3	2
22	PSCA (Prostate stem cell antigen preproprotein)	3	2
23	TCN1 (Transcobalamin-1)	3	2

In a second batch of functional, lab-purified MUC5AC (*i.e.*, MUC5AC/KTH), 38 different proteins were identified. Also here, only those protein matches were considered, for which at least three independent hits were recorded during the mass spectroscopic analysis. In this sample, gastric mucin MUC5AC outnumbered all other detected proteins: ~32 % (*i.e.*, 141 out of a total of 446 detected matches).

Table A1.4: Mass spectrometric analysis of MUC5AC/KTH. 38 different proteins were identified in this sample when the matches were tested against a porcine (*Sus scrofa*) protein database. Gastric mucin MUC5AC is highlighted in bold font.

#	Description: gene (protein)	No. of significant matches	No. of significant sequences
1	**MUC5AC (mucin 5AC = gastric mucin)**	**141**	**49**
2	N/A (uncharacterized protein) = IgM heavy chain constant region	23	8
3	ALB (Serum albumin)	22	11
4	HBB (Hemoglobin subunit beta)	19	9
5	ANXA2 (Annexin A2)	19	10
6	H4F3 (Histone H4)	13	5
7	KRT8 (Keratin, type II cytoskeletal 8 isoform 2)	13	7
8	MUC2 (Mucin 2)	10	6
9	COL1A1 (Collagen, Type I, alpha 1)	10	5
10	ANXA5 (Annexin A5)	10	6
11	BPIFB1 (Long palate lung and nasal epithelium protein 1)	10	6
12	DMBT1 (Deleted in malignant brain tumors 1 protein)	9	4
13	H2BC11 (Histone 2B)	9	4
14	CKMT1 (Creatine kinase U-type, mitochondrial)	9	5
15	MYH14 (Myosin 14)	9	6
16	ALDH1A1 (Retinal dehydrogenase 1)	9	7
17	ACTG1 (gamma-Actin)	8	4
18	N/A (uncharacterized protein) = Immunoglobulin lambda like polypeptide 5	8	3
19	OLFM4 (Olfactomedin 4)	8	5
20	FCGBP (IgGFc-binding protein)	8	5
21	HBA (Hemoglobin subunit alpha)	7	3
22	CLCA1 (Calcium-activated chloride channel regulator 1)	7	4
23	ANXA10 (Annexin A10)	5	2
24	N/A (uncharacterized protein; Ig light chain constant region)	5	3
25	CA2 (Carbonic anhydrase II)	5	3
26	GSTP1 (Glutathione S-transferase P)	5	4
27	ANXA1 (Annexin A1)	4	2
28	N/A (uncharacterized protein; immunoglobulin heavy variable 3-23)	4	2
29	KRT1 (Keratin 1)	4	2
30	LGALS4 (Galectin-4)	4	2
31	A2M (alpha-2-Macroglobulin)	4	2
32	PGA (Pepsin A)	4	2
33	PFN1 (Profilin 1)	4	3
34	PKM (Multifunctional fusion protein)	4	3
35	GDI2 (Rab GDP dissociation inhibitor beta)	4	3
36	TPI1 (Triosephosphate isomerase)	3	2
37	ENO1 (Enolase 1)	3	2
38	AGR2 (Anterior gradient protein 2 homolog)	3	2

Appendix

It is important to note that the numbers of peptide fragments detected for the different proteins in each sample do not reflect the quantitative composition of the three mucin preparations. This can be attributed to two reasons: First, since the proteins in the mucin samples come in various sizes (and thus with different numbers of target sites for tryptic digestion), the number of peptide fragments that can be obtained during sample preparation varies between different proteins. Second, the dense glycosylation of the mucin core region affects the result of the trypsin treatment; the glycosylated domain is efficiently protected from proteolytic degradation. Both their large size and the presence of posttranslational modifications (*i.e.*, the mucin glycan chains) render the identification of such non-fragmented mucin cores challenging. When the amino acid sequences of all peptide fragments that are assigned to gastric mucin in each sample are compared to the amino acid sequence deposited in the porcine proteome database for gastric mucin (accession number A0A287ANG4; 07/24/2021), a sequence coverage of ~24 % was obtained for MUC5AC, but coverage values of only ~0 % and ~2 %, respectively for the two commercial PGM variants.

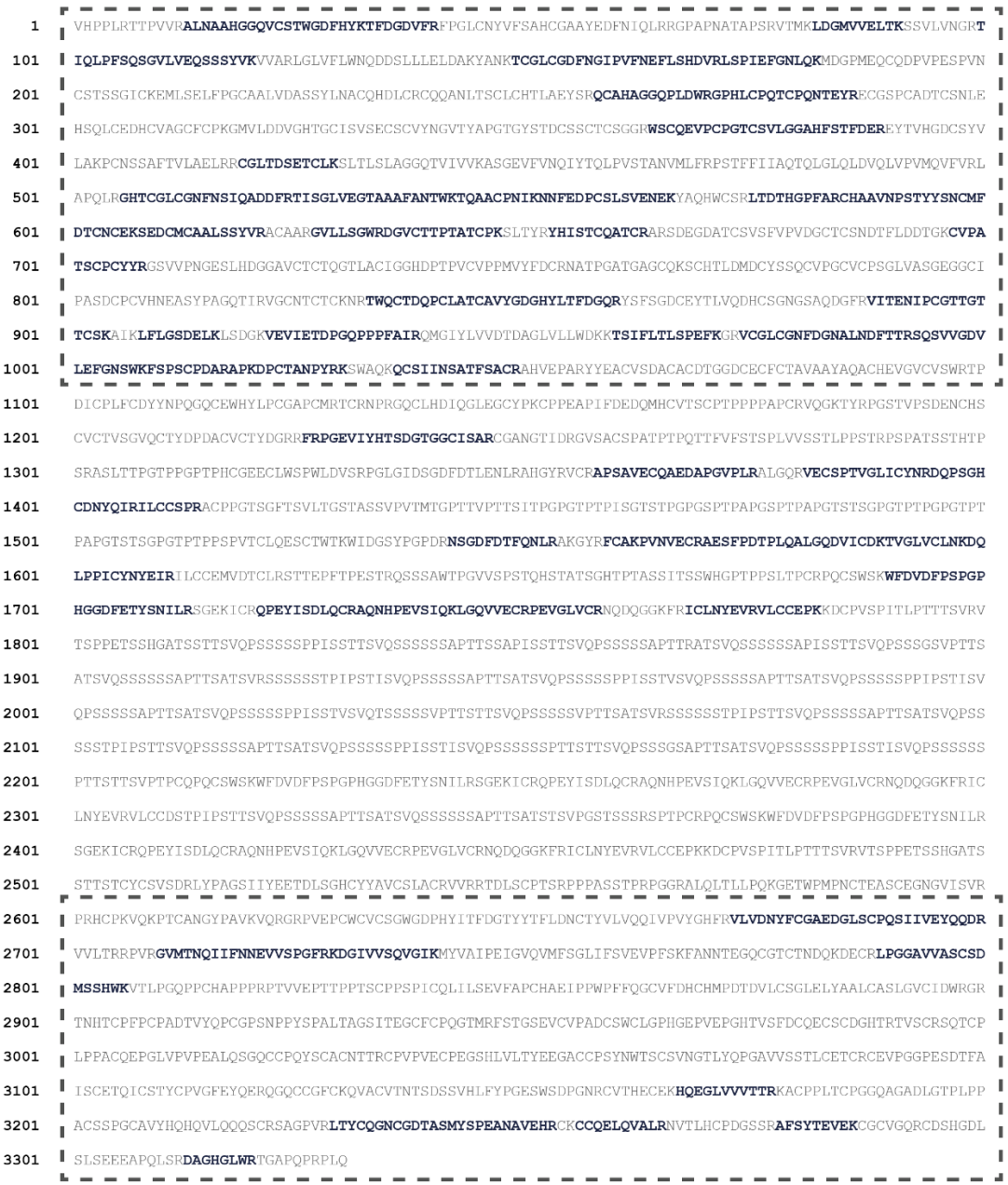

Sequence coverage: MUC5AC ~24 %

Fig. A1.1: Mass spectrometric analysis of trypsin treated MUC5AC. The peptides identified during the mass spectrometric analysis are highlighted in dark blue. The percentage of the MUC5AC amino acid sequence covered by the identified sequences is ~24 %. The accession number of the entry for MUC5AC, which was used for determining the coverage is A0A287ANG4 (07/24/2021). The dashed frames indicate the sequence sections, which were considered as mucin termini for the sequence analysis. If only those terminal sequences were considered for analysis, a sequence coverage of ~32 % is obtained.

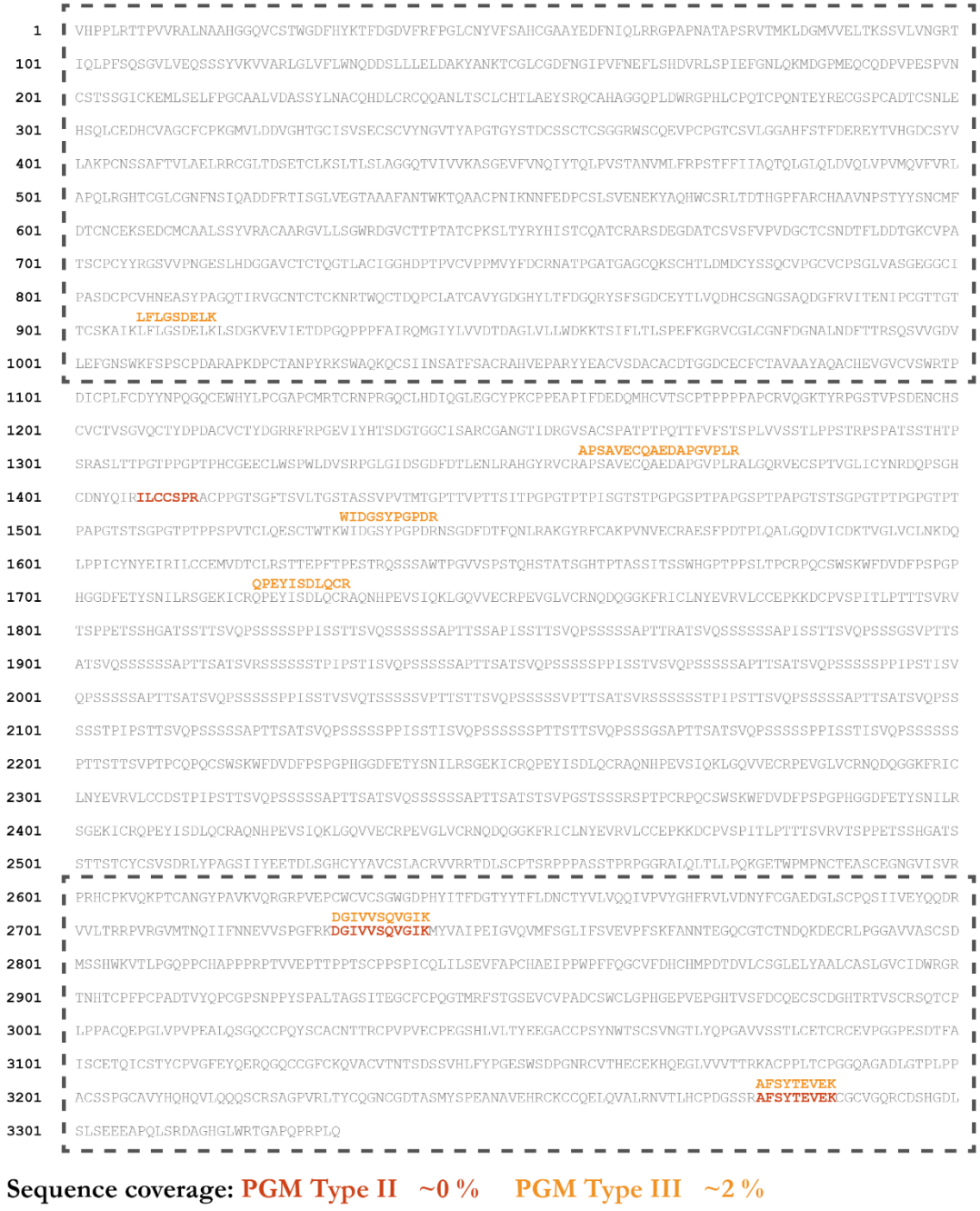

Sequence coverage: PGM Type II ~0 % PGM Type III ~2 %

Fig. A1.2: Mass spectrometric analysis of the two trypsin treated PGM variants. The peptides identified during the mass spectrometric analysis are highlighted in orange (PGM Type II) and yellow (PGM Type III). The percentages of the MUC5AC amino acid sequence covered by the identified sequences are ~0 % and ~2 %. The accession number of the entry for MUC5AC, which was used for determining the coverage is A0A287ANG4 (07/24/2021). The dashed frames indicate the sequence sections, which were considered as mucin termini for the sequence analysis. If only those terminal sequences were considered for analysis, sequence coverage values of ~1 % and ~2 % are obtained.

Fig. A1.3: Comparison of the predicted amino acid sequence of porcine gastric mucin MUC5AC with the sequence of the UniprotKB database entry A0A287ANG4_PIG. The predicted amino acid sequence (XP_020938242.1; 24/07/2021; based on an automated computational analysis of the genomic sequence NC_010444.4) of porcine gastric mucin is compared with the sequence (A0A287ANG4_PIG) that was used for identifying detected peptides during the mass spectrometric analyses. The latter sequence comprises mainly the mucin termini, whereas large sections of the glycosylated core protein are not covered. Black letters indicate peptide sequences covered by the UniprotKB entry A0A287ANG4_PIG, gray letters indicate sequences not covered by this entry.

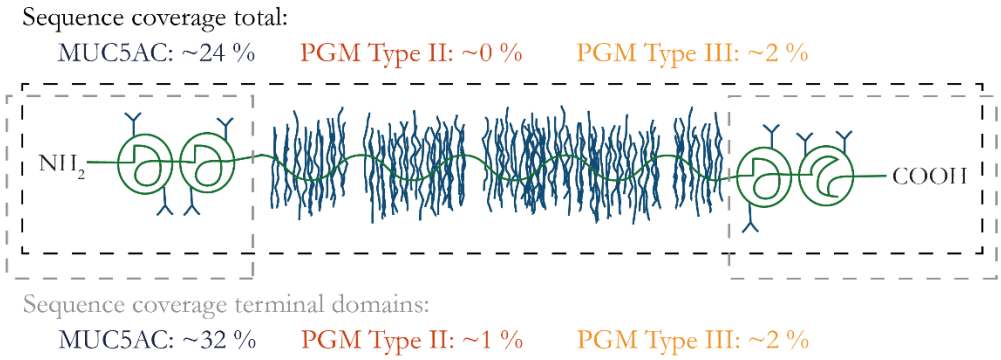

Fig. A1.4: Sequence coverage values obtained for lab-purified MUC5AC and the two commercial PGM variants. For lab-purified MUC5AC, a sequence coverage of ~24 % was obtained; in contrast, the matches obtained for the two PGM variants only covered ~0 and ~2 % of the same sequence, respectively. If only the amino acid sequences of the N- and C-termini were considered, a coverage of ~32 % was obtained for MUC5AC and coverage values of ~1 and ~2 %, respectively, for the two PGM variants.

To quantify the binding of chemical objects to mucins and determine binding affinities or the stoichiometry of binding events it is critical to know the molecular weight of MUC5AC. In the past, a broad spectrum of values ranging from ~1 MDa to up to ~15 MDa has been reported for the molecular weight of gastric mucin.[179, 273, 274] So far, both, the high level of intrinsic structural heterogeneity as well as the poor resolution of chromatography resins in the high molecular weight range rendered it difficult to accurately estimate the molecular of MUC5AC monomers. Combining size exclusion chromatography (SEC) with multi-angle laser light scattering (MALLS) allowed for obtaining more precise estimation of the molecular weight of this specific mucin variant. For this purpose, the lab-purified MUC5AC and the re-purified PGM samples were dissolved at concentrations between 0.5- 4.0 mg mL^{-1} in the eluent solution (*i.e.*, DMSO supplemented with 0.5 % (w/w) lithium bromide to promote molecule solubility and to limit both mucin aggregation and the association of mucins with DNA fragments) and analyzed by size exclusion chromatography (SECcurity 1260, Polymer Standard Services, Mainz, Germany) coupled to a refractive index detector (SECcurity 1260, Polymer Standard Services, Mainz, Germany) and a multi-angle laser light scattering device (MALLS, BIC-MwA7000, Brookhaven Instruments, New York). The refractive index increment (d*n*d*c*) for the mucin samples was calculated from sample injection at increasing concentrations to a value of 0.0594 mL g^{-1}. Separation was performed using a 100 Å GRAM pre-column and 30 Å and 10,000 Å analytical columns from PSS (Mainz, Germany) at a flow rate of 0.5 mL min^{-1} at 60 °C. Data was processed using the WinGPC (PSS, Mainz, Germany) software to obtain the SEC weight distributions, the absolute molecular weights (M_w) after Zimm extrapolation, and the radii of gyration (R_g). Hyphenation of MALLS to SEC separation enables the online

monitoring of the absolute molecular weight (M_w) and radius of gyration (R_g) for the mucin glycoproteins as they elute from the SEC column.

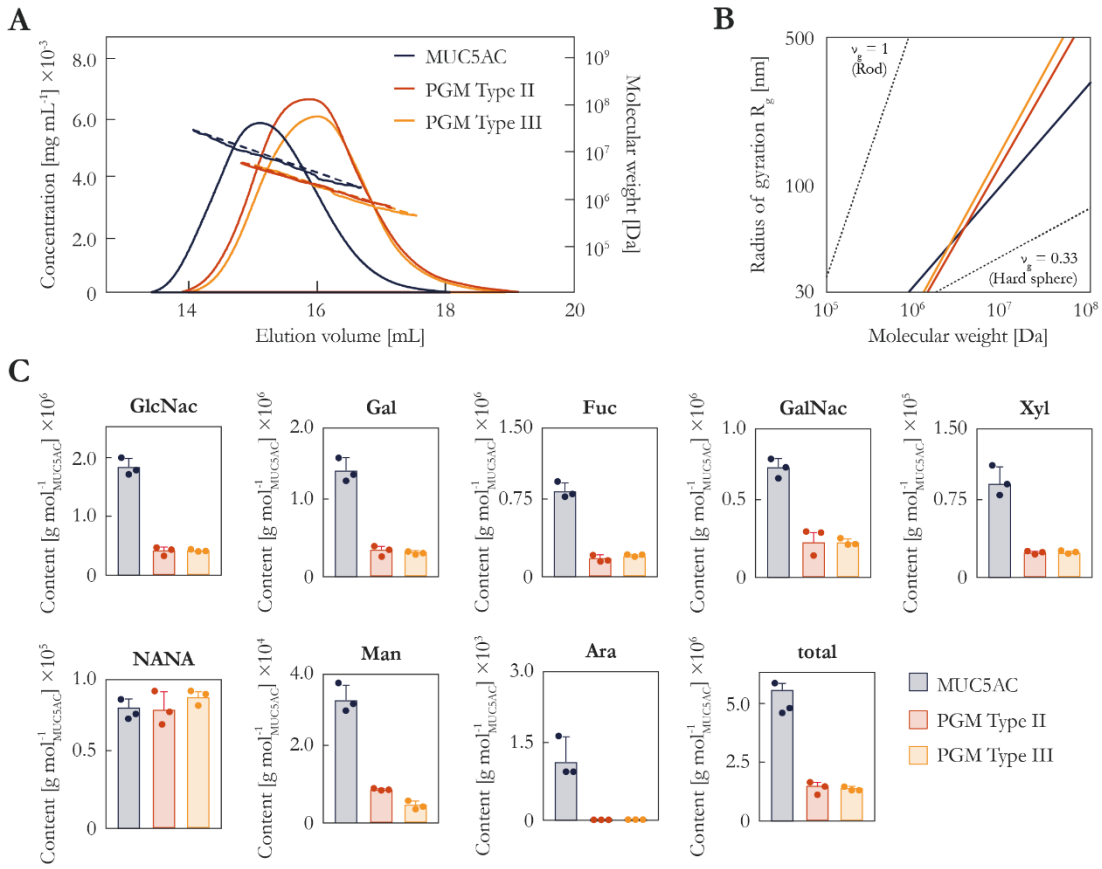

Fig. A1.5: Determination of molecular weights, fractal coefficients, and glycan contents of the different mucin variants. Peaks representing the MUC5AC concentration in the elution profiles (solid lines) and molecular weights of the three different mucin samples as determined by MALLS (dashed linear fits overlaying experimentally determined curves; **A**). Fractal dimension ν_g allows for assessing the mucin conformation. Whereas commercial PGM molecules exhibit a rather stiff conformation (ν_g ~0.70−0.75), lab-purified MUC5AC have a higher conformational flexibility (ν_g ~0.50−0.55; **B**). The amounts of eight different monosaccharides were quantified: *N*-acetylglucosamine (GlcNac), galactose (Gal), fucose (Fuc), *N*-acetylgalactosamine (GalNac), xylose (Xyl), *N*-acetyl-neuraminic acid (NANA; sialic acid), mannose (Man), and arabinose (Ara). Error bars indicate the standard deviation as obtained from three individual analyses (n = 3). The individual data points acquired at each condition are represented by points. To calculate molar concentrations for the different saccharide species, measured data were normalized to the molecular weights determined during the SEC-MALLS measurements (**C**).

An earlier elution of the lab-purified MUC5AC from the SEC column compared to the two commercial variants indicated that lab-purified mucins had a larger hydrodynamic size than commercial mucins. In accordance with previous studies, considerably smaller molecular weights were determined the two commercial PGM variants (~2.4 MDa and ~2.5 MDa, respectively) than

for lab-purified MUC5AC, for which a molecular weight of ~9.1 MDa was obtained (**Fig. A1.5 A**). Theoretically, the molecular weight of an individual porcine gastric mucin molecule can be easily approximated: based on the amino acid sequence computed for porcine MUC5AC, the molecular weight of the protein backbone alone is ~0.6 MDa. Additionally, an extensive glycan analysis (by means of high-performance anion-exchange chromatography with pulsed amperometry detection = HPAEC-PAD) of lab-purified MUC5AC and the two commercial PGM variants indicated that the total amount of glycans added up to ca. 3−5 MDa (**Fig. A1.5 C**). Based on these estimations, it appears reasonable to assume a total molecular weight of ca. 3.5−5.5 MDa for porcine gastric mucin.

Yet, this estimated value was somewhat smaller than those determined experimentally for MUC5AC (**Fig. A1.5 A**). However, these experimental values represented the average molecular weight of a population of mucins with a relatively broad molecular weight distribution. It has been repeatedly shown that the composition and the extent of the mucin glycan pattern is highly dependent on the health state and the dietary of the individual animal, and this also applies to the pigs from whom the stomachs are obtained.[208, 275] During the first step of the purification procedure, gastric mucus collected from dozens of individual pigs was pooled together – and this step might be responsible (at least in part) for the broad molecular weight distribution of mucins. Furthermore, mucins have a high propensity to associate into oligomers, and – even when dissolved in DMSO – not all mucin molecules might be in their monomeric state; instead, many of them might be present as dimers or oligomers.

Furthermore, light scattering also allowed for assessing the conformation of mucin molecules from the different samples as represented by the fractal dimension ν_g, which occurs as an exponent in the de Gennes scaling law concept and describes the protein architecture.[276] For lab-purified MUC5AC, ν_g adopted a value 0.51, which corresponds to a linear random coil conformation. For the two commercial PGM variants, ν_g adopted values of 0.70 and 0.76, respectively, which corresponds to a somewhat stiffer rod-like conformation (**Fig. A1.5 B**). The larger ν_g values determined for the two PGM variants might be attributed to the comparatively high conformational rigidity of the glycosylated mucin core (established by both repulsive electrostatic forces acting between anionic moieties and steric interactions), which – different from the terminal domains – seems to be preserved in commercial PGM preparations.[176]

Appendix A2: Modifications of the mucin purification procedure*

Although highly functional MUC5AC glycoproteins can be obtained following the state of the art procedure described by Schömig *et al.*[22], the achievable yields are still rather low (*i.e.*, ~100 mg purified mucin per pig stomach). To employ mucins in medical applications, a scale-up for the purification of functional mucins is required to satisfy the potentially high demand. Moreover, some process steps such as the initial mucus collection procedure are very time-consuming and require manual hand work. Thus, to reduce the 'production costs' for high-quality mucins, simplification, time reduction as well as a partial automatization of the mucin purification procedure are desired.

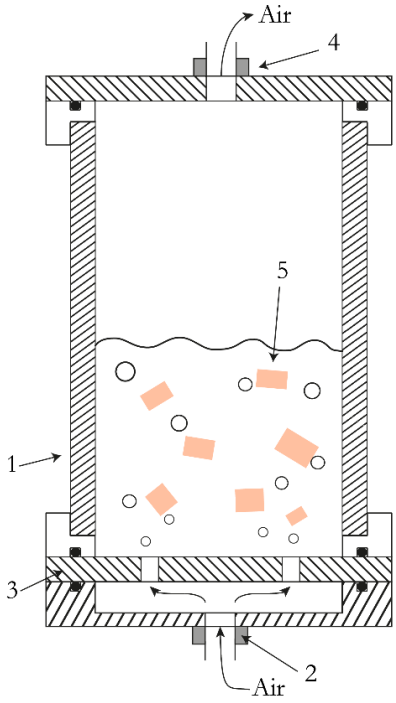

Fig. A2.1: Schematic of the aerated bubble column, which can be used for harvesting mucus from mucosal tissues. An aerated bubble column comprising a cylindrical main body (1), a bottom plate with gas inlet (2) and a non-return valve (3), and a lid with equipped with a gas outlet (4) was used to transfer mucus from the stomach internal surface (5) into a buffered solution. The bubble column is cooled to 4 °C, while a continuous mixing of the stomach/buffer mixture allows for dissolving the mucus and, in parallel, a homogenization of the fluid. By decanting the fluid afterwards through a grid an easy separation of liquid and solid parts is achieved, which reduces the number of required centrifugation steps afterwards.

To meet these demands, as a first modification step, the initial mucus collection procedure was semi-automatized. Using an aerated bubble column, mucin containing tissues was contacted with buffer, which led to an efficient transfer of mucins from the tissue surface into the buffer solution (**Fig. A2.1**). The bubble column used to establish this process modification comprised the following components: a hollow chamber made from polymethyl methacrylate (PMMA; **No. 1**), which served as liquid reservoir, an inlet for pressurized air or inert gas (**No. 2**), a non-return valve (**No. 3**), and a gas outlet (**No. 4**) with attached gas overflow filter and collecting flask. The gas inlet of the bubble column comprised several nozzles on the bottom of the column, and the gas outlet was mounted on

* This section follows in part the European patent application EP3792275A1.

top of the hollow chamber. The chamber of the bubble column has an inner diameter of 190 mm and a height of about 500 mm, which results in an operation volume of ~14 L. To provide cooling during operation, the column was placed in a cooling jacket made from PMMA that was filled with ice cubes and insulated to the outside with a 1 cm layer of styrofoam. For mucin purification, fresh pig stomachs were briefly rinsed under a stream of tap water, cut into 4-5 pieces each (**Fig. A2.1**, **No. 5**), and added into the hollow chamber together with pre-cooled buffer (3x PBS containing 1 M NaCl and 0.04 % (w/v) NaN_3, pH 8.0, cooled to 4 °C). Per 1 volume of stomach tissue 2 volumes of PBS buffer were added to the chamber. An increased ion concentration in the buffer was chosen on purpose to enhance the mucin transfer into the aqueous phase by inducing Deby screening effects, thus reducing binding interactions with the tissue surface and other mucus components. Moreover, the pH level of the buffer was increased to 8.0 to compensate for a putative acidification of the buffer over time due to operating the bubble column with (CO_2 containing) pressurized air. To operate the bubble column, the gas pressure was set to ~3 bar using a manometer. An efficient transfer of the mucins into the buffer solution was enabled by a constant aeration of the hollow chamber for 1-2 h, which induced a bubble driven circulation of the buffer and the stomach pieces, and thus a gentle solubilization of the mucins from the mucosal tissues.

A second process modification to the state of the art process was the introduction of subsequent filtration steps: raw mucus (either obtained using the bubble column or the conventional harvesting method) was subjected to at least two subsequent filtrations. First, the collected raw mucus was frozen at -80 °C. Aliquots of the frozen mucus were thawed and poured through a metal grid with an average pore size diameter of 1 mm. This filtered mucus was then subjected to filtration steps through one or several grids made from stainless steel with average pore size diameters of 500, 200, or 125 µm or combinations thereof (**Fig. A2.2**). Afterwards, the filtrates obtained with this procedure were further processed as described in Schömig *et al.* starting from SEC.[22] This particular process modification essentially allowed for the omission of the time consuming and costly (ultra-)centrifugation steps.

By introducing these process modifications, the total amount of mucins that could be obtained per pig stomach was increased to ~300 mg. For comparison, the state of the art process yielded only ~100 mg per stomach. Of course, one of the key requirements that come with the modification of an established purification protocol is maintaining the functionality of the obtained mucins. In fact, mucins that were purified employing the filtration-based protocol (in this particular case, harvesting of the raw mucus was performed manually) exhibited excellent lubricity (**Fig. A2.2 A**). Moreover,

their rheological properties were virtually identical to those of conventionally purified MUC5AC (**Fig. A2.2 B**).

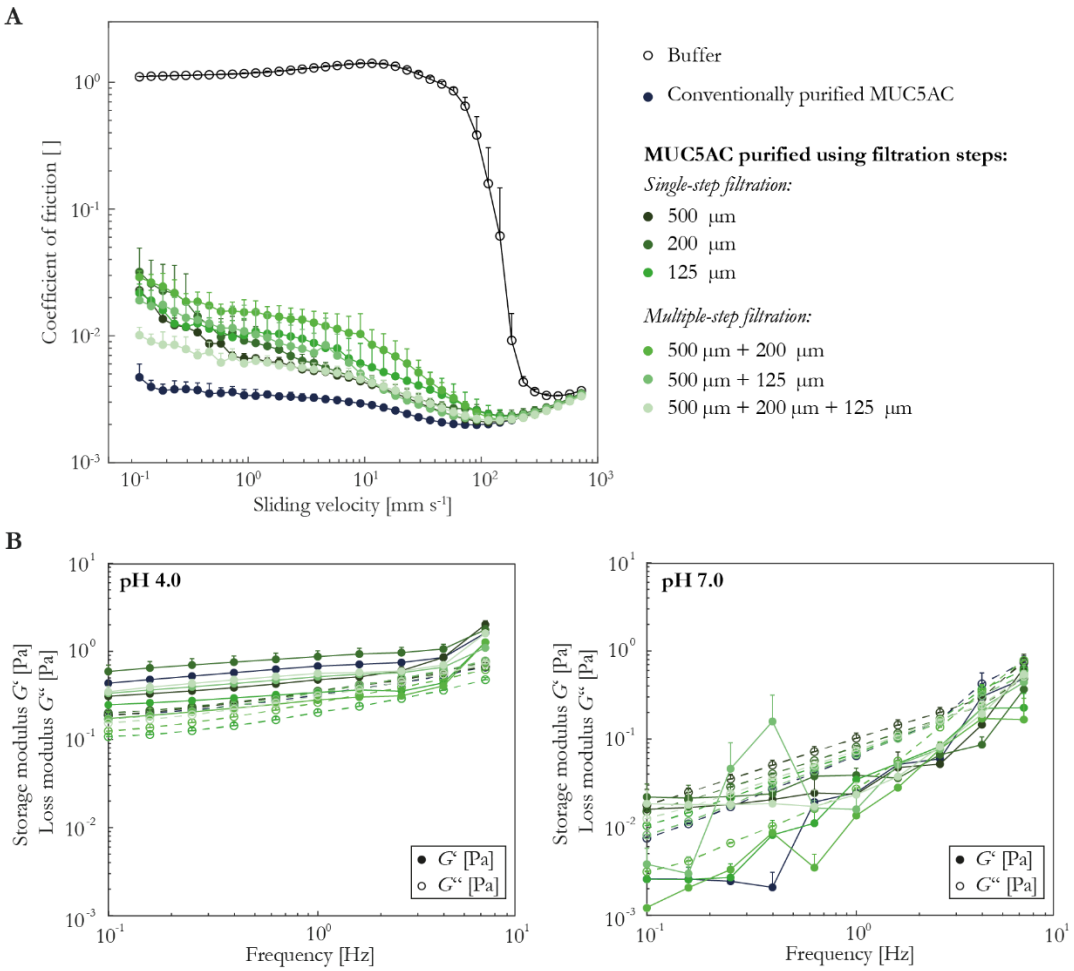

Fig. A2.2: Comparison of the tribological and gelation properties of conventionally purified MUC5AC and variants purified by performing single or multiple, consecutive filtration steps. The mucins obtained using an adapted purification protocol were compared to conventionally purified mucins for their lubricating properties: independent of the procedure used for purification, all mucins showed excellent lubricity over the entire range of probe sliding velocities (**A**). Moreover, the ability to undergo a sol-gel transition (*i.e*, gelation) in a pH-dependent manner was probed: indeed, all mucin variants successfully formed hydrogels at acidic conditions (storage modulus: solid lines, loss modulus: dashed lines; **B**).

Appendix A3: Amino acid sequences of the proteins used in this thesis*

Binding studies with mucin glycoproteins were performed with a variety of different peptides and proteins as binding partners. In addition to eight synthetic peptides, six variants of the protein αSN as well as BSA, lysozyme, and poly-L-lysine with a molecular weight of ~5 kDa were used.

Synthetic peptides

Six fluorescently labeled peptides and two non-fluorescent peptides were used to study mucin binding. The peptides were based on the three amino acids arginine (K, cationic), glutamic acid (E, anionic), and glutamine (Q, polar-uncharged). The detailed sequences are given in **Table A3.1**.

Table A3.1: Peptides used for mucin binding experiments. A total of eight different 24-meric peptides (of which six were labeled with the fluorophore 5,6-TAMRA) was used in this thesis. To estimate the net charge of each peptide/protein at pH levels of 4.0 and 7.0, elementary charges (e) were assigned to chemical groups that are positively charged (pH 4.0: Lys; pH 7.0: Lys) and negatively charged (pH 4.0: dye; pH 7.0: dye, Asp) at the respective pH.

#	Peptide/Protein	Fluorescence Label	Net charge (pH 4.0)	Net charge (pH 7.0)	Hydrophobic domains
1	5,6-TAMRA-$(KKK)_8$	Yes	+23 e	+23 e	Dye
2	5,6-TAMRA-$(QQK)_8$	Yes	+7 e	+7 e	Dye
3	5,6-TAMRA-$(Q_5K)_4$	Yes	+3 e	+3 e	Dye
4	5,6-TAMRA-$(Q_{11}K)_2$	Yes	+1 e	+1 e	Dye
5	5,6-TAMRA-$Q_{21}K_3$	Yes	+2 e	+2 e	Dye
6	5,6-TAMRA-$(EEE)_8$	Yes	-1 e	-25 e	Dye
7	$K_3Q_{18}K_3$	No	+6 e	+6 e	None
8	$Q_{21}K_3$	No	+3 e	+3 e	None

To estimate the net charge of each peptide at both acidic and neutral pH levels, full elementary charges were assigned to amino acid side chains and the conjugated dye. The side chain of the amino acid arginine is positively charged at both pH 4.0 and pH 7.0, whereas the dye was considered to be anionic at both pH levels. Since the pK_a value of the side chain carboxyl group of glutamic acid is ~4.07, in this simple model, this side chain group was considered to be protonated and thus

* This section follows in part the publication Marczynski *et al.*, Biomacromolecules (2019).

uncharged at pH 4.0. At pH 7.0, however, a negative elementary charge was assigned to the glutamic acid residues.

For a more accurate estimation of the charge state of the different oligopeptides, the publicly available charge calculator 'Protein Calculator v3.4' (http://protcalc.sourceforge.net/; 07/24/2021) was used. Since this calculator takes into account only the amino acid sequence but not the conjugated dye, for the six fluorescent peptides, the computed charge values were corrected by subtracting one full elementary charge (**Table A3.2**). Indeed, for all but the 5,6-TAMRA-$(EEE)_8$ peptide at acidic pH, the estimated values were virtually identical with the computed ones. For 5,6-TAMRA-$(EEE)_8$, the computed net charge at pH 4.0 is -7.7. Here, the comparatively larger disparity between the estimated and the computed value was due to the pK_a value of the δ-COOH group being very close (4.07) to the chosen acidic pH level of 4.0.

Expression, purification, and fluorescence labeling of αSN variants

The human wildtype αSN, the αSN truncation mutants αSN 1−108 (amino acid residues 109−140 deleted), αSN 60−140 (amino acid residues 1−59 deleted), αSN 1− 60 (amino acid residues 61−140 deleted), and an αSN variant containing the Parkinson's disease-related single amino acid mutation αSN A30P were all expressed in *E. coli* BL21 (DE3) cells transformed with a pT7-7 plasmid carrying one of the αSN constructs of interest. A details purification procedure for αSN was published by Sidhu *et al.* (2014),[277] and this procedure was followed for αSN 60−140 and αSN A30P. For the αSN 1−60 and αSN 1−108 proteins, the protocol was slightly adjusted. After precipitation, these proteins were resuspended in 50 mM glycine at pH 3.3 and loaded onto a ResourceS column. The αSN 1−60 and αSN 1−108 proteins were subsequently eluted using a linear gradient of NaCl (0−1 M) in 50 mM glycine at pH 3.3. After desalting, the protein stock solutions were stored at −80 °C at a concentration of 250 μM in 0.5 mL aliquots. To enable fluorescence labeling using maleimide functionalized dyes, proteins with an alanine-to-cysteine mutation at amino acid positions 9 and 140 were produced for wildtype αSN and αSN 60−140 and a serine-to-cysteine mutation at amino acid position 9 for αSN 1−108. These proteins were expressed following the abovementioned protocols with the additional inclusion of 1 mM dithiothreitol (DTT) as a reducing agent in all buffers to prevent the formation of disulfide bonds between cysteines. For labeling the αSN cysteine mutants, 1 mg of maleimide Alexa Fluor 647 (AF647; for the wildtype variant) or maleimide Alexa Fluor 488 (AF488; for the two truncated variants) was dissolved in dry dimethylsulfoxide to obtain 25 mM stock solutions. These stock solutions were aliquoted and stored at −20 °C until use. Prior to labeling,

freshly prepared DTT was added to the αSN cysteine mutants to a final concentration of 1 mM, to reduce putative interprotein disulfide bridges. After 30 min of incubation, the excess DTT was removed by using a Zeba Spin desalting column (7 kDa MWCO, 2 mL, Thermo Fisher Scientific). A 3× molar excess of AF647-maleimide was added, and the mixture was incubated in the dark at room temperature for 2 h. Then, excess dye was removed using two subsequent Zeba Spin desalting columns. The final protein concentration and the degree of labeling were calculated from absorbance spectra. The 140 amino acids long αSN amino acid sequence is given below (UniProt entry: P37840; 07/24/2021):

```
1    MDVFMKGLSK AKEGVVAAAE KTKQGVAEAA GKTKEGVLYV GSKTKEGVVH
51   GVATVAEKTK EQVTNVGGAV VTGVTAVAQK TVEGAGSIAA ATGFVKKDQL
101  GKNEEGAPQE GILEDMPVDP DNEAYEMPSE EGYQDYEPEA
```

The peptide sequence can be divided into three distinct domains: a central, hydrophobic region that drives the assembly of αSN into amyloid fibrils is flanked by an amphipathic N-terminal region, which adopts an α-helical conformation when bound to acidic lipid membranes both *in vitro* and *in vivo*, and a highly acidic C-terminal region that conveys an overall negative net charge to the αSN protein at neutral pH levels. However, at the acidic pH values found in the gastrointestinal tract (pH < 4.0), the overall net charge adopts positive values.

Other proteins used for mucin binding experiments

To estimate the net charge of BSA at the two relevant pH levels, the amino sequence as given below was used (UniProtKB entry: P02769; 07/24/2021):

```
1    DTHKSEIAHR FKDLGEEHFK GLVLIAFSQY LQQCPFDEHV KLVNELTEFA
51   KTCVADESHA GCEKSLHTLF GDELCKVASL RETYGDMADC CEKQEPERNE
101  CFLSHKDDSP DLPKLKPDPN TLCDEFKADE KKFWGKYLYE IARRHPYFYA
151  PELLYYANKY NGVFQECCQA EDKGACLLPK IETMREKVLA SSARQRLRCA
201  SIQKFGERAL KAWSVARLSQ KFPKAEFVEV TKLVTDLTKV HKECCHGDLL
251  ECADDRADLA KYICDNQDTI SSKLKECCDK PLLEKSHCIA EVEKDAIPEN
301  LPPLTADFAE DKDVCKNYQE AKDAFLGSFL YEYSRRHPEY AVSVLLRLAK
351  EYEATLEECC AKDDPHACYS TVFDKLKHLV DEPQNLIKQN CDQFEKLGEY
401  GFQNALIVRY TRKVPQVSTP TLVEVSRSLG KVGTRCCTKP ESERMPCTED
```

```
451   YLSLILNRLC VLHEKTPVSE KVTKCCTESL VNRRPCFSAL TPDETYVPKA
501   FDEKLFTFHA DICTLPDTEK QIKKQTALVE LLKHKPKATE EQLKTVMENF
551   VAFVDKCCAA DDKEACFAVE GPKLVVSTQT ALA
```

To estimate the net charge of lysozyme at the two relevant pH levels, the amino sequence as given below was used (UniProtKB entry: P00698; 07/24/2021):

```
1     KVFGRCELAA AMKRHGLDNY RGYSLGNWVC AAKFESNFNT QATNRNTDGS
51    TDYGILQINS RWWCNDGRTP GSRNLCNIPC SALLSSDITA SVNCAKKIVS
101   DGNGMNAWVA WRNRCKGTDV QAWIRGCRL
```

According to the manufacturer, the poly-L-lysine used in this work had an average molecular weight of ~5 kDa. As the molecular weight of the monomer L-lysine is 146.19 g mol^{-1}, each polypeptide comprised – on average – 34 L-lysine units.

In addition to charged amino acid side chains, both BSA and lysozyme also contain a number of hydrophobic amino acid residues, which allow for hydrophobic binding interactions with potential binding partners such as the mucin glycoprotein. Poly-L-lysine, however, is entirely composed of the charged amino acid L-lysine and does not carry any hydrophobic residues.

Table A3.2: Proteins used for mucin binding experiments. The six variants of proteins bovine serum albumin (BSA), lysozyme, and poly-L-lysine as well as six variants of α-synuclein, a protein that is associated with the onset of neurodegenerative disorders, were used. To estimate the net charge of each peptide/protein at pH levels of 4.0 and 7.0, elementary charges (e) were assigned to amino acid side chains that are positively charged (pH 4.0: Arg, His, Lys; pH 7.0: Arg, Lys) and negatively charged (pH 4.0: Asp; pH 7.0: Asp, Glu) at the respective pH.

#	Peptide/Protein	Fluorescence Label	Net charge (pH 4.0)	Net charge (pH 7.0)	Hydrophobic Domains
1	αSN, wildtype	No	+10 e	-9 e	Yes
2	αSN C9-AF647	Yes	+7 e	-12 e	Yes
3	αSN 1-60	No	+12 e	+4 e	Yes
4	αSN 1-108	No	+16 e	+3 e	Yes
5	αSN 60-140	No	-2 e	-12 e	Yes
6	αSN A30P	No	+10 e	-9 e	Yes
7	BSA	No	+59 e	-17 e	Yes
8	Atto488-BSA	Yes	+59 e	-17 e	Yes
9	Lysozyme	No	+12 e	+8 e	Yes
10	Poly-L-lysine (~5 kDa)	No	+34 e	+34 e	No

As explained above for the synthetic peptides, the net charges of the different protein variants at both pH 4.0 and 7.0 were estimated based on the pK_a values of the amino acid side chains and the charge state of the conjugate dye molecules (the dye Alexa Fluor 647 carries three sulfate groups, and each accounts for one negative elementary charge at both acidic and neutral pH). At pH 4.0, the side chain of aspartate is negatively charged, whereas the side chains of arginine, histidine, and lysine are positively charged. At pH 7.0, however, both aspartate and glutamate are negatively charged and only arginine and lysine contribute positive charges (**Table A3.2**).

Table A3.3: Comparison of the estimated and computed net charge values of the peptides/proteins used in this thesis. For estimation of the net charges of the different peptides/proteins, full elementary charges (e) were assigned to the amino acid residues and the conjugated dyes, whereas the public domain software 'Protein Calculator v3.4' was used for computing net charges.

#	Peptide/protein	Assuming full elementary Charges		Based on Protein Calculator v3.4	
		pH 4.0	**pH 7.0**	**pH 4.0**	**pH 7.0**
1	5,6-TAMRA-$(KKK)_8$	+23 e	+23 e	+23.1 e	+22.9 e
2	5,6-TAMRA-$(QQK)_8$	+7 e	+7 e	+7.1 e	+6.9 e
3	5,6-TAMRA-$(Q_5K)_4$	+3 e	+3 e	+3.1 e	+2.9 e
4	5,6-TAMRA-$(Q_{11}K)_2$	+1 e	+1 e	+1.1 e	+0.9 e
5	5,6-TAMRA-$Q_{21}K_3$	+2 e	+2 e	+2.1 e	+1.9 e
6	5,6-TAMRA-$(EEE)_8$	-1 e	-25 e	-7.7 e	-25.0 e
7	$K_3Q_{18}K_3$	+6 e	+6 e	+6.1 e	+5.9 e
8	$Q_{21}K_3$	+3 e	+3 e	+3.1 e	+2.9 e
9	αSN, wildtype	+10 e	-9 e	+9.3 e	-8.8 e
10	αSN C9-AF647	+7 e	-12 e	+6.3 e	-11.8 e
11	αSN 1-60	+12 e	+4 e	+10.1 e	+4.2 e
12	αSN 1-108	+16 e	+3 e	+12.7 e	+3.2 e
13	αSN 60-140	-2 e	-12 e	+0.3 e	-12.1 e
14	αSN A30P	+10 e	-9 e	+9.3 e	-8.8 e
15	BSA	+59 e	-17 e	+70.9 e	-13.9 e
16	Atto488-BSA	+59 e	-17 e	+70.9 e	-13.9 e
17	Lysozyme	+12 e	+8 e	+15.5 e	+7.9 e
18	Poly-L-lysine (~5 kDa)	+34 e	+34 e	+34.1 e	+33.9 e

Indeed, these estimated values were in good agreement with values calculated using the 'Protein Calculator v3.4' (**Table A3.3**). Also here, the computed charge value obtained for the 5(6)-TAMRA

labeled αSN variant, had to be corrected by subtracting three full elementary charges to account for the negative charges originating from the dye. No correction was required for the Atto488 labeled BSA variant, as this fluorophore is uncharged at both pH levels.

Appendix A4: Additional methods & results*

Hydration measurements

Proper hydration is essential for (bio-)molecules to be able to serve as lubricants. Accordingly, mucin glycoproteins have a very high water binding capacity, which they mainly owe to their large amounts of glycan chains.[164] Enzymatic modification of mucin glycoproteins, however, might affect their hydration state. Thus, the hydration of the different enzymatically treated MUC5AC and MUC5B variants was performed as described previously by Käsdorf *et al.*.[40]

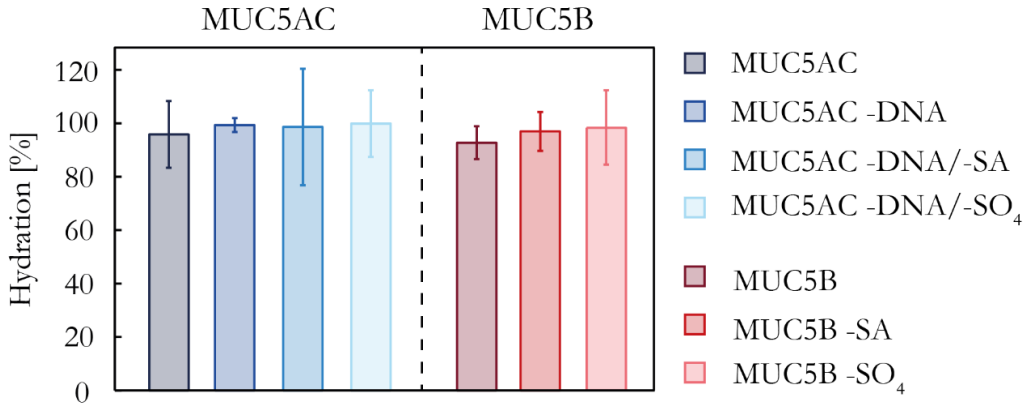

Fig. A4.1: Hydration of native and enzymatically modified mucin variants. The hydration state of different variants of porcine MUC5AC and human MUC5B was determined by performing both QCM-D and SPR measurements. The error bars denote the standard deviation as obtained from three (n = 3) independent measurements.

The hydration of mucin layers was calculated by combining the results of QCM-D measurements (E4 system, QSense, Gothenburg, Sweden) and surface plasmon resonance measurements (SPR, Biacore 2000, GE Healthcare). For this purpose, mucins were dissolved in 20 mM HEPES buffer (pH 7.0) at a concentration of 1 mg mL^{-1} for both measuring sets. The same HEPES buffer was used as a running buffer in both techniques. The hydrated mass of each mucin variant was calculated from the frequency and dissipation shifts obtained from QCM-D measurements based on a Voigt-based model (the density of the mucin coating was determined to be 1050 kg m^{-3})[278] using the Q-tool software. The dry mass was estimated by the response units (RU) obtained from SPR

* This section in part follows the publications Marczynski *et al.*, Biomaterials Science (2018), Marczynski *et al.*, Biomacromolecules (2019), Marczynski *et al.*, Colloids and Surfaces B: Biointerfaces (2020), Lutz *et al.*, Langmuir (2020), and Marczynski *et al.*, Biomacromolecules (2021).

measurements with the converting equation of 1 RU = 1 pg mm^{-2}.[279, 280] The hydration of the different mucin variants was then calculated according to the following equation:

$$\text{hydration } (\%) = \frac{\text{hydrated mass - dry mass}}{\text{hydrated mass}} \times 100\ \%$$

In fact, as indicated in **Fig. A4.1**, neither the removal of DNA from MUC5AC samples nor the removal of sialic acid or sulfate groups from either mucin variant significantly altered the hydration state of MUC5AC and MUC5B coatings.

Preparation of PDMS samples

PDMS is a silicone-based polymer that is commonly used in various medical and industrial applications. It is a chemically inert, non-toxic, biocompatible, and transparent elastomer. In this thesis, PDMS pins and kidney-shaped PDMS samples were used in tribology experiments. For sample preparation, a commercially available two-component PDMS system (Sylgard 184, Dow Corning, Midland, MI, USA) was used. Samples were prepared by first mixing the PDMS base with the curing agent in a 10:1 ratio and exposing the mixture to vacuum for 1 h to remove air bubbles. Afterwards, the PDMS mixture was filled into a mold using a displacement pipette before curing the silicone at 80 °C for 1 h. After curing, the samples were tempered at 100 °C for 2 h to remove unreacted low molecular weight residues.[281]

Microfluidics device fabrication

The channel geometry of the microfluidics chips was designed using AutoCAD (Autodesk, Munich, Germany), and the photomask was printed at a resolution of 64.000 dpi (Zitzmann, Eching, Germany). The master for casting PDMS chips was fabricated on a 3 inch silicon wafer (Siegert Wafer, Aachen, Germany) using EpoCore 50 (micro resist technology, Berlin, Germany) as a photoresist thus generating elevated structures needed for the following channel molding process (**Fig. A4.2 A**). Two spin coating steps using a WS-400B-6NPP/LITE spin coater (Laurell Technologies Corporation) at 300 rpm for 15 s and at 1000 rpm for 35 s, respectively, were used to apply an approximately 100 µm layer of photoresist onto the silicon wafer. Then, two prebaking steps were conducted to vaporize the solvent: first, at 65 °C for 5 min; then, at 95 °C for 10 min. After wafer cooling at room temperature, the photomask was placed onto the photoresist layer and the wafer was exposed to UV irradiation (λ = 365 nm, 500 mJ cm^{-2}) to induce photoresist cross-linking.

Two post-exposure baking steps were conducted at 65 °C for 5 min and at 95 °C for 20 min to harden the cross-linked structures. The wafer was developed by rinsing thoroughly with 1-methoxy-2-propanyl acetate (Sigma-Aldrich) to remove all remaining uncross-linked photoresist. Finally, the wafer was rinsed with isopropanol to remove any remaining developer.

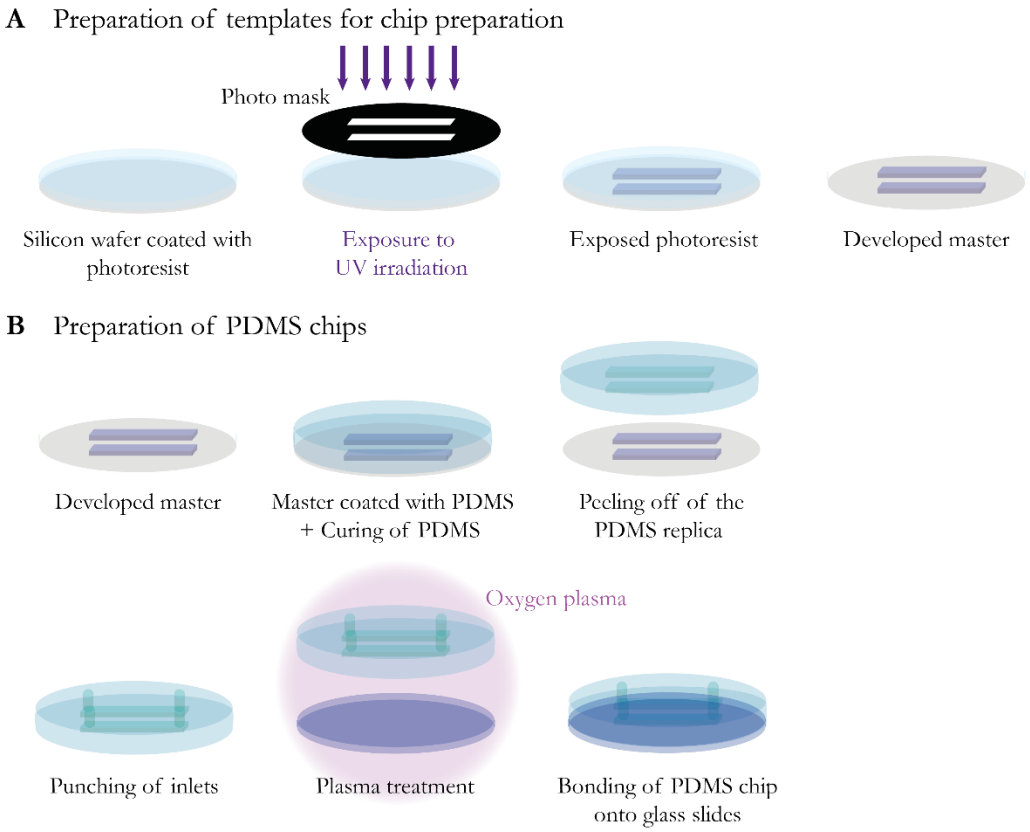

Fig. A4.2: Preparation of microfluidics chips. The templates for generating microfluidics chips were prepared by means of photolithography (**A**). The microfluidics chips were fabricated from PDMS and bonded onto glass slides (**B**).

For the fabrication of microfluidic chips (**Fig. A4.2 B**), the PDMS mixture was prepared as described above. After degassing for 1 h under vacuum, the mixture was cast into the master mold. The PDMS layer was cured at 70 °C for 1 h, peeled off, and access holes were punched. Afterwards, the PDMS chips were bonded to glass slides by treating both the glass slides and the PDMS replicas with oxygen plasma at 30 W for 30 s. The bonded devices were stored in an oven at 120 °C overnight so that the PDMS could recover its hydrophobic properties.

Exponential decay function fit to adsorption measurements onto PDMS surfaces conducted with MUC5B

Not only the adsorption efficiency of the two enzymatically modified MUC5B variants was altered compared to that of native MUC5B. The two modified variants also exhibited drastically slower adsorption kinetics. For quantification, an exponential decay function was fitted to the experimental data (**Fig. A4.3**).

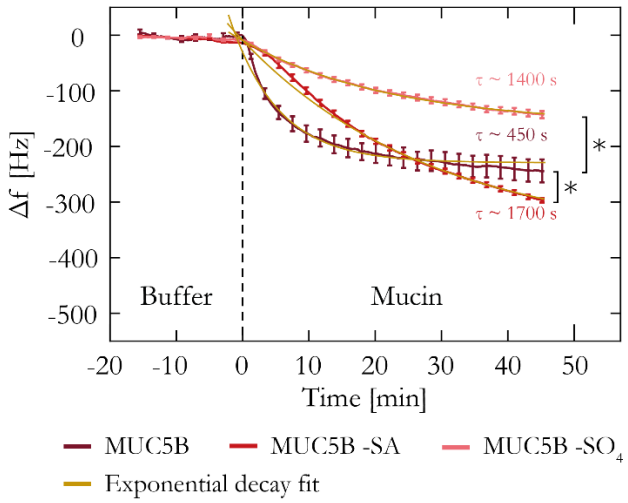

Fig. A4.3: Adsorption behavior of native and enzymatically treated MUC5B variants to PDMS surfaces. The adsorption kinetics of MUC5B was altered upon removal of sialic acid and sulfate groups. Red curves indicate exponential decays fits fitted to the experimental data. Error bars denote the standard error of the mean as obtained from at least three independent measurements. Asterisks indicate statistical significance ($p < 0.05$) as calculated for the final frequency shift determined at 45 min.

Dextran depletion assay performed with another mucin purification batch

The data shown below depicts an experimental repetition of the depletion tests shown in **Chapter 3.2** (**Fig. 3.3 A**); the data was obtained with MUC5AC and MUC5AC -DNA/-SO_4 mucins that have been obtained from another purification batch.

Both, cationic and anionic dextrans, bound strongly to the surface-attached layers of MUC5AC – for this specific, the anionic CM-dextrans were depleted from solution more strongly than the cationic DEAE-dextrans – although these difference were not statistically significant. In contrast, no binding of unmodified, neutral dextrans to the mucin surface layers could be detected. Upon enzymatic removal of DNA and sulfate groups, the capability of this mucin batch to deplete DEAE-dextrans from solution was completely diminished (**Fig. A4.4**). Yet, also the depletion of CM-dextrans was not as pronounced as for unmodified MUC5AC anymore.

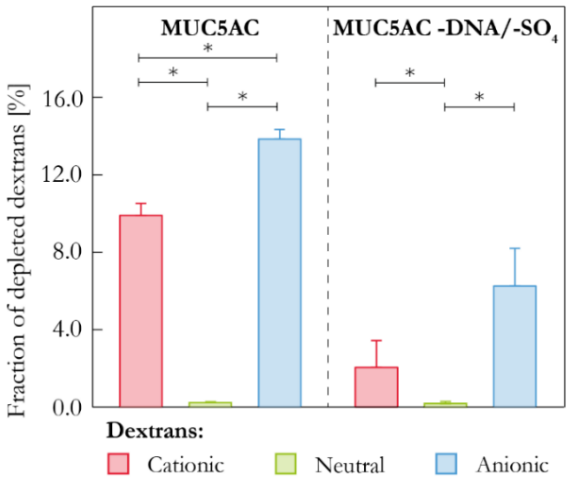

Fig. A4.4: Depletion assay to assess the binding interaction between native mucins MUC5AC and enzymatically treated mucins MUC5AC -DNA/-SO4 with different dextrans. Binding of cationic (blue), neutral (green), and anionic (red) dextrans to adsorbed mucin layers is compared for dextrans with a molecular weight of 150 kDa. The error bars represent the standard error of the mean as obtained from five individual samples ($n = 5$). Asterisks denote statistically significant differences of the dextran samples ($p < 0.05$).

Atomic force microscopy (AFM)

Atomic force microscopy is a technique that allows for imaging individual mucin molecules adsorbed onto both hydrophilic and hydrophobic surfaces.

Sample preparation

To obtain mucin functionalized mica (muscovite, diameter 10-12 mm, Plano, Wetzlar, Germany) or highly oriented pyrolytic graphite (HOPG) samples, the respective surface materials were first rinsed with acetone and cleaved using adhesive tape followed by cleaning in acetone (to remove tape residues) or a scalpel to obtain a clean and atomically flat substrate. The mica disks were functionalized on an AFM specimen (diameter: 15 mm) using the high-resolution replicating compound 101RF (Microset Products Ltd., Hinckley, Leicestershire, UK). HOPG samples (ZYH, 3.5° mosaic spread, µ-mash, Wetzlar, Germany) were cleaved and mucins were immobilized on the AFM specimen as given for mica as described in the following. For imaging, either native lab-purified MUC5B or the enzymatically modified derivatives (MUC5B -SA and MUC5B -SO_4) were dissolved in HEPES buffer (20 mM, pH 7.0) at room temperature to a concentration of 1 mg mL^{-1}. To dissociate mucin oligomers (and thus obtain monomeric mucins), tris-(2-carboxyethyl)-phosphine (TCEP) solution (containing 300 mM KOH) was added to the mucin solution to obtain a final TCEP concentration of 10 mM. After another 1 h, solutions containing a final mucin concentration of 0.001 mg mL^{-1}, 0.010 mg mL^{-1}, 0.025 mg mL^{-1}, 0.050 mg mL^{-1}, 0.100 mg mL^{-1} or 1.000 mg mL^{-1} were prepared. The imaging was started with a bare mica substrate in 200 µL of HEPES buffer. This solution was replaced by 200 µL of mucin solution at the lowest mucin concentration and imaging

was performed. Mucin imaging was carried out in the same way each time, using a higher concentration of mucin with every step as indicated above.

Sample imaging

AFM images were acquired on a Cypher ES (Asylum Research, an Oxford Instruments company, Santa Barbara, CA, USA) using a heating/cooling sample stage set to 25 °C. Imaging was performed using OMCLAC240TS cantilevers (Olympus, Tokyo, Japan) with a resonance frequency of about 70 kHz for AC mode imaging in air using piezo based excitation and BLAC40TS cantilevers (Olympus) with a resonance frequency of about 20–25 kHz for AC mode imaging in liquid using blueDrive (photothermal excitation). The cantilevers were rinsed in acetone prior to use. A scan velocity of 5 Hz and a scan angle of 90° (*i.e.*, perpendicular to cantilever axis) have been chosen. Using the commercial AFM software based on Igor Pro (WavMetrics Inc., Portland, OR, USA), AFM topography images were evaluated by using either a flattening or plane fit of 0^{th} and 1^{st} order to correct for imaging artifacts related to a tilted sample and the piezo scanner. Particle analysis was performed using the commercial AFM software (Asylum Research, an Oxford Instruments company). The threshold for masking was set to 1.10 nm and edge particles were omitted. Each AFM image represents a local state of the respective mica or HOPG surface.

For the three different variants of MUC5B (native MUC5B, MUC5B –SA, and MUC5B -SO_4), frequency distributions of height, diameter deconvoluted diameter, and deconvoluted volume values are given in **Fig. A4.5** and **Table A4.1**.

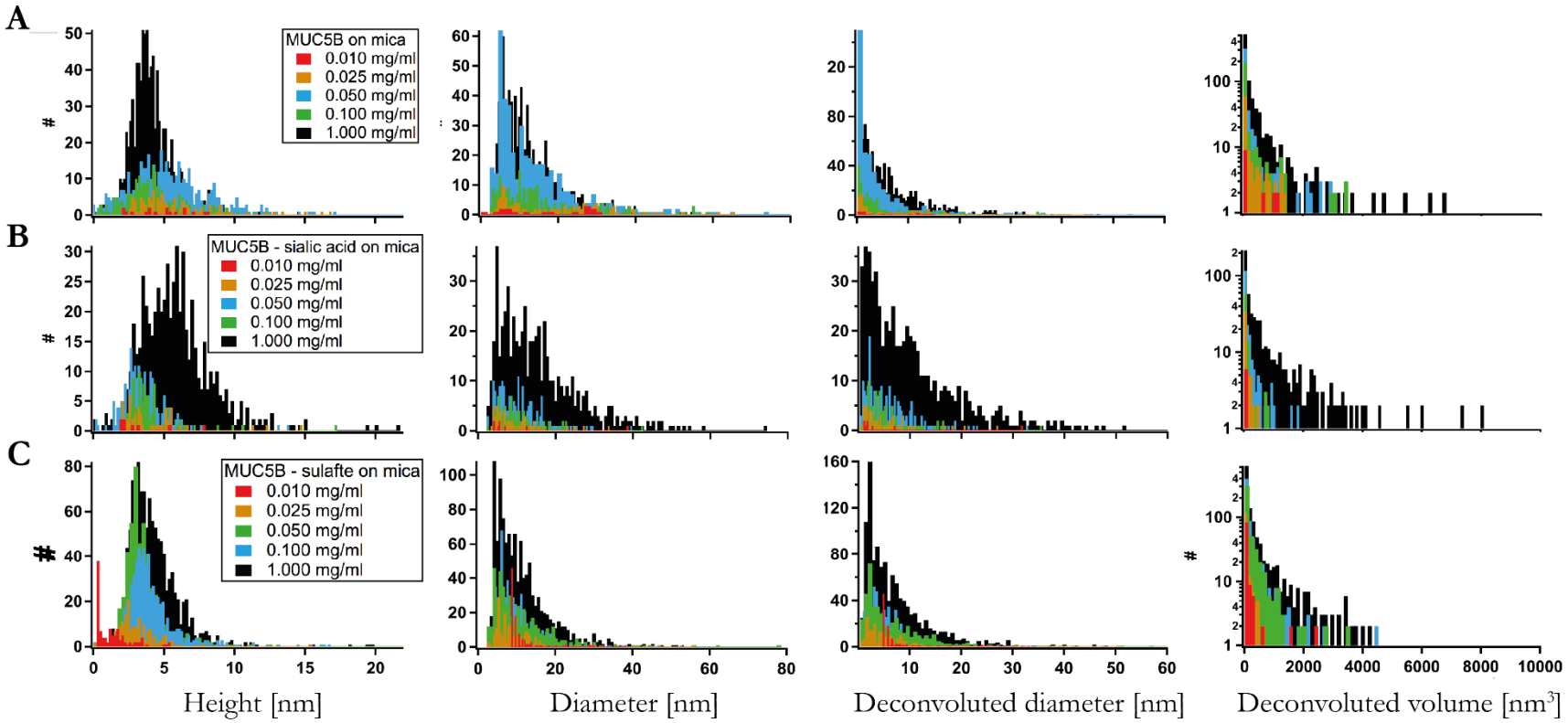

Fig. A4.5: Frequency distributions of native MUC5B and the enzymatically treated MUC5B variants on mica imaged in HEPES. 1 µm x 1 µm images were taken for particle analysis (commercial AFM software, Asylum Research, an Oxford Instruments company, CA, USA). The threshold for masking was set to 1.10 nm and edge particles were omitted. The height, the diameter, the real diameter after deconvolution using the respective tip radius and determined based on Engel *et al.*[282] as well as the resulting volume of the particles were determined for MUC5AC (**A**), MUC5AC –SA (**B**), and MUC5AC –SO_4 (**C**). Different concentrations of all MUC5B were imaged: 0.010 mg mL^{-1} (red) to 1.000 mg mL^{-1} (black). In particular, enzymatically treated MUC5B variants showed a shift toward higher values for increasing concentration. At the same time, a broader distribution of height, diameter and volume values was observed.

Table A4.1: Parameters of particle analysis of MUC5B AFM images on mica. Coverage, maximum height, area, diameter, number of particles for native, sialic acid-reduced and sulfate-reduced adsorbed MUC5B on mica were determined by particle analysis. MUC5B showed a slightly higher tendency toward particles with increased height and area (*i.e.*, aggregate formation) compared to the enzymatically treated MUC5B variants. For all three variants of MUC5B an increase of the concentration in solution led to a significantly higher coverage of the mica substrate.

MUC5B type	**MUC5B**	**MUC5B**	**MUC5B**	**MUC5B**	**MUC5B**	**MUC5B -SA**	**MUC5B -SA**	**MUC5B -SA**	**MUC5B -SA**	**MUC5B -SA**
Concentration [mg mL^{-1}]	0.010	0.025	0.050	0.100	1.000	0.010	0.025	0.050	0.100	1.000
Coverage [%]	0.17	4.75	9.24	13.43	16.65	0.23	0.29	0.89	2.21	17.53
Max. height [nm]	4.84 (±1.95)	5.67 (±2.79)	4.25 (±2.15)	5.35 (±3.15)	4.13 (±1.61)	3.38 (±2.15)	4.08 (±2.52)	4.06 (±2.00)	3.49 (±1.62)	5.81 (±2.57)
Diameter/10 [nm]	1.65 (±1.09)	1.81 (±1.28)	1.59 (±1.16)	1.43 (±1.21)	1.24 (±0.79)	1.02 (±1.19)	0.97 (±0.63)	1.06 (±0.60)	1.04 (±0.57)	1.56 (±1.05)
No. of particles	17	118	283	454	901	8	53	94	198	589

MUC5B type	**MUC5B -SO_4**	**MUC5B -SO_4**	**MUC5B -SO_4**	**MUC5B -SO_4**	**MUC5B -SO_4**
Concentration [mg mL^{-1}]	0.010	0.025	0.050	0.100	1.000
Coverage [%]	0.21	1.95	8.23	7.89	18.59
Max. height [nm]	1.33 (±1.23)	3.10(1.60)	3.75 (±2.33)	3.98 (±1.88)	4.23 (±1.87)
Diameter/10 [nm]	1.19 (±0.57)	0.92 (±0.58)	1.11 (±0.84)	1.00 (±0.61)	1.14 (±0.76)
No. of particles	110	199	479	647	1152

Lubricity of MUC5AC –SA and MUC5AC –SO_4

To remove sialic acids and sulfate groups from MUC5AC, neuraminidase and sulfatase treatments were used, respectively. No differences in terms of lubricity could be recorded for these variants compared to solutions of unmodified MUC5AC (**Fig. A4.6**).

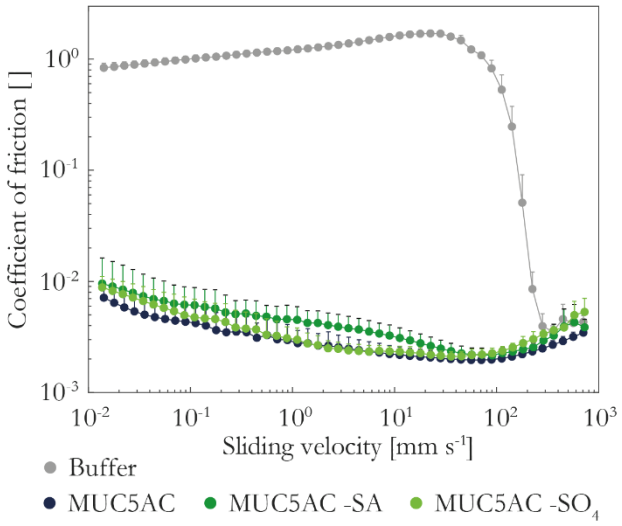

Fig. A4.6: Lubricity of native and enzymatically treated MUC5AC variants. Tribology measurements were performed with a steel/PDMS pairing in a ball-on-pins setup using different mucin solutions (0.1 % (w/v)) as lubricants (MUC5AC, MUC5AC –SA, and MUC5AC –SO_4. HEPES buffer devoid of any mucins is included as a reference (gray curve). Each point represents the mean value as obtained from three technical repetitions (n = 3) at a given sliding velocity and the error bars denote the corresponding standard error of the mean.

Determining the coating densities for covalently surface-attached mucin layers

To allow for a comparison of the surface coating densities obtained with lab-purified MUC5AC and the two commercial MUC5AC variants, each mucin variant was labeled with a green fluorescing dye (ATTO488, carboxy modified, ATTO-TEC GmbH; **Chapter 2.6**).

The conjugation reaction used for labelling targets amino groups, and accessible amino groups are mainly located in the termini of the mucin molecule. Thus, the labelling efficiency was expected to depend on the availability of such accessible amino groups. This labelling efficiency of the four mucin variants was determined by measuring the fluorescence intensity (ex.: 485 nm; em.: 535 nm) of a series of aqueous solutions generated from these four variants at different mucin concentrations ranging from 0.2 to 0.003 % (w/v). Since molecular weight measurements already indicated that the average molecular weights of the different variants vary significantly (**Fig. A1.5 A**), also the actual numbers of mucin molecules in each sample were expected to differ from each other. To determine labelling efficiencies, the mucin concentrations had to be corrected accordingly. When a linear

regression line was fitted to the data points, the intensity of a fluorescence signal emitted by a mucin solution at any concentration could be extrapolated. At a molar mucin concentration that corresponded to a weight concentration of 0.1 % (w/v), the fluorescence intensities determined for the two commercial PGM variants were ~2fold and ~3fold lower than that of MUC5AC (**Fig. A4.7 A**); this indicated a higher labelling efficiency for lab-purified MUC5AC.

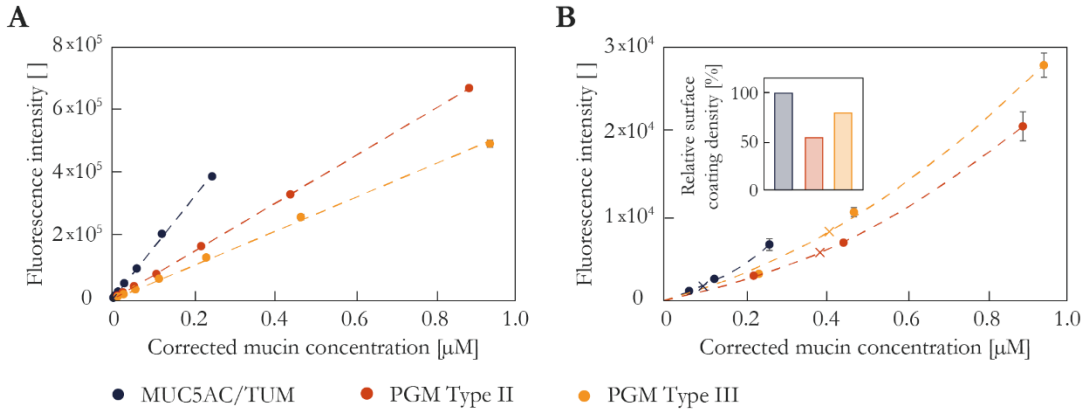

Fig. A4.7: Estimation of the labelling efficiencies and surface coating densities obtained for the three mucin variants. To account for relative differences in molecular weight (**Fig. A1.5 A**) between the different mucins, the molar mucin concentrations were corrected, accordingly. Shown are the fluorescence intensities of titration series prepared from the different mucin variants. A linear regression line was fitted to the data; here, the fit was forced to pass through the coordinate origin (**A**). Fluorescence intensities of covalently linked mucin layers: when a quadratic regression function was fitted to the corrected data points, relative surface coating densities could be calculated. Whereas the densest surface coating was obtained for MUC5AC, the maximal relative differences between two different coating variants were less than 2fold (**B**). Error bars represent the standard error of the mean as obtained from five individual experiments (n = 5). The crosses indicate the fluorescence intensities emitted by surface layers reconstituted from 0.1 % (w/v) mucin solutions, which were used to generate covalent mucin layers.

To determine relative differences in the coating densities obtained for the different mucin variants on polystyrene surfaces, fluorescent variants of each mucin type were covalently coupled to the wells of a 96-well microtiter plate; then, a titration series of mucin solutions was probed. After unbound mucins were removed by thoroughly washing the coated wells with buffer, fluorescence images of the coated surfaces were recorded and the fluorescence signals were quantified. Again, to be able to compare the fluorescence signals emitted by surface layers constituted by the different mucin variants, the used mucin concentrations had to be corrected to account for differences in molecular weight between the different mucin variants. The data was then further corrected to account for the different labelling efficiencies determined above. When a quadratic regression function was fitted to the corrected data points, values for the relative surface coating densities could be derived (**Fig. A4.7 B**).

Overall, the surface coating density values obtained for the different mucin variants were on the same order of magnitude. The densest mucin surface layer was obtained for MCU5AC, followed by PGM Type III, and PGM Type II (**Fig. A4.7 B**, inset).

Batch-to-batch variations in the viscoelastic properties of MUC5AC

To a certain extent, lab-purified mucins are always subject to batch-to-batch variability – and this also applies to the viscoelastic properties of different MUC5AC batches (**Fig. A4.8**). Different purification procedures can lead to differences in mucin purity. For instance, the differences in the pH-dependent viscoelastic behavior that were detected for two different MUC5AC batches (**Fig. A4.8**) can be attributed to slight differences in mucin purity. In the case of MUC5AC/KTH, certain batch contaminants might have acted as cross-linking agents that established intermolecular bonds between mucins. Those cross-linking molecules could then be responsible for the formation of a hydrogel even at a neutral pH level. In agreement with this notion, immunoglobulins were identified as contaminants that are likely to act as mucin cross-linking agents. A higher content of those immunoglobulins was detected in MUC5AC/KTH (~5.0 %) than in MUC5AC (~3.4 %).[176] Several authors have reported before that different isotypes of immunoglobulins (IgA, IgG, and IgM) can form cross-links between individual mucins on the one hand and between mucins and other objects such as viruses on the other hand.[206, 283, 284]

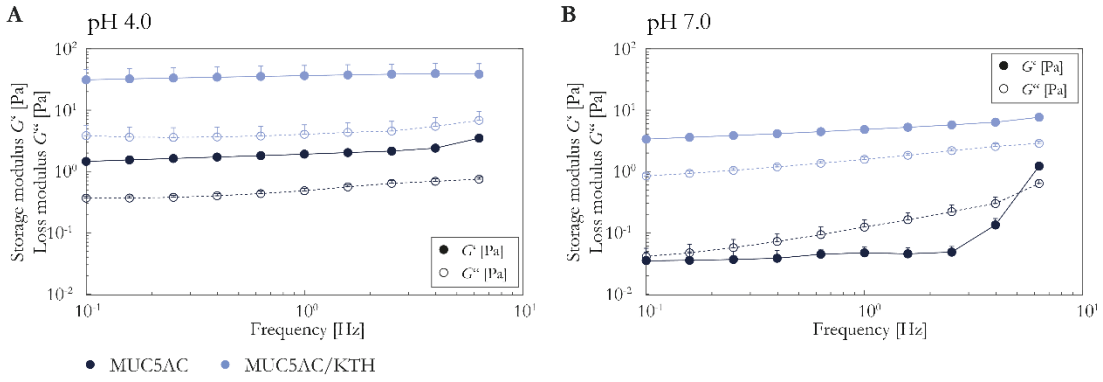

Fig. A4.8: Comparison of the pH-dependent viscoelastic properties of two batches of lab-purified MUC5AC. The viscoelastic frequency response of mucin samples is shown for both acidic (pH 4.0) and neutral (pH 7.0) buffer conditions. Closed symbols and solid lines denote the storage modulus *G'* and open symbols and dashed lines the loss modulus *G"*. Error bars represent the standard error of the mean as obtained from three independent measurements ($n = 3$).

Non-normalized penetration profiles of DEAE-dextrans into MUC5AC gels

Within the course of the penetration experiments, *i.e.*, within 20 min after injection of the fluorescently labeled dextrans, the accumulation peak in the penetration profile obtained for DEAE-dextrans seemed to increase with time. However, as indicated in **Fig. A4.9**, this was an artifact arising from the normalization procedure that had been applied to the data to correct for the bleaching of the fluorophore over time.

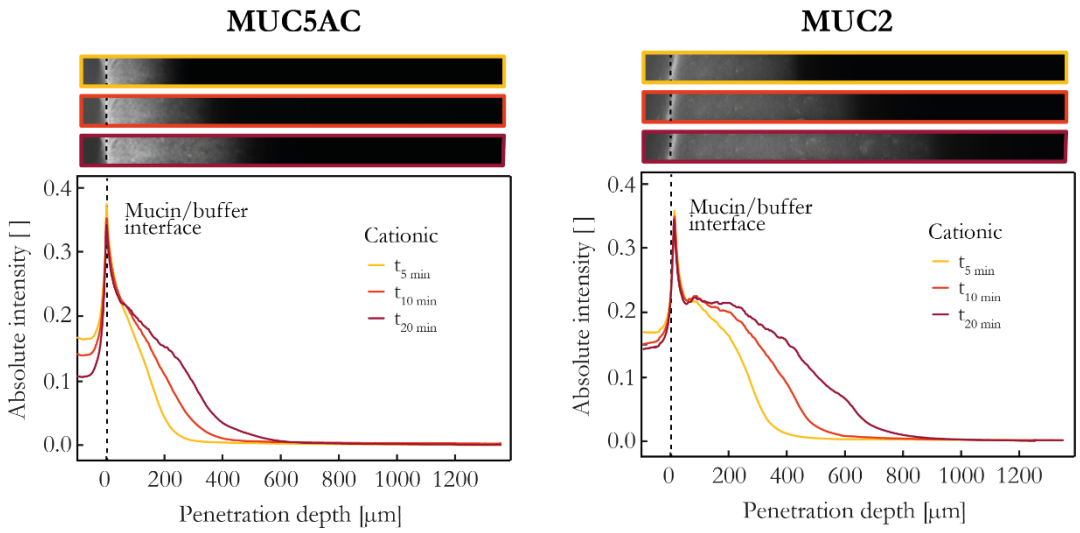

Fig. A4.9: Non-normalized penetration profiles of cationic dextrans into mucin gels. The barrier properties of mucin gels reconstituted from porcine gastric mucin MUC5AC (**A**) toward cationic DEAE-dextrans were compared to gels comprising purified porcine intestinal mucin MUC2 (**B**). Different from the curves shown in **Fig. 5.3** of the main text, the fluorescence intensity profiles determined at different time points of the experiment were not normalized and thus may contain photobleaching effects or other artifacts. However, those non-normalized profiles demonstrated that the height of the dextran accumulation peak did not increase over time and that the concentration of dextran molecules in the buffer compartment decreased as the penetration experiment progressed.

Binding properties of different mucin batches toward dextrans

For testing the binding affinity of three different dextran variants (cationic, electrostatically neutral, and anionic) toward different batches of MUC5AC and MUC2, depletion assays were performed as outlined in **Chapter 2.9.1**. In total, the relative binding affinities of eleven purification batches of MUC5AC and three purification batches of MUC2 were determined (**Fig. A4.10**).

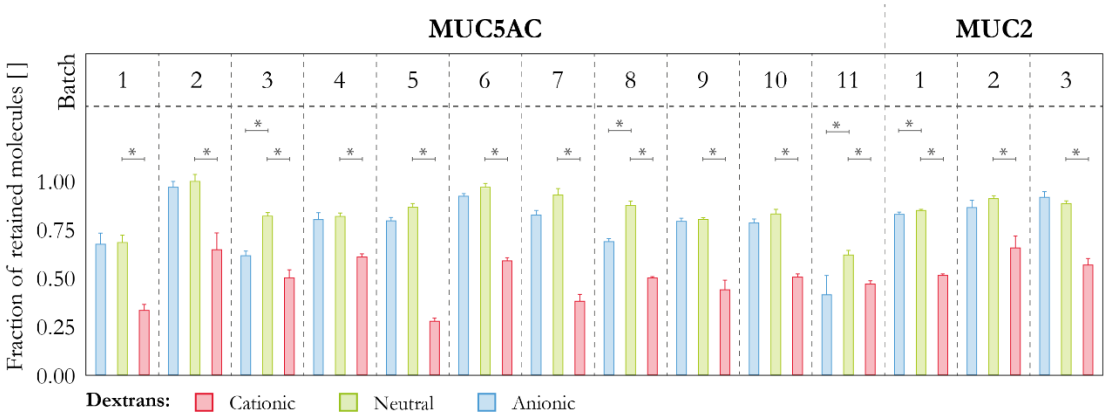

Fig. A4.10: Depletion assay performed on different purification batches of MUC5AC and MUC2, respectively. The binding behavior of three different dextran variants to surface layers of MUC5AC or MUC2, respectively, was compared by a depletion assay. In all tested mucin batches, cationic dextrans showed the highest binding efficiency. However, the amount of depleted cationic dextrans varied within the different batches. For at least two batches of gastric mucin (batch 3 and 8), an increased adsorption of anionic dextrans – compared to neutral dextrans – was observed. The error bars denote the standard error of the mean as obtained from five individual samples ($n = 5$). Asterisks indicate statistically significant differences ($p < 0.05$).

Increased density of mucins at gel/buffer interface in the microfluidics setup

To detect differences in the local concentration of mucins within reconstituted mucin gels on-chip, solutions of 1 % (w/v) MUC5AC and MUC2, respectively, were pre-mixed with 10 µg mL^{-1} of fluorescently labeled wheat germ agglutinin, which specifically binds to sialic acid residues. The solutions of lectin-labeled mucins were filled into microfluidics chips and a stable gel/buffer interface was generated as described in the main text. Fluorescence images were then acquired on a DMi8 Leica microscope (Leica, Wetzlar, Germany) using a 4x objective (HI PLAN 4x/0.10, Leica) with a digital camera (Orca Flash 4.0 C114400, Hamamatsu, Japan).

The fluorescence intensity correlates to the mucin concentration: a bright signal at a certain gel location indicates a high local mucin concentration, whereas a weak fluorescence signal corresponds to a low local mucin concentration. Locally increased mucin concentrations were detected at the gel/buffer interface for the majority of the MUC5AC gels, whereas this was only the case for some MUC2 gels. Also, the amount of such locally increased mucin concentration varied. At this point, it can only be speculated as to why this effect occurred at the buffer/gel interface. One possible explanation might be that this was an interfacial phenomenon arising from surface tension effects (since the mucin solution was injected into the channels first before the acidic buffer is added to

induce gelation). Alternatively, it might be a mechanical effect that was created by compressive forces that originated from filling the reservoir with buffer.

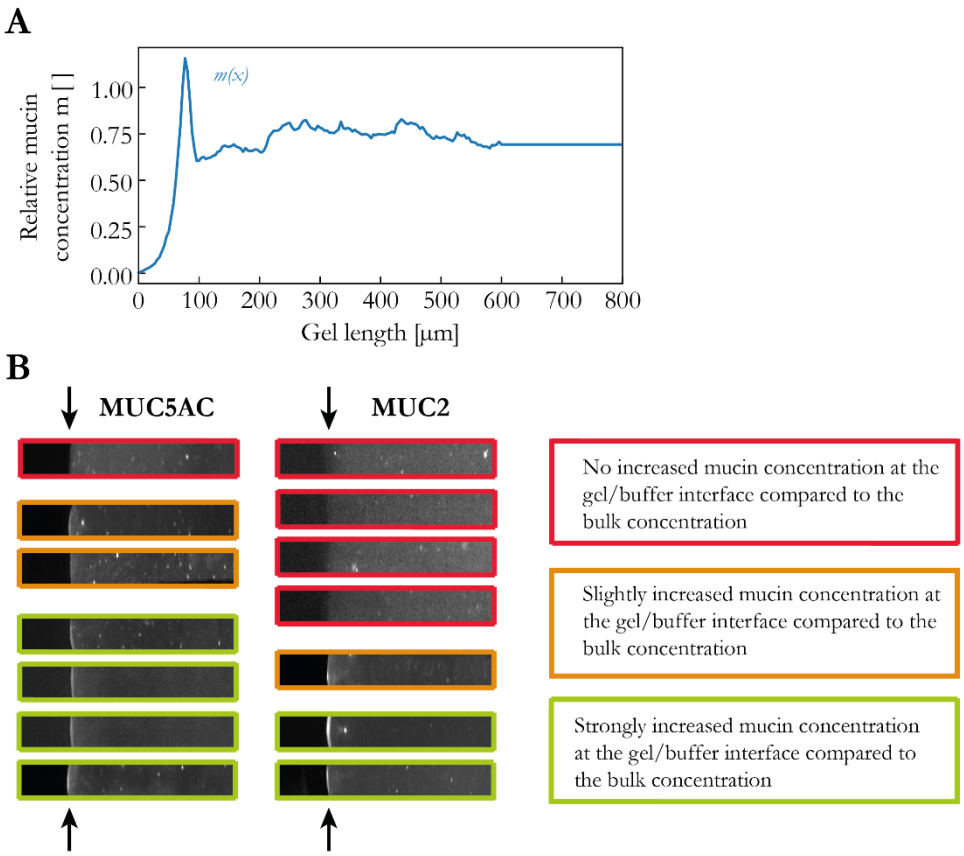

Fig. A4.11: Increased mucin concentration at the gel/buffer interface. By combining results obtained from the simulation with experimental data in a self-consistent iterative scheme, an averaged profile for the local mucin concentration within the mucin gel was obtained. This extracted mucin concentration profile *m*(x) was almost constant in the bulk phase of the gel but exhibited a clear peak at the gel/buffer interface (**A**). Exemplary fluorescence images of seven gel 'fingers' filled with a fluorescently labeled MUC5AC and MUC2 gel, respectively. For the majority of the MUC5AC gels, a locally increased mucin concentration at the gel/buffer interface was observed compared to the mucin concentration in the bulk phase of the gel. For MUC2 gels, such a locally increase mucin concentration at the buffer/gel interface could also be detected, albeit less frequently as for MUC5AC gels. The arrows indicate the position of the gel/buffer interface to guide the eye.

Assessing black carbon/mucin interactions using QCM-D

Binding interactions acting between mucin glycoproteins and black carbon (BC) nanoparticles were assessed using QCM-D (**Fig. A4.12**). First, the QCM-D sensors were coated with MUC5AC by

means of passive adsorption from a mucin containing solution (0.01 % (w/v) MUC5AC dissolved in either 20 mM HEPES buffer (pH 7.0) or 10 mM acetate buffer (pH 4.0)). Afterwards, unbound mucins were removed from the measuring cell by flushing with the respective buffer for 15 min. Then, BC nanoparticles (suspended in the respective buffer at a concentration of 10^{-2} %) were flushed into the measuring cell, and the ensuing shift in the frequency signal was recorded for 45 min.

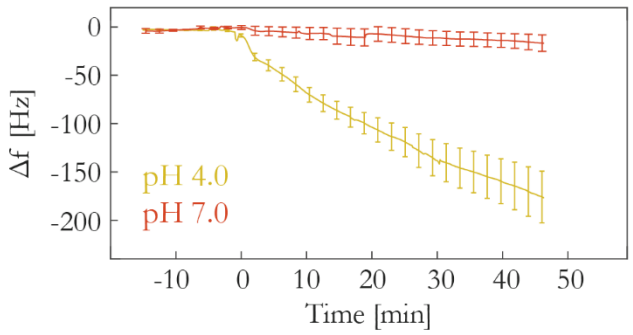

Fig. A4.12: Binding of BC nanoparticles to surface-attached mucin layers. Binding interactions acting between mucins and BC nanoparticles were assessed using QCM-D. A shift in the frequency signal indicated the binding of BC nanoparticles to the surface-attached mucin layers. Error bars represent the standard error of the mean as obtained from three technical repetitions (n = 3).

At a neutral pH level (pH 7.0), hardly any signal could be detected upon flushing of the BC nanoparticles into the measuring cell. This indicated that mucins and the BC nanoparticles did not interact (strongly) under these conditions. In contrast, at an acidic pH level (pH 4.0), a strong shift in the frequency signal upon flushing of the BC nanoparticles could be recorded. This indicated that, under these conditions, the nanoparticles interacted with the mucin layers.

Identification of the interactions governing the mucoadhesion of αSN proteins

Microscale thermophoresis (MST) experiments were conducted using MUC5AC and two different variants of αSN (wildtype and the truncation mutant αSN 60-140) as binding partners to identify the interactions modes, which govern the mucoadhesive properties of αSN (**Fig. A4.13**). MST measurements were conducted both at room temperature (*i.e.*, 22 °C) and at physiological body temperature (*i.e.*, 37 °C). An altered binding affinity at an elevated temperature was observed for αSN 60-140 but not for the wildtype variant. The former αSN mutant variant lacks the cationic N-terminal domain and thus exhibits a negative net charge even at pH 4.0; however, it comprised a large number of hydrophobic amino acids. Since only hydrophobic interactions but not electrostatic interactions exhibit a temperature dependency, this indicated that the mucoadhesive properties of αSN 60-140 might not be dominated by electrostatic interactions. In contrast, for the αSN wildtype

variant – which carries a large number of cationic binding sites – binding interactions seem to be dominated by electrostatic forces.

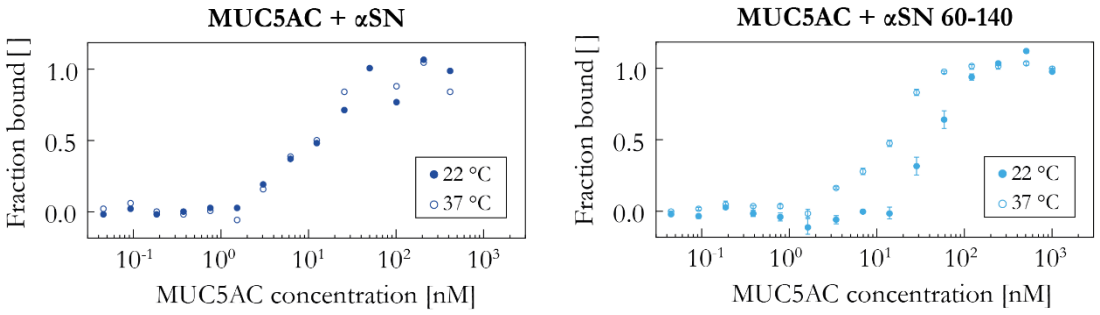

Fig. A4.13: Assessing binding interactions acting between MUC5AC and two variants of the protein αSN using MST. The binding affinity of wildtype αSN and N-terminally truncated αSN 60-140 toward MUC5AC was assessed. Whereas, for αSN, binding was independent of the ambient temperature, the binding affinity of αSN 60-140 exhibited a temperature dependency. Error bars denote the standard deviation as obtained from three independent measurements (n = 3).

Confocal laser scanning microscopy

To image networks of purified MUC5AC in either the absence or the presence of putative crosslinkers such as αSN, mucin gels with different compositions were prepared according to **Table A4.2**.

Table A4.2: Composition of the mucin gel samples used for CLSM imaging. Three different combinations of MUC5AC/αSN were studied: a MUC5AC hydrogel devoid of αSN, a non-fluorescent MUC5AC hydrogel supplemented with fluorescent αSN 9C-AF647, and a fluorescent MUC5AC hydrogel supplemented with fluorescent αSN 9C-AF647. All hydrogels were reconstituted in 10 mM acetate buffer (pH 4.0).

Sample	MUC5AC % (w/v)	MUC5AC-AF647 % (w/v)	MUC5AC-Atto488 % (w/v)	αSN μM	αSN 9C-AF647 μM
MUC5AC	0.98	0.02	-	0	0
αSN + MUC5AC	1.00	-	-	95.4	0.5
αSN + MUC5AC (co-localization)	0.96	-	0.04	95.4	0.5

Then, 10 μL of each composition were immediately deposited onto a glass slide. A cover slip (# 1.5, 20 × 20 mm) was gently placed on top of the sample, sealed to avoid evaporation, and left at rest for

the gels to form. Two hours after preparation, the samples were imaged using a confocal microscope (Nikon A1/Ti-E, Minato, Tokyo, Japan). The dyes Atto488 and Alexa Fluor 647 were excited using 488 nm (Sapphire 488-100CW CDRH, Coherent Inc., Santa Clara, CA, USA) and 647 nm (2RU-VFL-P-300-647, MPB Communication Inc., Montreal, Canada) lasers, respectively. The emission light was filtered with a 488/647 dichroic mirror, and the fluorescence signals from the green and the red dye were collected using 525/50 nm and 700/75 nm bandpass filters, respectively. Imaging was conducted using an Apo TIRF 100× Oil DIC N2 objective (Nikon).

The αSN-induced rearrangement of the mucin network was imaged using fluorescence CLSM. A double-labeling of the two interaction partners (MUC5AC-Atto488 and αSN-AF647) was performed to verify that the restructuring of the mucin network was, in fact, triggered by αSN. Indeed, it was found that the fluorescence signals originating from MUC5AC and αSN, respectively, colocalized. This confirmed that αSN induced a structural rearrangement of the three-dimensional mucin network (**Fig. A4.14**).

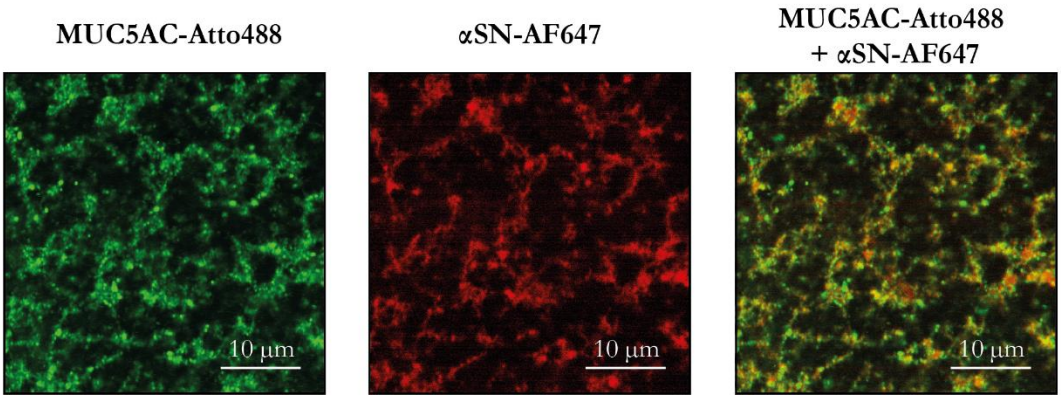

Fig. A4.14: Structural rearrangement of the mucin hydrogel by αSN as detected by fluorescence CLSM. A double staining of both, MUC5AC (*i.e.*, MUC5AC-Atto488) and αSN (*i.e.*, αSN-AF647) proved that, indeed, αSN triggered the rearrangement of the mucin gel microstructure.

Profiles recorded for the penetration of dextrans into αSN-contaminated MUC5AC hydrogels

To test how an αSN-induced restructuring of mucin hydrogels affects their permeability toward small molecules, penetration experiments were conducted with αSN-contaminated MUC5AC hydrogels and both, non-mucoadhesive (*i.e.*, neutral) and strongly mucoadhesive (*i.e.*, cationic) dextrans as

molecular probes. It was found that the penetration profiles at both conditions (pre-penetrated hydrogels *vs.* pristine hydrogels) were virtually identical (**Fig. A4.15**), which suggested that a rearrangement of the mucin network did not affect the penetration behavior of molecules smaller than the initial pore size of the untreated mucin hydrogel.

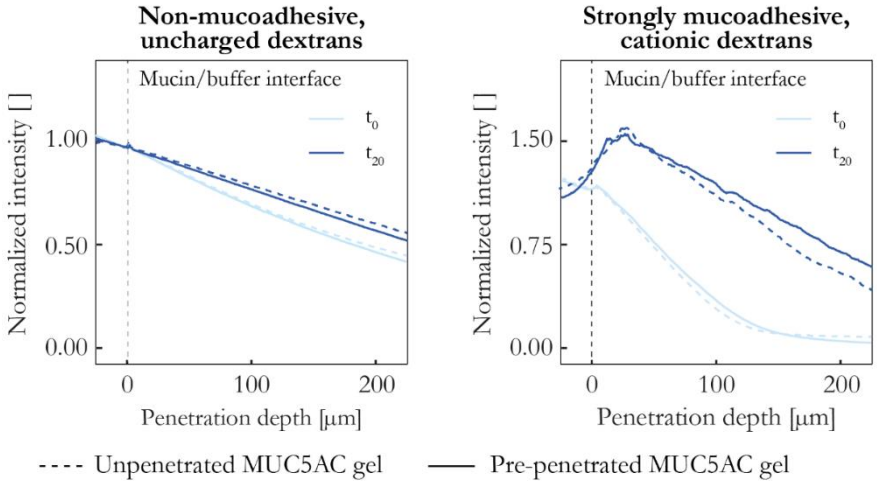

Fig. A4.15: Penetration behavior of uncharged (non-mucoadhesive) and cationic (strongly mucoadhesive) into mucin hydrogels. The barrier properties of 1 % (w/v) MUC5AC hydrogels toward two different dextran variants were compared for native mucin hydrogels (solid profiles) as well as mucin hydrogels that had been pre-penetrated by αSN before exposure to dextrans (dashed profiles). Penetration profiles were obtained from images taken right after filling of the microfluidic chips with fluorescent dextran molecules (t_0) and 20 min thereafter (t_{20}). For each condition, a minimum of nine ($n \geq 9$) individual fingers was evaluated.

Appendix A5: Numerical simulation of the MUC5AC molecules*

The numerical investigations conducted in this thesis aimed at investigating qualitative differences in the conformation of a mucin filament as a function of different effective line charge distributions.

General considerations

The simulation of the mucin molecule considered a single, initially straight filament, which was modeled by 3D beam theory and discretized in space by means of finite elements. Specifically, the geometrically exact Hermitian Simo−Reissner element formulation was applied here.[285] Thermal excitation and viscous damping of the mucin filament due to the implicitly modeled surrounding fluid were incorporated *via* the micromechanical continuum approach to Brownian dynamics.[286] The electrostatic (self-)interaction of the mucin filament was modeled by the so-called section−section interaction potential (SSIP) approach.[287] Steric repulsive forces based on the (self-)contact of the filament were accounted for by means of penalty beam contact formulation and precluded any mutual penetration.[288] The challenging combination of this beam contact formulation with the possibly attractive electrostatic forces from the SSIP approach has been verified in previous work.[287, 289] The software package used for the simulations was an in-house research code BACI developed by the research group of Prof. Dr. Wolfgang A. Wall (Institute for Computational Mechanics, TU München). Moreover, for this simulation, one end of the mucin filament was hinged by means of Dirichlet boundary conditions to comply with the experimental setup. Owing to a lack of knowledge and control over the fact which end of the filament had attached to the surface in the experiments, in this simulation, the N-terminus was chosen to be pinned.

Modelling of the detailed mucin conformation

The modelling approach was motivated by the presence of different structural motifs in the porcine gastric mucin (**Fig. 2.1 B**), and modelling was based on the amino acid sequence deposited in the UniProtKB data base (accession number A0A287ANG4; 09/25/2018): MUC5AC comprises a strongly glycosylated core domain core domain which is flanked by partially folded termini. These termini contain three von-Willebrand-factor (VWF)-like D domains in the N-terminus and one VWF-like D domain as well as two VWF-like C domains in the C-terminus. Here, the spherical VWF-like

* This section follows in part the publication Lutz *et al.*, Langmuir (2020).

domains were modelled as cylinders (**Fig. A5.1**), which are connected by other cylindrical segments corresponding to the respective protein strands. For each of VWF domains in the terminal domains the radius r was estimated based on the contour length l_c and the persistence length l_p of the corresponding peptide sequence according to the following equation:

$$r \approx \frac{2}{\sqrt{6}} l_p \sqrt{\frac{l_c}{2 l_p}}$$

The contour length l_c of the respective sequence was estimated by multiplying the number of amino acids in this sequence with the typical C_α-to-C_α distance of an amino acid, the latter of which was approximated as 3.5 Å.[290] The persistence length l_p was approximated with that of the small globular protein ubiquitin (i.e., l_p = 3.9 Å).[291]

The entire mucin glycoprotein was approximated as a continuous linear strand in which the peptide sequence is completely stretched. The globular domains, their connecting segments, and the remaining parts of the molecule are all modelled as flexible beam elements with an approximated cylindrical shape. The central, glycosylated region of the mucin was broken down into 48 segments of 50 amino acids each, and each of these segments was treated as a beam element with a persistence length of 50 nm.[132]

Table A5.1: Estimated charge distributions for different mucin variants as explained above. The segments corresponding to the N- and C-terminus are marked in gray, the VWF-domains in black, and the segments of the glycosylated core-domain in white.

#	Element length [nm]	Net charge of the protein sequence considering the sulfated groups and sialic acids				
		MUC5AC (pH 4.0)	**MUC5AC (pH 7.0)**	**MUC5AC –SO_4 (pH 7.0)**	**MUC5AC –SA (pH 7.0)**	**MUC5AC –SO_4/–SA (pH 7.0)**
1	25.00	11.5	8	8	8	8
2	6.00	-4.5	-8	-8	-8	-8
3	26.50	6	-3	-3	-3	-3
4	26.50	3	-6	-6	-6	-6
5	6.00	17	-2	-2	-2	2
6	22.25	4.5	0	0	0	0
7	22.25	2	-2	-2	-2	-2
8	22.25	2.5	-4	-4	-4	-4
9	22.25	3	-1	-1	-1	-1
10	6.00	14	-4	-4	-4	-4

11	17.50	-5	-5	-1	-4	0
12	17.50	-1	-1	0	-1	0
13	17.50	-8	-8	-3	-5	0
14	17.50	-8	-8	-1	-7	0
15	17.50	-19	-19	-5	-14	0
16	17.50	-9	-9	-3	-6	0
17	17.50	-4	-4	0	-4	0
18	17.50	-16	-16	-5	-11	0
19	17.50	-20	-20	-5	-15	0
20	17.50	-6	-6	-1	-5	0
21	17.50	-5	-5	-2	-3	0
22	17.50	-23	-23	-6	-17	0
23	17.50	-8	-8	-2	-6	0
24	17.50	-1	-1	-1	0	0
25	17.50	-23	-23	-4	-19	0
26	17.50	-36	-36	-6	-30	0
27	17.50	-14	-14	-4	-10	0
28	17.50	-2	-2	0	-2	0
29	17.50	-23	-23	-7	-16	0
30	17.50	-18	-18	-3	-15	0
31	17.50	-3	-3	-1	-2	0
32	17.50	-17	-17	-4	-13	0
33	17.50	-31	-31	-6	-25	0
34	17.50	-32	-32	-7	-25	0
35	17.50	-29	-29	-5	-24	0
36	17.50	-33	-33	-8	-25	0
37	17.50	-32	-32	-6	-26	0
38	17.50	-30	-30	-6	-24	0
39	17.50	-30	-30	-5	-25	0
40	17.50	-31	-31	-6	-25	0
41	17.50	-33	-33	-6	-27	0
42	17.50	-30	-30	-5	-25	0
43	17.50	-33	-33	-6	-27	0

44	17.50	-30	-30	-8	-22	0
45	17.50	-23	-23	-6	-17	0
46	17.50	-16	-16	-3	-13	0
47	17.50	-3	-3	0	-3	0
48	17.50	-12	-12	-4	-8	0
49	17.50	-26	-26	-7	-19	0
50	17.50	-8	-8	-1	-7	0
51	17.50	-2	-2	-1	-1	0
52	17.50	-20	-20	-5	-15	0
53	17.50	-30	-30	-6	-24	0
54	17.50	-23	-23	-6	-17	0
55	17.50	-11	-11	-2	-9	0
56	17.50	-11	-11	-2	-9	0
57	17.50	-8	-8	-2	-6	0
58	10.50	-6	-6	-1	-5	0
59	6.00	12	-7	-7	-7	-7
60	20.00	3	-4	-4	-4	-4
61	20.00	0	-3	-3	-3	-3
62	4.00	4	-5	-5	-5	-5
63	12.00	2	-3	-3	-3	-3
64	4.00	2.5	-4	-4	-4	-4
65	17.75	6	-2	-2	-2	-2
66	17.75	7	4	4	4	4
67	17.75	5.5	0	0	0	0
68	17.75	5.5	-3	-3	-3	-3

To define the net charge of each mucin variant at the respective pH value (pH 4.0 or 7.0), initially, a manual calculation was performed by allocating a full elementary charge to single amino acids if the pK_a value of the amino acid side chains is close to or above the pH level. With this approach, at pH 7.0, the basic (Arg, Lys) and acidic amino acid (Asp, Glu) were assigned one positive/negative charge each. In contrast, at pH 4.0, the basic amino acids (arg, his, lys) were assigned a full positive elementary charge, whereas the charge assignment at pH 4.0 was adjusted such that only half a negative elementary charge was assigned to aspartate. This adjustment was reasonable, since, for this particular amino acid having a pK_a value close to ~4.0, full deprotonation is unlikely. With this refined

estimation process, the spatial charge distribution for the whole mucin molecule based on the following set of information and assumptions was performed:

1. the amino acid sequence of gastric mucin MUC5AC (**Table A5.1**)

2. information on the amount of negatively charged sialic acids and sulfate groups in the core domain of the protein as obtained from quantifying the released residues during enzymatic treatments

3. assuming the amino acid sequence between the 3rd and 4th VWF-like domain to be strongly glycosylated. This assumption was reasonable since, in this area of the polypeptide chain, there are lots of threonines and serines, which are typical targets for *O*-glycosylations.[292]

Whereas charges established by amino acids in the mucin termini (segments 1-10 and 59-68) were considered as described above (**Table A5.1**), charges corresponding to amino acids in the glycosylated domain were neglected. This adjustment was based on the assumption that those charges are shielded the glycan chains extending from the mucin backbone. Instead, all sialic acids and sulfate groups (which were determined to occur in a ratio of 1:3.5; **Fig. 3.2 B**) in this glycosylated region were included into the charge distribution. They were assigned a full negative elementary charge each (elements 11-58, **Table A5.1**). The estimation of the spatial distribution of these negative charges was based on experimental data as follows: Sulfate groups constituted ~1.8 % (w/w) of the molecular weight of MUC5AC. By assuming a molecular weight of ~3 MDa for an individual MUC5AC molecule, the corresponding total amount of sulfate groups summed up to ~63 kDa per mucin molecule. Assuming a molecular mass of sulfate groups of ~96 g mol^{-1} for sulfates, in total, ~655 negative charges were established by sulfated glycans per mucin. Since the experimentally determined ratio of sulfate groups to sialic acids residues was 3.5:1, a number of 187 sialic acids per mucin molecule could be estimated. The total of ~842 negative charges was distributed in the glycosylated core domain of the mucin molecule. Since, only serines and threonines were assumed to be associated with glycans *via O*-glycosylation, only those amino acids received negative charges. For assigning elementary charges to enzymatically treated mucins, the contributions of the respective anionic glycans were removed from the charge profile, *i.e.*, a net charge of 0 was assigned to the respective motif (**Table A5.1**).

Quantities of interest

Goal of this simulation was to obtain information on the conformation of a mucin filament in dependence of its line charge density. Thus, as relevant parameters to properly describe the mucin conformation, the time- and configuration-averaged end-to-end distance L_{e2e} and the radius of gyration R_g were identified as the quantities of interest to be analyzed in the simulations. To ensure a sufficient sampling of these statistical quantities, the total simulation time was set to t_{end} = 2 s and five independent, random realizations for each set of parameters were computed. The radius of gyration was computed in a spatially discrete manner, *i.e.*, the contributions were evaluated at the 69 nodes used for the centerline discretization.

Validity check of the numerical model

Experimental results for the conformation of mucins indicated a very pronounced compaction of the mucin molecule upon reduction of the solvent pH from a neutral (7.0) to an acidic level (2.0).[137, 138]

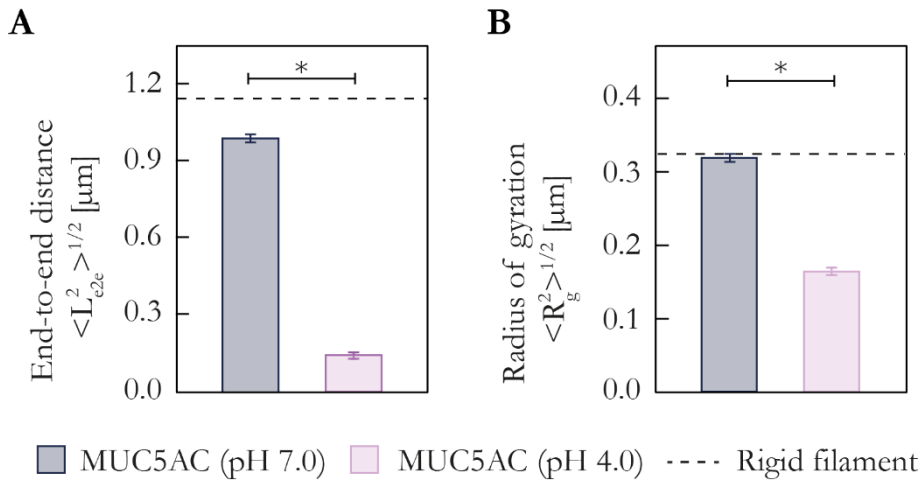

Fig. A5.1: Numerical simulation results obtained for native MUC5AC at neutral and acidic pH levels. The structural parameters, *i.e.*, the end-to-end distance and the radius of gyration, as calculated from the simulated mucins were determined at both, a neutral and an acidic pH level. The error bars depict to the standard error of the mean as obtained from five independent simulation runs (n = 5). Asterisks mark significant differences between samples as determined with a t-test (p < 0.05).

In accordance with experimental results obtained by AFM imaging, a compaction of the mucin molecules upon reduction of the solvent could be successfully predicted by the developed numerical model of the mucin molecule (**Fig. A5.1**).

Qualitatively similar results as for the simulation of MUC5AC –SO_4 could be obtained from simulated MUC5AC –SA (**Fig. A5.2**). However, in this case, the effects on the mucin conformation, *i.e.*, the reduction in both, end-to-end distance and radius of gyration, were less pronounced as for MUC5AC –SO_4 (**Fig. 3.6**).

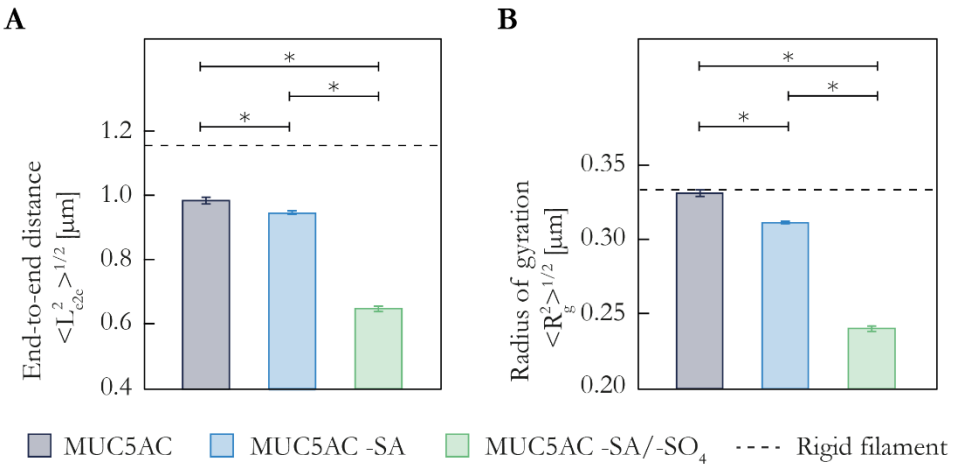

Fig. A5.2: Numerical simulation results obtained for native MUC5AC, MUC5AC –SA, and the double-treated variant MUC5AC –SO4/–SA at pH 7.0. The structural parameters, *i.e.*, the end-to-end distance and the radius of gyration, as calculated from the simulated mucins were determined for the two enzymatically modified MUC5AC variants. The error bars depict to the standard error of the mean as obtained from five independent simulation runs (n = 5). Asterisks mark significant differences between samples as determined with a t-test ($p < 0.05$).

Appendix A6: Mathematical model to describe molecule transport across mucin hydrogels*

The molecular penetration experiments presented in **Chapter 5.2** were supplemented with a theoretical description of these molecular transport processes based on diffusion-reaction equations. With this model, efficiency of the diffusive transport of charged objects across self-renewing physiological mucus barriers was predicted.

Estimation of the diffusion coefficient of dextran molecules in mucin gels

The diffusive travel distance (mean squared displacement, $\langle x^2 \rangle$) of a molecule in a viscous medium after a given time span t is linked to the molecules' diffusion coefficient D and the spatial dimension n *via* $\langle x^2 \rangle = 2 \times n \times D \times t$.

The diffusion coefficient D satisfies the Einstein Smoluchowski relation: $D = \frac{k_B \times T}{6 \times \pi \times \eta \times R}$ with the term $k_B \times T$ denoting the thermal energy, η the dynamic viscosity of the medium, and R the hydrodynamic radius of the diffusing object. When a local water-like viscosity within the mucin gel and a hydrodynamic radius $R = 1.4$ nm for the 4 kDa dextran molecules are assumed, a diffusion coefficient of $D = 175\ \mu m^2 s^{-1}$ is obtained. Considering a diffusion time of 20 min and a one-dimensional diffusion process (*i.e.*, n = 1), the average travel distance for such a molecule species can be calculated to $x = 648\ \mu m$.

Diffusion-reaction model

The system was modelled as a coupled one-dimensional reaction-diffusion system, described by the equations:

$$\frac{d}{dt}u(x,t) = D\ \frac{d^2}{dx^2}\ u(x,t) - r(x,t) \quad \text{and} \quad \frac{d}{dt}b(x,t) = r(x,t),$$

where $u(x,t)$ denotes the concentration of unbound (free) molecules at position x and time t, $b(x,t)$ denotes the corresponding concentration of bound molecules, and $r(x,t)$ is the reaction term. In the model, unbound molecules diffuse freely, with a diffusion constant of $D = 175\ \mu m^2\ s^{-1}$, whereas bound molecules cannot diffuse. Here, D corresponds to an effective, macroscopic diffusion

* This section follows in part the publication Marczynski *et al.*, Biomaterials Science (2018).

coefficient D_{eff} for the diffusion of objects through the mucin hydrogel matrix. In principle, this D_{eff} can be smaller than the microscopic diffusion coefficient. However, in this case, the difference between D and D_{eff} can be assumed to be negligibly small as the hydrodynamic radius of the probe molecules (*i.e.*, 4 kDa dextrans) is very small.[225, 293]

The reaction term $r(x,t)$ accounts for the binding and unbinding reactions:

$$r(x,t) = k^+ u(x,t) [m(x) - b(x,t)] - k^- b(x,t),$$

where the binding kinetics is described by the second order rate constant k^+ and the unbinding kinetics by the first-order rate constant k^-. Both rate constants are free parameters of the model. The local density of binding sites within the mucin gel is described by a profile $m(x)$. For comparison with the experiments, $m(x)$ was extracted from the averaged and normalized experimental data using a self-consistent parameter extraction scheme (see below), which also fixed the rate constants k^+ and k^-. Since the experimental profiles were normalized, the functions $u(x,t)$ and $b(x,t)$ are also dimensionless.

A generalized version of the model was used to account for the effects generated by mucus renewal *in vivo*. Thus, a constant drift velocity v in negative x-direction was introduced, which captures the transport effect arising from mucus renewal:

$$\frac{d}{dt}u(x,t) = D\,\frac{d^2}{dx^2}\,u(x,t) - v\frac{d}{dx}u(x,t) - r(x,t) \quad \text{and} \quad \frac{d}{dt}b(x,t) = -v\frac{d}{dx}b(x,t) + r(x,t).$$

For this explorative model, a homogeneous mucus profile $m(x) = m_0$ was assumed. In the absence of the binding reaction, the interplay between diffusive and convective transport is governed by the Peclet number, $Pe = vL/D$, where L is the length scale over which the transport occurs (here: the thickness of the mucus layer). For $Pe < 1$ diffusion dominates, whereas drift dominates for $Pe > 1$. In the presence of the binding reaction, an effective Peclet number Pe_{eff} was defined that has a similar interpretation. Since all molecules will experience the drift caused by mucus renewal, whereas only unbound molecules diffuse, the effective Peclet number is larger by a factor $(u+b)/u = 1+b/u$ than Pe, *i.e.*, the effect of the binding reaction on the interplay between diffusion and convection is determined by the bound-to-unbound ratio $a = b/u$. When a binding equilibrium is reached ($r = 0$), this ratio is fixed by the above equations to $a = \frac{m_0}{\left(u + \frac{k^-}{k^+}\right)}$.

Self-consistent estimation of the mucin binding site profile *m(x)*

The mucin binding site profile *m(x)* was extracted from the averaged and normalized experimental profiles using a parameter estimation scheme that also provided consistent values for the rate constants k^+ and k^-.

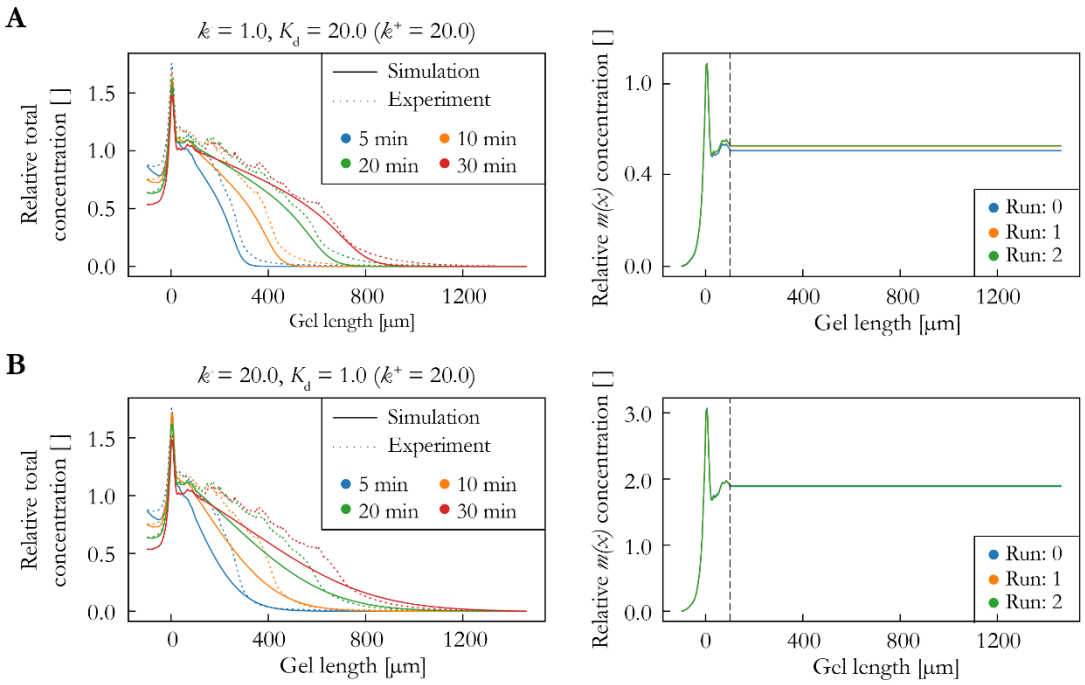

Fig. A6.1: Comparison of experiments (as obtained for a set of 'fingers' of one 'hand' filled with intestinal mucin MUC2 gels and positively charged dextrans) with simulations (left panel), and extracted *m(x)* concentration profiles (right panel) for different parameter values. In the *m(x)* profile a cut-off position was used, after which it was assumed to be constant to ensure convergence. The ratio of the transition rates $K_d = k^+/k^-$ was the most important parameter. The values $k^+ = 20$ and $k^- = 1$ gave the best fit for this dataset, and were thus used in the subsequent simulations (**A**). Another set of parameter values gave worse fits ($k^+ = 20$, $k^- = 20$): a low K_d also led to a different scale of the estimated *m(x)* profile (**B**).

For this purpose, a *m(x)* profile was assumed that is non-uniform only in the vicinity of the interface, but adopted a constant bulk value after a cut-off distance (indicated by the dashed vertical line in **Fig. A6.1**, right panel). The parameter estimation scheme was iterative and initial values for the rate constants k^+ and k^-, as well as an initial guess for the *m(x)* profile were chosen freely. The time-dependent concentration profiles *u(x,t)* and *b(x,t)* were obtained by solving the reaction-diffusion equations of the model numerically. The initial and boundary conditions were chosen as follows: a constant left boundary condition $u(x_0,t) = f(t) = 1$ and absorbing boundary conditions at the right-hand end, *i.e.*, $u(L,t) = 0$. Then the experimental data for the total concentration and the simulated

data for the unbound concentration (at the largest experimentally available time point) were used to get an updated estimate for *m(x)*. This procedure was iterated until convergence was reached (usually within three iterations) to determine a shape of the *m(x)* profile that was self-consistent (**Fig. A6.1**, right panel).

The obtained self-consistent *m(x)* profile that resulted from this procedure and, in particular, the absolute scale of *m(x)* depended on the chosen values for the rate constants. To get profiles that match the data, the rate constants k^+ and k^- were varied, and self-consistent *m(x)* estimation was repeated until agreement with the experimental data was successfully achieved for all times (**Fig. A6.1**, left panel). Importantly, multiple combinations of rate constant values yielded simulation results that adequately described the experimental profiles. Generally, the extraction of the rate constants and the *m(x)* profiles primarily served as a demonstration that a simple second-order mass-action binding model could, indeed, describe the observed transport behavior.

Bibliography

1. Lang, T.; Hansson, G. C.; Samuelsson, T., Gel-forming mucins appeared early in metazoan evolution. *Proc Natl Acad Sci USA* **2007,** *104* (41), 16209-16214.

2. Lang, T.; Klasson, S.; Larsson, E.; Johansson, M. E. V.; Hansson, G. C.; Samuelsson, T., Searching the Evolutionary Origin of Epithelial Mucus Protein Components—Mucins and FCGBP. *Mol Biol Evol* **2016,** *33* (8), 1921-1936.

3. Bakshani, C. R.; Morales-Garcia, A. L.; Althaus, M.; Wilcox, M. D.; Pearson, J. P.; Bythell, J. C.; Burgess, J. G., Evolutionary conservation of the antimicrobial function of mucus: a first defence against infection. *npj Biofilms Microbiomes* **2018,** *4* (1), 14.

4. Zintzen, V.; Roberts, C. D.; Anderson, M. J.; Stewart, A. L.; Struthers, C. D.; Harvey, E. S., Hagfish predatory behaviour and slime defence mechanism. *Sci Rep* **2011,** *1* (1), 131.

5. Bansil, R.; Turner, B. S., The biology of mucus: Composition, synthesis and organization. *Adv Drug Deliv Rev* **2018,** *124*, 3-15.

6. Toledo, R. C.; Jared, C., Cutaneous granular glands and amphibian venoms. *Comp Biochem Physiol Part A Physiol* **1995,** *111* (1), 1-29.

7. Johansson, M. E., Fast renewal of the distal colonic mucus layers by the surface goblet cells as measured by in vivo labeling of mucin glycoproteins. *PLoS One* **2012,** *7* (7), e41009.

8. Taherali, F.; Varum, F.; Basit, A. W., A slippery slope: On the origin, role and physiology of mucus. *Adv Drug Deliv Rev* **2018,** *124*, 16-33.

9. Cone, R. A., Barrier properties of mucus. *Adv Drug Deliv Rev* **2009,** *61* (2), 75-85.

10. Lieleg, O.; Lieleg, C.; Bloom, J.; Buck, C. B.; Ribbeck, K., Mucin biopolymers as broad-spectrum antiviral agents. *Biomacromolecules* **2012,** *13* (6), 1724-32.

11. Johansson, M. E. V.; Hansson, G. C., Immunological aspects of intestinal mucus and mucins. *Nat Rev Immunol* **2016,** *16* (10), 639-649.

12. Petrou, G.; Crouzier, T., Mucins as multifunctional building blocks of biomaterials. *Biomater Sci* **2018,** *6* (9), 2282-2297.

13. Schroeder, B. O., Fight them or feed them: how the intestinal mucus layer manages the gut microbiota. *Gastroenterol Rep* **2019,** *7* (1), 3-12.

14. Paone, P.; Cani, P. D., Mucus barrier, mucins and gut microbiota: the expected slimy partners? *Gut* **2020,** *69* (12), 2232-2243.

15. Wang, B. X.; Wu, C. M.; Ribbeck, K., Home, sweet home: how mucus accommodates our microbiota. *FEBS J* **2021,** *288* (6), 1789-1799.

16. Frenkel Erica, S.; Ribbeck, K.; Schottel, J. L., Salivary Mucins Protect Surfaces from Colonization by Cariogenic Bacteria. *Appl Environ Microbiol* **2015,** *81* (1), 332-338.

17. Andrianifahanana, M.; Moniaux, N.; Schmied, B. M.; Ringel, J.; Friess, H.; Hollingsworth, M. A.; Büchler, M. W.; Aubert, J.-P.; Batra, S. K., Mucin (MUC) gene expression in human pancreatic adenocarcinoma and chronic pancreatitis: a potential role of MUC4 as a tumor marker of diagnostic significance. *Clin Cancer Res* **2001,** *7* (12), 4033-4040.

18. Kufe, D. W., Mucins in cancer: function, prognosis and therapy. *Nat Rev Cancer* **2009,** *9* (12), 874-885.

19. Yamashita, M. S. A.; Melo, E. O., Mucin 2 (MUC2) promoter characterization: an overview. *Cell Tissue Res* **2018,** *374* (3), 455-463.

20. Madsen, F.; Eberth, K.; Smart, J. D., A Rheological Evaluation of Various Mucus Gels for Use in In-vitro Mucoadhesion Testing. *Pharm Pharmacol Commun* **1996,** *2* (12), 563-566.

21. Kočevar-Nared, J.; Kristl, J.; Šmid-Korbar, J., Comparative rheological investigation of crude gastric mucin and natural gastric mucus. *Biomaterials* **1997,** *18* (9), 677-681.

22. Schömig, V. J.; Käsdorf, B. T.; Scholz, C.; Bidmon, K.; Lieleg, O.; Berensmeier, S., An optimized purification process for porcine gastric mucin with preservation of its native functional properties. *RSC Adv* **2016,** *6* (50), 44932-44943.

23. Shankar, V.; Gilmore, M. S.; Elkins, R. C.; Sachdev, G. P., A novel human airway mucin cDNA encodes a protein with unique tandem-repeat organization. *Biochem J* **1994,** *300 (Pt 2)* (Pt 2), 295-8.

24. Lesuffleur, T.; Roche, F.; Hill, A. S.; Lacasa, M.; Fox, M.; Swallow, D. M.; Zweibaum, A.; Real, F. X., Characterization of a mucin cDNA clone isolated from HT-29 mucus-secreting cells. The 3' end of MUC5AC? *J Biol Chem* **1995,** *270* (23), 13665-73.

25. Linden, S. K.; Sutton, P.; Karlsson, N. G.; Korolik, V.; McGuckin, M. A., Mucins in the mucosal barrier to infection. *Mucosal Immunol* **2008,** *1* (3), 183-97.

26. Leal, J.; Smyth, H. D. C.; Ghosh, D., Physicochemical properties of mucus and their impact on transmucosal drug delivery. *Int J Pharm* **2017,** *532* (1), 555-572.

27. Allen, A.; Hutton, D. A.; Pearson, J. P., The MUC2 gene product: a human intestinal mucin. *Int J Biochem Cell Biol* **1998,** *30* (7), 797-801.

28. Zhao, H.; Jumblatt, J. E.; Wood, T. O.; Jumblatt, M. M., Quantification of MUC5AC protein in human tears. *Cornea* **2001,** *20* (8), 873-7.

29. Babu, S. D.; Jayanthi, V.; Devaraj, N.; Reis, C. A.; Devaraj, H., Expression profile of mucins (MUC2, MUC5AC and MUC6) in Helicobacter pylori infected pre-neoplastic and neoplastic human gastric epithelium. *Mol Cancer* **2006,** *5* (1), 10.

30. Spurr-Michaud, S.; Argüeso, P.; Gipson, I., Assay of mucins in human tear fluid. *Exp Eye Res* **2007,** *84* (5), 939-950.

31. Gipson, I. K.; Moccia, R.; Spurr-Michaud, S.; Argüeso, P.; Gargiulo, A. R.; Hill III, J. A.; Offner, G. D.; Keutmann, H. T., The amount of MUC5B mucin in cervical mucus peaks at midcycle. *J Clin Endocrinol Metab* **2001,** *86* (2), 594-600.

32. Van Klinken, B. J.-W.; Dekker, J.; Van Gool, S. A.; Van Marle, J.; Büller, H. A.; Einerhand, A. W., MUC5B is the prominent mucin in human gallbladder and is also expressed in a subset of colonic goblet cells. *Am J Physiol Gastrointest Liver Physiol* **1998,** *274* (5), G871-G878.

33. Thornton, D. J.; Khan, N.; Mehrotra, R.; Howard, M.; Sheehan, J. K.; Veerman, E.; Packer, N. H., Salivary mucin MG1 is comprised almost entirely of different glycosylated forms of the MUC5B gene product. *Glycobiology* **1999,** *9* (3), 293-302.

34. Bansil, R.; Turner, B. S., Mucin structure, aggregation, physiological functions and biomedical applications. *Curr Opin Colloid Interface Sci* **2006,** *11* (2), 164-170.

35. Imai, K.; Mitaku, S., Mechanisms of secondary structure breakers in soluble proteins. *Biophysics* **2005,** *1*, 55-65.

36. Jentoft, N., Why are proteins O-glycosylated? *Trends Biochem Sci* **1990,** *15* (8), 291-294.

37. Baos, S.; Phillips, D. B.; Wildling, L.; McMaster, T.; Berry, M., Distribution of sialic acids on mucins and gels: a defense mechanism. *Biophys J* **2012,** *102* (1), 176-184.

38. Marczynski, M.; Balzer, B. N.; Jiang, K.; Lutz, T. M.; Crouzier, T.; Lieleg, O., Charged glycan residues critically contribute to the adsorption and lubricity of mucins. *Colloids Surf B* **2020,** *187*, 110614.

39. Lutz, T. M.; Marczynski, M.; Grill, M. J.; Wall, W. A.; Lieleg, O., Repulsive Backbone–Backbone Interactions Modulate Access to Specific and Unspecific Binding Sites on Surface-Bound Mucins. *Langmuir* **2020,** *36* (43), 12973-12982.

40. Käsdorf, B. T.; Weber, F.; Petrou, G.; Srivastava, V.; Crouzier, T.; Lieleg, O., Mucin-inspired lubrication on hydrophobic surfaces. *Biomacromolecules* **2017,** *18* (8), 2454-2462.

41. Perez-Vilar, J.; Hill, R. L., The Structure and Assembly of Secreted Mucins* 210. *J Biol Chem* **1999,** *274* (45), 31751-31754.

42. Gum Jr, J. R.; Hicks, J. W.; Toribara, N. W.; Siddiki, B.; Kim, Y. S., Molecular cloning of human intestinal mucin (MUC2) cDNA. Identification of the amino terminus and overall sequence similarity to prepro-von Willebrand factor. *J Biol Chem* **1994,** *269* (4), 2440-2446.

43. Ambort, D.; van der Post, S.; Johansson, M. E.; MacKenzie, J.; Thomsson, E.; Krengel, U.; Hansson, G. C., Function of the CysD domain of the gel-forming MUC2 mucin. *Biochem J* **2011,** *436* (1), 61-70.

44. Ridley, C.; Kouvatsos, N.; Raynal, B. D.; Howard, M.; Collins, R. F.; Desseyn, J.-L.; Jowitt, T. A.; Baldock, C.; Davis, C. W.; Hardingham, T. E., Assembly of the respiratory mucin MUC5B: a new model for a gel-forming mucin. *J Biol Chem* **2014,** *289* (23), 16409-16420.

45. Taylor, C.; Allen, A.; Dettmar, P. W.; Pearson, J. P., Two rheologically different gastric mucus secretions with different putative functions. *Biochim Biophys Acta Gen Subj* **2004,** *1674* (2), 131-138.

46. Kesimer, M.; Ford, A. A.; Ceppe, A.; Radicioni, G.; Cao, R.; Davis, C. W.; Doerschuk, C. M.; Alexis, N. E.; Anderson, W. H.; Henderson, A. G.; Barr, R. G.; Bleecker, E. R.; Christenson, S. A.; Cooper, C. B.; Han, M. K.; Hansel, N. N.; Hastie, A. T.; Hoffman, E. A.; Kanner, R. E.;

Martinez, F.; Paine, R.; Woodruff, P. G.; O'Neal, W. K.; Boucher, R. C., Airway Mucin Concentration as a Marker of Chronic Bronchitis. *N Engl J Med* **2017,** *377* (10), 911-922.

47. Navazesh, M.; Mulligan, R. A.; Kipnis, V.; Denny, P. A.; Denny, P. C., Comparison of whole saliva flow rates and mucin concentrations in healthy Caucasian young and aged adults. *J Dent Res* **1992,** *71* (6), 1275-8.

48. Hattrup, C. L.; Gendler, S. J., Structure and function of the cell surface (tethered) mucins. *Annu Rev Physiol* **2008,** *70*, 431-457.

49. Govindarajan, B.; Gipson, I. K., Membrane-tethered mucins have multiple functions on the ocular surface. *Exp Eye Res* **2010,** *90* (6), 655-663.

50. Pelaseyed, T.; Hansson, G. C., Membrane mucins of the intestine at a glance. *J Cell Sci* **2020,** *133* (5), jcs240929.

51. Madsen, J. B.; Svensson, B.; Abou Hachem, M.; Lee, S., Proteolytic Degradation of Bovine Submaxillary Mucin (BSM) and Its Impact on Adsorption and Lubrication at a Hydrophobic Surface. *Langmuir* **2015,** *31* (30), 8303-8309.

52. Li, Leon D.; Crouzier, T.; Sarkar, A.; Dunphy, L.; Han, J.; Ribbeck, K., Spatial Configuration and Composition of Charge Modulates Transport into a Mucin Hydrogel Barrier. *Biophys J* **2013,** *105* (6), 1357-1365.

53. Martin, J. B., Molecular basis of the neurodegenerative disorders. *N Engl J Med* **1999,** *340* (25), 1970-1980.

54. Wong, Y. C.; Krainc, D., α-synuclein toxicity in neurodegeneration: mechanism and therapeutic strategies. *Nat Med* **2017,** *23* (2), 1-13.

55. Miake, H.; Mizusawa, H.; Iwatsubo, T.; Hasegawa, M., Biochemical characterization of the core structure of α-synuclein filaments. *J Biol Chem* **2002,** *277* (21), 19213-19219.

56. Hoyer, W.; Cherny, D.; Subramaniam, V.; Jovin, T. M., Impact of the acidic C-terminal region comprising amino acids 109− 140 on α-synuclein aggregation in vitro. *Biochemistry* **2004,** *43* (51), 16233-16242.

57. Fakhree, M. A.; Nolten, I. S.; Blum, C.; Claessens, M. M., Different conformational subensembles of the intrinsically disordered protein α-Synuclein in cells. *J Phys Chem Lett* **2018,** *9* (6), 1249-1253.

58. Horvath, I.; Weise, C. F.; Andersson, E. K.; Chorell, E.; Sellstedt, M.; Bengtsson, C.; Olofsson, A.; Hultgren, S. J.; Chapman, M.; Wolf-Watz, M., Mechanisms of protein oligomerization: inhibitor of functional amyloids templates α-synuclein fibrillation. *J Am Chem Soc* **2012,** *134* (7), 3439-3444.

59. Semerdzhiev, S. A.; Dekker, D. R.; Subramaniam, V.; Claessens, M. M., Self-assembly of protein fibrils into suprafibrillar aggregates: bridging the nano-and mesoscale. *ACS Nano* **2014,** *8* (6), 5543-5551.

60. Goedert, M., Alzheimer's and Parkinson's diseases: The prion concept in relation to assembled Aβ, tau, and α-synuclein. *Science* **2015,** *349* (6248).

61. Peelaerts, W.; Bousset, L.; Van der Perren, A.; Moskalyuk, A.; Pulizzi, R.; Giugliano, M.; Van den Haute, C.; Melki, R.; Baekelandt, V., α-Synuclein strains cause distinct synucleinopathies after local and systemic administration. *Nature* **2015,** *522* (7556), 340-344.

62. Shouren, G.; Kojio, K.; Takahara, A.; Kajiyama, T., Bovine serum albumin adsorption onto immobilized organotrichlorosilane surface: Influence of the phase separation on protein adsorption patterns. *J Biomater Sci Polym Ed* **1998,** *9* (2), 131-150.

63. Wetter, L. R.; Deutsch, H. F., Immunological studies on egg white proteins. IV. Immunochemical and physical studies of lysozyme. *J Biol Chem* **1951,** *192* (1), 237-42.

64. Long, C. M.; Nascarella, M. A.; Valberg, P. A., Carbon black vs. black carbon and other airborne materials containing elemental carbon: Physical and chemical distinctions. *Environ Pollut* **2013,** *181*, 271-286.

65. Kleeman, M. J.; Schauer, J. J.; Cass, G. R., Size and Composition Distribution of Fine Particulate Matter Emitted from Motor Vehicles. *Environ Sci Technol* **2000,** *34* (7), 1132-1142.

66. Paasonen, P.; Kupiainen, K.; Klimont, Z.; Visschedijk, A.; Denier van der Gon, H. A. C.; Amann, M., Continental anthropogenic primary particle number emissions. *Atmos Chem Phys* **2016,** *16* (11), 6823-6840.

67. Bond, T. C.; Doherty, S. J.; Fahey, D. W.; Forster, P. M.; Berntsen, T.; DeAngelo, B. J.; Flanner, M. G.; Ghan, S.; Kärcher, B.; Koch, D., Bounding the role of black carbon in the climate system: A scientific assessment. *J Geophy Res Atmos* **2013,** *118* (11), 5380-5552.

68. Organization, W. H., *Health effects of black carbon*. WHO: 2012.

69. Lieleg, O.; Vladescu, I.; Ribbeck, K., Characterization of particle translocation through mucin hydrogels. *Biophys J* **2010,** *98* (9), 1782-1789.

70. Winkeljann, B.; Leipold, P.-M. A.; Lieleg, O., Macromolecular Coatings Enhance the Tribological Performance of Polymer-Based Lubricants. *Adv Mater Interfaces* **2019,** *6* (16), 1900366.

71. Fahy, J. V.; Dickey, B. F., Airway mucus function and dysfunction. *N Engl J Med* **2010,** *363* (23), 2233-47.

72. Allen, A., The structure and function of gastrointestinal mucus. In *Attachment of organisms to the gut mucosa*, CRC Press: 2018; pp 3-12.

73. Kirkham, S.; Sheehan, J. K.; Knight, D.; Richardson, P. S.; Thornton, D. J., Heterogeneity of airways mucus: variations in the amounts and glycoforms of the major oligomeric mucins MUC5AC and MUC5B. *Biochem J* **2002,** *361* (3), 537-546.

74. Johansson, M. E.; Sjövall, H.; Hansson, G. C., The gastrointestinal mucus system in health and disease. *Nat Rev Gastroenterol Hepatol* **2013,** *10* (6), 352-361.

75. Celli, J. P.; Turner, B. S.; Afdhal, N. H.; Ewoldt, R. H.; McKinley, G. H.; Bansil, R.; Erramilli, S., Rheology of gastric mucin exhibits a pH-dependent sol-gel transition. *Biomacromolecules* **2007,** *8* (5), 1580-6.

76. Cao, X.; Bansil, R.; Bhaskar, K. R.; Turner, B. S.; LaMont, J. T.; Niu, N.; Afdhal, N. H., pH-dependent conformational change of gastric mucin leads to sol-gel transition. *Biophys J* **1999,** *76* (3), 1250-1258.

77. Song, J.; Winkeljann, B.; Lieleg, O., The lubricity of mucin solutions is robust toward changes in physiological conditions. *ACS Appl Bio Mater* **2019,** *2* (8), 3448-3457.

78. Hsu, S. M.; Gates, R. S., Boundary lubricating films: formation and lubrication mechanism. *Tribol Int* **2005,** *38* (3), 305-312.

79. Ma, L.; Gaisinskaya-Kipnis, A.; Kampf, N.; Klein, J., Origins of hydration lubrication. *Nat Commun* **2015,** *6* (1), 6060.

80. Neu, C. P.; Komvopoulos, K.; Reddi, A. H., The interface of functional biotribology and regenerative medicine in synovial joints. *Tissue Eng Part B Rev* **2008,** *14* (3), 235-47.

81. Boettcher, K.; Grumbein, S.; Winkler, U.; Nachtsheim, J.; Lieleg, O., Adapting a commercial shear rheometer for applications in cartilage research. *Rev Sci Instrum* **2014,** *85* (9), 093903.

82. Johnston, I.; McCluskey, D.; Tan, C.; Tracey, M., Mechanical characterization of bulk Sylgard 184 for microfluidics and microengineering. *J Micromech Microeng* **2014,** *24* (3), 035017.

83. Winkeljann, B.; Bussmann, A. B.; Bauer, M. G.; Lieleg, O., Oscillatory Tribology Performed With a Commercial Shear Rheometer. *Biotribology* **2018,** *14*, 11-18.

84. Sauerbrey, G., Verwendung von Schwingquarzen zur Wägung dünner Schichten und zur Mikrowägung. *Z Phys B* **1959,** *155* (2), 206-222.

85. Iruthayaraj, J.; Olanya, G.; Claesson, P. M., Viscoelastic Properties of Adsorbed Bottle-brush Polymer Layers Studied by Quartz Crystal Microbalance — Dissipation Measurements. *J Phys Chem C* **2008,** *112* (38), 15028-15036.

86. Shi, L.; Caldwell, K. D., Mucin adsorption to hydrophobic surfaces. *J Colloid Interface Sci* **2000,** *224* (2), 372-381.

87. Wienken, C. J.; Baaske, P.; Rothbauer, U.; Braun, D.; Duhr, S., Protein-binding assays in biological liquids using microscale thermophoresis. *Nat Commun* **2010,** *1* (1), 100.

88. Jerabek-Willemsen, M.; Wienken, C. J.; Braun, D.; Baaske, P.; Duhr, S., Molecular interaction studies using microscale thermophoresis. *Assay Drug Dev Technol* **2011,** *9* (4), 342-353.

89. Duhr, S.; Braun, D., Why molecules move along a temperature gradient. *Proc Natl Acad Sci USA* **2006,** *103* (52), 19678-19682.

90. Bara, J.; Chastre, E.; Mahiou, J.; Singh, R. L.; Forgue-Lafitte, M. E.; Hollande, E.; Godeau, F., Gastric M1 mucin, an early oncofetal marker of colon carcinogenesis, is encoded by the MUC5AC gene. *Int J Cancer* **1998,** *75* (5), 767-73.

91. Riener, C. K.; Kada, G.; Gruber, H. J., Quick measurement of protein sulfhydryls with Ellman's reagent and with 4,4'-dithiodipyridine. *Anal Bioanal Chem* **2002,** *373* (4-5), 266-76.

92. Song, D.; Cahn, D.; Duncan, G. A., Mucin Biopolymers and Their Barrier Function at Airway Surfaces. *Langmuir* **2020,** *36* (43), 12773-12783.

93. Benetti, E. M.; Spencer, N. D., Using Polymers to Impart Lubricity and Biopassivity to Surfaces: Are These Properties Linked? *Helv Chim Acta* **2019,** *102* (5), e1900071.

94. Yan, W.; Ramakrishna, S. N.; Romio, M.; Benetti, E. M., Bioinert and Lubricious Surfaces by Macromolecular Design. *Langmuir* **2019,** *35* (42), 13521-13535.

95. Yakubov, G. E.; McColl, J.; Bongaerts, J. H. H.; Ramsden, J. J., Viscous Boundary Lubrication of Hydrophobic Surfaces by Mucin. *Langmuir* **2009,** *25* (4), 2313-2321.

96. Knowles, M. R.; Boucher, R. C., Mucus clearance as a primary innate defense mechanism for mammalian airways. *J Clin Invest* **2002,** *109* (5), 571-577.

97. Liévin-Le Moal, V.; Servin, A. L., The front line of enteric host defense against unwelcome intrusion of harmful microorganisms: mucins, antimicrobial peptides, and microbiota. *Clin Microbiol Rev* **2006,** *19* (2), 315-337.

98. Carpenter, J.; Kesimer, M., Membrane-bound mucins of the airway mucosal surfaces are densely decorated with keratan sulfate: Revisiting their role in the Lung's innate defense. *Glycobiology* **2021,** *31* (4), 436-443.

99. McGuckin, M. A.; Lindén, S. K.; Sutton, P.; Florin, T. H., Mucin dynamics and enteric pathogens. *Nat Rev Microbiol* **2011,** *9* (4), 265-278.

100. Delaveris, C. S.; Webster, E. R.; Banik, S. M.; Boxer, S. G.; Bertozzi, C. R., Membrane-tethered mucin-like polypeptides sterically inhibit binding and slow fusion kinetics of influenza A virus. *Proc Natl Acad Sci USA* **2020,** *117* (23), 12643-12650.

101. Lindén, S. K.; Sheng, Y. H.; Every, A. L.; Miles, K. M.; Skoog, E. C.; Florin, T. H.; Sutton, P.; McGuckin, M. A., MUC1 limits Helicobacter pylori infection both by steric hindrance and by acting as a releasable decoy. *PLoS Pathog* **2009,** *5* (10), e1000617.

102. Dhar, P.; McAuley, J., The Role of the Cell Surface Mucin MUC1 as a Barrier to Infection and Regulator of Inflammation. *Front Cell Infect Microbiol* **2019,** *9*, 117.

103. Button, B.; Cai, L.-H.; Ehre, C.; Kesimer, M.; Hill, D. B.; Sheehan, J. K.; Boucher, R. C.; Rubinstein, M., A periciliary brush promotes the lung health by separating the mucus layer from airway epithelia. *Science* **2012,** *337* (6097), 937-941.

104. Button, B.; Goodell, H. P.; Atieh, E.; Chen, Y.-C.; Williams, R.; Shenoy, S.; Lackey, E.; Shenkute, N. T.; Cai, L.-H.; Dennis, R. G.; Boucher, R. C.; Rubinstein, M., Roles of mucus adhesion and cohesion in cough clearance. *Proc Natl Acad Sci USA* **2018,** *115* (49), 12501-12506.

105. Pallesen, L. T.; Berglund, L.; Rasmussen, L. K.; Petersen, T. E.; Rasmussen, J. T., Isolation and characterization of MUC15, a novel cell membrane-associated mucin. *Eur J Biochem* **2002,** *269* (11), 2755-2763.

106. Liu, B.; Yu, Z.; Chen, C.; Kling, D. E.; Newburg, D. S., Human milk mucin 1 and mucin 4 inhibit Salmonella enterica serovar Typhimurium invasion of human intestinal epithelial cells in vitro. *J Nutr* **2012,** *142* (8), 1504-9.

107. Sumiyoshi, M.; Ricciuto, J.; Tisdale, A.; Gipson, I. K.; Mantelli, F.; Argüeso, P., Antiadhesive character of mucin O-glycans at the apical surface of corneal epithelial cells. *Invest Ophthalmol Vis Sci* **2008,** *49* (1), 197-203.

108. Shi, L.; Ardehali, R.; Caldwell, K. D.; Valint, P., Mucin coating on polymeric material surfaces to suppress bacterial adhesion. *Colloids Surf B* **2000,** *17* (4), 229-239.

109. Crouzier, T.; Jang, H.; Ahn, J.; Stocker, R.; Ribbeck, K., Cell Patterning with Mucin Biopolymers. *Biomacromolecules* **2013,** *14* (9), 3010-3016.

110. Co, J. Y.; Crouzier, T.; Ribbeck, K., Probing the Role of Mucin-Bound Glycans in Bacterial Repulsion by Mucin Coatings. *Adv Mater Interfaces* **2015,** *2* (17), 1500179.

111. Song, J.; Lutz, T. M.; Lang, N.; Lieleg, O., Bioinspired Dopamine/Mucin Coatings Provide Lubricity, Wear Protection, and Cell-Repellent Properties for Medical Applications. *Adv Healthc Mater* **2021,** *10* (4), 2000831.

112. Robbe, C.; Capon, C.; Coddeville, B.; Michalski, J.-C., Structural diversity and specific distribution of O-glycans in normal human mucins along the intestinal tract. *Biochem J* **2004,** *384* (Pt 2), 307-316.

113. Andersch-Björkman, Y.; Thomsson, K. A.; Holmén Larsson, J. M.; Ekerhovd, E.; Hansson, G. C., Large scale identification of proteins, mucins, and their O-glycosylation in the endocervical mucus during the menstrual cycle. *Mol Cell Proteomics* **2007,** *6* (4), 708-16.

114. Reis, C. A.; Osorio, H.; Silva, L.; Gomes, C.; David, L., Alterations in glycosylation as biomarkers for cancer detection. *J Clin Pathol* **2010,** *63* (4), 322-9.

115. Larsson, J. M.; Karlsson, H.; Crespo, J. G.; Johansson, M. E.; Eklund, L.; Sjövall, H.; Hansson, G. C., Altered O-glycosylation profile of MUC2 mucin occurs in active ulcerative colitis and is associated with increased inflammation. *Inflamm Bowel Dis* **2011,** *17* (11), 2299-307.

116. Strombeck, D. R.; Harrold, D., Binding of cholera toxin to mucins and inhibition by gastric mucin. *Infect Immun* **1974,** *10* (6), 1266-72.

117. Loomis, R. E.; Prakobphol, A.; Levine, M. J.; Reddy, M. S.; Jones, P. C., Biochemical and biophysical comparison of two mucins from human submandibular-sublingual saliva. *Arch Biochem Biophys* **1987,** *258* (2), 452-64.

118. Nordman, H.; Davies, J. R.; Herrmann, A.; Karlsson, N. G.; Hansson, G. C.; Carlstedt, I., Mucus glycoproteins from pig gastric mucosa: identification ofdifferent mucin populations from the surface epithelium. *Biochem J* **1997,** *326* (3), 903-910.

119. Robinson, C. V.; Elkins, M. R.; Bialkowski, K. M.; Thornton, D. J.; Kertesz, M. A., Desulfurization of mucin by Pseudomonas aeruginosa: influence of sulfate in the lungs of cystic fibrosis patients. *J Med Microbiol* **2012,** *61* (Pt 12), 1644-1653.

120. Lindh, L.; Glantz, P.-O.; Carlstedt, I.; Wickström, C.; Arnebrant, T., Adsorption of MUC5B and the role of mucins in early salivary film formation. *Colloids Surf B* **2002,** *25* (2), 139-146.

121. Coles, J. M.; Chang, D. P.; Zauscher, S., Molecular mechanisms of aqueous boundary lubrication by mucinous glycoproteins. *Curr Opin Colloid Interface Sci* **2010,** *15* (6), 406-416.

122. Sotres, J.; Madsen, J. B.; Arnebrant, T.; Lee, S., Adsorption and nanowear properties of bovine submaxillary mucin films on solid surfaces: influence of solution pH and substrate hydrophobicity. *J Colloid Interface Sci* **2014,** *428*, 242-50.

123. Zhou, H.-X.; Pang, X., Electrostatic Interactions in Protein Structure, Folding, Binding, and Condensation. *Chem Rev* **2018,** *118* (4), 1691-1741.

124. Norde, W., Driving forces for protein adsorption at solid surfaces. *Macromol Symp* **1996,** *103* (1), 5-18.

125. Yano, Y. F., Kinetics of protein unfolding at interfaces. *J Phys Condens Matter* **2012,** *24* (50), 503101.

126. Pan, H.; Qin, M.; Meng, W.; Cao, Y.; Wang, W., How Do Proteins Unfold upon Adsorption on Nanoparticle Surfaces? *Langmuir* **2012,** *28* (35), 12779-12787.

127. Round, A. N.; Berry, M.; McMaster, T. J.; Corfield, A. P.; Miles, M. J., Glycopolymer charge density determines conformation in human ocular mucin gene products: an atomic force microscope study. *J Struct Biol* **2004,** *145* (3), 246-53.

128. Marczynski, M.; Käsdorf, B. T.; Altaner, B.; Wenzler, A.; Gerland, U.; Lieleg, O., Transient binding promotes molecule penetration into mucin hydrogels by enhancing molecular partitioning. *Biomater Sci* **2018,** *6* (12), 3373-3387.

129. Karlsson, N. G.; Nordman, H.; Karlsson, H.; Carlstedt, I.; Hansson, G. C., Glycosylation differences between pig gastric mucin populations: a comparative study of the neutral oligosaccharides using mass spectrometry. *Biochem J* **1997,** *326* (3), 911-917.

130. Padra, M.; Adamczyk, B.; Flahou, B.; Erhardsson, M.; Chahal, G.; Smet, A.; Jin, C.; Thorell, A.; Ducatelle, R.; Haesebrouck, F.; Karlsson, N. G.; Lindén, S. K., Helicobacter suis infection alters glycosylation and decreases the pathogen growth inhibiting effect and binding avidity of gastric mucins. *Mucosal Immunol* **2019,** *12* (3), 784-794.

131. Menchicchi, B.; Fuenzalida, J. P.; Bobbili, K. B.; Hensel, A.; Swamy, M. J.; Goycoolea, F. M., Structure of Chitosan Determines Its Interactions with Mucin. *Biomacromolecules* **2014,** *15* (10), 3550-3558.

132. Round, A. N.; Berry, M.; McMaster, T. J.; Stoll, S.; Gowers, D.; Corfield, A. P.; Miles, M. J., Heterogeneity and Persistence Length in Human Ocular Mucins. *Biophys J* **2002,** *83* (3), 1661-1670.

133. McMaster, T. J.; Berry, M.; Corfield, A. P.; Miles, M. J., Atomic force microscopy of the submolecular architecture of hydrated ocular mucins. *Biophys J* **1999,** *77* (1), 533-41.

134. Zappone, B.; Patil, N. J.; Madsen, J. B.; Pakkanen, K. I.; Lee, S., Molecular Structure and Equilibrium Forces of Bovine Submaxillary Mucin Adsorbed at a Solid–Liquid Interface. *Langmuir* **2015,** *31* (15), 4524-4533.

135. Grant, L. M.; Ederth, T.; Tiberg, F., Influence of surface hydrophobicity on the layer properties of adsorbed nonionic surfactants. *Langmuir* **2000,** *16* (5), 2285-2291.

136. Mendez-Vilas, A.; Gonzalez-Martin, M.; Labajos-Broncano, L.; Nuevo, M., Experimental analysis of the influence of surface topography on the adhesion force as measured by an AFM. *J Adhes Sci Technol* **2002,** *16* (13), 1737-1747.

137. Hong, Z.; Chasan, B.; Bansil, R.; Turner, B. S.; Bhaskar, K. R.; Afdhal, N. H., Atomic force microscopy reveals aggregation of gastric mucin at low pH. *Biomacromolecules* **2005,** *6* (6), 3458-66.

138. Maleki, A.; Lafitte, G.; Kjøniksen, A.-L.; Thuresson, K.; Nyström, B., Effect of pH on the association behavior in aqueous solutions of pig gastric mucin. *Carbohydr Res* **2008,** *343* (2), 328-340.

139. Thaplyal, P.; Bevilacqua, P. C., Experimental approaches for measuring pKa's in RNA and DNA. *Methods Enzymol* **2014,** *549*, 189-219.

140. Wenz, C.; Jeltsch, A.; Pingoud, A., Probing the Indirect Readout of the Restriction Enzyme EcoRV: MUTATIONAL ANALYSIS OF CONTACTS TO THE DNA BACKBONE (*). *J Biol Chem* **1996,** *271* (10), 5565-5573.

141. Corfield, A. P.; Wagner, S. A.; O'Donnell, L. J.; Durdey, P.; Mountford, R. A.; Clamp, J. R., The roles of enteric bacterial sialidase, sialate O-acetyl esterase and glycosulfatase in the degradation of human colonic mucin. *Glycoconj J* **1993,** *10* (1), 72-81.

142. Flynn, J. M.; Niccum, D.; Dunitz, J. M.; Hunter, R. C., Evidence and Role for Bacterial Mucin Degradation in Cystic Fibrosis Airway Disease. *PLoS Pathog* **2016,** *12* (8), e1005846.

143. Gubareva, L. V.; Kaiser, L.; Hayden, F. G., Influenza virus neuraminidase inhibitors. *Lancet* **2000,** *355* (9206), 827-35.

144. Cohen, M.; Zhang, X.-Q.; Senaati, H. P.; Chen, H.-W.; Varki, N. M.; Schooley, R. T.; Gagneux, P., Influenza A penetrates host mucus by cleaving sialic acids with neuraminidase. *Virol J* **2013,** *10* (1), 321.

145. Yang, X.; Steukers, L.; Forier, K.; Xiong, R.; Braeckmans, K.; Van Reeth, K.; Nauwynck, H., A beneficiary role for neuraminidase in influenza virus penetration through the respiratory mucus. *PLoS One* **2014,** *9* (10), e110026-e110026.

146. Tailford, L. E.; Crost, E. H.; Kavanaugh, D.; Juge, N., Mucin glycan foraging in the human gut microbiome. *Front Genet* **2015,** *6* (81).

147. Shon, D. J.; Kuo, A.; Ferracane, M. J.; Malaker, S. A., Classification, structural biology, and applications of mucin domain-targeting proteases. *Biochem J* **2021,** *478* (8), 1585-1603.

148. Praharaj, A. B.; Dehury, B.; Mahapatra, N.; Kar, S. K.; Behera, S. K., Molecular dynamics insights into the structure, function, and substrate binding mechanism of mucin desulfating sulfatase of gut microbe Bacteroides fragilis. *J Cell Biochem* **2018,** *119* (4), 3618-3631.

149. Luis, A. S.; Jin, C.; Pereira, G. V.; Glowacki, R. W. P.; Gugel, S.; Singh, S.; Byrne, D. P.; Pudlo, N.; London, J. A.; Baslé, A.; Reihill, M.; Oscarson, S.; Eyers, P. A.; Mirjam, C.; Michel, G.; Barbeyron, T.; Yates, E. A.; Hansson, G. C.; Karlsson, N. G.; Cartmell, A.; Martens, E. C., A single bacterial sulfatase is required for metabolism of colonic mucin O-glycans and intestinal colonization by a symbiotic human gut bacterium. *bioRxiv* **2020**, 2020.11.20.392076.

150. Rho, J. H.; Wright, D. P.; Christie, D. L.; Clinch, K.; Furneaux, R. H.; Roberton, A. M., A novel mechanism for desulfation of mucin: identification and cloning of a mucin-desulfating glycosidase (sulfoglycosidase) from Prevotella strain RS2. *J Bacteriol* **2005,** *187* (5), 1543-51.

151. Ma, J.; Rubin, B. K.; Voynow, J. A., Mucins, mucus, and goblet cells. *Chest* **2018,** *154* (1), 169-176.

152. Wagner, C. E.; Wheeler, K. M.; Ribbeck, K., Mucins and Their Role in Shaping the Functions of Mucus Barriers. *Annu Rev Cell Dev Biol* **2018,** *34* (1), 189-215.

153. Sheehan, J. K.; Thornton, D. J.; Somerville, M.; Carlstedt, I., The structure and heterogeneity of respiratory mucus glycoproteins. *Am Rev Respir Dis* **2012**.

154. Marczynski, M.; Winkeljann, B.; Lieleg, O., Advances in Mucin Biopolymer Research: Purification, Characterization, and Applications. In *Biopolymers for Biomedical and Biotechnological Applications*, 2021; pp 181-208.

155. Sweeney, M. P.; Bagg, J.; Baxter, W. P.; Aitchison, T. C., Clinical trial of a mucin-containing oral spray for treatment of xerostomia in hospice patients. *Palliat Med* **1997,** *11* (3), 225-232.

156. Vinke, J.; Kaper, H. J.; Vissink, A.; Sharma, P. K., Dry mouth: saliva substitutes which adsorb and modify existing salivary condition films improve oral lubrication. *Clin Oral Investig* **2020,** *24* (11), 4019-4030.

157. Sarkar, A.; Xu, F.; Lee, S., Human saliva and model saliva at bulk to adsorbed phases - similarities and differences. *Adv Colloid Interface Sci* **2019,** *273*, 102034.

158. Payment, S. A.; Liu, B.; Offner, G. D.; Oppenheim, F. G.; Troxler, R. F., Immunoquantification of Human Salivary Mucins MG1 and MG2 in Stimulated whole Saliva: Factors Influencing Mucin levels. *J Dent Res* **2000,** *79* (10), 1765-1772.

159. Chaudhury, N. M. A.; Shirlaw, P.; Pramanik, R.; Carpenter, G. H.; Proctor, G. B., Changes in Saliva Rheological Properties and Mucin Glycosylation in Dry Mouth. *J Dent Res* **2015,** *94* (12), 1660-1667.

160. Chan, S. M. T.; Neu, C. P.; DuRaine, G.; Komvopoulos, K.; Reddi, A. H., Tribological altruism: A sacrificial layer mechanism of synovial joint lubrication in articular cartilage. *J Biomech* **2012,** *45* (14), 2426-2431.

161. Winkeljann, B.; Bauer, M. G.; Marczynski, M.; Rauh, T.; Sieber, S. A.; Lieleg, O., Covalent Mucin Coatings Form Stable Anti-Biofouling Layers on a Broad Range of Medical Polymer Materials. *Adv Mater Interfaces* **2020,** *7* (4), 1902069.

162. Klein, J., Hydration lubrication. *Friction* **2013,** *1* (1), 1-23.

163. Sarkar, A.; Andablo-Reyes, E.; Bryant, M.; Dowson, D.; Neville, A., Lubrication of soft oral surfaces. *Curr Opin Colloid Interface Sci* **2019,** *39*, 61-75.

164. Crouzier, T.; Boettcher, K.; Geonnotti, A. R.; Kavanaugh, N. L.; Hirsch, J. B.; Ribbeck, K.; Lieleg, O., Modulating Mucin Hydration and Lubrication by Deglycosylation and Polyethylene Glycol Binding. *Adv Mater Interfaces* **2015,** *2* (18), 1500308.

165. Biegler, M.; Delius, J.; Käsdorf, B. T.; Hofmann, T.; Lieleg, O., Cationic astringents alter the tribological and rheological properties of human saliva and salivary mucin solutions. *Biotribology* **2016,** *6*, 12-20.

166. Ma, S.; Lee, H.; Liang, Y.; Zhou, F., Astringent Mouthfeel as a Consequence of Lubrication Failure. *Angew Chem Int Ed* **2016,** *55* (19), 5793-5797.

167. Rudge, R. E. D.; Fuhrmann, P. L.; Scheermeijer, R.; van der Zanden, E. M.; Dijksman, J. A.; Scholten, E., A tribological approach to astringency perception and astringency prevention. *Food Hydrocoll* **2021,** *121*, 106951.

168. Schömig, V.; Isik, E.; Martin, L.; Berensmeier, S., Solid liquid liquid extraction of porcine gastric mucins from homogenized animal material. *RSC Adv* **2017,** *7* (63), 39708-39717.

169. Tsui, S.; Tandy, J.; Myant, C.; Masen, M.; Cann, P. M., Friction measurements with yoghurt in a simulated tongue-palate contact. *Biotribology* **2016,** *8*, 1-11.

170. Boettcher, K.; Winkeljann, B.; Schmidt, T. A.; Lieleg, O., Quantification of cartilage wear morphologies in unidirectional sliding experiments: Influence of different macromolecular lubricants. *Biotribology* **2017,** *12*, 43-51.

171. Larhed, A. W.; Artursson, P.; Gråsjö, J.; Björk, E., Diffusion of drugs in native and purified gastrointestinal mucus. *J Pharm Sci* **1997,** *86* (6), 660-5.

172. Lee, S.; Müller, M.; Rezwan, K.; Spencer, N. D., Porcine Gastric Mucin (PGM) at the Water/Poly(Dimethylsiloxane) (PDMS) Interface: Influence of pH and Ionic Strength on Its Conformation, Adsorption, and Aqueous Lubrication Properties. *Langmuir* **2005,** *21* (18), 8344-8353.

173. Joyner, K.; Song, D.; Hawkins, R. F.; Silcott, R. D.; Duncan, G. A., A rational approach to form disulfide linked mucin hydrogels. *Soft Matter* **2019,** *15* (47), 9632-9639.

174. Witten, J.; Samad, T.; Ribbeck, K., Molecular characterization of mucus binding. *Biomacromolecules* **2019,** *20* (4), 1505-1513.

175. Sohna Sohna, J. E.; Cooper, M. A., Does the Sauerbrey equation hold true for binding of peptides and globular proteins to a QCM?: A systematic study of mass dependence of peptide and protein binding with a piezoelectric sensor. *Sens Bio-Sens Res* **2016,** *11*, 71-77.

176. Marczynski, M.; Jiang, K.; Blakeley, M.; Srivastava, V.; Vilaplana, F.; Crouzier, T.; Lieleg, O., Structural Alterations of Mucins Are Associated with Losses in Functionality. *Biomacromolecules* **2021,** *22* (4), 1600-1613.

177. McDermott, A. M., Antimicrobial compounds in tears. *Exp Eye Res* **2013,** *117*, 53-61.

178. Mall, A. S.; Habte, H.; Mthembu, Y.; Peacocke, J.; de Beer, C., Mucus and Mucins: do they have a role in the inhibition of the human immunodeficiency virus? *Virol J* **2017,** *14* (1), 192.

179. Jumel, K.; Fiebrig, I.; Harding, S. E., Rapid size distribution and purity analysis of gastric mucus glycoproteins by size exclusion chromatography/multi angle laser light scattering. *Int J Biol Macromol* **1996,** *18* (1-2), 133-9.

180. Gillis, R. B.; Adams, G. G.; Wolf, B.; Berry, M.; Besong, T. M.; Corfield, A.; Kök, S. M.; Sidebottom, R.; Lafond, D.; Rowe, A. J.; Harding, S. E., Molecular weight distribution analysis by ultracentrifugation: adaptation of a new approach for mucins. *Carbohydr Polym* **2013,** *93* (1), 178-83.

181. Almutairi, F. M.; Cifre, J. G.; Adams, G. G.; Kök, M. S.; Mackie, A. R.; de la Torre, J. G.; Harding, S. E., Application of recent advances in hydrodynamic methods for characterising mucins in solution. *Eur Biophys J* **2016,** *45* (1), 45-54.

182. Swaminathan, C. P.; Surolia, N.; Surolia, A., Role of Water in the Specific Binding of Mannose and Mannooligosaccharides to Concanavalin A. *J Am Chem Soc* **1998,** *120* (21), 5153-5159.

183. Nikogeorgos, N.; Patil, N. J.; Zappone, B.; Lee, S., Interaction of porcine gastric mucin with various polycations and its influence on the boundary lubrication properties. *Polymer* **2016,** *100*, 158-168.

184. Ahmad, M.; Ritzoulis, C.; Chen, J.; Meigui, H.; Bushra, R.; Jin, Y.; Xiao, H., Xanthan gum − mucin complexation: Molecular interactions, thermodynamics, and rheological analysis. *Food Hydrocoll* **2021,** *114*, 106579.

185. Luka, B.; Arbter, V.; Sander, K.; Duerrschnabel, A.; Schlueter, N., Impact of mucin on the anti-erosive/anti-abrasive efficacy of chitosan and/or F/Sn in enamel in vitro. *Sci Rep* **2021,** *11* (1), 5285.

186. Olăreţ, E.; Bălănucă, B.; Onaş, A. M.; Ghiţman, J.; Iovu, H.; Stancu, I.-C.; Serafim, A., Double-Cross-Linked Networks Based on Methacryloyl Mucin. *Polymers* **2021,** *13* (11), 1706.

187. Lai, S. K.; Wang, Y. Y.; Wirtz, D.; Hanes, J., Micro- and macrorheology of mucus. *Adv Drug Deliv Rev* **2009,** *61* (2), 86-100.

188. Sellers, L. A.; Allen, A.; Morris, E. R.; Ross-Murphy, S. B., Mucus glycoprotein gels. Role of glycoprotein polymeric structure and carbohydrate side-chains in gel-formation. *Carbohydr Res* **1988,** *178* (1), 93-110.

189. Wagner, C. E.; Turner, B. S.; Rubinstein, M.; McKinley, G. H.; Ribbeck, K., A Rheological Study of the Association and Dynamics of MUC5AC Gels. *Biomacromolecules* **2017,** *18* (11), 3654-3664.

190. Meldrum, O. W.; Yakubov, G. E.; Bonilla, M. R.; Deshmukh, O.; McGuckin, M. A.; Gidley, M. J., Mucin gel assembly is controlled by a collective action of non-mucin proteins, disulfide bridges, Ca2+-mediated links, and hydrogen bonding. *Sci Rep* **2018,** *8* (1), 5802.

191. Curnutt, A.; Smith, K.; Darrow, E.; Walters, K. B., Chemical and Microstructural Characterization of pH and [Ca2+] Dependent Sol-Gel Transitions in Mucin Biopolymer. *Sci Rep* **2020,** *10* (1), 8760.

192. Madsen, F.; Eberth, K.; Smart, J. D., A rheological examination of the mucoadhesive/mucus interaction: the effect of mucoadhesive type and concentration. *J Control Release* **1998,** *50* (1), 167-178.

193. Hoffmann, W., TFF2, a MUC6-binding lectin stabilizing the gastric mucus barrier and more (Review). *Int J Oncol* **2015,** *47* (3), 806-16.

194. Bastholm, S. K.; Samson, M. H.; Becher, N.; Hansen, L. K.; Stubbe, P. R.; Chronakis, I. S.; Nexo, E.; Uldbjerg, N., Trefoil factor peptide 3 is positively correlated with the viscoelastic properties of the cervical mucus plug. *Acta Obstet Gynecol Scand* **2017,** *96* (1), 47-52.

195. Grande, G.; Milardi, D.; Vincenzoni, F.; Pompa, G.; Biscione, A.; Astorri, A. L.; Fruscella, E.; De Luca, A.; Messana, I.; Castagnola, M.; Marana, R., Proteomic characterization of the qualitative and quantitative differences in cervical mucus composition during the menstrual cycle. *Mol Biosyst* **2015,** *11* (6), 1717-1725.

196. Hill, D. B.; Long, R. F.; Kissner, W. J.; Atieh, E.; Garbarine, Ian C.; Markovetz, M. R.; Fontana, N. C.; Christy, M.; Habibpour, M.; Tarran, R.; Forest, M. G.; Boucher, R. C.; Button, B., Pathological mucus and impaired mucus clearance in cystic fibrosis patients result from increased concentration, not altered pH. *Eur Respir J* **2018,** *52* (6), 1801297.

197. Henderson, A. G.; Ehre, C.; Button, B.; Abdullah, L. H.; Cai, L. H.; Leigh, M. W.; DeMaria, G. C.; Matsui, H.; Donaldson, S. H.; Davis, C. W.; Sheehan, J. K.; Boucher, R. C.; Kesimer, M., Cystic fibrosis airway secretions exhibit mucin hyperconcentration and increased osmotic pressure. *J Clin Invest* **2014,** *124* (7), 3047-60.

198. Hill, D. B.; Vasquez, P. A.; Mellnik, J.; McKinley, S. A.; Vose, A.; Mu, F.; Henderson, A. G.; Donaldson, S. H.; Alexis, N. E.; Boucher, R. C.; Forest, M. G., A Biophysical Basis for Mucus Solids Concentration as a Candidate Biomarker for Airways Disease. *PLoS One* **2014,** *9* (2), e87681.

199. Celli, J.; Gregor, B.; Turner, B.; Afdhal, N. H.; Bansil, R.; Erramilli, S., Viscoelastic properties and dynamics of porcine gastric mucin. *Biomacromolecules* **2005,** *6* (3), 1329-33.

200. Bhaskar, K. R.; Gong, D. H.; Bansil, R.; Pajevic, S.; Hamilton, J. A.; Turner, B. S.; LaMont, J. T., Profound increase in viscosity and aggregation of pig gastric mucin at low pH. *Am J Physiol* **1991,** *261* (5 Pt 1), G827-32.

201. Wang, Y.-Y.; Lai, S. K.; Ensign, L. M.; Zhong, W.; Cone, R.; Hanes, J., The microstructure and bulk rheology of human cervicovaginal mucus are remarkably resistant to changes in pH. *Biomacromolecules* **2013,** *14* (12), 4429-4435.

202. Vukosavljevic, B.; Murgia, X.; Schwarzkopf, K.; Schaefer, U. F.; Lehr, C. M.; Windbergs, M., Tracing molecular and structural changes upon mucolysis with N-acetyl cysteine in human airway mucus. *Int J Pharm* **2017,** *533* (2), 373-376.

203. Yuan, S.; Hollinger, M.; Lachowicz-Scroggins, M. E.; Kerr, S. C.; Dunican, E. M.; Daniel, B. M.; Ghosh, S.; Erzurum, S. C.; Willard, B.; Hazen, S. L.; Huang, X.; Carrington, S. D.; Oscarson, S.; Fahy, J. V., Oxidation increases mucin polymer cross-links to stiffen airway mucus gels. *Sci Transl Med* **2015,** *7* (276), 276ra27-276ra27.

204. Fahrbach, K. M.; Malykhina, O.; Stieh, D. J.; Hope, T. J., Differential Binding of IgG and IgA to Mucus of the Female Reproductive Tract. *PLoS One* **2013,** *8* (10), e76176.

205. Wang, Y.-Y.; Harit, D.; Subramani, D. B.; Arora, H.; Kumar, P. A.; Lai, S. K., Influenza-binding antibodies immobilise influenza viruses in fresh human airway mucus. *Eur Respir J* **2017,** *49* (1), 1601709.

206. Schroeder, H. A.; Newby, J.; Schaefer, A.; Subramani, B.; Tubbs, A.; Gregory Forest, M.; Miao, E.; Lai, S. K., LPS-binding IgG arrests actively motile Salmonella Typhimurium in gastrointestinal mucus. *Mucosal Immunol* **2020,** *13* (5), 814-823.

207. Tran, D. T.; Ten Hagen, K. G., Mucin-type O-glycosylation during development. *J Biol Chem* **2013,** *288* (10), 6921-6929.

208. Reily, C.; Stewart, T. J.; Renfrow, M. B.; Novak, J., Glycosylation in health and disease. *Nat Rev Nephrol* **2019,** *15* (6), 346-366.

209. Jordan, N.; Newton, J.; Pearson, J.; Allen, A., A novel method for the visualization of the in situ mucus layer in rat and man. *Clin Sci* **1998,** *95* (1), 97-106.

210. Lewis, O. L.; Keener, J. P.; Fogelson, A. L., A physics-based model for maintenance of the pH gradient in the gastric mucus layer. *Am J Physiol Gastrointest Liver Physiol* **2017,** *313* (6), G599-g612.

211. Ogata, S.; Uehara, H.; Chen, A.; Itzkowitz, S. H., Mucin gene expression in colonic tissues and cell lines. *Cancer Res* **1992,** *52* (21), 5971-8.

212. Atuma, C.; Strugala, V.; Allen, A.; Holm, L., The adherent gastrointestinal mucus gel layer: thickness and physical state in vivo. *Am J Physiol Gastrointest Liver Physiol* **2001,** *280* (5), G922-9.

213. Strugala, V.; Allen, A.; Dettmar, P. W.; Pearson, J. P., Colonic mucin: methods of measuring mucus thickness. *Proc Nutr Soc* **2003,** *62* (1), 237-43.

214. Lehr, C.-M.; Poelma, F. G. J.; Junginger, H. E.; Tukker, J. J., An estimate of turnover time of intestinal mucus gel layer in the rat in situ loop. *Int J Pharm* **1991,** *70* (3), 235-240.

215. Quintana-Hayashi, M. P.; Padra, M.; Padra, J. T.; Benktander, J.; Lindén, S. K., Mucus-Pathogen Interactions in the Gastrointestinal Tract of Farmed Animals. *Microorganisms* **2018,** *6* (2), 55.

216. Cu, Y.; Saltzman, W. M., Drug delivery: Stealth particles give mucus the slip. *Nat Mater* **2009,** *8* (1), 11-3.

217. Suk, J. S.; Lai, S. K.; Boylan, N. J.; Dawson, M. R.; Boyle, M. P.; Hanes, J., Rapid transport of muco-inert nanoparticles in cystic fibrosis sputum treated with N-acetyl cysteine. *Nanomedicine* **2011,** *6* (2), 365-75.

218. Chai, G.; Hassan, A.; Meng, T.; Lou, L.; Ma, J.; Simmers, R.; Zhou, L.; Rubin, B. K.; Zhou, Q.; Longest, P. W.; Hindle, M.; Xu, Q., Dry powder aerosol containing muco-inert particles for excipient enhanced growth pulmonary drug delivery. *Nanomed Nanotechnol Biol Med* **2020,** *29*, 102262.

219. Crater, J. S.; Carrier, R. L., Barrier properties of gastrointestinal mucus to nanoparticle transport. *Macromol Biosci* **2010,** *10* (12), 1473-83.

220. Ensign, L. M.; Henning, A.; Schneider, C. S.; Maisel, K.; Wang, Y. Y.; Porosoff, M. D.; Cone, R.; Hanes, J., Ex vivo characterization of particle transport in mucus secretions coating freshly excised mucosal tissues. *Mol Pharm* **2013,** *10* (6), 2176-82.

221. Georgiades, P.; Pudney, P. D.; Thornton, D. J.; Waigh, T. A., Particle tracking microrheology of purified gastrointestinal mucins. *Biopolymers* **2014,** *101* (4), 366-77.

222. Murgia, X.; Pawelzyk, P.; Schaefer, U. F.; Wagner, C.; Willenbacher, N.; Lehr, C.-M., Size-Limited Penetration of Nanoparticles into Porcine Respiratory Mucus after Aerosol Deposition. *Biomacromolecules* **2016,** *17* (4), 1536-1542.

223. Merrill, E. W.; Dennison, K. A.; Sung, C., Partitioning and diffusion of solutes in hydrogels of poly(ethylene oxide). *Biomaterials* **1993,** *14* (15), 1117-26.

224. Arends, F.; Sellner, S.; Seifert, P.; Gerland, U.; Rehberg, M.; Lieleg, O., A microfluidics approach to study the accumulation of molecules at basal lamina interfaces. *Lab Chip* **2015,** *15* (16), 3326-3334.

225. Lieleg, O.; Ribbeck, K., Biological hydrogels as selective diffusion barriers. *Trends Cell Biol* **2011,** *21* (9), 543-551.

226. Armstrong, J. K.; Wenby, R. B.; Meiselman, H. J.; Fisher, T. C., The hydrodynamic radii of macromolecules and their effect on red blood cell aggregation. *Biophys J* **2004,** *87* (6), 4259-4270.

227. De Jong, W. H.; Borm, P. J., Drug delivery and nanoparticles:applications and hazards. *Int J Nanomedicine* **2008,** *3* (2), 133-49.

228. Wilczewska, A. Z.; Niemirowicz, K.; Markiewicz, K. H.; Car, H., Nanoparticles as drug delivery systems. *Pharmacol Rep* **2012,** *64* (5), 1020-37.

229. Saputra, D.; Yoon, J.-H.; Park, H.; Heo, Y.; Yang, H.; Lee, E. J.; Lee, S.; Song, C.-W.; Lee, K., Inhalation of carbon black nanoparticles aggravates pulmonary inflammation in mice. *Toxicol Res* **2014,** *30* (2), 83-90.

230. Sahu, S.; Tiwari, M.; Bhangare, R.; Pandit, G., Particle size distribution of mainstream and exhaled cigarette smoke and predictive deposition in human respiratory tract. *Aerosol Air Qual Res* **2013,** *13* (1), 324-332.

231. Polymeropoulos, M. H.; Lavedan, C.; Leroy, E.; Ide, S. E.; Dehejia, A.; Dutra, A.; Pike, B.; Root, H.; Rubenstein, J.; Boyer, R.; Stenroos, E. S.; Chandrasekharappa, S.; Athanassiadou, A.; Papapetropoulos, T.; Johnson, W. G.; Lazzarini, A. M.; Duvoisin, R. C.; Di Iorio, G.; Golbe, L. I.; Nussbaum, R. L., Mutation in the alpha-synuclein gene identified in families with Parkinson's disease. *Science* **1997,** *276* (5321), 2045-7.

232. Spillantini, M. G.; Schmidt, M. L.; Lee, V. M. Y.; Trojanowski, J. Q.; Jakes, R.; Goedert, M., α-Synuclein in Lewy bodies. *Nature* **1997,** *388* (6645), 839-840.

233. Braak, H.; Rüb, U.; Gai, W. P.; Del Tredici, K., Idiopathic Parkinson's disease: possible routes by which vulnerable neuronal types may be subject to neuroinvasion by an unknown pathogen. *J Neural Transm* **2003,** *110* (5), 517-36.

234. Borghammer, P., How does parkinson's disease begin? Perspectives on neuroanatomical pathways, prions, and histology. *Mov Disord* **2018,** *33* (1), 48-57.

235. Natale, G.; Pasquali, L.; Ruggieri, S.; Paparelli, A.; Fornai, F., Parkinson's disease and the gut: a well known clinical association in need of an effective cure and explanation. *Neurogastroenterol Motil* **2008,** *20* (7), 741-9.

236. Bohórquez, D. V.; Shahid, R. A.; Erdmann, A.; Kreger, A. M.; Wang, Y.; Calakos, N.; Wang, F.; Liddle, R. A., Neuroepithelial circuit formed by innervation of sensory enteroendocrine cells. *J Clin Invest* **2015,** *125* (2), 782-6.

237. Olanow, C. W.; Prusiner, S. B., Is Parkinson's disease a prion disorder? *Proc Natl Acad Sci USA* **2009,** *106* (31), 12571-2.

238. Chandra, R.; Hiniker, A.; Kuo, Y. M.; Nussbaum, R. L.; Liddle, R. A., α-Synuclein in gut endocrine cells and its implications for Parkinson's disease. *JCI Insight* **2017,** *2* (12).

239. Kim, S.; Kwon, S. H.; Kam, T. I.; Panicker, N.; Karuppagounder, S. S.; Lee, S.; Lee, J. H.; Kim, W. R.; Kook, M.; Foss, C. A.; Shen, C.; Lee, H.; Kulkarni, S.; Pasricha, P. J.; Lee, G.; Pomper, M. G.; Dawson, V. L.; Dawson, T. M.; Ko, H. S., Transneuronal Propagation of Pathologic α-Synuclein from the Gut to the Brain Models Parkinson's Disease. *Neuron* **2019,** *103* (4), 627-641.e7.

240. Killinger, B. A.; Labrie, V., Vertebrate food products as a potential source of prion-like α-synuclein. *npj Parkinson's Dis* **2017,** *3* (1), 33.

241. Buisine, M. P.; Desreumaux, P.; Leteurtre, E.; Copin, M. C.; Colombel, J. F.; Porchet, N.; Aubert, J. P., Mucin gene expression in intestinal epithelial cells in Crohn's disease. *Gut* **2001,** *49* (4), 544-51.

242. Strugala, V.; Dettmar, P. W.; Pearson, J. P., Thickness and continuity of the adherent colonic mucus barrier in active and quiescent ulcerative colitis and Crohn's disease. *Int J Clin Pract* **2008,** *62* (5), 762-9.

243. Petersson, J.; Schreiber, O.; Hansson, G. C.; Gendler, S. J.; Velcich, A.; Lundberg, J. O.; Roos, S.; Holm, L.; Phillipson, M., Importance and regulation of the colonic mucus barrier in a mouse model of colitis. *Am J Physiol Gastrointest Liver Physiol* **2010,** *300* (2), G327-G333.

244. Lee, B.; Litt, M.; Buchsbaum, G., Rheology of the vitreous body: part 3. Concentration of electrolytes, collagen and hyaluronic acid. *Biorheology* **1994,** *31* (4), 339-51.

245. Donlan, R. M., Biofilms: microbial life on surfaces. *Emerg Infect Dis* **2002,** *8* (9), 881-90.

246. Sophia Fox, A. J.; Bedi, A.; Rodeo, S. A., The basic science of articular cartilage: structure, composition, and function. *Sports Health* **2009,** *1* (6), 461-468.

247. Salbreux, G.; Charras, G.; Paluch, E., Actin cortex mechanics and cellular morphogenesis. *Trends Cell Biol* **2012,** *22* (10), 536-45.

248. Lieleg, O.; Claessens, M. M. A. E.; Bausch, A. R., Structure and dynamics of cross-linked actin networks. *Soft Matter* **2010,** *6* (2), 218-225.

249. Heinemann, F.; Vogel, Sven K.; Schwille, P., Lateral Membrane Diffusion Modulated by a Minimal Actin Cortex. *Biophysical Journal* **2013,** *104* (7), 1465-1475.

250. Abu Shah, E.; Keren, K., Symmetry breaking in reconstituted actin cortices. *Elife* **2014,** *3*, e01433-e01433.

251. Tibbitt, M. W.; Anseth, K. S., Hydrogels as extracellular matrix mimics for 3D cell culture. *Biotechnol Bioeng* **2009,** *103* (4), 655-663.

252. Nicolas, J.; Magli, S.; Rabbachin, L.; Sampaolesi, S.; Nicotra, F.; Russo, L., 3D Extracellular Matrix Mimics: Fundamental Concepts and Role of Materials Chemistry to Influence Stem Cell Fate. *Biomacromolecules* **2020,** *21* (6), 1968-1994.

253. Bansil, R.; Turner, B. S., The biology of mucus: Composition, synthesis and organization. *Advanced Drug Delivery Reviews* **2018,** *124*, 3-15.

254. Smart, P.; Neville, A.; Bryant, M., Tribocorrosion of dental tissues: The role of mucin. *Tribol Int* **2020,** *148*, 106337.

255. Shogren, R.; Gerken, T. A.; Jentoft, N., Role of glycosylation on the conformation and chain dimensions of O-linked glycoproteins: light-scattering studies of ovine submaxillary mucin. *Biochemistry* **1989,** *28* (13), 5525-5536.

256. Wang, B. X.; Wheeler, K. M.; Cady, K. C.; Lehoux, S.; Cummings, R. D.; Laub, M. T.; Ribbeck, K., Mucin Glycans Signal through the Sensor Kinase RetS to Inhibit Virulence-Associated Traits in Pseudomonas aeruginosa. *Curr Biol* **2021,** *31* (1), 90-102.e7.

257. Kim, H. J.; Boedicker, J. Q.; Choi, J. W.; Ismagilov, R. F., Defined spatial structure stabilizes a synthetic multispecies bacterial community. *Proc Natl Acad Sci USA* **2008,** *105* (47), 18188-93.

258. Lu, H.-P.; Lai, Y.-C.; Huang, S.-W.; Chen, H.-C.; Hsieh, C.-h.; Yu, H.-T., Spatial heterogeneity of gut microbiota reveals multiple bacterial communities with distinct characteristics. *Sci Rep* **2014,** *4* (1), 6185.

259. Eraga, S. O.; Arhewoh, M. I.; Iwuagwu, M. A.; Ukponahiusi, O. E., Formulation and in vitro release studies of pegylated mucin based matrix tablets. *Pak J Pharm Sci* **2015,** *28* (1), 113-8.

260. Ofokansi, K. C.; Adikwu, M. U.; Okore, V. C., Preparation and evaluation of mucin-gelatin mucoadhesive microspheres for rectal delivery of ceftriaxone sodium. *Drug Dev Ind Pharm* **2007,** *33* (6), 691-700.

261. Laurén, P.; Paukkonen, H.; Lipiäinen, T.; Dong, Y.; Oksanen, T.; Räikkönen, H.; Ehlers, H.; Laaksonen, P.; Yliperttula, M.; Laaksonen, T., Pectin and Mucin Enhance the Bioadhesion of Drug Loaded Nanofibrillated Cellulose Films. *Pharm Res* **2018,** *35* (7), 145.

262. Mumuni, M. A.; Kenechukwu, F. C.; Ofokansi, K. C.; Attama, A. A.; Díaz, D. D., Insulin-loaded mucoadhesive nanoparticles based on mucin-chitosan complexes for oral delivery and diabetes treatment. *Carbohydr Polym* **2020,** *229*, 115506.

263. Nowald, C.; Penk, A.; Chiu, H.-Y.; Bein, T.; Huster, D.; Lieleg, O., A Selective Mucin/Methylcellulose Hybrid Gel with Tailored Mechanical Properties. *Macromol Biosci* **2016,** *16* (4), 567-579.

264. Kimna, C.; Lieleg, O., Engineering an orchestrated release avalanche from hydrogels using DNA-nanotechnology. *J Control Release* **2019,** *304*, 19-28.

265. Kimna, C.; Winkeljann, B.; Song, J.; Lieleg, O., Smart Biopolymer-Based Multi-Layers Enable Consecutive Drug Release Events on Demand. *Adv Mater Interfaces* **2020,** *7* (19), 2000735.

266. Rolando, M.; Refojo, M. F.; Kenyon, K. R., Increased tear evaporation in eyes with keratoconjunctivitis sicca. *Arch Ophthalmol* **1983,** *101* (4), 557-8.

267. Kwan, C.-S.; Cerullo, A. R.; Braunschweig, A. B., Design and Synthesis of Mucin-Inspired Glycopolymers. *ChemPlusChem* **2020,** *85* (12), 2704-2721.

268. Canton, I.; Warren, N. J.; Chahal, A.; Amps, K.; Wood, A.; Weightman, R.; Wang, E.; Moore, H.; Armes, S. P., Mucin-Inspired Thermoresponsive Synthetic Hydrogels Induce Stasis in Human Pluripotent Stem Cells and Human Embryos. *ACS Cent Sci* **2016,** *2* (2), 65-74.

269. Wallert, M.; Nie, C.; Anilkumar, P.; Abbina, S.; Bhatia, S.; Ludwig, K.; Kizhakkedathu, J. N.; Haag, R.; Block, S., Mucin-Inspired, High Molecular Weight Virus Binding Inhibitors Show Biphasic Binding Behavior to Influenza A Viruses. *Small* **2020,** *16* (47), 2004635.

270. Kruger, A. G.; Brucks, S. D.; Yan, T.; Cárcarmo-Oyarce, G.; Wei, Y.; Wen, D. H.; Carvalho, D. R.; Hore, M. J. A.; Ribbeck, K.; Schrock, R. R.; Kiessling, L. L., Stereochemical Control Yields Mucin Mimetic Polymers. *ACS Cent Sci* **2021,** *7* (4), 624-630.

271. Sharma, A.; Thongrom, B.; Bhatia, S.; von Lospichl, B.; Addante, A.; Graeber, S. Y.; Lauster, D.; Mall, M. A.; Gradzielski, M.; Haag, R., Polyglycerol-Based Mucus-Inspired Hydrogels. *Macromol Rapid Commun* **2021,** *n/a* (n/a), 2100303.

272. Srivastava, V.; Rezinciuc, S.; Bulone, V., Quantitative Proteomic Analysis of Four Developmental Stages of Saprolegnia parasitica. *Front Microbiol* **2018,** *8* (2658).

273. Rousseau, K.; Kirkham, S.; McKane, S.; Newton, R.; Clegg, P.; Thornton, D. J., Muc5b and Muc5ac are the major oligomeric mucins in equine airway mucus. *Am J Physiol Lung Cell Mol Physiol* **2007,** *292* (6), L1396-404.

274. Harding, S. E.; Gillis, R. B.; Almutairi, F.; Erten, T.; Kök, M. Ş.; Adams, G. G., Recent Advances in the Analysis of Macromolecular Interactions Using the Matrix-Free Method of Sedimentation in the Analytical Ultracentrifuge. *Biology* **2015,** *4* (1).

275. Montagne, L.; Piel, C.; Lallès, J. P., Effect of diet on mucin kinetics and composition: nutrition and health implications. *Nutr Rev* **2004,** *62* (3), 105-14.

276. De Gennes, P.-G.; Gennes, P.-G., *Scaling concepts in polymer physics*. Cornell University Press: 1979.

277. Sidhu, A.; Segers-Nolten, I.; Subramaniam, V., Solution conditions define morphological homogeneity of α-synuclein fibrils. *Biochim Biophys Acta Proteins Proteom* **2014,** *1844* (12), 2127-2134.

278. Voinova, M. V.; Rodahl, M.; Jonson, M.; Kasemo, B., Viscoelastic acoustic response of layered polymer films at fluid-solid interfaces: continuum mechanics approach. *Phys Scr* **1999,** *59* (5), 391.

279. Stenberg, E.; Persson, B.; Roos, H.; Urbaniczky, C., Quantitative determination of surface concentration of protein with surface plasmon resonance using radiolabeled proteins. *J Colloid Interface Sci* **1991,** *143* (2), 513-526.

280. Patching, S. G., Surface plasmon resonance spectroscopy for characterisation of membrane protein–ligand interactions and its potential for drug discovery. *Biochim Biophys Acta Biomembr* **2014,** *1838* (1), 43-55.

281. Kim, J.; Chaudhury, M. K.; Owen, M. J., Hydrophobic Recovery of Polydimethylsiloxane Elastomer Exposed to Partial Electrical Discharge. *J Colloid Interface Sci* **2000,** *226* (2), 231-236.

282. Engel, A.; Schoenenberger, C. A.; Müller, D. J., High resolution imaging of native biological sample surfaces using scanning probe microscopy. *Curr Opin Struct Biol* **1997,** *7* (2), 279-84.

283. Olmsted, S. S.; Padgett, J. L.; Yudin, A. I.; Whaley, K. J.; Moench, T. R.; Cone, R. A., Diffusion of macromolecules and virus-like particles in human cervical mucus. *Biophys J* **2001,** *81* (4), 1930-7.

284. Henry, C. E.; Wang, Y.-Y.; Yang, Q.; Hoang, T.; Chattopadhyay, S.; Hoen, T.; Ensign, L. M.; Nunn, K. L.; Schroeder, H.; McCallen, J.; Moench, T.; Cone, R.; Roffler, S. R.; Lai, S. K., Anti-PEG antibodies alter the mobility and biodistribution of densely PEGylated nanoparticles in mucus. *Acta Biomater* **2016,** *43*, 61-70.

285. Meier, C.; Grill, M. J.; Wall, W. A.; Popp, A., Geometrically exact beam elements and smooth contact schemes for the modeling of fiber-based materials and structures. *Int J Solids Struct* **2018,** *154*, 124-146.

286. Cyron, C.; Wall, W., Numerical method for the simulation of the Brownian dynamics of rod-like microstructures with three-dimensional nonlinear beam elements. *Int J Numer Methods Eng* **2012,** *90* (8), 955-987.

287. Grill, M. J.; Wall, W. A.; Meier, C., A computational model for molecular interactions between curved slender fibers undergoing large 3D deformations with a focus on electrostatic, van der Waals, and repulsive steric forces. *Int J Numer Methods Eng* **2020,** *121* (10), 2285-2330.

288. Meier, C.; Popp, A.; Wall, W. A., A finite element approach for the line-to-line contact interaction of thin beams with arbitrary orientation. *Comput Methods Appl Mech Eng* **2016,** *308*, 377-413.

289. Grill, M. J.; Meier, C.; Wall, W. A., Investigation of the peeling and pull-off behavior of adhesive elastic fibers via a novel computational beam interaction model. *J Adhes* **2021,** *97* (8), 730-759.

290. Ainavarapu, S. R.; Brujic, J.; Huang, H. H.; Wiita, A. P.; Lu, H.; Li, L.; Walther, K. A.; Carrion-Vazquez, M.; Li, H.; Fernandez, J. M., Contour length and refolding rate of a small protein controlled by engineered disulfide bonds. *Biophys J* **2007,** *92* (1), 225-33.

291. Stirnemann, G.; Giganti, D.; Fernandez, J. M.; Berne, B. J., Elasticity, structure, and relaxation of extended proteins under force. *Proc Natl Acad Sci USA* **2013,** *110* (10), 3847-3852.

292. Gum, J. R.; Hicks, J. W.; Toribara, N. W.; Rothe, E. M.; Lagace, R. E.; Kim, Y. S., The human MUC2 intestinal mucin has cysteine-rich subdomains located both upstream and downstream of its central repetitive region. *J Biol Chem* **1992,** *267* (30), 21375-21383.

293. Peppas, N. A.; Hansen, P. J.; Buri, P. A., A theory of molecular diffusion in the intestinal mucus. *Int J Pharm* **1984,** *20* (1), 107-118.

Author contributions

This thesis follows a total number of 5 research articles, 2 review articles, 1 book chapter and 1 European patent application to which I contributed during my time as doctoral candidate. Those publications, which built the fundament of the individual chapters, are indicated at the beginning of every sub-chapter in a footnote. My individual contribution to these publications is listed below:

1) **Marczynski, M.**; Käsdorf, B. T.; Altaner, B.; Wenzler, A.; Gerland, U.; Lieleg, O., Transient binding promotes molecule penetration into mucin hydrogels by enhancing molecular partitioning. *Biomaterials Science* **2018**, *6* (12), 3373-3387.

   Individual contribution: I contributed to the conception of this study, the design and performance of the experiments, the data analysis, and writing of the manuscript.

2) **Marczynski, M.**; Rickert, C. A.; Semerdzhiev, S.; van Dijk, W.; Segers-Nolten, I.; Claessens, M. M. A. E.; Lieleg, O., α-Synuclein penetrates mucin hydrogels despite its mucoadhesive properties. *Biomacromolecules* **2019**, *20* (12), 4332-4344.

   Individual contribution: I contributed to the conception of this study, the design and performance of the experiments, the data analysis, and writing of the manuscript.

3) **Marczynski, M.**; Balzer, B. N.; Jiang, K.; Lutz, T. M.; Crouzier, T.; Lieleg, O., Charged glycan residues critically contribute to the adsorption and lubricity of mucins. *Colloids and Surfaces B: Biointerfaces* **2020**, *187*, 110614.

   Individual contribution: I contributed to the conception of this study, the design and performance of the experiments, the data analysis, and writing of the manuscript.

4) Lutz, T. M.; **Marczynski, M.**; Grill, M.; Wall, W. A.; Lieleg, O., Repulsive backbone-backbone interactions modulate access to specific and unspecific binding sites on surface-bound mucins. *Langmuir* **2020**, *36* (43), 12973-12982.

   Individual contribution: I contributed to the conception of this study, the design and performance of the experiments, the data analysis, and writing of the manuscript.

5) **Marczynski, M.**; Jiang, K.; Blakeley, M.; Srivastava, V.; Vilaplana, F.; Crouzier, T.; Lieleg, O., Structural alterations of mucins are associated with losses in functionality. *Biomacromolecules* **2021**, *22* (4), 1600-1613.

Individual contribution: I contributed to the conception of this study, the design and performance of the experiments, the data analysis, and writing of the manuscript.

6) **Marczynski, M.**; Kimna, C.; Lieleg, O., Purified mucins in drug delivery research. *Advanced Drug Delivery Reviews* **2021**, *in press*.

Individual contribution: I contributed to the conception, the literature review and writing of the manuscript.

7) **Marczynski, M.**; Lieleg, O., Forgotten but not gone: particulate matter as contaminations of mucosal systems. *Biophysics Reviews* **2021**, *2* (3), 031302.

Individual contribution: I contributed to the conception, the literature review and writing of the manuscript.

8) **Marczynski, M.**; Winkeljann, B.; Lieleg, O., Advances in mucin biopolymer research: purification, characterization, and applications. *In: Biopolymers for Biomedical and Biotechnological Applications*, edited by Bernd Rehm & M. Fata Moradali. **2021**, 181-208.

Individual contribution: I contributed to the conception, the literature review and writing of the book chapter.

9) Lieleg, O.; **Marczynski, M.**; Weber-Hohengrund, M.; Winkeljann, B., Method of isolating mucin from mucin containing tissue. *European patent application EP3792275A1,* **2021**.

Individual contribution: I contributed to the conception of this invention, performance of experiments, data analysis, and writing of the text.

Full list of publications

Journal articles (peer-reviewed)

1) **Marczynski, M.**; Käsdorf, B. T.; Altaner, B.; Wenzler, A.; Gerland, U.; Lieleg, O., Transient binding promotes molecule penetration into mucin hydrogels by enhancing molecular partitioning. *Biomaterials Science* **2018**, *6* (12), 3373-3387.

2) **Marczynski, M.**; Rickert, C. A.; Semerdzhiev, S.; van Dijk, W.; Segers-Nolten, I.; Claessens, M. M. A. E.; Lieleg, O., α-Synuclein penetrates mucin hydrogels despite its mucoadhesive properties. *Biomacromolecules* **2019**, *20* (12), 4332-4344.

3) **Marczynski, M.**; Balzer, B. N.; Jiang, K.; Lutz, T. M.; Crouzier, T.; Lieleg, O., Charged glycan residues critically contribute to the adsorption and lubricity of mucins. *Colloids and Surfaces B: Biointerfaces* **2020**, *187*, 110614.

4) Winkeljann, B.; Bauer, M. G.; **Marczynski, M.**; Rauh, T.; Sieber, S. A.; Lieleg, O., Covalent mucin coatings form stable anti-biofouling layers on a broad range of medical polymer materials. *Advanced Materials Interfaces* **2020**, *7* (4), 1902069.

5) Rickert, C. A.; Lutz, T. M.; **Marczynski, M.**; Lieleg, O., Several sterilization strategies maintain the functionality of mucin glycoproteins. *Macromolecular Bioscience* **2020**, *20* (7), 2000090.

6) Lutz, T. M.; **Marczynski, M.**; Grill, M.; Wall, W. A.; Lieleg, O., Repulsive backbone-backbone interactions modulate access to specific and unspecific binding sites on surface-bound mucins. *Langmuir* **2020**, *36* (43), 12973-12982.

7) Jiang, K.; Yan, H.; Rickert, C. A.; **Marczynski, M.**; Sixtensson, K.; Vilaplana, F.; Lieleg, O.; Crouzier, T., Modulating the bioactivity of mucin hydrogels with crosslinking architecture. *Advanced Functional Materials* **2021**, *31* (10), 2008428.

8) **Marczynski, M.**; Jiang, K.; Blakeley, M.; Srivastava, V.; Vilaplana, F.; Crouzier, T.; Lieleg, O., Structural alterations of mucins are associated with losses in functionality. *Biomacromolecules* **2021**, *22* (4), 1600-1613.

9) **Marczynski, M.**; Kimna, C.; Lieleg, O., Purified mucins in drug delivery research. *Advanced Drug Delivery Reviews* **2021**, *in press*.

10) **Marczynski, M.**; Lieleg, O., Forgotten but not gone: particulate matter as contaminations of mucosal systems. *Biophysics Reviews* **2021**, *2* (3), 031302.

11) Zachos, I.; Genth, R.; Sutiono, S.; **Marczynski, M.**; Lieleg, O.; Sieber, V., Hot flows: Evolving an archael glucose dehydrogenase for carba-$NADP^+$ using microfluidics at elevated temperatures. *ACS Catalysis, submitted.*

Book chapters

1) **Marczynski, M.**; Winkeljann, B.; Lieleg, O., Advances in mucin biopolymer research: purification, characterization, and applications. *In: Biopolymers for Biomedical and Biotechnological Applications*, edited by Bernd Rehm & M. Fata Moradali. **2021**, 181-208.

Patents

1) Lieleg, O.; **Marczynski, M.**; Weber-Hohengrund, M.; Winkeljann, B., Method of isolating mucin from mucin containing tissue. *European patent application EP3792275A1,* **published 17th March 2021**.

2) Lieleg, O.; **Marczynski, M.**; Winkeljann, B., A method of isolating mucins based on filtrations steps. *Patent application no. EP20196327.9*, date of filing:**15th September 2020**.

Acknowledgement

An dieser Stelle möchte ich allen danken, die auf verschiedene Arten am Gelingen dieser Arbeit beteiligt waren.

Ein ganz großer Dank gebührt natürlich meinem Doktorvater Prof. Dr. Oliver Lieleg. Danke für die Aufnahme in Deine Arbeitsgruppe und die Möglichkeit, ein spannendes Thema zu bearbeiten. Vielen Dank für Deine intensive Betreuung, für wissenschaftliche Förderung, das Schärfen rhetorischer Fertigkeiten, das Korrigieren zahlreicher Manuskripte und das Schaffen einer motivierenden Arbeitsatmosphäre.

Außerdem danke ich den Mitgliedern der Prüfungskommission für die Übernahme ihrer jeweiligen Aufgaben als Prüfungsvorsitz und Zweitprüfer.

Ein besonderer Dank gilt ferner allen Kollegen und Kollaborationspartnern außerhalb der Arbeitsgruppe, mit denen ich in den vergangenen Jahren zusammenarbeiten durfte: Prof. Dr. Thomas Crouzier, Kun Jiang, Dr. Matthew Blakeley, Dr. Hongji Yan, Dr. Vaibhav Srivastava, Prof. Dr. Francisco Vilaplana, Prof. Dr. Mireille M. A. E. Claessens, Dr. Slav Semerdzhiev, Dr. Ine Segers-Nolten, Dr. Bizan N. Balzer, Prof. Dr. Wolfgang A. Wall, Dr. Maximilian Grill, Prof. Dr. Stephan A. Sieber, Dr. Theresa Rauh, Prof. Dr. Ulrich Gerland und Dr. Bernhard Altaner.

Ich bedanke mich außerdem herzlich bei allen aktuellen und ehemaligen Mitgliedern der Professur für Biomechanik für ihre Kollegialität und gute Zusammenarbeit. Insbesondere gilt mein Dank Dr. Benjamin Winkeljann für gemeinsame Bierpausen, Spaziergänge und natürlich für die Hilfe mit den Rheometern. Ich danke Ceren Yağmur Kımna, Bernardo Miller Naranjo und Maria Bauer für zahlreiche Kaffeepausen, nicht ganz so zahlreiche Prosecco-Nächte, *dad jokes* und das Wehklagen über die ~~Nichtigkeiten~~ Widrigkeiten des (Labor-/Arbeits-)Alltags. Vielen Dank an Iris König-Decker und Tobias Fuhrmann für Unterstützung in administrativen und technischen Angelegenheiten sowie für *assistance with mucin purification*. Natürlich danke ich auch Theresa Lutz für morgendliche Gespräche und das Zutagefördern charmanter mundartlicher Absonderlichkeiten. Ich danke Euch allen für Eure Freundschaft.

Marvin Ertelt und Carolin Ricky Rickert: Ich fürchte, dass ich die Dankbarkeit, die ich Euch gegenüber verspüre, gar nicht adäquat in Worte fassen kann. Euretwegen bin ich immer gerne in die Arbeit gekommen. Danke für Alles! ♡ ♡ ♡

Natürlich möchte ich auch meiner Familie und Freunden danken. Auch wenn Euer inhaltlicher Beitrag zu diesem Werk eher gering ausgefallen ist, so war der moralische Beitrag umso größer: Danke!

Zu guter Letzt gebührt ein riesiges Dankeschön meinem Ehemann Claus Pommer: Vielen Dank für Deine Liebe und Unterstützung. Danke, dass du während meiner Promotionszeit immer für mich da warst und mich nach weniger erfolgreichen Arbeitstagen aufgebaut hast.